Additives for Improved Analysis of Lipids by

Mass Spectrometry

by

Rian Lara-Kim Griffiths

A thesis submitted to The University of Birmingham for the

degree of a Doctor of Philosophy

School of Chemistry

University of Birmingham

May 2014

UNIVERSITY OF BIRMINGHAM

University of Birmingham Research Archive

e-theses repository

Abstract

Matrix-assisted laser desorption/ionisation (MALDI) has rapidly been established as a suitable technique for lipid analysis. In MALDI lipids form a range of adducts (protonated ($[M+H]^+$) and cationic ($[M+Na]^+$, $[M+K]^+$)), leading to spectral complexity. Promotion of a single adduct type is therefore desirable. This thesis describes optimised sample preparation strategies for MALDI-MS and imaging of lipids in biological samples.

Inclusion of salt additives in MALDI matrix solutions for analysis of biological samples is considered. Nitrate salt additives are found to increase sensitivity of a given adduct type in extract samples. Similar preparations deposited via airspray for imaging are shown to have limited use owing to blockage of the spray nozzle. Incorporation of lithium into tissue samples via formal fixation is demonstrated, enabling *in situ* structural characterisation of highly abundant lithium-lipid adducts in MALDI-MS and imaging.

Analysis of formal fixed tissues is also shown to be compatible with a relatively new surface sampling technique: liquid-extraction surface-an) complexes, was used to allow electron-transfer dissocation (ETD) of $[Mg+L_2]^{2+}$ and $[Ca+L_2]^{2+}$, giving rise to highly abundant fatty acid side-chain informative product ions.

Declaration

I hereby declare that the work presented in this thesis is entirely my own, except where indicted by reference in the text. I also declare that this thesis has not been submitted for a degree at any other institution.

Work presented in Section 2 of this thesis has been published in the following:

R. L. Griffiths and J. Bunch. A survey of useful salt additives in matrix-assisted laser desorption/ionization mass spectrometry and tandem mass spectrometry of lipids: introducing nitrates for improved analysis. *Rapid Communications in Mass Spectrometry*, 2012. **26**(13): p 1557-1566.

Work presented in Sections 3-5 of this thesis has been published in the following:

R. L. Griffiths, J. Sarsby, E. J. Guggenheim, Alan M Race, Rory T. Steven, J. Fear, P. F. Lalor and J. Bunch. Formal Lithium Fixation Improves Direct Analysis of Lipids in Tissue by Mass Spectrometry, 2013. *Analytical Chemistry*, **85**(15): p 7146-7153.

Acknowledgements

TABLE OF CONTENTS

4. FORMAL LITHIUM FIXATION AS A ROUTE TO LITHIUM ION INCORPORATION INTO TISSUE FOR IMPROVED *IN SITU* ANALYSIS OF PHOSPHOLIPIDS BY MALDI .138

List of Figures

List of Tables

List of Abbreviations

alpha-hydroxycinnamic acid	CHCA
Atmospheric pressure	AP
Collision-induced dissociation	CID
Desorption electrospray ionisation	DESI
Direct current	DC
Dithranol	DIT
Electron-capture dissociation	ECD
Electron-transfer dissociation	ETD
Electrospray ionisation	ESI
Fourier transform ion cyclotron resonance	FT ICR
Gas chromatography	GC
High-energy collision-induced dissociation	HE-CID
Infrared	IR
Infrared multiphoton dissociation	IRMPD
Liquid chromatography	LC
Liquid-extraction surface analysis	LESA
Liquid micro-junction surface sampling	LMJ-SS
Matrix-assisted laser desorption ionisation	MALDI
Mass Spectrometry	MS
Mass spectrometry imaging	MSI
Mass to charge ratio	m/z
Neodymium Yttrium Aluminium Garnet	Nd:YAG
Neodymium Yttrium Lithium Fluoride	Nd:YLF
Neodymium Yttrium Vanadate	$Nd:YVO_4$
Ozone-induced dissociation	OzID

para-Nitroaniline	PNA
Phosphatidylcholine	PC
Phosphatidylethanolamine	PE
Phosphatidylglycerol	PG
Phosphatidylinositol	PI
Phosphatidylserine	PS
Post source decay	PSD
Radio frequency	RF
Sinapinic acid	SPA
Secondary ion mass spectrometry	SIMS
Sphingomyelin	SM
Tandem mass spectrometry (Dissocition experiment)	MS/MS
Time-of-flight	TOF
Trifluoroacetic acid	TFA
Ultraviolet	UV
Ultraviolet photo dissociation	UVPD
Quadrupole time-of-flight	Q-TOF
2,5-Dihyroxybenzoic acid	DHB
2,6-Dihydroxyacetophenone	DHA
2,4,6-Trihydroxyacetophenone	THAP
3-hydroxypicolinic acid	HPA
9-Aminoacridine	9-AA

1. Introduction

Mass spectrometry (MS) analysis was first developed in the late *1900s* and enables analysts to measure the mass to charge ratio (*m/z*) of ionised species. To conduct a mass spectrometry (MS) experiment molecules must first be ionised. Once charged species have been formed these are separated according to their mass-to -charge ratio (*m/z*) in a mass analyser and then detected. Traditionally species were ionised by electron ionisation (EI). This ionisation technique leads to a large degree of molecule fragmentation; hence it is unsuitable for the analysis of larger molecules with masses of hundreds or thousands of Daltons, such as those found in biological systems. Softer desorption ionisation techniques such as electrospray ionisation (ESI) and matrix-assisted laser desorption/ionisation (MALDI) developed in the 1980s were shown to be more suitable for the analysis of biomolecules [1, 2].

There is considerable interest in the analysis of biomolecules in order to improve scientific understanding of biological processes. The natural presence, relative abundance and/or the spatial distributions of biological molecules such as proteins, lipids and other metabolites in tissues can vary with the onset and/or progression of disease. Hence changes in the normal abundance and localisation of certain species can be considered as biomarkers for a particular disease. As mass spectrometry enables consideration of a large number of different analytes in a single analysis it is an attractive route to gaining understanding the natural composition of different species

(such as proteins, drugs or lipids) in a sample. Furthermore, with the introduction of mass spectrometry imaging (MSI) techniques such as secondary ion mass spectrometry (SIMS) [3], desorption electrospray ionisation [4] (DESI) and MALDI imaging [5], it is also possible to obtain spatial information, hence compositional changes can be considered alongside changes in localisation.

In the presented work matrix-assisted laser desorption/ionisation (MALDI) will be the ionisation method considered. Both liquid and solid samples can be considered by MALDI-MS analysis and imaging experiments can also be conducted. For the analysis of liquid samples, solutions are generally spotted onto a multi well target plate and introduced to the mass spectrometer after drying, whereupon the laser is fired across the sample well. For the analysis of solid samples, such as thin tissue sections, the surface can either be analysed by manually selecting an area of interest and firing the laser in this selected area or large areas can be analysed in a single analysis by performing an imaging experiment. These can be performed either by firing the laser at discrete sequential and incremental locations across a pre-defined region of interest or by rastering the laser across the sample region.

1.1 Matrix-Assisted Laser Desorption/Ionisation (MALDI)

Desorption ionisation was first described by Beckey with the introduction of field desorption [6]. This was the first technique to separately desorb and then ionise an analyte. A solution of the analyte sample is deposited on a filament covered with microneedles, where, upon heating, the sample melts and ions formed accumulate at the microneedle tips before being desorbed [7]. This forms ions with low internal energy, hence highly abundant molecular ions and little or no fragment ions are detected in the resultant mass spectrum. This is particularly suitable for the analysis of high molecular weight and/or thermally labile species. Laser desorption ionisation followed. In this approach, a laser beam is irradiated onto a surface on which the sample of interest has been deposited. This enabled the detection of intact molecules with biological relevance such as glycosides, nucleotides, amino acids and oligopeptides [8]. Laser desorption ionisation was first performed with an IR wavelength laser, however UV wavelength lasers were later shown to be useful also [9].

Matrix-assisted laser desorption/ionisation (MALDI) was developed in the late 1980's simultaneously by two groups; Karas and Hillenkamp [10] and Tanaka *et al.* [2]. Laser desorption ionisation, although enabling the analysis of biologically relevant molecules, was limited to those with relatively low molecular masses (hundreds of Daltons). Tanaka *et al.* showed, for the first time, the (UV) laser desorption ionisation of proteins with masses of thousands of Daltons by first preparing the sample surface with glycerol and cobalt powder [2]. Karas and Hillenkamp also showed (UV) laser desorption ionisation of high molecular weight proteins, however they used a conjugated organic acid (nicotinic acid) with a strong molar absorptivity at the laser wavelength as an absorbing matrix [10].

Today, matrix-assisted laser desorption/ionisation is usually achieved by first introducing a matrix (either a single compound or a mixture) which efficiently absorbs energy at the wavelength of the laser employed. Laser irradiation of this mixed matrix/analyte sample mixture leads to desorption/ionisation of the sample material. Both IR and UV wavelength lasers have been described in MALDI, however only UV MALDI will be considered in this thesis. In UV MALDI, matrix molecules are generally low molecular weight and highly conjugated organic compounds which efficiently absorb energy at the specific wavelength of the laser employed, similar to the approach described by Karas and Hillenkamp [10]. Upon laser irradiation, energy is absorbed by matrix molecules and then transferred to the analyte species, leading to desorption/ionisation of both matrix and analyte species.

Matrix molecules are deposited in molar excess to analyte molecules; historically, ratios of up to 10 000 to 1 have been described, however more recently lower matrix to analyte ratios have been shown to provide better results for low molecular weight analytes [11, 12]. Generally co-crystallisation of matrix molecules with analyte species is believed to be crucial for the ionisation process. For this reason, solvent selection is a particularly important parameter in the MALDI experiment. A simplified schematic of the process is provided in Figure 1. After ionisation, either positively or negatively charged species (depending on the ion mode selected) are extracted into the mass analyser and separated by, for example, their time-of flight (TOF), before detection as a mass to charge ratio (*m/z*).
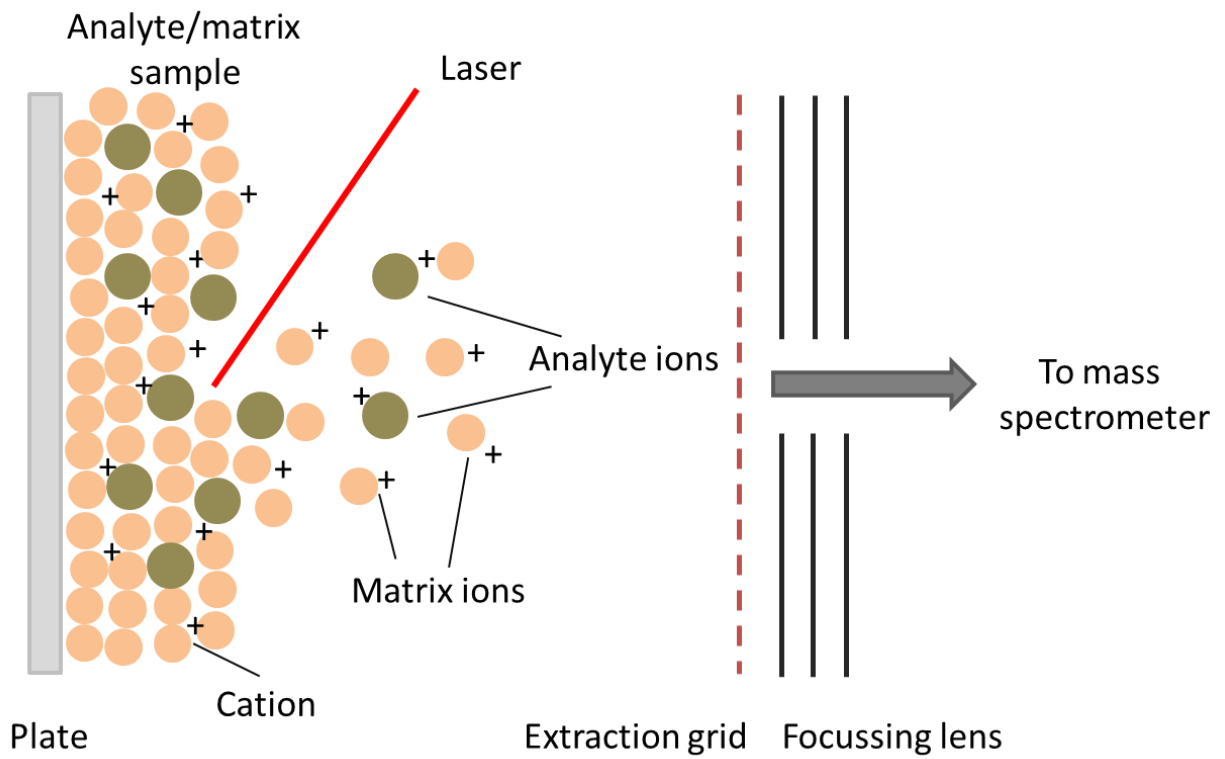
Figure 1 A simplified schematic of the MALDI process. Matrix/analyte crystals deposited on a MALDI target plate are ablated with a pulsed laser. Energy from the laser is absorbed by matrix molecules and transferred to analyte species, aiding desorption and ionisation. Ionised species are extracted into the mass spectrometer.

1.1.1 Matrix selection

A wide range of molecules have been reported as suitable matrix compounds for UV-MALDI experiments. Studies have shown that different compounds are particularly suitable for the analysis of specific classes of analytes. A summary of recommended matrices for a range of different analytes is provided in Table 1. In addition, certain matrix molecules may be better suited to positive ion mode analysis than to negative ion mode. Generally, matrix structures should be vacuum-stable, soluble in a solvent system suitable for the analysis of the analyte in question whilst also exhibiting high molar absorptivity (ε) at the laser wavelength and promote ion formation (such as protonation in positive ion mode).

Owing to these many different requirements, the design of matrix compounds has proven challenging. The introduction of atmospheric pressure MALDI (AP-MALDI) and the use of solvent-free sample preparations such as dry-coating have reduced the number of different requirements. However, matrix selection and optimisation remains an intensive area of research and the reasons why one structure is particularly suited to the analysis of a specific analyte are still not often well understood. This thesis describes the analysis of lipid analytes only, hence these will be discussed in greater detail.
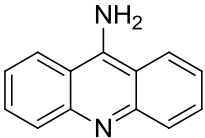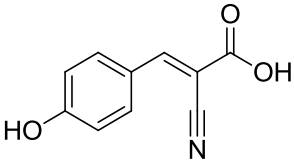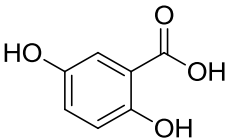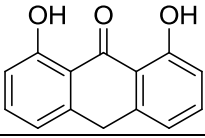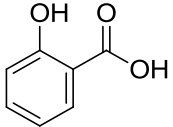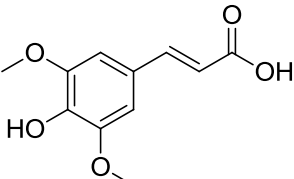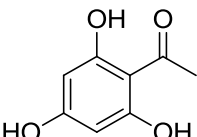
Matrix Compound	Structure	Analytes
9-amino acridine (9-AA)		Lipids [13]
α-cyano-4-hydroxycinammic acid (CHCA)		Peptides [14] Proteins
2,5-Dihydroxybenzoic acid (DHB)		Lipids [13] Polymers [15]
Dithranol (DIT)		Lipids [16] Polymers [15]
3-hydroxypcolinic acid (HPA)		Oligonucleotides [17]
Sinapinic acid (SPA)		Proteins [14]
Trihydroxyacetophenone (THAP)		Carbohydrates [18] Oligonucleotides Lipids [13, 19]

Table 1 Common UV-MALDI matrices and analytes they are useful for.

Historically, low molecular weight organic acids were employed in MALDI experiments in order to promote protonation of analyte species during the ionisation process. However more recently a range of neutral and basic compounds have been shown to be useful also. To date the most commonly reported matrices for spot analysis of lipids are 2,5-dihydroxybenzoic acid (DHB) [20-32], 2,6-dihydroxyacetophenone (DHA) [22, 33, 34] and 2,4,6-trihydroxyacetophenone (THAP) [19, 35-38]. However the basic nature of 9-aminoacridine (9-AA) and *para*-nitroaniline (PNA) matrices have been shown to improve negative ion mode lipid analysis compared to acidic matrices [39, 40].

For tissue imaging, matrix properties such as the typical crystal size and vacuum stability, can have a limiting impact on the experiment. Although the use of DHB in imaging has been reported [23, 26, 41], many groups favour α-cyano-4-hydroxycinnamic acid (CHCA) [42-44] as smaller crystals are formed. Large crystals which are formed by DHB and THAP matrices can cause delocalisation (spreading) of analytes [45] which is detrimental to imaging experiments. Furthermore, DHA and PNA matrices have been shown to exhibit poor vacuum stability over long time periods [22, 46], hence they are unsuitable for lengthy imaging experiments in vacuum MALDI which can require hours of data acquisition for a single experiment. However, recently, matrices such as PNA have been shown to be suitable for MALDI imaging of lipids on intermediate-pressure instrumentation [39] and should not have limited use in AP-MALDI.

A number of different approaches have been considered in the search for suitable matrix compounds. Several groups have explored the use of binary matrix systems (a combination of two different matrix compounds) in an attempt to gain mutual benefits [47-51]. Shanta *et al.* reported that combining CHCA matrix, which is commonly reported in positive ion, but not in negative ion, mode analysis of lipids, with DHB increased signal intensities and/or signal to noise ratios of lipid species, enabling imaging analysis in both ionisation modes [48]. Gua *et al.* also describe improved spectral quality (reduced background peaks and better signal-to-noise) and lower laser fluence requirements when combining CHCA and 9-AA for positive and negative ion mode analysis [51]. In a different approach, Teuber *et al.* showed that design of a compound based on existing matrix compounds could be advantageous, thus, synthesis of α-cyano-2,4-difluorocinnamic acid (di-FCCA),which is not commercially available, gave rise to sensitivity improvements in the analysis of a variety of lipid species [52].

Less conventional matrix structures based on aromatic molecules, which characteristically display a large degree of conjugation, have also been reported for lipid analysis, such as acenaphthene [27] and 1,5-diaminonaphthalene [53]. Thomas *et al.* showed the application of 1,5-diaminonaphthalene for dual polarity analysis of lipids in thin tissue sections [53]. Graphite and graphene structures have also been shown to be useful MALDI matrices; the delocalised electrons which exist in these structures act as UV absorbers, similar to the delocalised electrons in highly conjugated organic molecules. The use of graphite for the analysis of several lipid classes has been reported

for lipid standards, complex extracts and *in situ* tissue analysis of a range of lipid analytes [54-56]. A particular advantage of replacing an organic matrix compound with graphite or graphene is the reduced spectral complexity afforded by the removal of background matrix peaks which can mask the detection of some small-molecule analytes [55]. Other structures such as gold nanoparticles [28] and ionic matrices [57] have also been reported as useful matrix compounds in recent years. Gold nanoparticles enabled preferential detection of cerebroside lipid species for thin tissue sections, which were not typically detected when an organic matrix, DHB, was used [28]. Ionic liquid matrices based on the conjugate base of CHCA have been shown to reduce the extent of fragmentation of phospholipid species compared to traditional organic matrices, increase signal intensity and improve sample homogeneity [58].

1.1.2 Matrix Deposition

Once an appropriate matrix compound for analysis has been selected it must be deposited onto the MALDI target alongside the analyte. Generally, when handling liquid samples, solutions of matrices and analyte samples are spotted onto MALDI target well plates. A range of different spotting techniques have been described in the literature for spot sample analysis. Directly pipetting a solution containing a mixture of the analyte and matrix is described in dried-droplet preparation [59]. Alternatively, analyte and matrix solutions can be spotted separately, with the matrix solution applied as an overlayer after the analyte solution has dried [60]. Finally, the analyte sample can be 'sandwiched' between matrix layers.

Traditionally it was believed that co-crystallisation of matrix and analyte molecules is integral to the MALDI ionisation process. For this reason, the choice of solvent has played a significant role in preparation procedures and has been investigated widely. However a number of studies have challenged this understanding. The use of a number of different positional isomers of DHB was considered by Horneffer *et al.* for protein analysis. The group showed that analyte incorporation into matrix crystals, although helpful, was not a requirement for MALDI [61].

The successful employment of solvent-free sample preparation methods also challenges this idea [62]. For sample preparations which involve lipid and matrix samples in solution, a particular advantage is the solubility of many lipid and organic matrix molecules in the same organic solvents [63]. When pipetting sample solutions, retention inside the sample well on the MALDI target plate is aided by the hydrophobic outer edge. The hydrophobic edge maintains water inside the well, hence even if sample solutions are prepared in organic solvents, a small amount of water is often still added.

When performing tissue analysis, it is important to form a homogeneous layer of matrix crystals across a large sample area. For this reason, spraying techniques were the first sample preparation method considered. Commonly, manual deposition techniques such as using an artist's airspray gun or a thin layer chromatography sprayer have been reported [64]. Nebulisation of the sprayed solution can also help to ensure small matrix crystals are formed [65]. The analyst must ensure that sufficient matrix molecules are deposited to enable ionisation, however care must be taken to ensure analyte delocalisation from solvent wetting does not occur. It can be advantageous in spraying techniques to incorporate a percentage of water into the solvent system as this reduces problems with evaporation of more volatile organic solvents before they reach the MALDI target plate.

Manual deposition methods have suffered from user dependency and problems with reproducibility, hence a number of automated deposition techniques have been developed to reduce these problems. Automated acoustic deposition[66], automated inkjet printing[67] and robotic sample preparation instrumentation have all been described [68, 69]. More recently the use of solvent-free techniques in MALDI imaging analysis of lipids has been described. Hankin *et al.* describe sublimation of matrix powders onto MALDI target plates for improved (homogeneous) coverage [70]. Furthermore, Puolitaival *et al.* describe dry-coating of ground matrix powders through an analytical sieve (20 μm mesh) [62]. These solvent-free deposition techniques remove potential problems with analyte delocalisation. These methods could provide a less user dependent and therefore more reproducible alternative to manual spraying techniques.

1.1.3 Laser Selection

Traditionally N_2 (Nitrogen) gas lasers (337 nm) have been employed in UV MALDI-MS analysis [2]. These lasers are relatively cheap, commercially available and have a reasonable life span of approximately 2-6 x 10^7 shots [71]. The financial implications of maintaining the laser is an important consideration. MS imaging (which requires lengthier data acquisition) a drive towards improved instrumentation has led to the introduction of diode-pumped solid-state lasers (DPSS) [71], which typically have lifetimes of 1 x 10^9 shots. Most of these are based on Neodymium and all are frequency-tripled: Nd:YAG (Yttrium Aluminium Garnet) [72], Nd:YVO$_4$ (Yttrium Vanadate) [71] and Nd:YLF (Yttrium Lithium Fluoride) [73]. These lasers offer the advantage of higher repetition rates which can allow for shorter acquisition times for similar data collection and hence higher throughput analysis in comparison to N_2 lasers [71, 73]. The typical properties of these lasers discussed are listed in Table 2.

Characteristics	**N_2**	**Nd:YAG**	**Nd:YLF**	**Nd:YVO$_4$**
Wavelength (nm)	337	355	349	355
Power (µJ per pulse)	< 150	< 300	5	< 20
Repetition Rate	1-60 Hz	200Hz-1 KHz	200Hz-5 KHz	1-20 KHz
Pulse Width	800 ps – 3 ns	< 500 ps	*n.r*	1.5>t>1.25 ns

Table 2 Typical properties of N_2 and Neodymium-based UV-MALDI lasers according to the following publications [71, 74-79], *n.r* – not reported.

1.1.4 Ion Formation in Matrix-Assisted Laser Desorption-Ionisation (MALDI)

MALDI was introduced nearly three decades ago and studies to probe the exact nature of the ion formation process continue to be explored. Knochenmuss proposed that ion formation is a two-step process involving generation of primary ions during, or shortly after, the laser pulse, followed by conversion to the 'most favourable secondary ion products' in the desorption plume via a number of different mechanisms [80, 81]. This two-step process is the most widely accepted model and subsequent literature has discussed the role of these primary [82-85] and secondary [86-89] processes in detail.

Primary processes during laser ablation are not currently as well understood as secondary reactions in the MALDI plume because the formation of the ions that are detected masks these primary reactions. However a number of theories have been postulated, for example, energy pooling of excited states (M*) [81], leading to photoionisation of a single matrix (M) or analyte molecule (A) [83, 90]:

$$MM \xrightarrow{2(h\nu)} M^*M^* \longrightarrow M^{+\bullet} + e^-$$

$$M^*M^* + A \longrightarrow MM + A^{+\bullet} + e^-$$
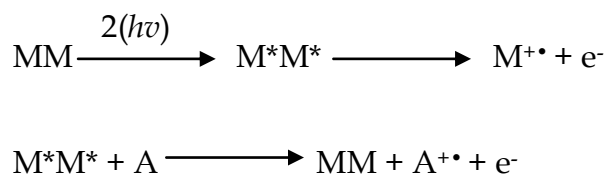
As a single matrix compound may be useful in both positive and negative ionisation modes, the possibility of disproportionation reactions has also been proposed [90]:

$$2M \xrightarrow{n(h\nu)} (MM)^* \longrightarrow (M-H)^- + MH^+$$
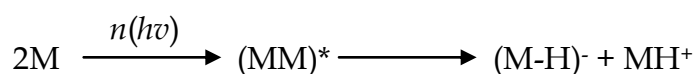
The possibility of desorbing ions that are pre-formed in the matrix-analyte solid solution has also been suggested [91]. Although this has remained difficult to prove, it is an interesting theory where salt doping studies are concerned.

Radical cations ($M^{+\bullet}$) formed during primary ionisation (desorption) can undergo further reactions in the MALDI plume. A wide range of secondary reactions have been proposed, such as proton (H) and cation (C) transfer:

Proton transfer $M^{+\bullet} + M \longrightarrow (M-H) + MH^{+\bullet}$

$M^{+\bullet} + A \longrightarrow (M-H) + AH^{+\bullet}$

Cation transfer $MC^{+\bullet} + A \longrightarrow (M-C) + AC^{+\bullet}$
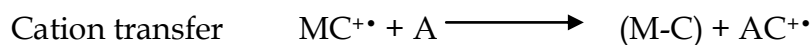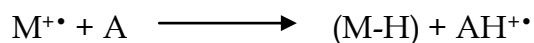
Electron capture and/or transfer have also been described in detail by Knochenmuss and Zenobi [88]. The potential role of matrix-analyte clusters has also been debated [92]. The importance of considering the effect of ionisation energy and the internal energy of matrix and analyte molecules has also been highlighted[76, 93]. Clearly the ionisation process is very complex and studies are on-going to determine the exact mechanisms occurring. Gas-phase thermodynamics are particularly important when considering in-plume processes such as proton and cation transfer, which can only occur if the analyte has a greater (proton or cation) affinity than the matrix molecule. Proton and cation affinities and gas-phase interactions of a range of common matrix compounds and analyte species have been determined experimentally and/or computationally [89, 94-96].

Experimental reports agree that the formation of singly charged ions appears to be most favourable, even when multiply charged metal ions are included as cationising agents [97]. Karas *et al.* discussed in detail the possible reasons for this, such as neutralisation via proton transfer and electron capture [98], and a number of reviews provide comprehensive summaries of the many potential mechanisms postulated for both primary (initial laser irradiation) and secondary (in-plume) mechanisms [85, 90, 99].

It has been shown that a number of experimental factors also affect the desorption and/or ionisation process. Sample preparation parameters, such as the matrix selected, alongside instrumental settings, such as the laser characteristics, must be considered

when attempting to understand the complex processes of ion formation [100-103]. In addition, the transfer of internal energy from matrix to analyte molecules has been shown to be affected by laser characteristics [76], further highlighting the complexity of the ionisation process.

1.1.5 Sample Analysis

Data can be acquired in a number of ways and both liquid and solid samples can be analysed. In order to analyse liquid samples, such as lipid standard solutions or biological lipid extract samples, matrix and analyte solutions are generally pipetted manually onto a MALDI target plate which contains spot wells. These spot wells are surrounded by a hydrophobic cell wall in order to aid sample retention. The laser is often fired in random locations across the sample well, in order to generate a mean spectrum for each spot.

Solid samples can also be analysed by MALDI; this provides the opportunity to directly analyse biological tissues. For the analysis of tissue organs or blocks, samples are sectioned in a cryostat before thaw mounting onto a plain MALDI target plate. Subsequent deposition of the matrix, often via a spraying technique, prepares the sample for introduction into the mass spectrometer. Imaging experiments can be conducted on tissue sections. This enables visualisation of the data in one of two ways, as a mass spectrum at each pixel location or by showing the spatial distribution of a

single *m/z* of interest (an image). A simplified scheme of MALDI-MS and mass spectrometry imaging (MSI) analysis is shown in Figure 2.
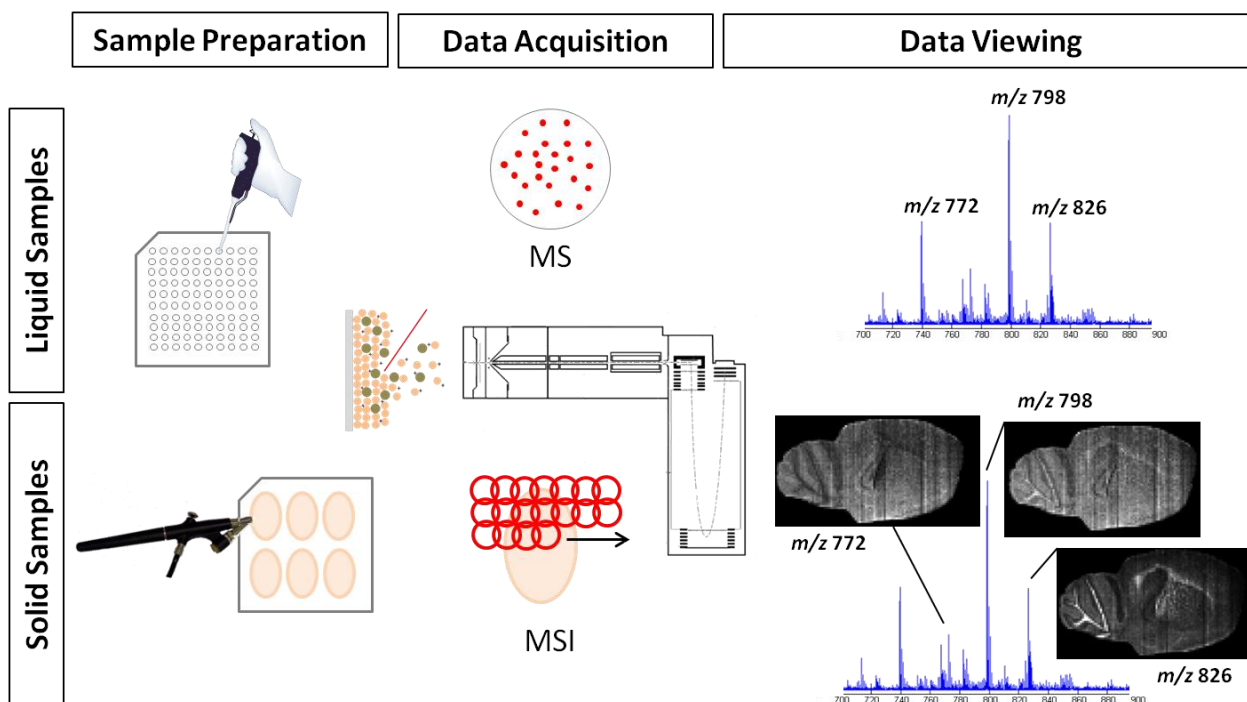
Figure 2 Diagrammatic schemes of sample preparation, data acquisition and data viewing of liquid and solid biological samples by MALDI mass spectrometry. Pippetting of liquid samples onto multi-well target plates, followed by firing of the laser in random locations across each sample well is depicted. Spraying of matrix solutions onto plain MALDI target plates before raster imaging data acquisition is also portrayed. Spot sample data is viewed as a mean mass spectrum providing compositional information. Imaging datasets can be viewed as single pixel spectra or as images showing the spatial distribution of a single *m/z* of interest, providing spatial and compositional information.

1.2 Electrospray Ionisation (ESI)

ESI operates via the application of a strong electric field to a liquid sample flowing through a capillary tube at atmospheric pressure [104]. The electric field generated induces charge accumulation at the liquid surface, forming highly charged droplets. Injection of a carrier gas disperses the spray and solvent molecules are removed via heating. Once the electric field is great enough, desorption from the droplet surface occurs [104]. Figure 3 provides a simplified schematic of the electrospray ionisation process. This was developed further to nano-electrospray, which creates a spray from a fine tip, hence it can handle low flow rates and generates smaller droplets [105].
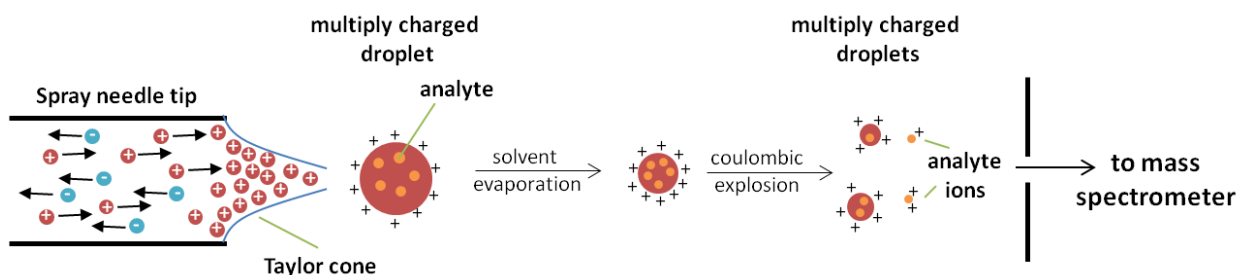
Figure 3 Simplified schematic of the electrospray ionisation (ESI) process.

Traditionally ESI analysis of biological tissues has been achieved by performing an extraction procedure combined with chromatographic separation techniques such as LC or GC, which can be directly coupled to the ESI source ref. A range of lipids have been analysed previously by ESI in this way including ceramides [106, 107], sphingoid bases [107], phospholipids [108-110] and neutral species such as fatty acids [107], cholesterol [106, 111], cholesterol esters [112] and triacylglycerols [113]. One of the main advantages of ESI over MALDI is that a wider variety of different analytes can be dissolved in a single solvent system and thus ionised, without the requirement for lengthy optimisation of experimental parameters such as matrix compound. In this way a wider variety of analyte species can be analysed in a single experiment, without the requirement for optimisation of parameters such as matrix selection for separate analytes. However ESI is less tolerant of salts than MALDI, which is particularly important when considering samples such as biological tissues which contain relatively high concentrations of salts.

1.2.1 Ion Formation in ESI

There are two models which have been proposed for the mechanism of ionisation in electrospray. The ion evaporation model proposes that as the spray droplets reach a particular radius the electric field is sufficient to afford desorption of the solvated ions [114, 115]. Conversely, the charge residue model suggests that the spray droplets undergo evaporation and fission cycles, eventually leading to droplets containing one analyte ion or less [115, 116]. Gas phase ions are then formed by a process of solvent evaporation, leaving the analyte species with all the charges that were present. A schematic representation is provided in Figure 4.
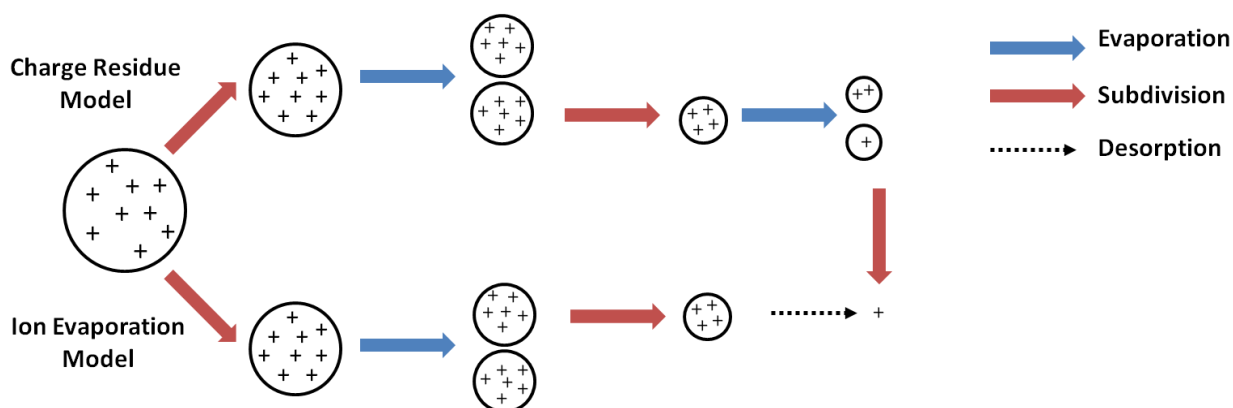
Figure 4 Schematic representations of the charge residue and ion evaporation models for the ionisation mechanism of electrospray

1.2.2 Liquid Extraction Surface Analysis (LESA)

Owing to the lengthy sample preparation times (extraction and separation prior to mass spectrometry analysis), alternative mass spectrometry techniques, which offer direct tissue surface analysis and the opportunity for imaging, have been favoured by some groups. More recent developments in surface-sampling techniques, which are compatible with ESI sources such as liquid micro-junction surface sampling (LMJ-SS) and desorption electrospray ionisation (DESI), offer the opportunity to combine spatial information with compositional information.

Liquid micro-junction surface sampling was reported in 2001 by Wachs and Henion, The miniaturised sprayer they described, can be used to form a liquid micro-junction with a sample surface prior to electrospray [117]. Van Berkel *et al.* introduced a similar device for automated liquid micro-junction surface sampling in 2005 [118] and later developed the device to allow automated formation and withdrawal of a liquid micro-junction [119]. This was later commercialised and is commonly referred to as liquid-extraction surface-analysis (LESA). A simplified schematic of the process is provided in Figure 5.

Liquid micro-junction surface sampling has been shown to be suitable for a wide range of different applications. Various surfaces and analytes have been successfully sampled; dyes on TLC plates [118], inks on paper [118], skin blanching agents [120], drug metabolites, lipids and drug analytes in thin tissue sections [119-123], drug metabolites and proteins in blood spots [124, 125] and lipids on used contact lenses (polymer surface) [126]. This final example is of particular interest as surface sampling allows the opportunity to separately assess the accumulation of lipid species on the air and eye sides of the lens which provides greater insight as to the biological condition [126].
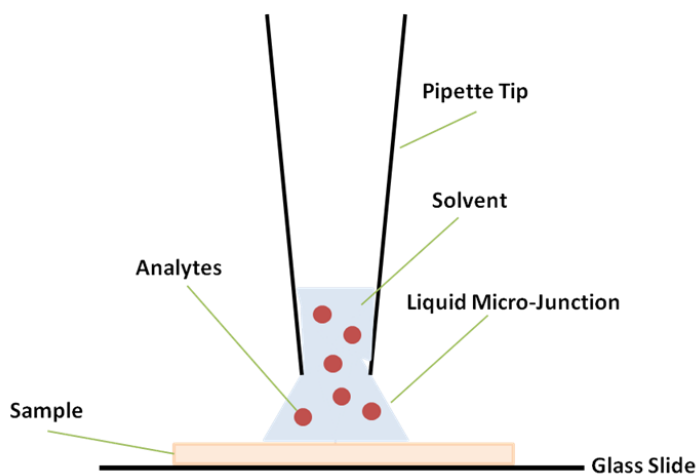
Figure 5 Simplified schematic of the liquid-extraction surface-analysis (LESA) process. A solvent is dispensed onto the sample surface, maintaining a liquid micro-junction between the sample surface and the pipette tip, which enables analyte extraction from the sample before then solvent is the re-aspirated and introduced to the mass spectrometer via ESI.

Desorption electrospray was introduced in 2004 by Cooks *et al.* The technique involves electrospraying a solvent onto a surface, which extracts the analytes of interest, before the projectile droplets are desorbed from the surface by a combination of pneumatic and electrostatic forces [4]. A simplified schematic of the desorption electrospray process is provided in Figure 6.
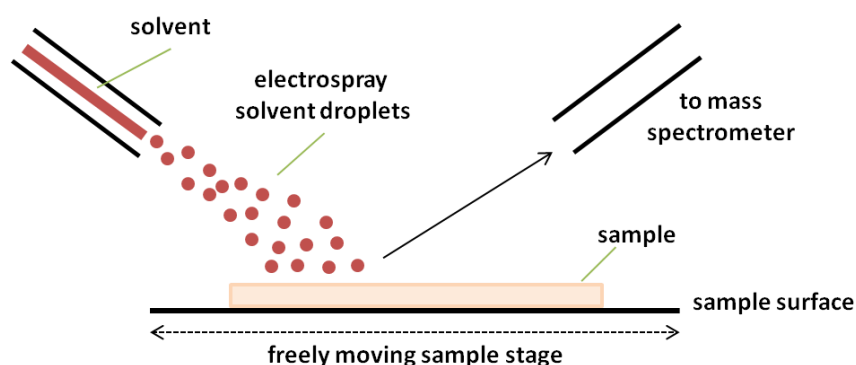
Figure 6 A simplified schematic of the desorption electrospray ionistion (DESI) process. Solvent molecules are ionised via electrospray and directed onto the sample surface. These ions extract analyte species, before they are extracted into the mass analyser.

Surface sampling and desorption electrospray techniques offer the advantage of reduced sample preparation and reduced spectral complexity in the low *m/z* region in comparison to MALDI-MS and MSI as no matrix is required [127]. However, in terms of MSI, DESI suffers with inferior spatial resolution of approximately 200 μm [127] when compared to MALDI and SIMS, which can resolve spatial information within 10 μm [128] and on the nm scale [129] respectively, hence using multiple techniques is often complimentary.

Both LESA and DESI have been shown to support MALDI mass spectrometry analysis. The corroboration of results between MALDI and LESA techniques from direct surface analysis strengthens results [120]. Although LESA cannot provide spatial resolution comparable to MALDI [120], it has been shown that analysis of MALDI spot samples by LESA-ESI, *post* MALDI analysis, can support the information obtained by MALDI, ionising species which are not detected in the first analysis [119]. Furthermore, DESI imaging has been used in support of MALDI imaging to separately analyse different analytes of interest, such as both lipids and proteins [130]. The analysis of thin tissue sections by LESA-ESI, to obtain data which supports that obtained in MALDI experiments will be presented in chapter 5 of this thesis.

1.3 Lipid ion formation in MALDI and ESI

Lipid analytes form both protonated (denoted $[M+H]^+$) and cationic adducts (such as sodium $[M+Na]^+$ and potassium $[M+K]^+$). It is important to note here that M denotes the analyte species in both MALDI and ESI in these annotations. This is the convention adopted in literature reports and should not be confused for the matrix. Phospholipids in particular can undergo laser-induced fragmentation in MALDI, leading to the detection of relatively highly abundant head-group peaks; however, the degree of fragmentation is affected to an extent by the matrix used. When analysing tissue samples, high concentrations of potassium and sodium salts in tissue samples, combined with the use of acidic matrix compounds and/or protic solvent systems, leads to the detection of a range of different lipid adducts when analysing tissue sections in a single experiment.

Although tissue salts are removed during extraction procedures, trace soluble metal impurities present in commercially available matrix compounds and solvents means various lipid adducts are also detected in liquid analysis. Therefore, cationic adducts are still detected when analysing extract and lipid standard samples, leading to the formation of three different adducts for any given lipid species in a single analysis. This complicates analysis, introducing the problem of overlapping nominal mass to charge ratio (*m/z*) values of different adducts of different lipids, leading to decreased sensitivity

for the detection of a single analyte. Overlapping *m/z* values are a particular problem for instruments which do not have high mass resolution capabilities.

Adducts of a limited number of different phosphocholine (PC) lipid species, which are detected at the same nominal mass, are highlighted in Table 3. The protonated adduct of PC 38:4 at *m/z* 810.6008 and the sodium adduct of PC 36:1 at *m/z* 810.5984 will be detected at the same *m/z* on instruments which can only have sufficient resolving power to report values in the region *m/z* 700-900 to one decimal place. The same problem will be encountered for the protonated adduct of PC 36:4 and the sodium adduct of PC 34:1, which would both be reported at *m/z* 782.6. In complex samples, such as biological tissues, it can be difficult to assign which lipid species have actually been detected in the experiment owing to such overlapping peaks. Thus routes to promote the formation of a single lipid adduct are desirable. Doping of MALDI matrix solutions with salt additives [19, 131-133] in an attempt to achieve spectral simplification have been described and is a major focus of this thesis.

Lipid Species	*m/z* [M+H]⁺	*m/z* [M+Na]⁺	*m/z* [M+K]⁺
PC 34:1	760.5851	**782.5671**	798.5411
PC 36:1	788.6165	**810.5984**	826.5723
PC 38:4	**810.6008**	832.5828	848.5567
PC 36:4	**782.6031**	804.5850	820.5589

Table 3 Mass to charge ratios (*m/z*) of protonated, sodium and potassium adducts of a range of phosphocholine (PC) lipid species.

1.4 Mass Analysis

Once ions have been formed, they are separated by a mass analyser and then detected. Ions can be separated in a number of ways. A range of instrumentation is available commercially, such as time-of-flight, quadrupole and more recently ion trapping mass analysers. In the presented thesis, a tandem mass spectrometer, which contains two separate mass analysers was used. This enables further opportunities with respect to the type of experiments that can be performed. Tandem instruments can be used to perform dissociation studies; in these experiments, only a selected *m/z* (parent ion) is transmitted through the first mass analyser. Ions of the selected *m/z* are then dissociated (fragmented) in a collision cell before fragment (product) ions are separated in the second mass analyser.

1.4.1 Quadrupole Time-of Flight (Q-TOF)

Morris *et al.* reported the first use of a quadrupole orthogonal time-of-flight instrument (Q-TOF) in 1996 [134]. A schematic of the instrument is provided in **Figure 8**. Their ideas were developed as a variation of the triple quadrupole instrument (QQQ). They used collision-activated decomposition (now described as collision-induced dissociation or CID) to sequence a biopolymer. Replacement of the final quadrupole with a time-of-flight (TOF) mass analyser improved the signal-to-noise ratio of obtained MS/MS spectra, providing mass accuracies in their study of product ions 'within 0.1 Dalton' [134], which enabled the determination of isotope patterns in MS/MS spectra [134] and

significantly improved the ability to assign charge states of fragment ions, which is particularly important for the analysis of biological analytes.

These initial experiments demonstrated the basic characteristics of the instrumental set-up; signal-to-noise and product ion mass accuracy, resolution better than 3000 (FWHM) and the ability to produce MS/MS spectra from low concentrations of sample [134]. This was first described with an electrospray ion source, however instruments with other ion sources, such as MALDI are also available [77, 135]. Chernushevich *et al.* have presented a comprehensive review of Q-TOF instrumentation [136].

1.4.1.1 Quadrupoles

Quadrupole mass analysers separate ions according to trajectory. Positive ions entering the space in between the rods will be attracted to the negative rod. Changing the potential before the ion discharges onto the rod will change the direction of the ion. Ions travelling along the axis of the poles are subjected to a total electric field comprising a quadrupolar alternating field superposed on a constant field which is resultant from the application of potentials upon the rods:

$$\phi_0 = +(U - V \cos \omega t) \text{ and } -\phi_0 = -(U - V \cos \omega t)$$

where ϕ_0 is the potential applied to the rods, ω is the angular frequency, U is the direct potential and V is the zero-to-peak amplitude of the radio frequency (RF) voltage. Only ions with a stable trajectory are transmitted. In, order to separate ions over a mass range, U is constant and V potentials are scanned across a predetermined range, transmitting

ions with stable trajectories over the desired *m/z* range. This is described as RF (V) only mode.

However, during dissociation experiments (MS/MS) Q_1 operates in mass-resolving mode via the application of a resolving DC voltage, only transmitting ions of a selected *m/z* (parent ions) and q_0 and q_2 remain in the RF only mode, transmitting ions across an *m/z* range. Figure 7 shows stable trajectories with changing or constant potentials. Fragment ions (product ions) formed by collision with a neutral gas (nitrogen) at a collision energy of up to 100 eV are detected across a chosen *m/z* range in the time-of-flight mass analyser.

$(U - V \cos \omega t)$

$-(U - V \cos \omega t)$

U

m_3

m_1 m_2

V

+

-

-

+
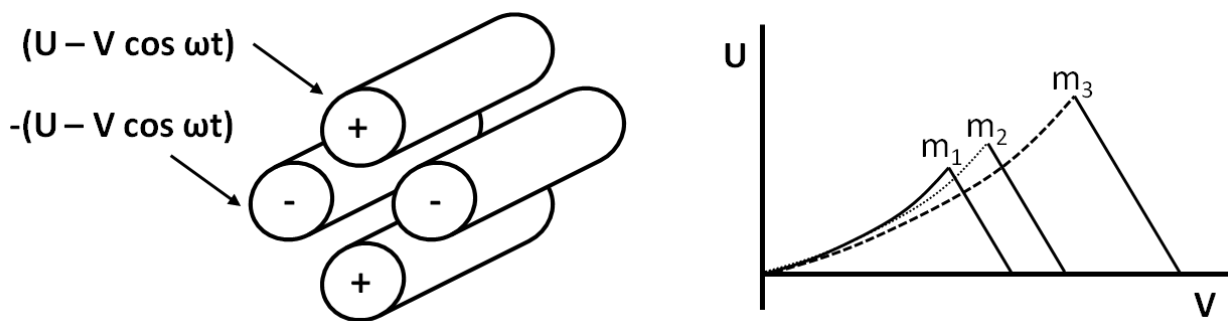
Figure 7 Schematic of the potentials applied to the quadrupole rods and a graph showing the stability area of ions with increasing masses ($m_1 < m_2 < m_3$) as a function of direct potential (U) and radio frequency potential (V).
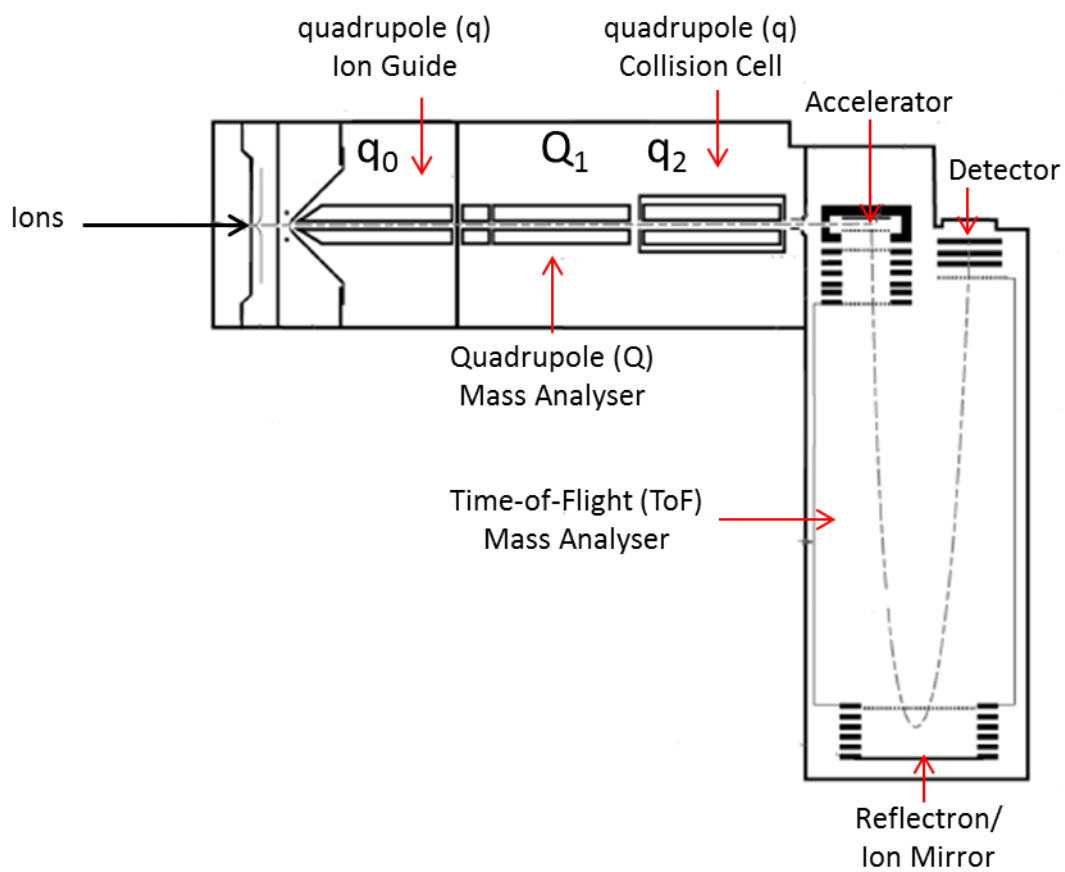
Figure 8 Schematic of the quadrupole time-of-flight (Q-TOF) instrumentation used to acquire MALDI mass spectrometry data in this thesis.

1.4.1.2 Time-of Flight (TOF)

Ions in the time-of-flight (TOF) mass analyser are separated according to their velocity when drifting in a free-field region (flight tube), after initial acceleration by an electric field. Ions are ejected from the source in packets, hence TOF mass analysers are particularly well suited to a pulsed laser source such as those used in MALDI. During acceleration all ions acquire the same kinetic energy; hence velocity differs according to mass. m/z ratios are calculated by measurement of the time taken to travel through the flight tube to the detector. An ion with mass m and charge $q= ze$ is accelerated by a potential of V_x. The electric potential is converted into kinetic energy (KE):

$$KE = \frac{mv^2}{2} = qV_x$$

Thus, velocity can be calculated by rearrangement of this equation:

$$v = (2zeV_x/m)^{1/2}$$

The ion travels at constant velocity, taking time t to travel a distance L to the detector:

$$t = \frac{L}{v}$$

Rearrangement of this equation, substituting v for the value shown above gives the following:

$$t^2 = \frac{m}{z}\left(\frac{L^2}{2eV_x}\right)$$

Hence m/z can be calculated from measuring t^2.

A reflectron, an electrostatic mirror, is also present in the TOF mass analyser. This creates a retarding field which deflects ions, sending them back through the flight tube. This achieves two things: first, increasing the flight path, enabling better separation of ions and secondly, correction of kinetic energy dispersion of ions accelerated with the same *m/z*. Ions with greater kinetic energy and thus greater velocity permeate the reflectron to a greater extent than ions with less kinetic energy. Therefore, faster ions spend longer in the reflectron, and reach the detector at the same time as slower ions with the same *m/z* according to the following equation:

$$d = \frac{KE}{qE} = \frac{qV_x}{qV_{y/D}} = \frac{DV_x}{V_y}$$

where V_y is the potential inside the reflectron, D is the length inside and the electric field in the reflectron $E = V_y/D$. A schematic of the reflectron time-of-flight set-up is provided in Figure 9.
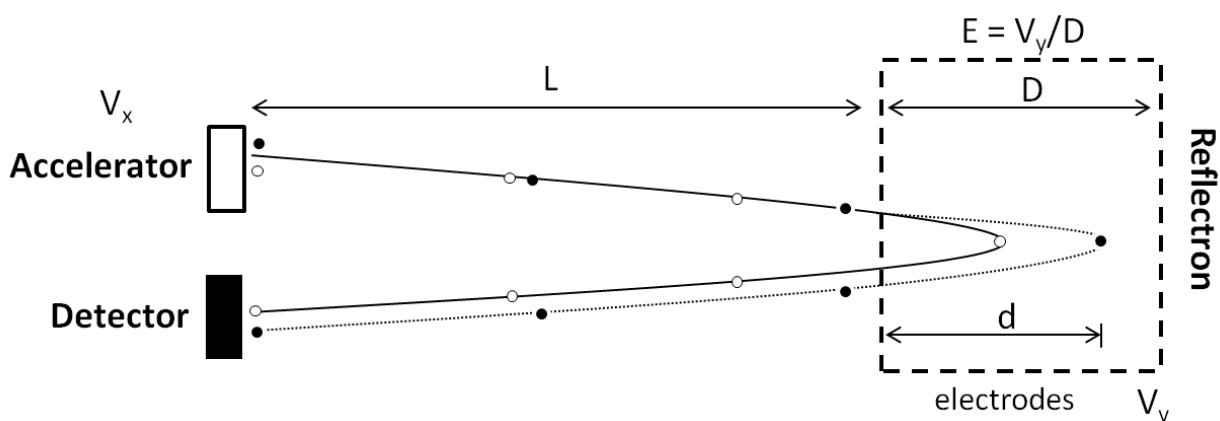
Figure 9 Schematic of the reflectron TOF mass analyser.

1.4.2 Electrostatic Trapping Instruments

The development of fourier transform ion cyclotron resonance [137] (FT ICR) mass spectrometry and the subsequent introduction of a number of trapping instruments [138, 139] provided the inspiration for the orbitrap mass analyser. Marakarov introduced the electrostatic field orbital trapping instrument in 2000 [140]. In this mass analyser, ions are trapped while orbiting an axial electrode, performing harmonic oscillations along the electrode [140]. Oscillations are converted into mass spectra using fourier transform, similar to FT ICR. The high mass resolution and mass accuracy afforded by FT ICR [137] lends the technique particularly suitable to the analysis of complex mixtures as molecules with very similar, but not the same, *m/z* can be separated with 1 000 000 ppm accuracy.

Marakov went on to couple the orbitrap mass analyser to an electrospray ion source [141] for the analysis of complex biological samples. This is particularly useful in lipid analysis as many lipid species have similar nominal masses. Analysis of lipids on this type of instrument can dramatically reduce problems regarding overlapping peaks. Other benefits of this instrumental set-up include a good dynamic range and considerable mass to charge range [142]. Analysis of thin tissue sections by a surface sampling technique compatible with electrospray ionisation on an orbitrap mass analyser will be considered in Chapter 5 of this thesis.

1.4.2 Orbitrap

Orbitrap mass analysers separate ions according to the frequency of their oscillation around an inner spindle shaped electrode which has an electrostatic voltage on the order of magnitude of several kilovolts and an outer barrel shaped electrode at ground potential. Ions with mass m and charge $q = ze$ are introduced along the r axis (see Figure x) and are accelerated along the z axis owing the force induced by the electric field. The potential inside the trap (U) is defined according to the following equation:

$$U(r, z) = \frac{k}{2}\left(z^2 - \frac{r^2}{2}\right) + \frac{k}{2}\ (R_m)2\ \ln\left(\frac{r}{R_m}\right) + C$$

where r and z are cylindrical coordinates, k is field curvature, R_m is the characteristic radius and C is a constant. Ions oscillate harmonically around the inner electrode. The frequency of oscillation ω of an ion is linked to the m/z as follows and is independent of its kinetic energy.

$$\omega = \sqrt{\left(\frac{q}{z}\right)k}$$

Mass spectra are generated by performing a fourier transform of the broadband current created by the ions and converting it into individual frequencies and intensities. A schematic representation of the orbitrap mass analysis is provided in Figure 10.
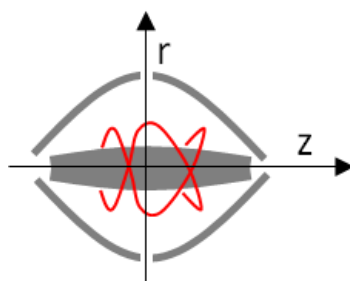
Figure 10 Schematic representation of the orbitrap mass analyser and the oscillation of ions (red).

1.4.3 Dissociation Studies

During dissociation experiments (MS/MS) a single *m/z* of interest is selected and then dissociated, which can activated via numerous methods. The fragment (product) ions formed, hopefully at structurally informative locations, are then detected. Obtaining structural information is particularly important when attempting to identify biomarkers of disease.

Dissociation of selected parent ions can be initiated in a number of ways. The most commonly report method is via collision with a neutral gas (such as nitrogen) in the collision cell. This is termed collision-induced dissociation (CID) and has been widely reported for lipid analytes [19, 34, 130, 143-145]. CID is the method which is available on the quadrupole time-of flight instrument used to acquire data presented in this thesis and is therefore the main focus of structural characterisation work.

Although CID is the only dissociation method available on the Q-TOF instrument, there is instrumentation available that can perform CID at comparatively higher energies, referred to as high energy-CID or HE-CID. Other available dissociation methods such as electron-mediated methods (electron transfer or capture dissociation (ETD or ECD)), infrared multiphoton dissociation (IRMPD), ultraviolet photo dissociation (UVPD), ozone- induced dissociation (OzID) and post-source decay (PSD), have all been reported in the structural analysis of lipids in recent years [146-150]. In order to perform electron-mediated dissociation, multiply charged species are preferable as this technique only works well for higher charge state ions (≥2), hence this is not commonly reported for ions formed by MALDI as these are usually only singly charged. Conversely, PSD is specific to ions generated via MALDI. Both PSD and OzID have been reported for lipid ions generated by MALDI.

PSD generates similar product ions to those described in CID studies [150, 151], however OzID has been shown to provide increased structural information with respect to double bond positioning in fatty acid side chains [152]. However, to date, few dissociation studies compare a range of different techniques for structural elucidation of lipid analytes. Yet, it has been suggested that the consideration of varied dissociation techniques can provide complimentary data. For example, Liang *et al*. report that ETD of doubly sodiated lipids generates similar product ions to CID in different relative abundances; hence a combination of techniques provided highly abundant productions which can together enhance structural elucidation [148].

Dissociation studies can enable the analyst to determine not only which lipid adduct is detected (protonated, potassium or sodium adduct), but also the components which make up larger lipids, such as phospholipids. In these molecules, the identity of the phosphate head-group in addition to each fatty acid side-chain is required in order to allow complete structural identification of detected lipid species. Once the lipid adduct is detected and phosphate head-group is known, a general formula can be used to describe the species detected. For example, a phosphocholine lipid is denoted as a PC species. The combined numbers of carbon atoms which comprise the two fatty acid side-chains are then described followed by the total number of double bonds in those fatty acid side-chains. Determination of the identity of each fatty acid and their relative positions along the glycerol backbone is also desirable. Figure 11 provides a schematic of a PC phospholipid and the side-chain annotations.
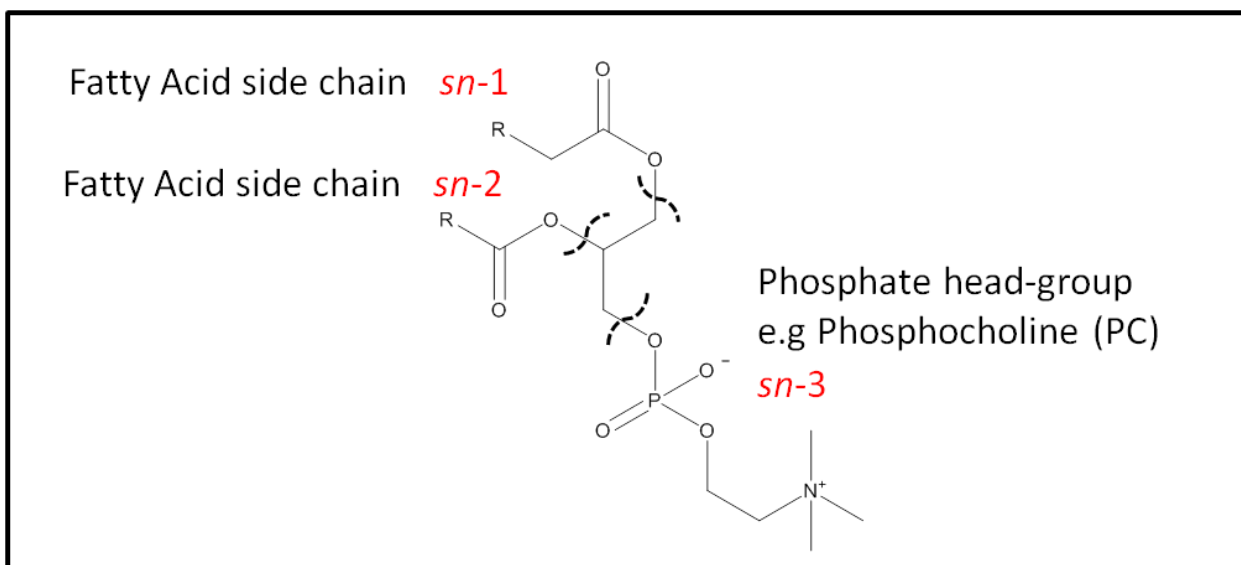
Figure 11 Phosphocholine (PC) lipid structure indicating the three substituents esterified along the glycerol backbone. Two fatty acids are esterified in the *sn*-1 and *sn*-2 positions and the PC head-group is denoted in the *sn*-3 position along the glycerol backbone, according to a stereochemical numbering system.

The phosphate head-group is denoted in the *sn*-3 position along the glycerol backbone, with the two fatty acid acid side chains denoted in *sn*-1 and *sn*-2 positions. In shorthand nomenclature these lipids are described first using the head-group annotation shown in Table 4, section 1.2 of this thesis, PC for phosphcholine in this example, and then second by describing the number of carbons in the fatty acyl chains followed by the number of double bonds. If the identities of each fatty acid are unknown a general formula is used to describe the lipid, for example PC 34:1. If the identities of each fatty acid are known then they are described, for example PC (16:0, 18:1). The order in which the fatty acids are described is *sn*-2 then *sn*-1 after the head-group annotation.

The identities of the substituents along the glycerol back bone can be determined either by detection of a particular *m/z* or by a characteristic neutral loss. For example, the detection of acyl ions of fatty acid substituents ($RC^+=O$) or the detection of a peak at *m/z* 184 indicating the protonated PC head-group provide structural information. In addition, characteristic neutral losses such as that of the intact fatty acid side-chain (RCOOH) or the neutral loss of the zwitterionic head-group (183 u) also aid structural elucidation. As lipids form a variety of different adducts (protonated and cationic), it is important to consider whether the number and types of product ions detected upon dissociation of each adduct provides useful structural information. This issue will be discussed throughout this thesis. Salt additives will be considered in order to assess whether the formation of non-natural cationic lipid adducts can be advantageous in dissociation experiments.

1.4.3.1 Collision-induced Dissociation in the Q-TOF

In order perform MS/MS analysis in this instrument, Q_1 acts as an ion filter in RF/DC mode, only allowing a selected *m/z* through to the collision cell q_2. For further details of the working of the quadrupole mass analyser in this type of experiment refer to chapter 1.1.7.1.1. Prior to introduction to the collision cell, the selected ions, described as parent ions, are accelerated by a potential voltage up to 100 eV. In the collision cell parent ions undergo fragmentation caused by collision with a neutral gas, which is nitrogen in this instrument. Ions are subsequently detected in the TOF analyser. A schematic is provided in Figure 12.

| Parent ion Selection in First Mass Analyser | Dissociation of Selected *m/z* in Collision Chamber | Detection of Product Ions in Second Mass Analyser |

Q_1 Q_2 ToF
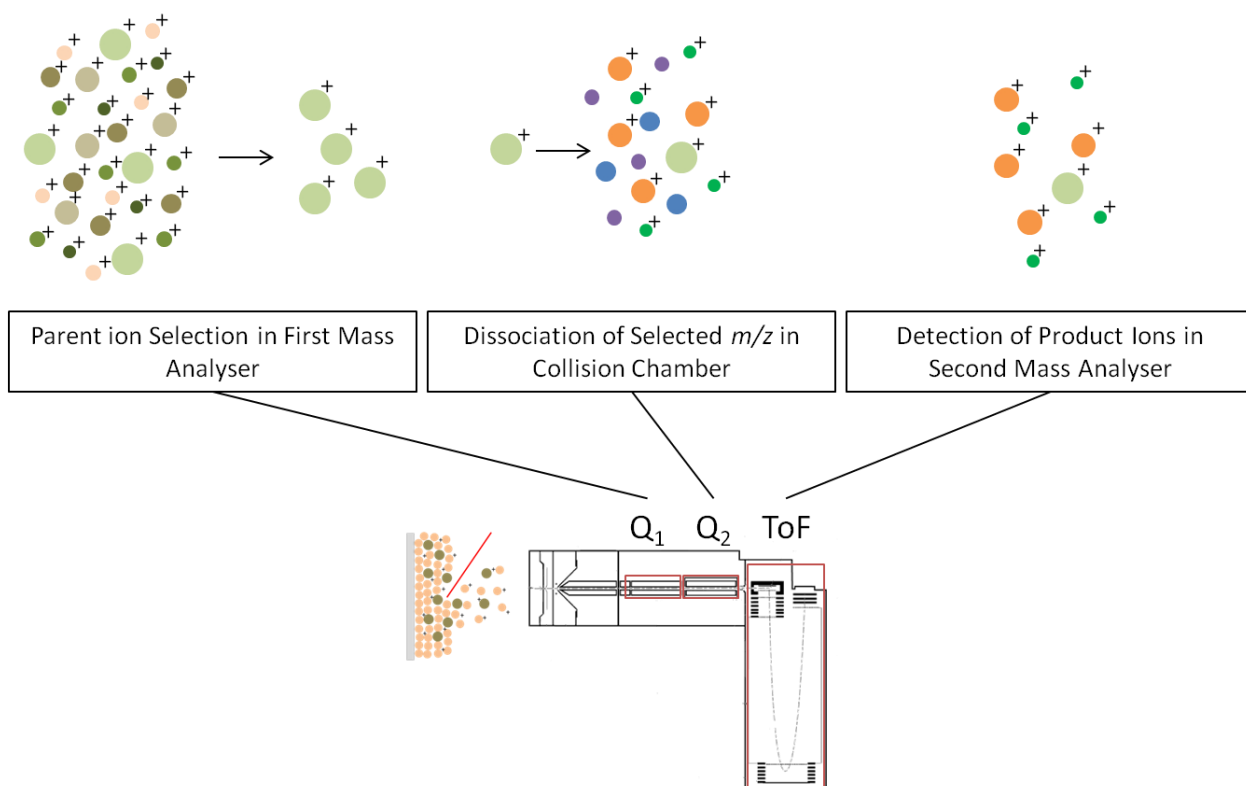
Figure 12 Diagrammatic scheme of a parent ion collision-induced dissociation (CID) experiment performed on a Q-TOF mass spectrometer. A chosen *m/z* is selectively transmitted through the quadrupole mass analyser (Q_1) and then dissociated in a collision chamber (Q_2) by bombarding with a neutral gas. Conditions are optimised with the aim of initiating bond breakages at structurally informative sites. Product (fragment) ions are detected in the time of flight (TOF) mass analyser.

1.4.3.2 Collision-induced Dissociation in the Orbitrap Mass Analyser

As shown in Figure 13, the use of this mass analyser also provides the user with the opportunity to consider various dissociation techniques. A comparison of CID, HE-CID and ETD techniques for the analysis of lipid species will be considered in chapter 6 of this thesis.

In this instrument parent ions for CID are mass selected by a quadrupole in-between the C-trap (ion trap) and the collision cell. An ion trap is based on similar principles to a quadrupole, however a ring electrode is surrounded by electrodes from above and below, hence the ions inside experience applied potentials in three dimensions. As a result only a particular range of ions are stable within the trap. This limits detection inn CID experiments to ions with approximately one third of the m/z of the parent ion or higher.

1.1.4.2 High Energy- Collision-induced Dissociation (HE-CID) in a quadrupole

As described earlier for the Q-TOF instrument, the quadrupole is in RF only mode in order to transmit ions across a mass range after collision with a neutral gas (nitrogen) before detection in the orbitrap mass analyser. The difference between CID and HE-CID is the relative voltages experienced by parent ions in the collision cell. In HE-CID, parent ions experience a field of the order of several keV, hence these ions and the subsequent product ions formed have much greater kinetic energies when compared to CID, which operates between 1 and 100 eV.

CID   HE-CID   ETD

quadrupole Ion Guide   Octopole   High pressure cell   Low pressure cell   quadrupole Mass Filter   C-trap   quadrupole Collision Cell   Transfer Multipole   Reagent Ion Source

Ions

ETD Reagent Gas

Orbitrap mass analyser
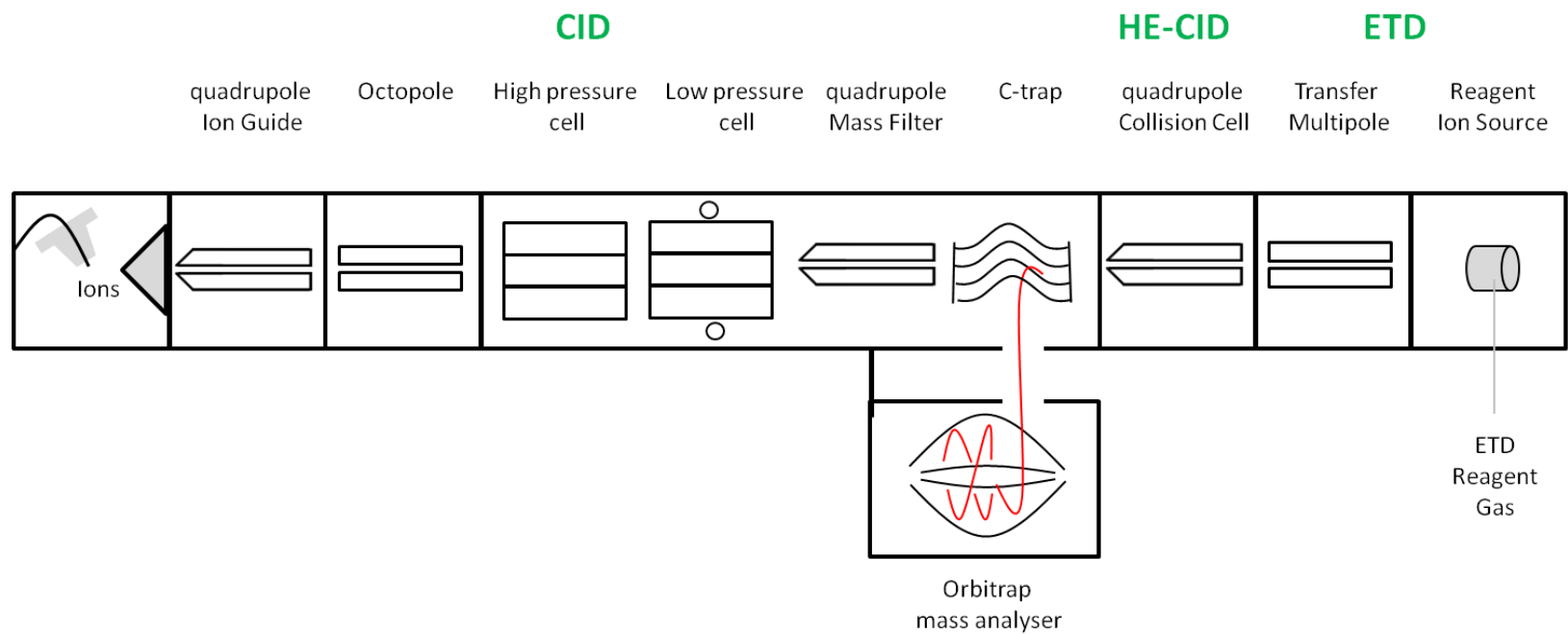
Figure 13 Schematic of the orbitrap instrumentation used to acquire ESI and LESA-ESI mass spectrometry data in this thesis.

A few recent lipid dissociation studies by HE-CID have suggested that increased structural information can be obtained in comparison to (lower energy) CID. Harvey *et al*. showed that the determination of double bond positioning was possible by performing HE-CID studies of fatty acid related species, proposing a charge associated mechanism[153]. Shimma *et al*. report similar data for phospholipids detected directly *in situ* [154]. Clearly consideration of this dissociation technique, alongside dissociation data, could provide enhanced structural information when compared to CID alone.

1.4.3.4 Electron-transfer Dissociation in a quadrupole

Electron-mediated dissociation techniques are a relatively recent development. Zubarev *et al*. introduced electron-capture dissociation, which involves bombardment of positive ions with low energy electrons [155, 156]. It is thought that charge state reduction leads to the formation of a radical positive ion which then dissociates. However this method is not compatible with ion trap based mass analyser, owing to practicalities concerning the strong electric field used in trapping instruments. Hence electron-transfer dissociation was introduced by Syka *et al*. [157]. This was first described for a Finnigan LTQ mass spectrometer [157] but has since been described for orbitrap instrumentation [158]. Electron transfer from a singly charged anthracene anion, generated in the reagent ion source indicated in **Figure 13**, occurs in order to achieve dissociative results analogous with ECD.

Initial studies have focussed on the analysis of multiply charged protein and peptide analytes, yielding greater structural information when performed alongside CID [157]. However, some recent ECD and ETD studies of lipid species have shown some promising results. For example, James *et al*. report that product ions indicative of fatty acyl chain identities are detected upon ECD of divalent metal-phospholipid complexes [146]. Furthermore, Liang *et al*. describe the detection of structurally informative product ions which enabled assignment of *sn*-1, *sn*-2 and *sn*-3 side-chains of phospholipid species upon ETD of doubly sodiated lipid species [148].

1.5   Lipids

1.5.1 Lipidomics

Mass spectrometry analysis offers the opportunity to consider a wide range of different molecules in a single analysis. Hence the introduction of MALDI and electrospray (ESI) ionisation techniques enables consideration of a range of different analytes of a particular molecule type (such as proteins, drugs or lipids) in a single analysis. The study of proteins to better understand their structure and functions in biological systems, defined as proteomics, is one of the most widely studied areas in MALDI. However, with improving understanding of biological functions, the need to explore the roles of other fundamental, smaller, biological species such as nucleotides, amino acids and lipids, is becoming increasingly important. Research in this thesis will concentrate on the analysis of lipid species.

Lipids are important biological molecules involved in a range of biological processes. Lipids classify a range of different molecules and many types of lipid species have been shown to have biological relevance. For example, phospholipids are major components of cell membranes and are involved in cell signalling. It follows that changes in the metabolism of various lipid classes have been implicated in a variety of diseases. Changes in the natural presence of lipid species have been implicated in a range of diseases, for example Alzheimer's disease [106, 159-161], liver diseases [162, 163] and a

range of cancers [47, 164-166]. Many of these diseases affect large numbers of the population; hence the importance of lipid research (lipidomics [167]).

There are a great number and variety of lipids which can vary quite significantly in their structure and chemical properties; it follows that lipid species can differ considerably in their biological functions. Owing to these varied properties, a number of classification systems have been developed. Different systems classify lipids by different characteristics, such as polarity, solubility or degree of saturation. For simplicity the Fahy classification system will be adopted throughout this thesis [168, 169]. The Fahy system separates lipids into eight main categories of lipids based (chemically) on structure: fatty acyls (FA), glycerolipids (GL), glycerophospholipids (GP), sphingolipids (SP), saccharolipids (SL), sterol lipids (ST), prenol lipids (PR) and polyketides (PK). The basic structure of each lipid class is indicated in Figure 14. Sterol lipids, prenol lipids and polyketides are not included as they do not have a common generic structure. Sterol and prenol lipids are linked by way of their biosynthetic pathway, however they do not express structural similarities. Polyketides are an assorted group of molecules sourced from plants and microbacteria. There are a wide range of different sub-groups associated with each of these main categories. A summary of lipids discussed in this thesis, alongside shorthand notations, is provided in Table 4.
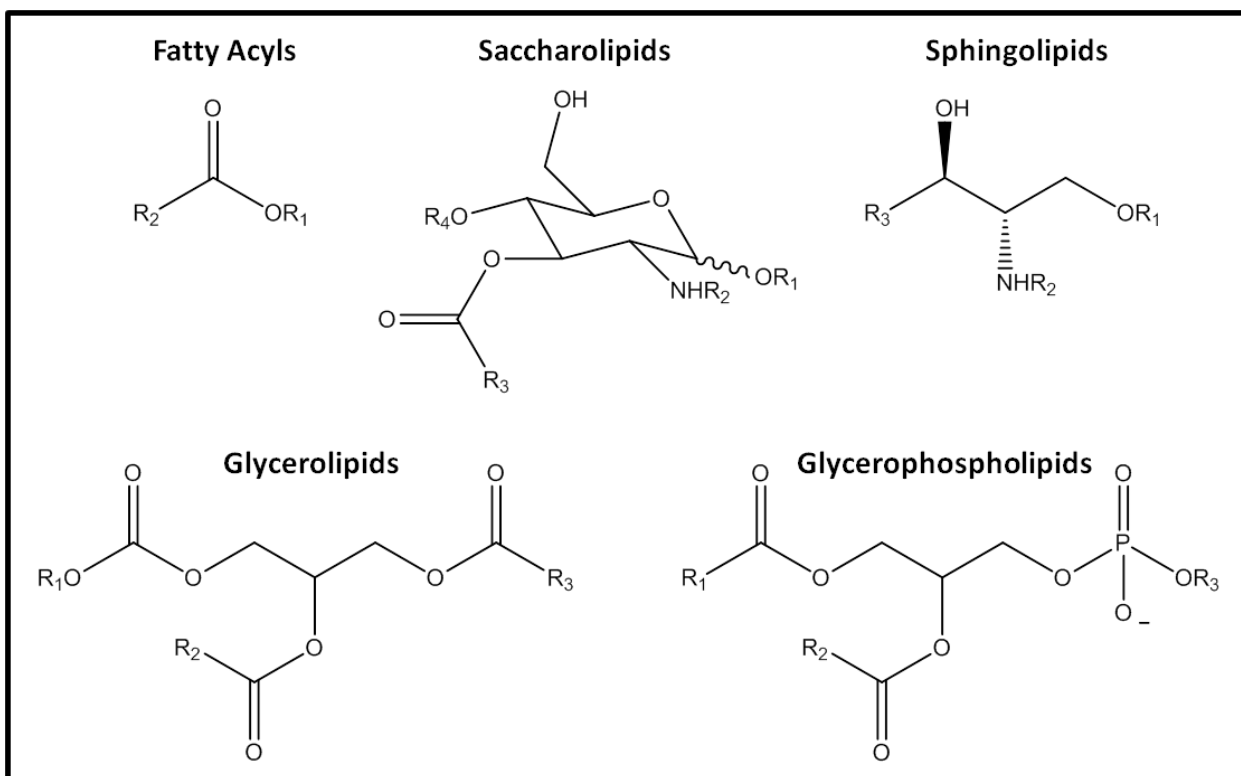
Figure 14 General chemical structure of lipid species according to their lipid classification.

Lipid Class and Sub-Classes	Abbreviation	Lipid Class and Sub-Classes	Abbreviation
Glycerophospholipids GP		**Fatty Acyls FA**	
Phosphocholines	PC	Fatty Acids and Conjugates	
Phosphoethanolamines	PE	Octadecanoids	
Phosphoserines	PS	Eicosanoids	
Phosphoglycerols	PG	Docosanoids	
Phosphoglycerolphosphates	PGP	Fatty Alcohols	
Phosphoinositols	PI	Fatty Aldehydes	
Phosphoinositol monophosphate	PIP	Fatty Esters	
Phosphoinositol biphosphate	PIP2	Fatty Amides	
Phosphoinositol triphosphate	PIP3	Fatty Nitriles	
Phosphates (Phosphatidic Acid)	PA	Fatty Ethers	
Pyrophosphates	PPA	Hydrocarbons	
Phosphoglycerophosphoglycerols (Cardiolopins)	CL	Oxygenated Hydrocarbons Other	
Sphingolipids SP		**Glycerolipids GL**	
Sphingoid bases		Monorady glycerols	MG
Ceramides	Cer	Diradyl glycerols	DG
Phosphosphingolipids	SM	Trirady glycerols	TG
Neutral glycosphingolipids	[glycan]-Cer	Other	
Acidic glycosphingolipids			
Basic glycosphingolipids			
Amphoteric glycosphingolipids			
Arsenoshingolipids			
Other			

Table 4 A summary of lipid species which will be discussed in this thesis in terms of their classification and sub-classification, according to the Fahy system, and their abbreviations.

Mass spectrometric studies of diseased tissues samples have considered lipid species from a range of these main categories and their sub-groups. Fatty acids can be metabolised in biosystems to form part of larger lipid species. For example, a fatty acid may be esterified onto the glycerol backbone of a glycerophospholipid. Hence changes in lipid compositions and distributions can be implied by both smaller and larger lipid structures belonging to different lipid categories. Fatty acids are described by shorthand notation, first describing the total number of carbon atoms in the chain and then describing the total number of double bonds, separated by a semi colon. Examples of this shorthand notation are shown in Table 5. Reference to both the systematic (according to chain length and the presence of double bonds) and the corresponding trivial name often described in literature reports is also provided.

It is worth noting that a number of fatty acids which have the same mass are present in various isomeric forms. For example, oleic and elaidic acids each have one double bond between carbon 9 and 10, however the double bond in oleic acid has the (z)-configuration and that in elaidic acid the (E)- configuration. In addition, a number of fatty acids can have the same number of carbon atoms and double bonds in the chain, yet these may be positioned between different carbons in the chain, hence they are different fatty acids. In Table 5 three fatty acids are listed with 20 carbon atoms and 3 double bonds; however the double bonds are positioned differently along the carbon chain in each one. This further highlights the complicated nature of lipid species and the importance of developing methods for their structural characterisation.

Systematic Fatty Acid Name	Trivial Name	Number of Carbons	Number of Double Bonds	Shorthand
Tetradecanoic Acid	Myristic Acid	14	0	14:0
Hexadecanoic Acid	Palmitic Acid	16	0	16:0
c-9-Hexadecanoic Acid	Palmitoleic Acid	16	1	16:1
Octadecanoic Acid	Stearic Acid	18	0	18:0
c-9-Octadecenoic Acid	Oleic Acid	18	1	18:1
t-9-Octadecenoic Acid	Elaidic Acid	18	1	18:1
c-9,12-Octadecadienoic	Linoleic Acid	18	2	18:2
Eiocosanoic Acid	Arachidic Acid	20	0	20:0
c-9- Eiocosenoic Acid	Gadoleic Acid	20	1	20:1
c-11,14- Eiocosadienoic Acid	Dihomolinoleic Acid	20	2	20:2
c-11,14,17- Eiocosatrienoic Acid	Dihomolinolenic Acid	20	3	20:3
c-8,11,14- Eiocosatrienoic Acid	Dihomogammalinolenic Acid	20	3	20:3
c-5,8,11- Eiocosatrienoic Acid	Mead Acid	20	3	20:3
c-5,8,11.14- Eiocosatetranoic Acid	Arachidonic Acid	20	4	20:4
c-5,8,11,14,17- Eiocosapentanoic Acid	Eiocosapentanoic Acid	20	5	20:5
Docosanoic Acid	Behenic Acid	22	0	22:0
c-13- Docosenoic Acid	Erucic Acid	22	1	22:1

Table 5 Examples of fatty acid systematic and trivial names with standard nomenclature.

1.5.2 Implication of lipids in Disease

A variety of different lipid species have been implicated in Alzheimer's disease. A number of recent reviews detail the role of the free fatty acid docosahexanoic acid and sphingolipids in Alzheimer's disease [159-161, 170]. Changes in the abundances of cholesterol and oxidised lipids have been shown to be potential biomarkers of multiple sclerosis [171]. Changes in the ratio of two free fatty acids, arachidonic acid and α-linolenic acid, have been observed in sufferers of coronary artery disease [172]. Furthermore, increased concentrations of oxidized lipids have been detected in patients suffering from non-alcoholic steatohepatitis liver disease[163] and decreases in the ratio of phosphatidylcholine to phosphatidylethanolamine lipids have been reported in non-alcoholic fatty liver disease [162]. Finally, changes in lipid abundances and spatial distributions have been indicated in a number of different cancers [50, 164, 166, 173-176].

It is clear from these selected examples that changes in both the relative abundance and spatial distribution of a wide range of lipid species can be informative of a particular disease. Therefore it is important to develop a detailed knowledge of normal lipid abundances and spatial localisations of lipid analytes in tissue and an understanding of lipid metabolism in biological systems. For this reason there has been increasing interest in the study of lipids in recent years.

Mass spectrometry is of particular interest when performing analytical studies owing to the ability to detect a large number of analytes in a single experiment with minimal sample preparation. A number of reports demonstrate that there is interest in both rapid profiling of lipid extract samples and direct surface sampling of thin tissue sections by ionisation techniques such as MALDI [47, 176, 177] and ESI [163, 178]. An increasing number of reports also consider the use of mass spectrometry imaging techniques, which combine compositional information similar to that obtained from analysing lipid extract samples with spatial information.

Analysis of lipids by MALDI has been a topic of much recent interest and the technique has been used to identify lipid biomarkers in diseases such as Fabry disease [179], Tay Sachs/Sandhoff disease [65] and cancers [49, 50]. Both the relative abundances and localisation of lipid species have been implicated in these diseases, hence understanding the normal presence and distribution of lipids in biological samples is key to understanding these diseases and development of appropriate treatments. With opportunities for analysis of complex, unseparated lipid mixtures and direct analysis of thin tissue sections, MALDI imaging is an attractive method for profiling lipids in healthy and diseased tissue.

1.6 Aims and Objectives

MALDI-MS and MS imaging have widespread applications in the analysis of biological molecules. Lipids are important biological species, the analysis of which is complicated by the fact that they form various different adducts in the MALDI experiment. Routes to improving the analysis of lipids by MALDI-MS can be addressed at the sample preparation stage by doping the MALDI matrix solution with an additive in order to promote the formation of a particular adduct. This strategy can lead to decreased spectral complexity and improved sensitivity for a given lipid analyte.

Salt additive selection in matrix doping experiments for the analysis of a complex lipid extract sample will be discussed in detail in Chapter 2. Improved sensitivity and reduced spectral complexity afforded by the inclusion of a particular salt additive will be reviewed. Furthermore, as it is important to structurally characterise lipid analytes when considering lipids as disease biomarkers, collision-induced dissociation of the various lipid adducts formed will be considered. The inclusion of salt additives in MS/MS experiments will be explored in order to determine which lipid adduct(s) provides the most informative structural information in dissociation studies.

The incorporation of salt additives into tissue samples will be discussed in Chapters 3 and 4 as a route to improve *in situ* analysis and imaging of thin tissue sections. The inclusion of salt additives in matrix solutions or powders prior to matrix application will be described in Chapter 3. Formal fixation as a route to additive incorporation, leading

to the formation of highly abundant lipid adducts which provide useful structural information will be presented in Chapter 4.

Direct surface sampling of fixed tissue samples by a relatively new technique, liquid-extraction surface-analysis (LESA) for electrospray ionisation (ESI), will be considered in Chapter 5. This will be coupled to a type of trap mass analyser (orbitrap) which has high mass-resolving power. Structural information that can be obtained from lipid analytes using high-energy collision-induced dissociation and electron transfer dissociation techniques will be assessed in Chapter 6.

2. Investigations into the use of salt additives in MALDI-MS analysis of lipids

2.1 Introduction

The inclusion of additives to MALDI matrices has been investigated by a number of groups for the analysis of a range of analytes. Addition of these additives aims to favour a particular adduct, reduce the relative abundance of another adduct or act as a cationising agent [19] in MALDI-MS experiments. Salt additives have been included in the matrix solution [19], used in matrix washing procedures [132] and have also been used as tissue washing solutions [180] prior to MALDI-MS analysis.

Various salts have been considered for lipid analysis including ammonium acetate [181], ammonium citrate [19, 182] and diammonium hydrogen citrate [150, 181], sodium acetate [19, 150, 182-184], potassium acetate[72, 135], potassium chloride[182, 184], lithium acetate [19, 135, 145, 150] , lithium chloride [77, 143, 145], lithium citrate [145], lithium iodide [145] and lithium trifluoroacetate [145], caesium chloride [131-133, 185-187] and silver nitrate [27] but few studies compare a selection. Furthermore, the concentrations of additives reported are varied.

Several infrequently reported additives have also been shown to improve lipid analysis: such as urea [181], guanadinium chloride [181], calcium chloride [188] and

ethylenediaminetetraacetic acid ammonium salt [189], indicating that a trial of wider additive selections would be beneficial. External cationic sources such as lithium and caesium (sodium and potassium are present in the matrices themselves) might be advantageous as they could be utilised as internal standards in tissue investigations. It is also suggested that the lithium isotope pattern could be useful in adduct confirmation of complex mixtures [19]. Caesium in particular could be incredibly useful as caesium adducts form outside of the usual lipid *m/z* window of interest, again simplifying adduct confirmation and overcoming the problem of overlapping peaks of different adducts [187].

A range of other additives have been used in the analysis of other analytes by MALDI. For example, ammonium acetate [190], ammonium citrate [190, 191] and ammonium phosphate [191, 192], diammonium citrate [190] and phosphoric acid [193] have all been used in phosphopetide and/or protein analysis to promote protonation. Lithium and caesium chlorides have been reported to show different selectivity's for a range of polyethers [194]. In addition, silver nitrate has been employed as a cationsing agent in the analysis of non-polar polymers such as polyisoprene, polystyrene, and polybutadiene, extending the detection range to a distribution of up to 6 000 u [195]. Furthermore, tetraamine spermine [196] and polyamine [197] have been reported to improve oligonucleotide analysis, simplifying spectra by eliminating cation adduction or acting as a proton sink respectively. Finally, zinc sulfate heptahydrate [198] was

reported to simplify spectra by enhancing the detection of protonated adducts, in the analysis of peptide toxins in cyanobacteria.

Comparison of the additive cation with various counteranions in positive ion mode experiments allows systematic evaluation of additive selection. A number of studies have considered groups of additives in this way. A range of lithium salts were investigated by Cerruti *et al.* for lipid analysis in tissue imaging[145]. A range of chlorides (lithium, potassium, caesium and rubidium) were investigated in the detection of aspirin [199]. In addition, a large study was conducted by Choi *et al.* in the analysis of carbohydrates [200]. Lithium, sodium, potassium and caesium were investigated as cationising agents in a number of salt forms: trifluoroacetates, hydroxides and chlorides. Various forms of silver salts have been investigated for the analysis of polybutadiene [201]. Several counteranions have been considered in negative ion mode analysis of oligonucleotides [202].

Furthermore, cation selection has been shown to have a profound effect on the relative number of different product ions in CID studies [19, 150, 203]. Lithium lipid adducts have been reported to provide the most useful product ions with respect to structural characterisation [19, 143, 150]. However dissociation studies of caesium lipid adducts (of the form $[M+Cs]^+$) have not been reported. Here a comprehensive investigation into the structural information afforded by CID of various adducts of a PC lipid standard is presented, extending the range of investigated cations.

The aim of this research was to evaluate the use of various salt additives in various anionic and cationic forms, over a wide concentration range, for MALDI-MS analysis of lipids for a variety of applications: promotion of a particular adduct, improving sensitivity and reducing spectral complexity. A wide range of additives were considered, some of which have previously been considered for lipid analysis, others have been employed in the analysis of other analytes and some, such as nitrates, completely novel. In this study ammonium, sodium and potassium cations were investigated in a variety of salt forms; acetates, chlorides and nitrates. Lithium and caesium salts were also considered in order to evaluate the use of non-endogenous cations.

2.2 Experimental

2.2.1 Materials

All salts (NH$_4$Cl, NH$_4$CH$_3$CO$_2$, NaCH$_3$CO$_2$, NaCl, NaNO$_3$, KCH$_3$CO$_2$, KCl, KNO$_3$, LiCl, LiNO$_3$, CsCl), trifluoroacetic acid (TFA, 99% purity) and matrices (α-cyano-4-hydroxycinnamic acid (CHCA), 2,5-dihydroxybenzoic acid (DHB), and 2,4,6-trihydroxyacetophenone (THAP)) were purchased from Sigma-Aldrich (Gillingham, Dorset, UK). Lipid standard 1-palmitoyl-2-oleyl-*sn*-glycero-3-phosphocholine PC (16:0/18:1) was purchased from Avanti Polar Lipids Inc. (Delfzyl, The Netherlands). The water used was purified by an ELGA Option 3 system (Marlow, UK). Rat brain samples were supplied by AstraZeneca (Alderley Park, UK) and stored at -80 °C.

2.2.2 Sample Preparation

2.2.2.1 Lipid Extraction

Lipids were extracted from thawed rat brain according to a modified version of the Folch method[204]: 2 g of rat brain tissue was extracted with 50 mL of 2:1 CHCl$_3$: CH$_3$OH. No salts were added to the aqueous phase during the tissue washing stage. The mixture was allowed to separate whilst standing.

2.2.2.2 Spotting of Lipid Extract Samples for MALDI-MS experiments

Matrices were prepared at 10 mg mL^{-1} for matrix optimisation experiments. All matrix additives (NH$_4$CH$_3$CO$_2$, NH$_4$Cl, NaCH$_3$CO$_2$, NaCl, NaNO$_3$, KCH$_3$CO$_2$, KCl, KNO$_3$, LiCl,

LiNO$_3$, and CsCl) were prepared in 80% CH$_3$OH/20% H$_2$O. DHB at 10 mg mL^{-1} (80% MeOH/20% H$_2$O/0.1% TFA) was prepared incorporating 0, 5, 10, 20, 40, 80 mM of additive. All MALDI-MS samples were spotted as separate overlayers[60] on a stainless steel MALDI target (AB SCIEX, Frammingham, USA) 0.25 μL of lipid extract followed by 0.5 μL matrix allowing approximately 2 minutes drying time between applications.[205, 206] Eight replicate spots of each sample were prepared for MS experiments.

2.2.2.3 MALDI-MS/MS analysis of PC (18:1, 16:0)

Samples prepared with – 0 or 5 mM (LiCl, or CsCl) were used for *MS/MS* analysis. All samples were spotted as overlayers. 0.5 μl of 1 mg ml^{-1} PC (16:0/18:1) followed by 0.5 μL of 10 mg mL^{-1} DHB matrix (with or without additive), with time allowed for drying between applications. Five replicate spots of each sample were prepared.

2.2.3 Mass Spectrometry

A hybrid quadrupole time of flight (Q-TOF) mass spectrometer (Qstar XL, AB Sciex, Frammingham, USA) equipped with an orthogonal MALDI ion source was used to acquire MALDI-MS and MS/MS data. A pulsed N$_2$ laser (337 nm, operated at 20 Hz) delivered through a 200 μm fibre delivering 30 % of the available power was controlled by Analyst 1.1 software (Applied Biosystems). All data were acquired in positive ion mode. Spot samples were interrogated using a circular laser pattern, summing 15 scans per spectrum and ablating most material within the well. Ion transmission was

optimised and a focusing potential (FP) of 60 V and a declustering potential (DP2) of 20 V were used in all experiments. For *MS/MS* experiments the number of scans summed was increased from 15 to 60. Nitrogen was used as a collision gas. The collision energy used was optimised in the range 10-100 eV.

2.2.4 In-source Photographs of Matrix-Additive Crystals

DHB matrix prepared with or without the inclusion of 5 mM additive 80% CH_3OH (with 0.1% TFA). The lipid standard solution was prepared in $CHCl_3$. 0.5µL of the lipid standard solution was spotted onto a stainless steel MALDI target plate (Waters Ltd, Elstree, UK), followed by 0.5µL of the matrix solution with time allowed for drying between applications. A MALDI-TOF (Time of Flight) instrument (MALDI micro MX, Waters) equipped with a pulsed N_2 laser (337 nm, operated at 10 Hz) and a 1.24 m flight path, was controlled by Mass Lynx 4.1 software (Waters Ltd, Elstree, UK) and used to obtain screen shots showing crystal morphology.

2.3 Results and Discussion

2.3.1 Matrix System Optimisation

Initial investigations evaluated which matrix compound (CHCA, DHB or THAP) was optimal for the analysis of a complex lipid extract. DHB is the most commonly reported matrix for lipid analysis[65]. More recently 2,4,6-trihydroxyacetophenone (THAP) [19] has been shown to be a viable alternative for lipid analysis, hence it was included in this evaluation. Both were compared to CHCA which is also widely reported. All were evaluated with the addition of 0.1% trifluoroacetic acid (TFA)[65], which has been shown to enhance the signal to noise ratio in the mass spectra obtained [207] and enhance cationisation [132]. These properties can be attributed to the strong ion pairing ability of TFA [208].

A representative MALDI mass spectrum acquired when the complex biological lipid extract sample was analysed with CHCA matrix is shown in Figure 15. The most abundant ion in the spectrum is *m/z* 184 which is characteristic of the phosphocholine head-group of PC lipid species. Lower abundances of phospholipid head-group fragment ions were detected in the region *m/z* 50-300; *m/z* 86, 104, 125 and 146, shown in Table 6 below, have all been previously reported [135]. Other peaks in this region relate to CHCA matrix ions: *m/z* 190 [M+H]$^+$, 212 [M+Na]$^+$ and 228 [M+K]$^+$.
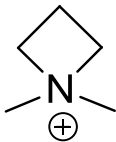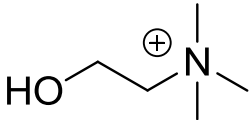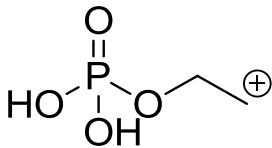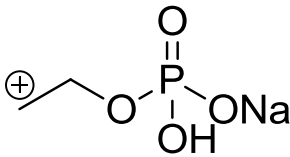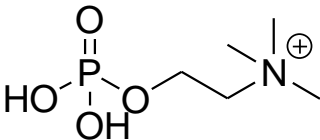
m/z	Fragment Identity
86	
104	
125	
146	
184	

Table 6 Common phospholipid head-group fragments detected in MALDI analysis

Intact lipid ions in the highlighted region between *m/z* 700-900 of phosphatidylcholine lipids such as PC 34:1, PC 32:0 and PC 36:1 were detected in relatively low abundance in comparison to other peaks in the spectrum. Further lipid fragment ions were detected in the region *m/z* 400-600; these ions can be attributed to neutral losses of the PC head-group and the fatty acid side-chains as they are similar to those detected in CID experiments described in this chapter and in further detail in chapter 4 of this thesis.

Fragment ions in MALDI-MS experiments have previously been described to be similar to those detected in PSD and low-energy CID experiments [209]. Stubiger *et al.* also found that the use of CHCA matrix in lipid investigations led to extensive fragmentation during ionisation [19]. This is probably owing to the fact that CHCA is a hot matrix [93] for lipid analytes, typically producing analyte ions with greater internal energies compared to those generated using other matrix compounds [76]. Protonated lipid adducts $[M+H]^+$ were detected in highest abundance when CHCA matrix was used. This is perhaps unsurprising owing to the fact that it is a carboxylic acid and is thus likely to promote protonation of analyte species.

When THAP matrix was used to analyse this lipid sample the most abundant ion in the spectrum was *m/z* 169 which is the protonated adduct $[M+H]^+$ of THAP matrix. Other matrix peaks $[M+Na]^+$ and $[M+K]^+$ at *m/z* 191 and 207, respectively, were detected in much lower abundance. Lipid fragment ions were also detected in lower abundances when compared to using the CHCA matrix. This is probably owing to the fact that THAP is a cool matrix for lipid analytes. In addition, ion counts of detected lipid species increased when the THAP matrix was used. High abundances of both protonated $[M+H]^+$ and cationic lipid adducts ($[M+Na]^+$ and $[M+K]^+$) were detected, probably owing to the fact that THAP is a neutral compound, and therefore does not promote protonation to the same extent as CHCA, for example. As fewer lipid fragments and higher abundances of intact lipid species were detected when THAP was used for lipid analysis it was deemed more suitable than CHCA.
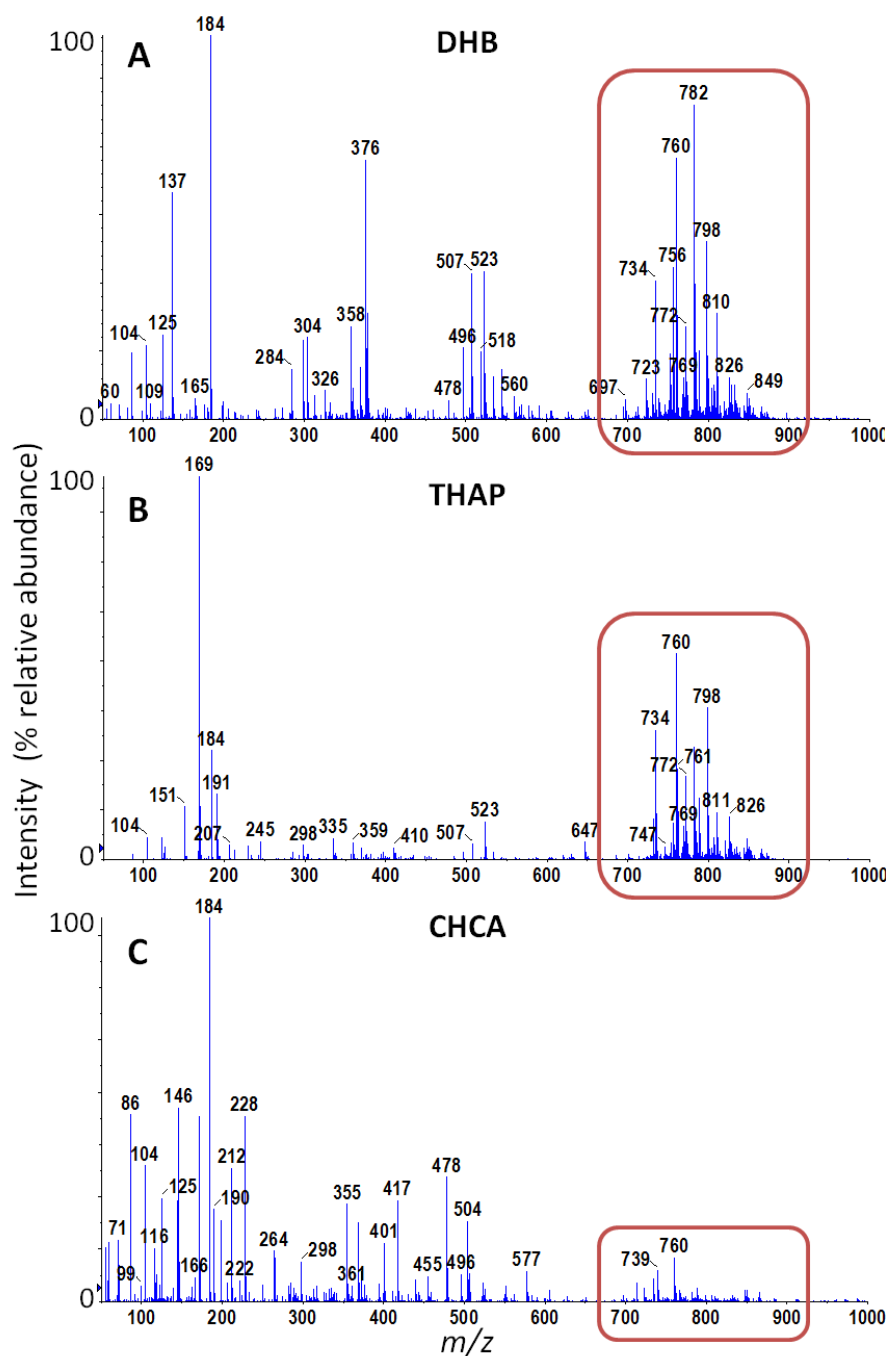
Figure 15 Representative MALDI-MS spectra of rat brain lipid extract sample prepared with DHB (top), THAP (middle) or CHCA (bottom) matrix. The phospholipid region *m/z* 700-900 is highlighted. Highest ion counts of lipid species were detected when DHB matrix was used.

The most abundant ion detected when DHB matrix is used to analyse the lipid extract sample was at m/z 184, indicating the PC head-group of lipid species. Matrix ions were not detected in significantly high abundance, except for $[M+H-H_2O]^+$ at m/z 137. Significantly higher ion count, double or triple that of other matrices, of intact phospholipid species were detected in the region m/z 700-900 when DHB matrix was used compared to THAP and CHCA matrices, as illustrated in Figure 15. Furthermore, cationic lipid adducts were detected in relatively high abundance; sodium lipid adducts $[M+Na]^+$ were the most abundant detected of a range of lipid species as demonstrated in Figure 16.
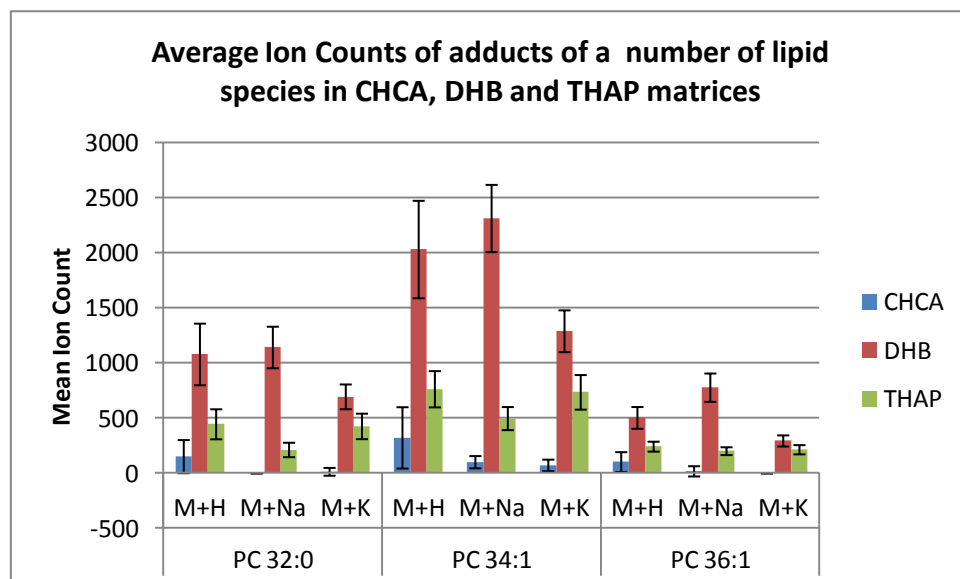
Figure 16 Mean ion counts of $[M+H]^+$, $[M+Na]^+$ and $[M+K]^+$ adducts of 3 abundant phospholipids (PC 32:0, PC 34:1 and PC 36:1) detected when rat brain lipid extract is analysed with CHCA, DHB and THAP matrices. Error bars indicate one standard deviation above and below the mean.

It is perhaps surprising that similar abundances of protonated and cationic adducts are not detected as DHB is an acidic molecule and therefore it might be expected that use of this matrix would promote protonation. Even though protonated adducts were also detected in high abundance, the use of DHB matrix appeared to lead to the detection of a range of lipid adducts, all in relatively high abundance. DHB and THAP matrices have similar gas-phase basicities for both sodium and potassium [89]. Gas-phase basicity is related to cation affinity and theoretical calculations have shown that their sodium binding energies differ by just 4 kJ mol^{-1} [96]. Low cation affinities and gas-phase basicities, shown in Table 7, of DHB and THAP matrix compounds could account for the increased abundances of cationic lipid adducts detected when these are used for lipid analysis, in comparison to CHCA. Overall DHB matrix was deemed a suitable candidate for additive studies.

Although lipid fragment ions were detected in the region m/z 400-600, their abundance was relatively low in comparison to when CHCA matrix was used. Knochenmuss and Zenobi's investigations of in-plume processes suggest that the internal energy of analytes in the MALDI plume is dependent on the exothermicity of the proton transfer reaction [88]. As this is greater for CHCA than DHB, and THAP is a neutral molecule, this could account for the trend in decreasing lipid fragmentation that is observed. As DHB matrix offered the particular benefit of significantly higher ion counts of lipid species, and promoted the formation of various different lipid adducts, this matrix was selected for a detailed study of salt additives.

MALDI matrix	Proton Affinity (kJ mol^{-1})	Sodium Cation Affinity (kJ mol^{-1})	Gas phase basicity (kJ mol^{-1})	Gas-Phase Sodium Basicity (kJ mol^{-1})	Gas-Phase Potassium Basicity (kJ mol^{-1})
CHCA	841	193	908	*n.f*	*n.f*
DHB	841-866	< 100	*n.f*	158	99
THAP	892	> 114	864	154	97

Table 7 Proton and cation affinities and gas-phase basicities of CHCA, DHB and THAP matrices, as reported in the following [89, 94, 96, 210-212]. *n.f* values not found.

2.3.2 Additives in MALDI-MS Analysis of Complex Lipid Samples

2.3.2.1 Crystal Homogeneity

The homogeneity of spotted crystals was markedly different upon addition of different salts to the matrix and with varying salt concentration, as shown in Table 8. When DHB matrix was spotted, rod-like crystals were formed largely around the outside of the sample well with smaller crystals inside. This is in agreement with previous reports of the type of crystal morphology exhibited when DHB matrix is prepared by the dried droplet method [213].

Upon addition of an acetate salt, crystal homogeneity was significantly improved. Much smaller and rounder crystals were formed and therefore homogeneity was increased. The addition of a chloride salt did not alter the crystal formation at most investigated concentrations, however it was slightly improved at higher chloride salt concentrations. The only exception in this study was caesium chloride, smaller crystals were detected when caesium chloride was added however these were not very homogeneous. The addition of a nitrate salt led to the formation of smaller and rounder crystals at higher additive concentrations (20 mM and above) however the characteristic (for DHB) rod-like crystals formed at lower concentrations. Table 8 shows photos of crystal appearance. Although a number of other lipid studies have considered the effect of salt additives in MALDI at varied salt concentration [19, 182], the resultant crystal formation is not

commented upon. Most studies focus on describing the effect of salt addition on the detection of lipid analytes with respect to adduct formation.

Investigations probing the crystallisation process in dried droplet samples have reported that alkali ions remain in solution for as long as possible during the drying process, leading to principal localisation in the central area of the sample well [214] . Hence they are segregated from the larger matrix crystals formed around the edge [214]. The same study revealed that drying time has a significant impact on crystal homogeneity; slower crystallisation leads to larger crystal formation and faster crystal formation leads to reduced component segregation. Increased solute (salt) concentrations will lead to faster evaporation of the solvent upon deposition; hence this could help explain why more homogeneous crystals are formed at higher salt concentrations. Furthermore, it has been shown that more polar analytes, with greater affinities for metal ions will co-crystallise [214]. Phospholipids are polar and will therefore have an affinity for alkali ions. Combined with the above described effects this could explain why overall increased homogeneous crystal formation between matrix, salt and analyte was observed at higher additive concentrations. This does not however explain why this was prevalent at lower salt concentrations for some additives but not others.
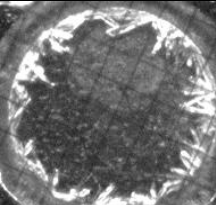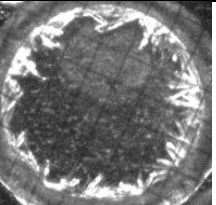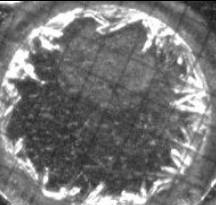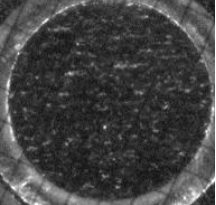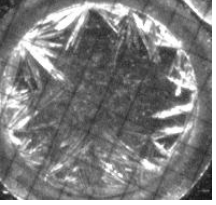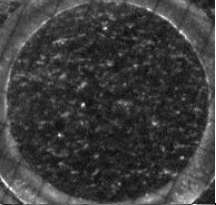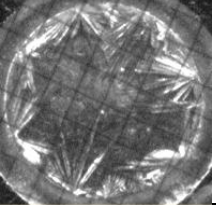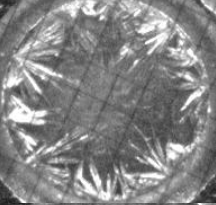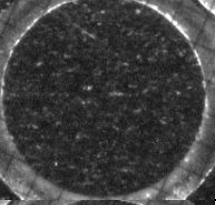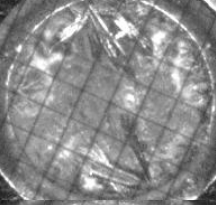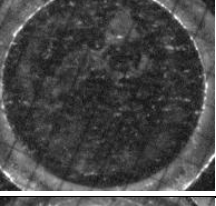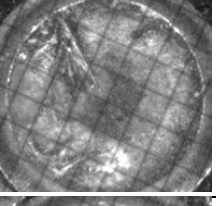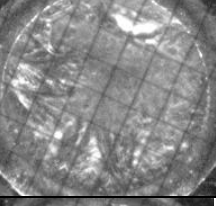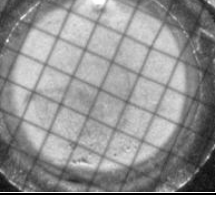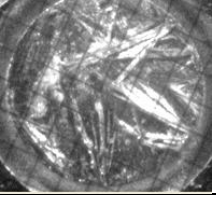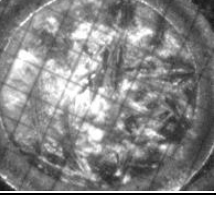
Additive concentration	Sodium Acetate (NaOAc)	Sodium Chloride (NaCl)	Sodium Nitrate (NaNO₃)
0 mM (DHB only)			
5 mM			
10 mM			
20 mM			
40 mM			
80 mM			

Table 8 In-source photographs of MALDI sample spots. Images show lipid extract prepared with 20 mg ml^{-1} DHB matrix with the addition of 0-80 mM of sodium acetate, sodium chloride or sodium nitrate. Sodium additives are shown as an example of general trends. Spot wells are 2.5 mm in diameter.

2.3.2.2 Acetate Salt Additives

The inclusion of low concentrations of ammonium acetate in the MALDI matrix led to increased ion counts of all lipid species of various adducts. Based on a mean average, there is a two-fold increase in the ion counts of detected lipid species of any adduct type when 5 mM ammonium acetate is included in the matrix. This could be a route to increasing the sensitivity by detecting lipids which are present in low abundance and/or have lower ionisation efficiency than the readily ionised PC lipid species. However the standard deviation indicates that the reproducibility of this outcome is poor, as shown in Figure 18.

Ammonium acetate has also proved useful as a tissue desalting wash, reducing sodium and potassium content in tissue and increasing ion counts of protonated adducts of lipid analytes, though in that study, a much more concentrated solution (160 mM) was considered [180]. Angel *et al.* agree that the use of an ammonium salt-based wash solution leads to the removal of potassium and sodium adducts [215]. The addition of this salt to MALDI matrices has also proven useful in the analysis of analytes such as phosphopeptides [190], leading to enhanced detection, however it has not been considered as a matrix dopant for lipids previously.

The addition of sodium acetate to the matrix did not increase the ion counts for the sodium adducts. However suppression of potassium adducts at *m/z* 772 (PC 32:0), *m/z* 798 (PC 34:1) and *m/z* 826 (PC 36:1) and protonated adducts at *m/z* 734, *m/z* 760 and *m/z*

788, respectively, in comparison to the control experiment, were noticeable, as demonstrated in Figure 17. In the presented study, overall the spectra were less complex than control samples. Stubiger *et al.* reported similar findings when sodium acetate was included in the matrix solution in complex lipid analysis; sodium adducts of PC lipids were detected in high abundance while signal intensity of other adducts decreased, relatively [19].

The addition of potassium acetate to the matrix led to increased ion counts/relative abundance of potassium adducts at *m/z* 772 (PC 32:0), 798 (PC 34:1) and 826 (PC 36:1), in comparison to the control experiment, as shown in Figure 17. Sugiura *et al.* also reported increased potassium adduct formation of PC lipids in rat brain homogenates by addition of this salt [72]. Sodium adducts of the same lipids were suppressed at *m/z* 756, 772 and 810, respectively. Therefore reduced spectral complexity is achieved by inclusion of this salt. Reduced ion counts of protonated adducts were also detected, agreeing with Sugiura *et al.*; Reduced protonated adduct generation of a lyso-PC species has also been reported by addition of this salt [72].

The inclusion of high concentrations of any of these acetate salts dramatically affected the detection of lipids. Spectral quality became poorer with increasing additive concentration and no lipid ions were detected when ≥ 40 mM of any of these acetate salts were added to the matrix, see Figure 18. Many reports of acetate salts in similar dopant studies only consider low salt concentrations (10-20 mM) [135, 145, 150, 183] and

it has been reported that the inclusion of high concentrations of sodium acetate (> 20 mM) leads to a complete loss in lipid signal of PC species [182]. This was particularly interesting. Although crystal homogeneity was improved with increasing acetate additive concentration (Table 8) it would seem that MALDI-MS analysis of these samples is not enhanced. It has been demonstrated that the formation of more homogeneous matrix crystals leads to more homogenous analyte distribution leading to improved signal reproducibility [216], however this does not necessarily consider samples with particularly high salt composition. High salt concentrations have previously been shown to obstruct the formation of crystalline matrix crystals [217]. It is probable that the addition of high concentrations of salts impedes analysis by MALDI for this reason.

Sugiura *et al.* reported that MALDI-MS spectra could not be obtained when 60 mM potassium acetate was added to DHB matrix, however this was possible at lower salt concentrations (10, 20 mM) [72]. In this study amorphous crystallisation is described to be the limiting factor [72]. This further supports the postulate that the addition of high salt concentrations has a marked effect on crystal formation which is detrimental to the MALDI experiment. We reveal similar findings in acetate salts across a wider surveyed concentration range.
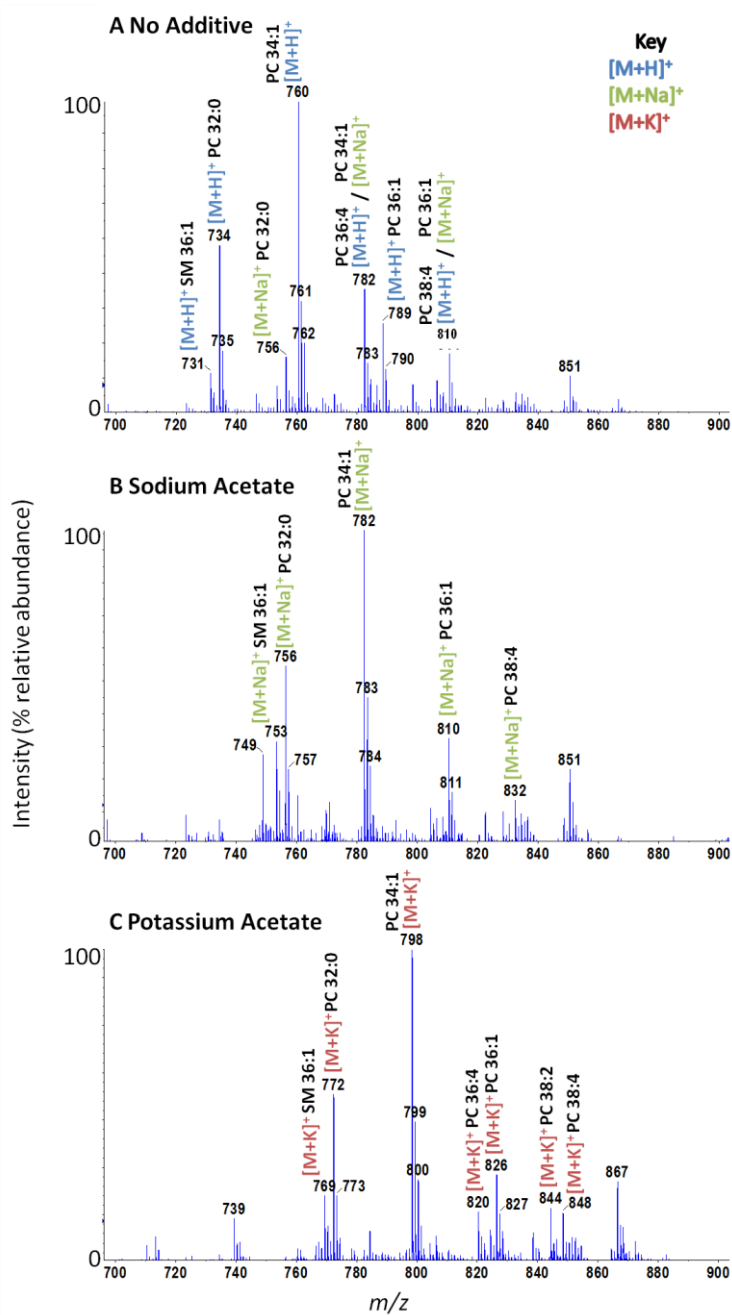
Figure 17 Representative MALDI-MS spectra of rat brain lipid extract sample prepared with DHB matrix including A) no additive, B) 5 mM sodium acetate or C) 5 mM potassium acetate. The phospholipid region *m/z* 700-900 is shown. Changes in the most abundant lipid adduct detected with changing additive and the reduction in spectral complexity achieved by the inclusion of low concentrations of these acetate salts is shown.
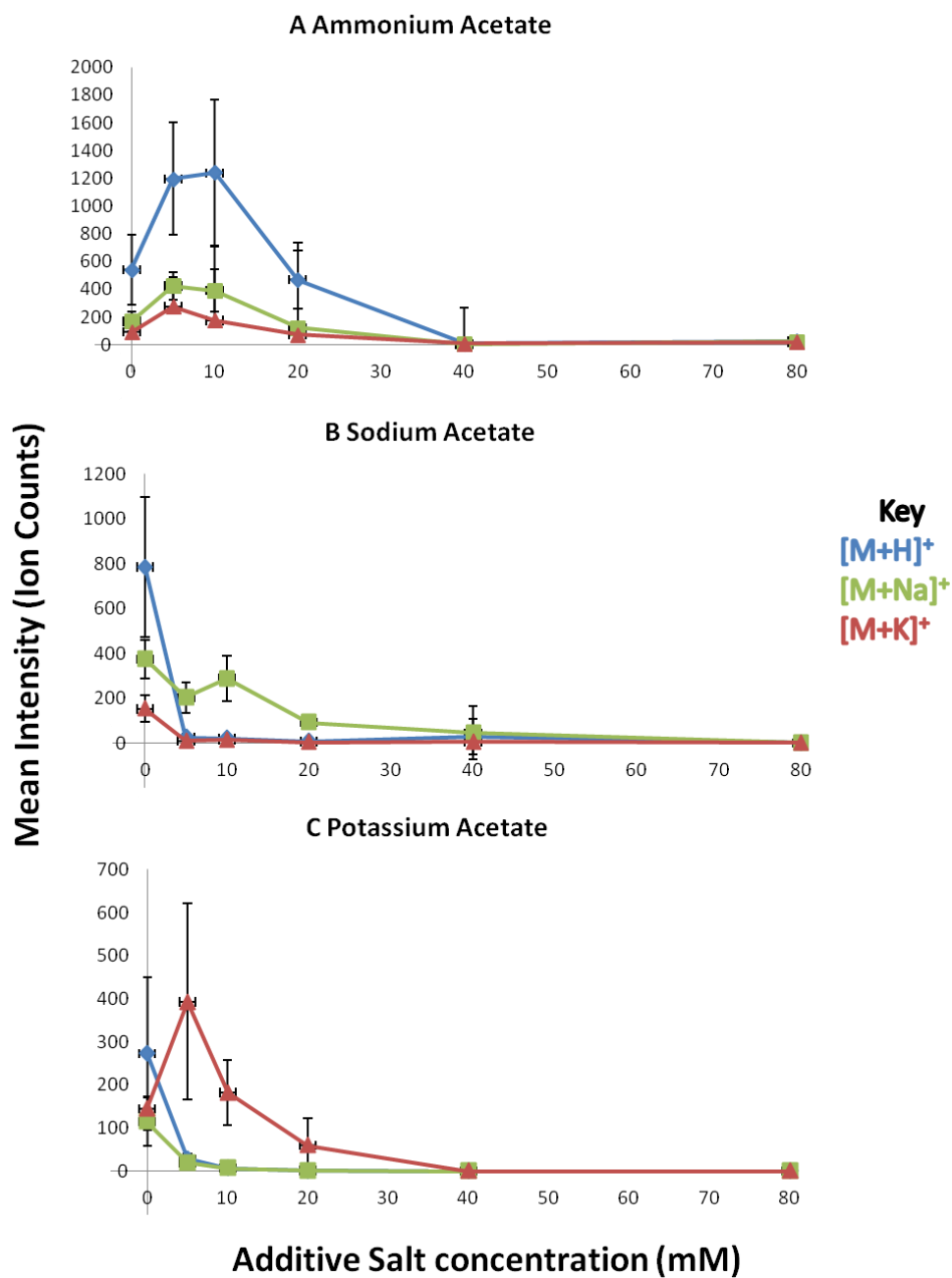
Figure 18 Mean ion counts of [M+H]+, [M+Na]+ and [M+K]+ adducts of PC 34:1 detected in rat brain lipid extract sample in the presence of ammonium (top), sodium (middle) and potassium (bottom) acetate at varied additive salt concentration (0-80 mM). Error bars show one standard deviation above and below the mean ion count. No lipid ions were detected at high acetate concentrations.

2.3.2.3 Chloride Salt Additives

The addition of ammonium chloride to the matrix solution led to decreased intensities of sodium and potassium adducts in comparison to control spectra containing no salt additive. The ion counts of the corresponding protonated species increased at low additive concentrations (≤ 10 mM), but decreased with increasing ammonium chloride concentration thereafter. Despite this, decreases in the relative abundances of cationic adducts resulted in reduced spectral complexity. Although a range of ammonium salts have been considered in tissue washing protocols prior to MALDI analysis of lipids [215], only ammonium citrate had previously been investigated as a matrix additive in MALDI-MS analysis of lipids as a route to promoting protonation (over cationisation) [19, 182]. Here it is shown that the inclusion of ammonium chloride in the MALDI matrix solution gives rise to similar results; however the usefulness of this salt as a matrix additive exhibits a degree of concentration dependence within the investigated range.

Similar observations were made when the chloride salts of sodium and potassium were added to the MALDI matrix. Lipid adducts of the additive cation appear to be preferably formed compared to other lipid adducts, such as protonated and other cationic adducts. The inclusion of sodium chloride in the matrix did not increase the ion counts of sodium lipid adducts (*m/z* 756, 782 and 810 (PC 32:0, 34:1 and 36:4)) or significantly suppress the detection of protonated adducts (*m/z* 734, 760, 788), however

potassium adducts appeared to be suppressed (*m/z* 772, 798 and 826), as shown in Figure 19. Therefore, overall spectral complexity was reduced to an extent. A significantly increased relative abundance of a phosphatidylinositol-monophosphate lipid when this salt is added to the matrix has been reported by Muller *et al.*[188]. In these experiments it appeared that although the average ion counts of sodium adducts remain similar, the relative abundance of sodium adducts (in comparison to protonated and potassium adducts) increases.

The use of potassium chloride as an additive increases the ion counts/relative abundance of potassium lipid adducts at *m/z* 772, 798 and 826 (PC 32:0, PC 34:1 and PC 36:4), in comparison to protonated and sodium adducts, at additive concentrations ≤ 20mM. Lower ion counts of protonated adducts (*m/z* 734, 760, 788) and sodium adducts (*m/z* 756, 782, 810) of these lipids were detected in comparison to the control sample, as illustrated in Figure 19. In this way, the inclusion of potassium chloride in the matrix led to reduced spectral complexity. This was observed across a range of additive concentrations; however, sensitivity in lipid detection decreased with increasing concentration. Here the range of potassium salts considered as matrix additives for the analysis of lipids is extended from acetates to chlorides, showing that chlorides exhibit similar benefits across a greater concentration range.
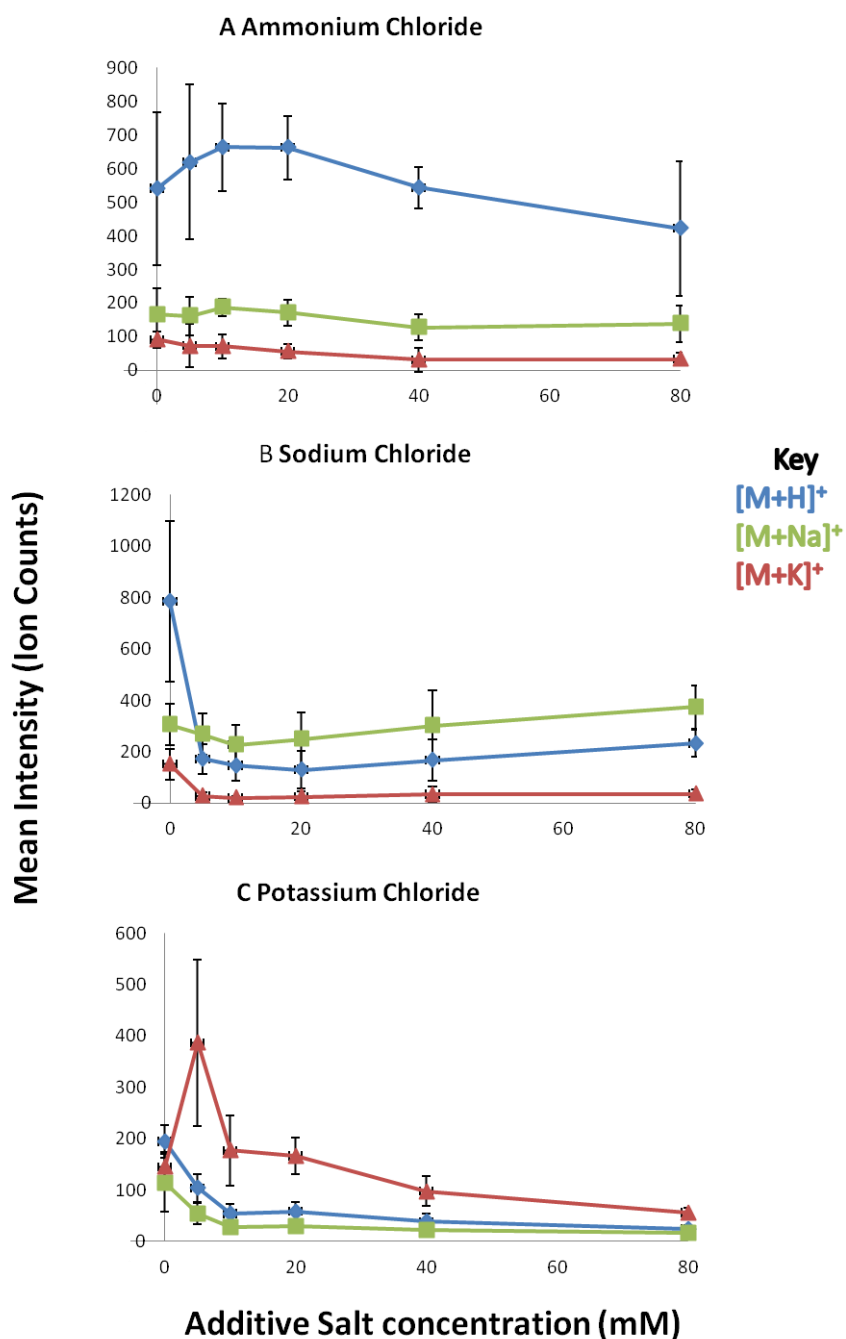
Figure 19 Mean ion counts of [M+H]⁺, [M+Na]⁺ and [M+K]⁺ adducts of PC 34:1 detected in rat brain lipid extract sample in the presence of A) ammonium, B) sodium and C) potassium chloride salts at varied additive salt concentration (0-80 mM). Error bars show one standard deviation above and below the mean ion count.

Detection of caesium lipid adducts eliminates the potential problems with overlapping adduct peaks of different lipids. The peak detected at *m/z* 810 could be attributed to the protonated adduct of PC 38:4 or the sodium adduct of PC 36:1. The addition of caesium chloride led to the detection of caesium lipid adducts of each of these lipids at *m/z* 920 and 942. Therefore it is likely that both were present at *m/z* 810 in different adduct forms. The addition of caesium significantly reduced spectral complexity and aided lipid assignment. Caesium lipid adducts detected are in good agreement with previous reports [132, 133, 185, 187, 218] of PC 32:0, 34:1, 36:1and 38:4, respectively. Ion counts of all other adducts ([M+H]$^+$, [M+Na]$^+$ and [M+K]$^+$) were significantly reduced, or no longer detected, resulting in less complex spectra. For example [M+H]$^+$, [M+Na]$^+$ and [M+K]$^+$ adducts of PC 36:1 detected at *m/z* 734, 756 and 772, respectively, are replaced by a single peak at *m/z* 920.

Furthermore, the formation of caesium adducts between *m/z* 850-1000 leads to a mass shift of 132 u from protonated adducts detected in the region *m/z* 700-850, as shown in Figure 20, shifting. This is particularly advantageous for assignment purposes as no overlapping peaks of other lipids are expected in this mass region. A number of other groups have reported the particular benefit of using caesium chloride as an auxiliary reagent in phospholipid analysis for this purpose in complex sample analysis [131, 132, 187]. Here systems of known caesium ion concentration are investigated at a range of concentrations, demonstrating that only relatively low concentrations of this salt offer these benefits.

Other studies have considered caesium chloride addition at a low additive concentration (10 mM) [185, 186], however Wang *et al.* reported the formation of caesium-lipid adducts incorporating 200 mM caesium chloride into DHB matrix. This is clearly much higher than we found to be useful however their experiments were conducted *in situ* and so it is difficult to directly compare results with respect to lipid concentration and crystal formation [133].

Lipid	[M+H]$^+$	[M+Na]$^+$	[M+K]$^+$	[M+Cs]$^+$
PC 32:0	734	756	772	866
PC 34:1	760	782	798	892
PC 36:1	788	810	826	920
PC 38:4	810	832	848	942
PC 36:4	782	804	820	914
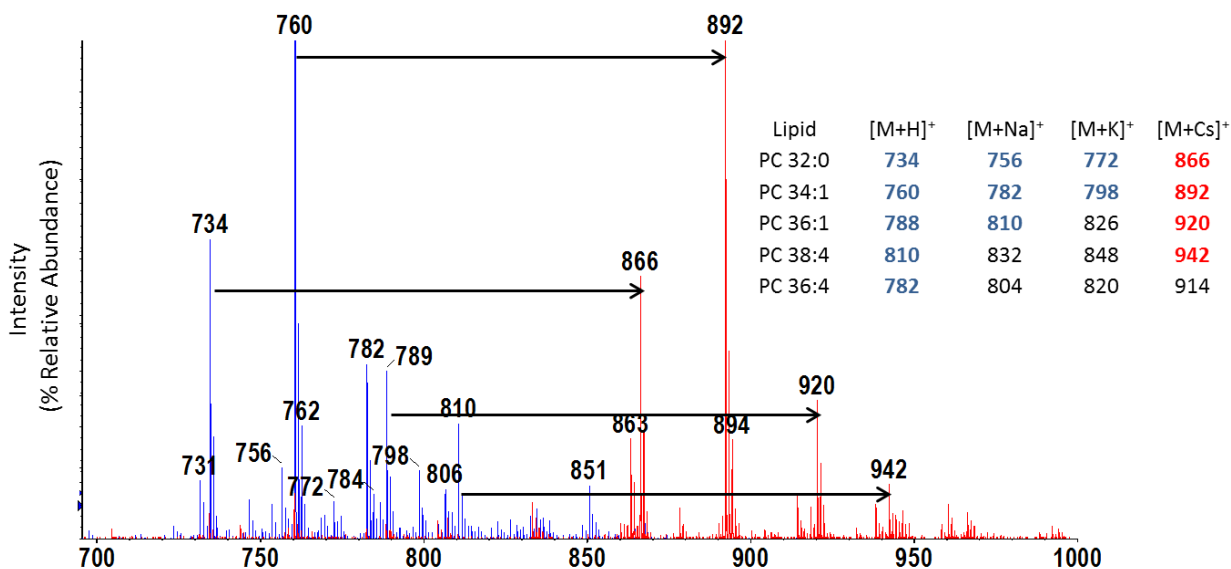
Figure 20 Representative spectra showing phospholipid species detected in the region *m/z* 700-1000 in a non-additive doped sample (blue) and between 700-1000 with the addition of 5 mM caesium chloride (red) to rat brain extract. A table showing the detected *m/z* values of different adducts of a variety of PC lipid species is shown in the table to the right. Peaks detected in the non-additive doped sample are highlighted in blue in the table and those detected in the caesium chloride doped sample are shown in red.

The addition of lithium chloride to the matrix led to the formation of several lithium-lipid adducts at *m/z* 740, 760 and 794 for PC 32:0, 34:1 and 36:1 respectively, in agreement with reported values from *in situ* tissue analysis by Jackson *et al.* [143]. Lithium cationisation appeared to be favoured over sodium and potassium cationisation; sodium and potassium adducts of these lipids were not detected when lithium chloride was included in the matrix. However protonated adducts (*m/z* 734, 760 and 788) of these lipid species were detected at most of the investigated concentrations (5-80 mM). As lithium lipid adducts of many lipids are detected in the *m/z* window as protonated adducts of other lipids, overlapping *m/z* values remains problematic. For example, the protonated adduct of PC 36:1 and the lithium adduct of PC 36:4 are both expected at *m/z* 788. Thus, the employment of lithium chloride as a matrix additive led to reduced spectral complexity, but only to a limited extent.

Few MALDI-MS studies consider the use of lithium chloride in lipid analysis with a view to reducing spectral complexity; most reports of lithium salts consider their use in CID studies [19, 143, 150]. Jackson *et al.* showed that the inclusion of a high concentration of lithium chloride (100 mM) in matrix solutions leads to the formation of lithium-lipid adducts in thin tissue sections, although protonated and potassium adducts were also detected [143]. Unfortunately, data collected without the inclusion of lithium chloride in the matrix is not reported. It is therefore difficult to comment upon the relative complexity of the spectrum. More commonly, lithium acetate has been considered in the analysis of complex lipid extracts and phospholipid standard, leading

to the formation of lithium-lipid adducts and providing useful structural information in CID studies [19, 182].

In my experiment, at an additive concentration of 80 mM, only lithium- lipid adducts were detected. However the spectral quality deteriorated with increasing lithium chloride concentration. The signal to noise ratio of the spectra acquired decreases with increasing additive concentration. Furthermore, the ion counts of species detected in the lipid region of interest were significantly lower in the lithium-doped samples than those in the control samples over a range of additive concentrations (5-80 mM). Stubiger *et al.* reported that lithium-lipid adducts dominate spectra (compared to other adducts) at a lithium acetate additive concentration of 50 mM, however they do not comment upon whether or not the spectral quality is affected.

Lithium chloride and lithium acetate have been considered as matrix additives by some groups as a route to forming lithium-lipid adducts for dissociation studies. These investigations do not offer commentary on the relative use of lithium salts in terms of spectral complexity and spectral quality. It is possible that the particular benefit of using lithium salts in lipid analysis will be indicated in dissociation studies which will be discussed in Chapter 2.3.4. This study shows that the inclusion of lithium chloride in the MALDI matrix is useful to an extent in terms of reducing spectral complexity; however its use is limited at high additive concentrations.

2.3.2.4 Nitrate Salt Additives

The addition of sodium nitrate to the matrix led to decreased spectral complexity owing to increased [M+Na]$^+$ (at *m/z*s 756, 782 and 810) rather than [M+K]$^+$, when compared to control samples, however protonated species were also detected. These observations were found over a range of additive concentrations (5-80 mM). Spectral quality appeared to be unaffected by increasing salt concentration unlike with other salts, as demonstrated in Figure 21 and Figure 22. Sodium nitrate has not been reported as an additive in MALDI-MS previously; here we demonstrate that significant improvements in sensitivity in the detection of sodium lipid adducts are afforded by inclusion of this salt at a range of salt concentrations in MALDI matrix solutions.

The addition of potassium nitrate also led to increased detection of [M+K]$^+$ rather than [M+Na]$^+$ adducts, although protonated adducts were also detected. In this instance reduced ion counts of peaks detected at *m/z* 756, 782 and 810 ([M+Na]$^+$ (PC 32:0, 34:0 and PC 36:1 respectively) were observed. Again protonated adducts of these lipids were detected at *m/z* 734, 760 and 788 in similar relative abundance to the control (no additive) experiments. The potassium adducts of these lipids at *m/z* 772, 798 and 826 had significantly increased ion counts in the additive spectra when compared to the control sample, see Figure 21 and Figure 22. Again, this salt has not previously been considered as an additive in MALDI-MS of lipids and was found to increase sensitivity of potassium adducts over a range of additive concentrations (5-80 mM).

Spectral quality appeared to be unaffected by salt concentration. This work was published by me and Dr Josephine Bunch in 2012. More recently Lee *et al.* have also shown that nitrate salts were most useful in their lipid investigations, particularly for enhanced detection of cerebroside lipids [219].
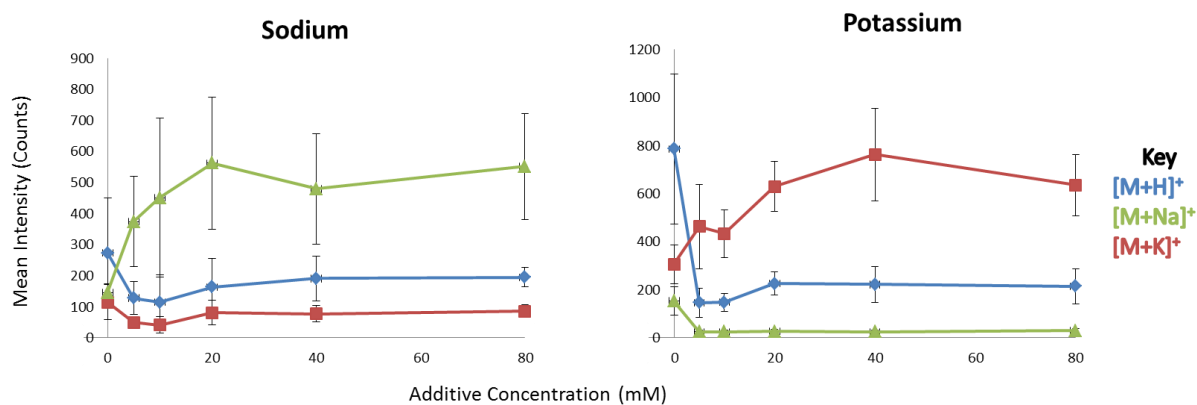
Figure 21 Mean ion counts of [M+H]⁺, [M+Na]⁺ and [M+K]⁺ adducts of PC 34:1 detected in rat brain lipid extract sample in the presence of sodium (left) and potassium (right) nitrate at varied additive salt concentration (0-80 mM). Error bars show one standard deviation above and below the mean ion count.
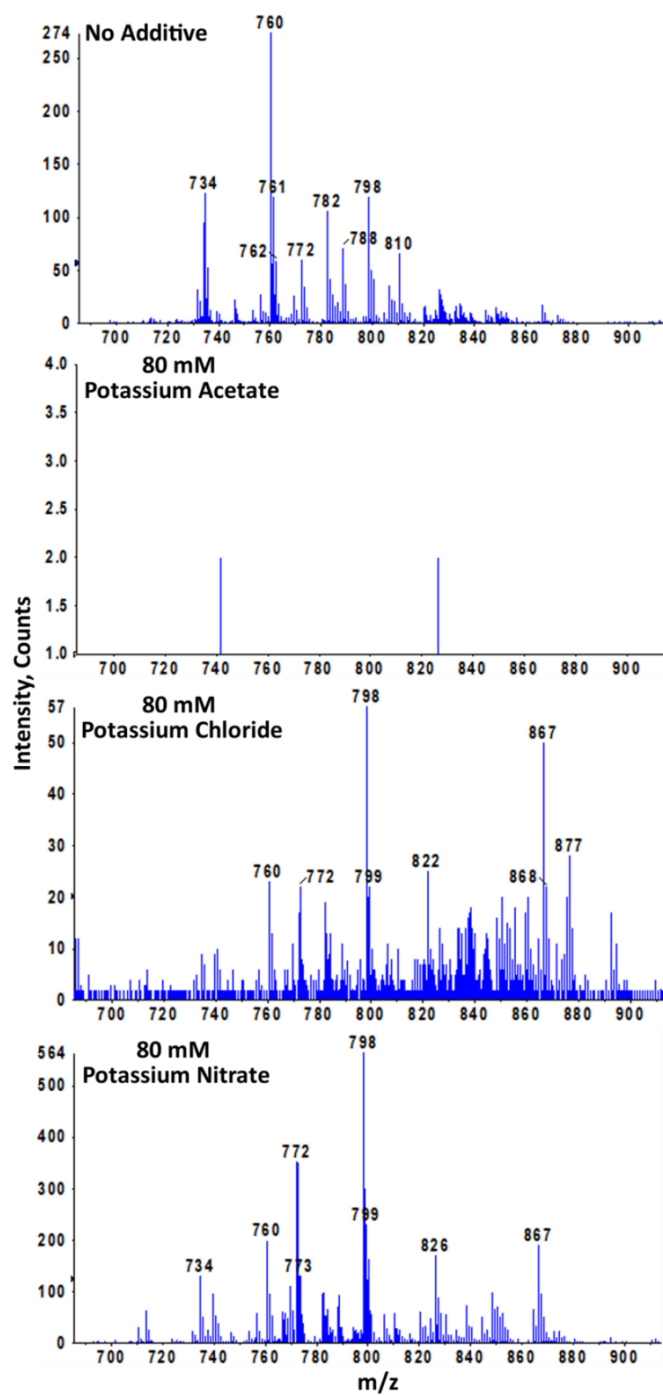
Figure 22 Representative MALDI-MS spectra of lipid extract analysed with a) no additive, b) 80 mM potassium acetate, c) 80 mM potassium chloride and d) 80 mM potassium nitrate.

2.3.3 Summary of Additives in MALDI-MS and MS/MS

Evaluation of ammonium, sodium and potassium acetates and chlorides, alongside sodium and potassium nitrates and lithium and caesium chorides as salt additives has revealed one stark trend; overcoming cationisation pathways in favour of protonation was achieved more readily. The inclusion of ammonium chloride favoured protonation, suppressing cationic adduct signals. However, overcoming protonation in favour of any cationic pathway proved much more difficult. This seems to support Knochenmuss' idea that protonated adduct formation has a lower activation barrier than cationisation [83].

The inclusion of a number of salts (potassium, sodium and ammonium acetates or lithium and caesium chlorides) at high concentrations led to poor spectral quality or no detection of lipid ions. This is clearly undesirable and therefore careful consideration of additive concentration is advised. A summary of results from this MALDI-MS analysis of the complex lipid extract is provided in Table 10. Applications for both improved ion counts and reduced spectral complexity are considered across a range of additive concentrations.

It is not clear why some salts exhibit concentration-dependent effects when others do not in terms of their use in MALDI-MS detection of lipids as illustrated in Figure 23. Nitrates show no concentration dependence, chlorides show some concentration dependence and acetates show strong additive concentration dependence.

Consideration of anion size and basicity does not explain the observed trend between salt types. The lattice energy of the nitrate salts are lower in comparison to the respective chloride and acetate salts, as shown in Table 9 below, and could potentially account at least in part to the observations, however it is not known whether the same trend remains in the crystalline solid solution formed upon deposition of the salt-matrix solutions. A wide range of different experimental factors can be affected by the inclusion of salts in the MALDI matrices, such as the crystal morphology. For this reason it is difficult to postulate with any certainty which properties are responsible for the apparent trend.

	Caesium	Potassium	Sodium	Lithium
Acetate	682	749	828	*n.r*
Chloride	657	707	769	834
Nitrate	648	685	755	662

Table 9 Lattice Enthalpies of salts of Caesium, Potassium, Sodium and Lithium in the form of acetates, chlorides and nitrates [220]. *n.r* not reported.

Matrix Additive	Additive Concentration				
	5 mM	10 mM	20 mM	40 mM	80 mM
Ammonium Acetate (NH₄OAc)	-	-	-	-	-
	ooo	ooo	o	-	-
Ammonium Chloride (NH₄Cl)	++	++	++	++	+
	-	-	-	-	-
Sodium Acetate (NaOAc)	-	++	+	-	-
	-	-	-	-	-
Sodium Chloride (NaCl)	+	+	+	+	+
	-	-	-	-	-
Sodium Nitrate (NaNO₃)	++	++	++	++	++
	o	o	oo	ooo	oo
Potassium Acetate (KOAc)	+++	+++	+++	-	-
	oo	-	-	-	-
Potassium Chloride (KCl)	++	+	+	+	-
	oo	-	-	-	-
Potassium Nitrate (KNO₃)	++	++	+	+	-
	oo	ooo	ooo	ooo	ooo
Lithium Chloride (LiCl)	n.e	+	-	-	-
	n.e	-	-	-	-
Caesium Chloride (CsCl)	+++	++	++	-	-
	o	-	-	-	-

Table 10 Suitability of matrix additives for first altering the ionisation pathway (+) and secondly improving sensitivity (o) in the MALDI-MS analysis of PC lipids in positive ionisation mode with DHB matrix (- not useful, + useful, ++ very useful, +++ extremely useful) (- not useful, o useful, oo very useful, ooo extremely useful) (*n.e* not evaluated)
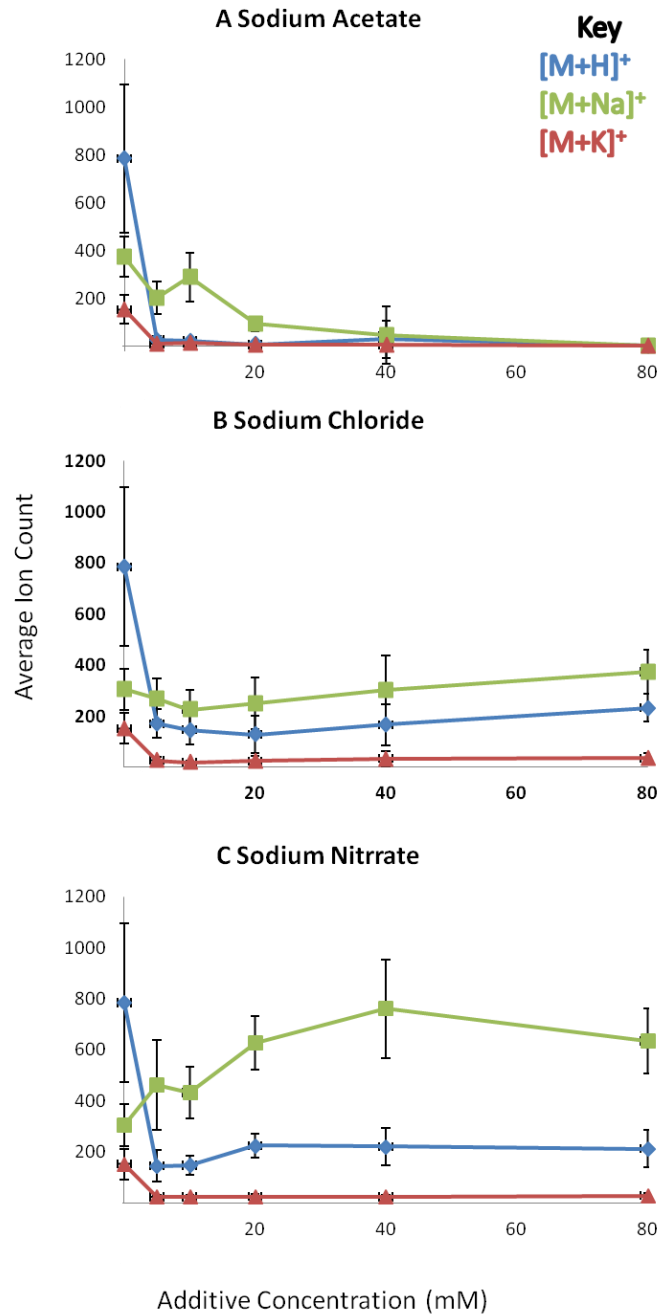
Figure 23 Mean ion counts of [M+H]+, [M+Na]+ and [M+K]+ adducts of PC 34:1 detected in rat brain lipid extract sample in the presence of sodium a) acetate b) chloride and c) nitrate at varied additive salt additive concentration (0-80 mM). Error bars show one standard deviation above and below the mean ion count.

2.3.4 Collision-induced dissociation Studies of Lipid Adducts

A study of the collision-induced dissociation (CID) of various adducts of PC (18:1/16:0) was investigated. Dissociation of [M+H]$^+$, [M+Na]$^+$ and [M+K]$^+$ adducts was explored with a sample prepared with DHB matrix only. In order to assess lithium ([M+Li]$^+$) and caesium ([M+Cs]$^+$) lipid adducts, 5 mM of the respective chloride salt was added to the matrix solution. The collision energy of the nitrogen gas introduced into the collision chamber was optimised between 10-100 eV and the most useful data in terms of structural characterisation is presented.

A product ion at *m/z* 184 was detected in greatest abundance when the protonated lipid adduct ([M+H]$^+$) was dissociated. This can most likely be attributed to the protonated phosphocholine head-group, as described in a number of literature reports of CID of protonated lipid adducts by different ionisation techniques [19, 143, 145, 221-223]. This ion has also been reported as the predominant product ion by other dissociation methods, such as post source decay[150]. Although some smaller *m/z* product ions were detected in low abundance these do not provide further insight into the identity of the lipid. Overall, only product ions indicative of the phospholipid head-group, in the *sn*-3 position along the glycerol backbone, were detected, which is in good agreement with MS/MS reports of protonated adducts [19, 145, 224].

Dissociation of the potassium adduct ([M+K]$^+$) led to the detection of different product ions in comparison to that of the protonated adduct. The product ions detected were characeristic of the PC head-group identity via neutral losses: m/z 739 [M+K-59]$^+$ where 59 u is the mass of the choline moiety of the head-group (N(CH$_3$)$_3$), m/z 615 [M+K-183]$^+$ where 183 u relates to the intact zwitterionic PC head-group (PO$^-_4$C$_2$H$_5$N$^+$(CH$_3$)$_3$) and m/z 577 indicates the further loss of potassium. The most abundant product ion was detected at m/z 163, which is indicative of the phosphate moiety of the head-group associated with potassium (PO$_4$C$_2^+$H$_5$K). Once again only the identity of the (*sn*-3) head-group could be confirmed. Hence, dissociation of the potassium lipid adduct did not prove to be useful for complete structural characterisation as product ions indicative of the two fatty acid side-chain identities were not detected. Similar product ions have been reported by Jackson *et al.* from MALDI-MS/MS of the potassium adduct of PC 32:0 detected *in situ* who agree that dissociation of potassium adducts of PC species did not yield product ions indicative of fatty acid side-chain indicative product ions [143].

Dissociation of the sodium adduct ([M+Na]$^+$) led to the detection of similar product ions indicative of the PC head- to those described for dissociation of the potassium adduct. However, additional product ions were detected in relatively low abundance in the region m/z 200-550. Product ions detected at m/z 239 and 265 are indicative of the acyl ions (RCO$^+$) of palmitic (16:0) and oleic (18:1) fatty acid side-chains, respectively. In addition, product ions detected at m/z 441 and 467 are indicative of the neutral loss of each fatty acid side-chain alongside the neutral loss of choline (59 u). The detection of

these fragments is adequate to enable elucidation of each fatty acid side-chain identity, but these were not detected consistently across five repeats. These product ions were detected in similar relative abundance to one another and hence no conclusions can be drawn as to which fatty acid resides in the *sn*-1 position on the glycerol backbone and which in the *sn*-2 position.

Previous studies considering CID of sodium lipid adducts vary in their recommendations. Some groups have reported the dissociation of sodium lipid adducts enables complete structural assignment [183]. Other reports suggest that product ions that are characteristic of the fatty acid side-chain identities are not detected by dissociation of sodium adducts [143]. Although these results appear to agree with Garrett *et al.* [183] that dissociation of sodium adducts can provide product ions which aid structural assignment, they also appear to show that assignment of fatty acid esterification positions (*sn*-1 and *sn*-2) along the glycerol backbone may not be possible. This is critical when considering lipids as biomarkers of disease, consequently dissociation of alternative lipid adducts which are not naturally present in biological samples must be considered.

The most informative product ion spectrum when the caesium-lipid [M+Cs]$^+$ adduct was dissociated indicated neutral loss of 59 u (choline moiety of the head-group) and free caesium at *m/z* 133. Although caesium-lipid adducts were shown to be particularly useful in MALDI-MS experiments for reducing spectral complexity (and have been

included in MALDI-MS preparations by a number of groups for this reason [132]), clearly structural elucidation of PC lipid species cannot be achieved from CID of these adducts. Wang *et al.* reported that dissociation of [M+Cs$^+$-2H]$^-$ adducts of cardiolipin lipid species were useful in structural characterisation [225], however CID of [M+Cs]$^+$ adducts of lipid species have not been reported previously. Here it is demonstrated that dissociation of caesium-lipid adducts do not provide product ion spectra which enables complete structural characterisation of PC species.

Dissociation of the lithium-lipid adduct [M+Li]$^+$ provided the most product ion rich spectra compared to protonated and all other cationic lipid adducts ([M+K]$^+$, [M+Na]$^+$ and [M+Cs]$^+$). The most abundant product ions detected were similar to those detected during dissociation of other cationic adducts; neutral loss of the choline moiety of the head-group (*m/z* 707) and neutral loss of the intact phosphocholine head-group (*m/z* 583, further loss of lithium at *m/z* 577). The lithium adduct of the phosphate moiety of the head-group (*m/z* 131) was also observed, however this was detected in much lower abundance than analogous product ions detected in dissociation experiments of sodium and potassium cationic adducts.

In contrast to dissociation of other cationic adducts, or the protonated lipid adduct, a variety of product ions were detected in the region *m/z* 200-550 in relatively high abundance. All of the product ions detected in this region are indicative of the identities of the two fatty acid side-chains: neutral loss of palmitic and oleic fatty acid side-chains,

respectively (*m/z* 510 and 484), the further neutral loss of choline (*m/z* 451 and 425), neutral loss of the lithium salt of each fatty acid (*m/z* 504 and 478) and detection of acyl ions (RCO⁺) at *m/z* 239 and 265 as shown in Figure 24.
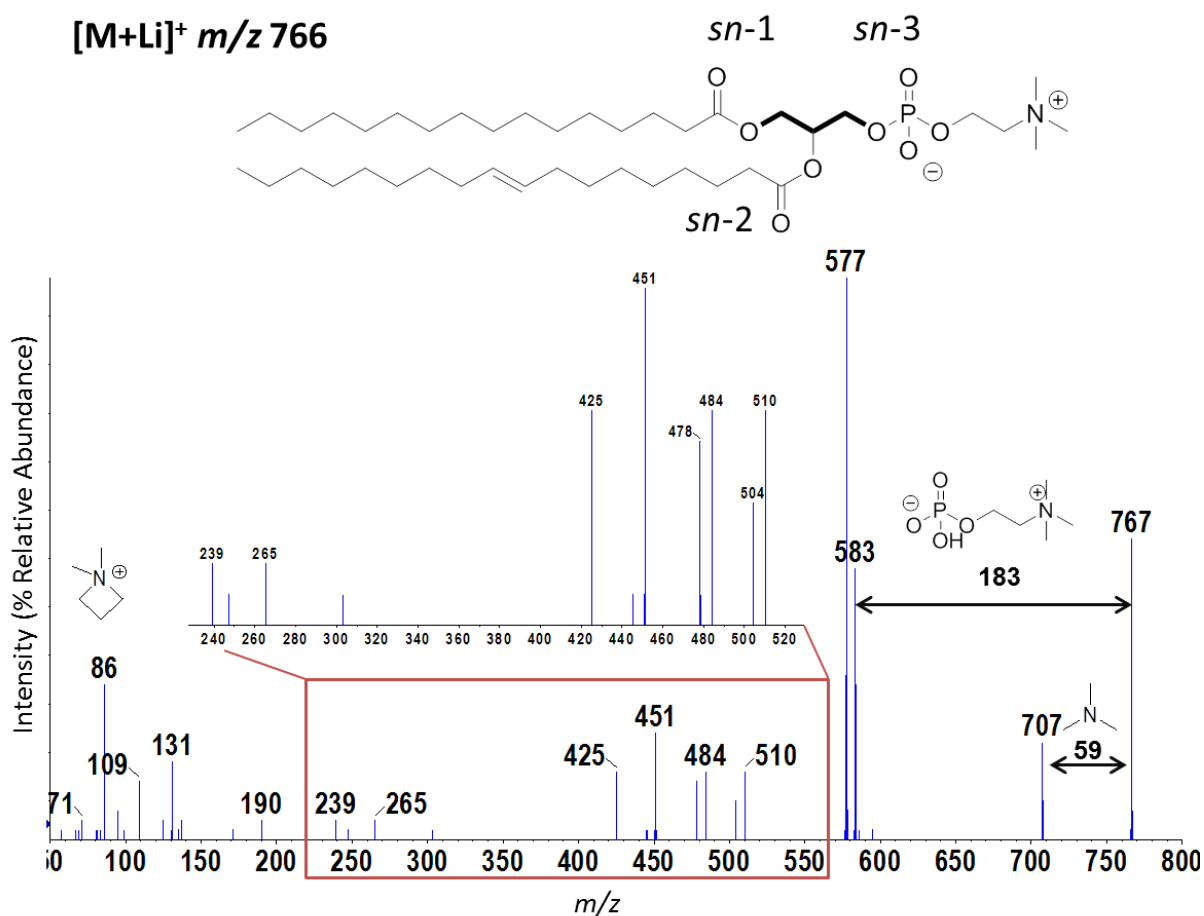
Figure 24 Representative product ion spectrum acquired during dissociation of *m/z* 766 corresponding to the [M+Li]⁺ adduct of PC (16:0/18:1) in DHB matrix. The structure of PC (16:0/18:1) is shown above the spectrum and the *sn*-1, *sn*-2 and *sn*-3 positions along the glycerol backbone indicated. Product ions detected are indicative of the *sn*-3 phosphocholine head-group, the two fatty acid side-chain identities and their relative positions along the glycerol backbone.

Collision-induced dissociation of lithium-lipid adducts has commonly been reported as the most useful for gaining structurally characteristic information from phospholipid analytes (owing to the detection of the above described product ions in a single MALDI-MS/MS experiment) [77, 143, 145, 151]. The structural information obtained from CID of a variety of other different lipid species such as tri- and diacylglycerols [203], fatty acids [226] and galactosyl ceramides [145] has also been reported to be enhanced by dissociation of lithium-lipid adducts compared to other adduct forms. Similar findings have also been described by groups investigating CID of lipid ions formed by ESI [113, 227-230].

In this study, it was found that neutral loss of the fatty acid side-chain alongside that of choline were the most abundant product ions characteristic of the fatty acid side-chains. The product ion indicating neutral loss of the *sn*-1 fatty acid (*m/z* 451) alongside choline was repeatedly detected in greater abundance than neutral loss of the *sn*-2 fatty acid (*m/z* 425). Stubiger *et al.* described similar findings in MALDI-MS/MS experiments with a phospholipid standard [150]. Hence it is possible to assign fatty acid side-chain positions. This is particularly important when considering samples of unknown composition; understanding the trends in relative abundances of characteristic product ions is key to structurally characterising lipid species detected *in situ*, for example, when attempting to identify biomarkers.

2.3.5 Conclusions

Overall the use of additives for a variety of applications is described. Careful consideration of the additive of choice with respect to the intended use is recommended. For the purpose of MALDI-MS analysis: if the detection of a particular adduct is required , specifically $[M+H]^+$, $[M+Na]^+$ or $[M+K]^+$, the addition of ammonium chloride, sodium acetate or potassium acetate, respectively, are the recommended additives for affording improved sensitivity whilst simultaneously reducing spectral complexity. However their usefulness is limited at high concentrations. Inclusion of caesium chloride is recommended to reduce spectral complexity whilst simultaneously shifting the detected *m/z* outside of that region viewed in the control, allowing unambiguous assignment of caesium-lipid adducts. However this salt also has limited use at high additive concentrations.

The addition of sodium or potassium nitrate to the matrix is recommended for improved sensitivity of sodium and potassium adducts respectively as a concentration-tolerant additive. Sodium and potassium nitrates were the only additives which may be utilised as usefully across a range of concentrations and are shown to be particularly useful for increasing ion counts of a particular ion with benefit in MALDI-MS analysis of lipids. These salts could be particularly useful when considering the incorporation of additive salts in MALDI-MS and imaging analysis of thin tissue sections as optimisation of the additive concentration may not be required.

It is also clear from these studies that the relative degree of structural information obtained by CID of different cationic adducts of lipids increases with decreasing cation size. The structural information obtained by dissociation of $[M+Li]^+$ > $[M+Na]^+$ > $[M+K]^+$ > $[M+Cs]^+$ lipid adducts improve. Lithium lipid adducts are shown to provide the most structurally informative product ions. These findings are in agreement with previous reports in the dissociative trends of different cationic lipid adducts [19, 150].

In order to achieve structural characterisation, dissociation of lithium-lipid adducts generated the most useful product ions reliably. These were detected in high relative abundance and reliably inferred the relative *sn*-1 and *sn*-2 positions of each fatty acid along the glycerol backbone. Lithium-lipid adducts are not naturally abundant in tissue samples. As these were most useful in dissociation studies, the need to pursue strategies leading to the introduction of lithium ions into tissue samples for imaging experiments, in order to achieve *in situ* structural characterisation of lipids in thin tissue sections is highlighted.

Dissociation of sodium adducts yielded sufficiently informative product ions for determination of the head-group and fatty acid side-chain; however relative *sn*-1 and *sn*-2 fatty acid side-chain positions could not be deduced. This could still be important when conducting *in situ* structural characterisation analysis as sodium lipid adducts are detected naturally in fresh tissue, hence promoting the detection of these adducts may prove more favourable than forming lithium adducts. The formation of lithium adducts

in these MALDI-MS investigations via inclusion of lithium chloride in the matrix solution led to lower ion counts (reduced sensitivity) in comparison to other lipid adducts.

3. The inclusion of additives for MALDI-MS *in situ* analysis of lipids

3.1 Introduction

Mass spectrometry imaging offers analysts the opportunity to simultaneously acquire information regarding both the sample composition and the spatial distribution of analytes. Tissue features, such as white and grey matter, in murine brain can be distinguished in thin tissue sections at a spatial resolution of 100 µm, which is commonly reported in MALDI-S imaging analysis. Different lipid species are often preferentially localised in different tissue regions, for example certain species will be prevalent in white matter in brain cerebellum and other species will have a greater prevalence in the grey matter. This is particularly important when considering the analysis of disease model tissue sections when spatial distributions of some species may differ from normal. Gaining an understanding of both the lipid composition whilst also obtaining insight as to the spatial distributions of lipid species is of the utmost importance when investigating changes between normal and diseased state tissues.

MALDI-MS imaging of lipids in tissue samples has been reported widely by a number of different groups. Murine, bovine [16] and porcine organs such as brain [48, 57], liver [57] and ocular tissue [128] have all been examined for tissue imaging analysis of lipids. These studies optimised parameters such as matrix selection [16, 39, 45, 48, 57], matrix deposition technique [23, 70] and processing options [42]. Optimised methods have been

described in lipid investigations of normal and diseased tissue models [23, 29]. A number of recent studies have considered human disease tissues or regions [53, 231].

As described in Chapter 2, lipids form protonated [M+H]$^+$ and cationic adducts such as [M+Na]$^+$ and [M+K]$^+$ in MALDI-MS experiments. Therefore the inclusion of additive salts in MALDI matrix solutions has been considered as a route to decreasing spectral complexity and/or improving sensitivity in MALDI-MS experiments. The following additives have been investigated in MALDI-MS imaging analysis of lipids with a view to optimising *in situ* lipid analysis: ammonium acetate was employed in a tissue washing protocol to remove potassium and sodium ions from samples [180]. The inclusion of either sodium or potassium acetate in matrix solutions has been shown to lead to selective imaging of different lipid species [184]. Sodium acetate has also been included in matrix solutions as a cationising agent in lipid imaging studies and has been show to aid *in situ* structural characterisation of lipid species [183].

Dissociation studies, such as those described in Chapter 2, have shown that lithium-lipid adducts provide the most useful structural information. For this reason the incorporation of lithium salts into tissue is also of particular interest to lipid analysts. Lithium is not endogenous in most tissues and lithium-lipid adducts are not detected in MALDI-MS imaging experiments, hence the problem of lithium ion introduction arises. To date, this has been accomplished for *in situ* tissue profiling CID studies simply via pipetting a matrix solution containing a lithium salt directly onto the tissue [77, 143].

However, analyte delocalisation is a concern with this approach, and hence structural elucidation of lipid species from a single specific anatomical region is unrealistic. Furthermore, imaging experiments cannot be prepared in this manner.

A range of approaches have been considered for the introduction of lithium into tissue samples via spraying deposition methods for MALDI-MS imaging studies: Synthesis of a lithium salt of DHB matrix for the analysis of neutral lipids in plants and insects [232]. By this preparation lithium adducts of a number of wax ester analytes were detected and their spatial distribution (images) shown. A range of lithium salts have been considered as additives to CHCA matrix solutions deposited as an aerosol using a robot via a heated nebuliser for tissue imaging analysis [145]. By this method, images of lithium adducts of phospholipid species in cerebellum tissue have been generated.

Solvent-free matrix application preparations have also been considered in additive introduction strategies: mixing of matrix compounds with additive salts by ball milling or vortexing for dry-coating preparation for the analysis of polymers [233], free fatty acids [226] and peptides and proteins [234] has been described. Solvent-free dry-coating of matrix compounds onto tissue samples for imaging analysis of phospholipids has also been shown to be beneficial, enabling acquisition of high quality images of phospholipids [62]. Here the use of mixtures of matrix-salt powders as a route to additive introduction for imaging is considered.

In the present study, the range of sodium additives considered for tissue imaging of lipids is extended to chlorides and nitrates. Counteranion trends observed in lipid extract analysis are confirmed in imaging experiments and sodium nitrate is shown to be a useful cationising agent. Furthermore, the use of lithium salts for imaging is extended to lithium nitrate which has been shown to increase ion counts of lithium-lipid adducts in comparison to lithium chloride for lipid extract analysis [235]. Finally, the inclusion of additive salts in MALDI matrix solutions for airspray deposition is compared to a solvent-free dry-coating method in which additive salts are mixed with matrix powders.

3.2 Experimental

3.2.1 Materials

All salts (NaCH$_3$CO$_2$, NaCl, NaNO$_3$, LiCl and LiNO$_3$), α-cyano-4-hydroxycinnamic acid matrix (CHCA) , *p*-nitroaniline (PNA) and 2,5- dihydroxybenzoic acid (DHB) were purchased from Sigma Aldrich (Gillingham, UK). Methanol (HPLC grade) was purchased from Fisher Scientific (Leicestershire, UK). Water was purified by an ELGA Option 3 system (Marlow, UK). Stainless steel MALDI target plates were purchased from AB Sciex (Framingham, USA).

3.2.2 Matrix Application

Matrix solutions of PNA, CHCA and DHB (20 mg/mL, 80 % CH$_3$OH) were used for initial investigations. CHCA (20 mg/mL, 80 % CH$_3$OH) with or without the inclusion of 5-20 mM NaCH$_3$CO$_2$, NaCl, NaNO$_3$, LiCl or LiNO$_3$ were deposited using an artist airbrush purchased from Draper (Hampshire, UK) propelled by dry N$_2$. Two consecutive spray passes were followed by ten seconds drying time, until 10 mL was deposited, from a distance of 20 cm from the plate. For dry-coating[62], CHCA matrix (2 g) was ground for 10 minutes in a pestle and mortar with or without 5 mM equivalent LiCl or LiNO$_3$. Matrix samples were deposited onto the MALDI target plate through a 20 μm mesh sieve.

3.2.3 Mass Spectrometry

MALDI-MSI and MS/MS imaging studies of murine samples were carried out on a QSTAR XL Q-TOF mass spectrometer (AB Sciex). An Elforlight (Daventry, UK) Nd:YVO$_4$ DPSS laser (355 nm) was triggered by a Thurlby Thandar Instruments (Huntingdon, Cambridgeshire) TGP110 10 MHz pulse generator, coupled to the MALDI source via a 100 µm core diameter fiber optic patchcord (Edmund Optics, NA=0.22) and operated at 5 kHz and approximately 8 µJ. Analysis was performed in positive ion mode with a pixel size of 100 by 100 µm, *m/z* range 400-900, focusing potential (FP) of 85 and declustering potential (DP2) of 35. For MS/MS imaging CID was performed with N$_2$ gas at collision energy of 40 eV. Images were collected in raster mode at a speed of 1 mm s^{-1} (acquired in ≈ 25 minutes per section), 0.3 mm s^{-1} (acquired in ≈ 70 minutes) or 0.2 mm s^{-1} (acquired in ≈ 100 minutes).

3.2.4 Data Conversion and Analysis

MALDI data acquired using the QSTAR XL were analysed using Analyst QS 1.1 and MATLAB. The data were converted from the AB Sciex .wiff proprietary file format to mzML using AB MS Data Converter (AB Sciex version 1.3) and then converted to imzML using imzMLConverter[236] and processed in MATLAB (version 7.8.0 (2009a), Math Works Inc, USA). For all of the images displayed, peak information is the summed ion intensity from within a 0.1 Dalton window centred on the peak of interest.

3.3 Results and Discussion

3.3.1 MALDI-MS and Imaging of lipids using an Nd:YVO$_4$ Laser

With a view to developing techniques which could be suitable for tissue imaging it is important to consider sample analysis time. Conventional N$_2$ lasers deliver relatively high energies (up to 100 μJ) at relatively low repetition rates (up to hundreds of Hz). More recent laser developments consider the use of high repetition rates (tens of thousands of Hz), which offer considerably greater throughput but also operate at lower laser energies (up to 10 μJ). Here the use of a diode-pumped solid-state (DPSS) laser (Nd:YVO$_4$) is used.

Preliminary experiments investigating the analysis of a PC lipid standard with a range of MALDI matrices acquired using an Nd:YVO$_4$ laser showed that a different matrix compound is optimal for analysis with this laser compared to the N$_2$ laser described in earlier work. Analysis of the lipid standard (PC 18:1/16:0) with CHCA, DHB and THAP matrices led to the detection of high relative abundances of lipid ions, such as protonated [M+H]$^+$ and cationic adducts [M+Na]$^+$ and [M+K]$^+$ at *m/z* 760, 782 and 798, respectively. However the ion counts of the detected lipid species were significantly higher when CHCA matrix was employed using the Nd:YVO$_4$ laser as illustrated in Figure 25.

Even though CHCA matrix is hot in character when analysing lipids, leading to the detection of high abundances of lipid fragment ions such as the neutral loss of the PC head-group (*m/z* 577) and each fatty acid side-chain (*m/z* 478 and 504) as demonstrated in Figure 26, the overall ion counts of lipid ions detected were so much greater that CHCA was selected for analysis. This result was surprising as DHB and THAP are the most commonly reported MALDI matrices for the analysis of lipid species with N_2 lasers [19-21, 35] and had been found to be most useful in our previous studies.
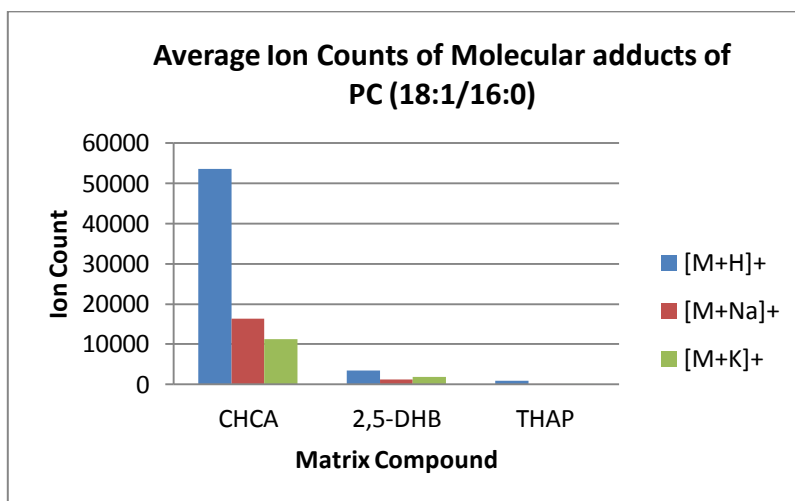
Figure 25 Average Ion Count of [M+H]+, [M+Na]+ and [M+K]+ adducts of PC (18:1/16:0) analysed with a range of organic matrices with an Nd:YVO$_4$ laser.
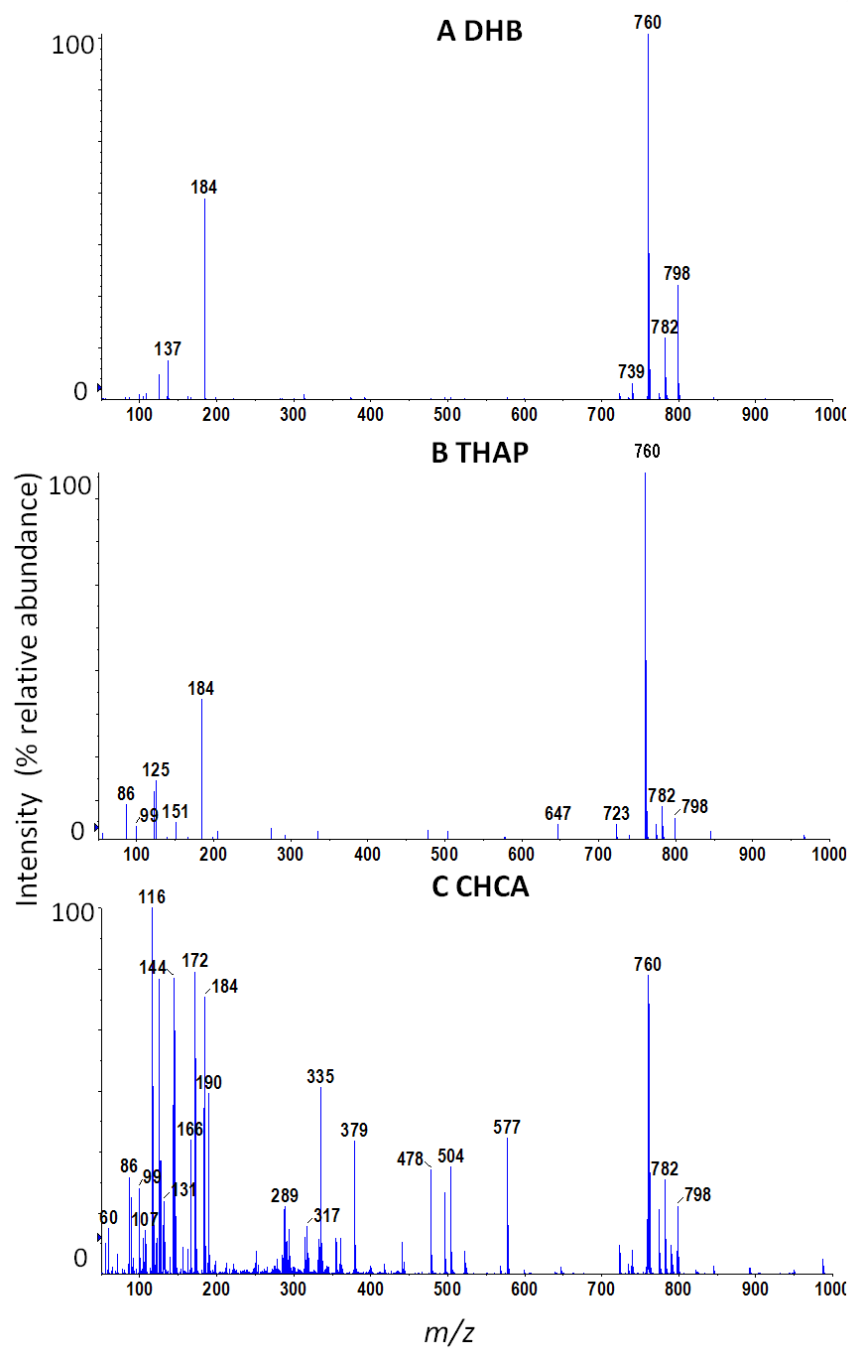
Figure 26 Representative MALDI mass spectra of PC (18:1/16:0) analysed with A) DHB, B) THAP or C) CHCA matrices with an Nd:YVO₄ laser.

A variety of different characteristics determine whether a molecule is a suitable matrix candidate for UV MALDI experiments. Some factors, such as vacuum stability are independent of the laser employed in the experiment and are unaffected by the laser used; others are very strongly dependent on the specific laser used or are affected by the laser properties such as the laser wavelength [237], laser fluence [79] and beam profile [79].

Consideration of the differing laser properties could help to rationalise the observed results. Traditional N_2 lasers are capable of delivering much higher laser powers than the high repetition rate Nd:YVO_4 counterpart (up to 100 µJ compared to 10 µJ). In the described experiments (in Chapter 2) the N_2 laser was operated between 25-40 µJ and the Nd:YVO_4 laser was operated at 8 µJ. It is possible that the decreased laser power available with the Nd:YVO_4 laser contributes to the poorer ionisation efficiency. Although operated at different laser powers, the use of a smaller diameter fibre for delivery (100 µm compared to 200 µm) leads to a similar fluence experience (energy per unit area). It has been shown that light penetrates different depths of the prepared sample when the laser wavelength is changed [238]. Hence higher laser fluences are required in lasers operating at 355 nm (such as the Nd:YVO_4 laser described here) in order to deposit the same energy on a certain unit volume when compared to lasers operating at 337 nm (such as N_2). This could contribute to the apparent difference in matrix suitability of the same analytes when the laser is changed.

Furthermore, matrices that form larger or more dense crystals in comparison to those which form small crystals by dried droplet deposition often require even greater laser powers or fluences. THAP matrix forms quite dense crystals, DHB forms quite large rod-like crystals and CHCA forms much smaller and less dense crystals as shown in Table 11. As it was not possible to increase the laser power for experiments performed with the Nd:YVO$_4$ laser at 355 nm, this could have contributed to the poor ionisation efficiency of these matrices when compared to CHCA.
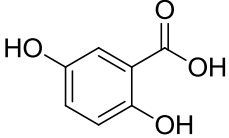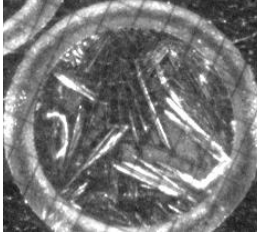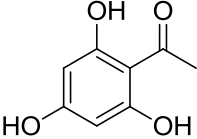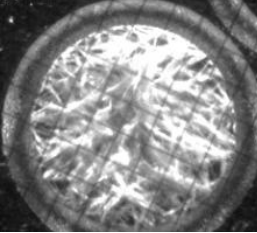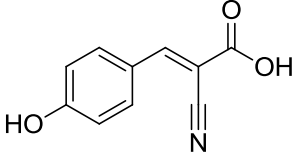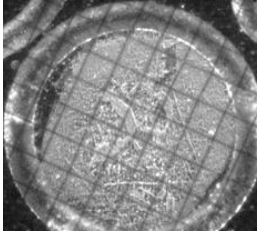
Matrix compound	Crystal Appearance In Source
2,5-Dihydroxybenzoic acid (DHB)	
2,4,6-Trihydroxyacetophenone (THAP)	
α-Cyanohydroxycinnamic acid (CHCA)	

Table 11 Showing the structures of DHB, THAP and CHCA matrices and the appearance of the typical crystals formed upon spotting of these matrices onto a stainless steel MALDI target.

In addition, the absorption efficiency of each matrix compound varies with changing wavelength. As these lasers operate at different wavelengths, the molar absorptivity of these matrix compounds could be very different at each wavelength which can have a significant impact on detection [239]. Profiles of the UV-vis absorption of CHCA and DHB have been documented in the literature. The extinction coefficient (ε) of CHCA is reported to be significantly higher than that of DHB in solution at both 337 nm and 355 nm [209]. However solid-state absorption profiles have revealed that the molar absorptivity of the two compounds is actually similar at these wavelengths, see Table 12 for details. Arguably it is therefore unlikely that this property of the matrix is causing the observed difference in selectivities of the two lasers.

Matrix	Extinction coefficient (ε) at 337 nm (soln) $dm^3\,mol^{-1}\,cm^{-1}$	Absorption$_{solid}$ at 337 nm (ss) rel. units	Extinction coefficient (ε) at 355 nm (soln) $dm^3\,mol^{-1}\,cm^{-1}$	Absorption$_{solid}$ at 355 nm (ss) rel. units
CHCA	27 500	0.95	12 500	0.95
DHB	1 200	0.93	500	0.95

Table 12 Molar absorptivity, extinction coeffeicients (ε), of CHCA and DHB matrices at 337 nm and 355 nm in solution (soln) and by solid state experiments (ss). These valuas are approximated from data reported in [209].

3.3.2 Incorporation of Sodium Additives via Inclusion in MALDI matrix solutions for Airspray Deposition

Additive salts were prepared in CHCA matrix solutions prior to airspray deposition. Initial experiments considered the addition of 5 mM sodium acetate, chloride or nitrate. Sample preparation via airspray deposition using an artist's airspray gun was first used to deposit matrix solutions. This deposition technique necessitates a degree of skill in the user, which comes with a lot of practice. It is important when depositing the matrix solution onto tissue sections to wet the tissue section sufficiently for extraction of analyte molecules however it is also important not to wet the tissue too much as this can lead to analyte delocalisation.

A large number of early attempts of image acquisition failed owing to insufficient tissue wetness or due to analyte delocalisation. Example images of fresh tissue sections which have been sprayed poorly with CHCA matrix via the airspray deposition technique are shown in Figure 27 a-c. The spatial distribution of potassium adducts of the three most abundant lipids in the tissue (PC 34:1, PC 32:0 and PC 36:1) are not confined to the tissue region but are delocalised around the tissue section on the MALDI target plate. Examples of more successful matrix deposition, which did not result in lipid delocalisation, are shown in Figure 27 d-i. These examples also demonstrate the importance of pixel size in imaging experiments. Example ion images acquired at 100

µm resolution (Figure 27 g-i) show anatomical features of the tissue more clearly than those acquired at 250 µm (Figure 27 d-f), enabling tissue features to be distinguished.
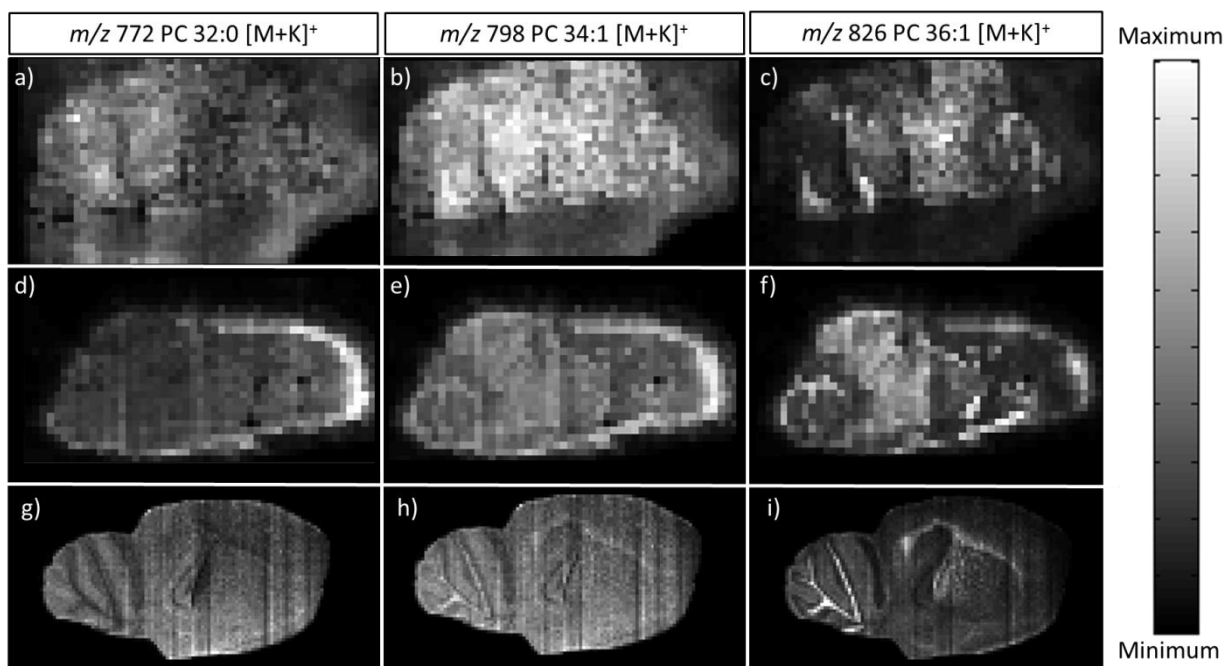
Figure 27 Ion images showing the spatial distribution of three PC lipids detected in mouse brain prepared by airspray deposition with CHCA matrix. Examples of tissue sprayed too wettly leading to analyte delocalisation are show in (a) PC 32:0, (b) PC 34:1 and (c) PC 36:1 (250 µm x 250 µm pixel resolution). Examples of tissue which has not been sprayed less wettly are show in (d) PC 32:0, (e) PC 34:1 and (f) PC 36:1 (250 µm x 250 µm pixel resolution). Examples of tissue which has not been sprayed too wettly are show in (g) PC 32:0, (h) PC 34:1 and (i) PC 36:1 (100 µm x 100 µm pixel resolution). Areas of no signal intensity are shown in black; regions of high signal intensity are shown in white.

It follows that ensuring reproducibility is a challenge for airspray deposition. A number of automatic deposition techniques have been developed in order to improve the reproducibility of matrix deposition for (tissue) imaging studies. Automated deposition technologies such as an acoustic droplet ejector [66], and an inkjet printer [67] have been described. A number of automated deposition robots, such as the TM Sprayer (Leap Technologies) and MALDI Sun Collect Spotter (SunChrom), are also now commercially available and have been used to prepare MALDI imaging tissue samples [145, 240, 241]. These automated instruments provide much greater controls of the deposition parameters in comparison to manual airspray deposition; small volumes of the matrix solution can be sprayed at precise flow rates of either 40 or 300 µL min^{-1} and higher temperatures than ambient, either 120 or 150 °C, depending on the salt. These deposition devices also offer the advantage of crystal size control (improved crystal homogeneity) and improved reproducibility.

Initial experiments were conducted at a raster speed of 1 mm s^{-1}; this is a compromise between acquiring data at 100 µm resolution at the fastest possible raster speed within the available instrumental parameters. Various lipid species were detected in tissue samples sprayed with CHCA matrix only. Relatively high abundances of potassium adducts of PC lipids were detected at *m/z* 798, 772 and 826 indicating the presence of PC lipids 32:0, 34:1 and 36:1, respectively. However, lipid ions were not readily detected in tissue sections sprayed with a solution containing a sodium salt. Very low intensity or

no lipid ions were detected in many locations when the tissue was sprayed with CHCA

containing a salt additive, as illustrated in Figure 28.
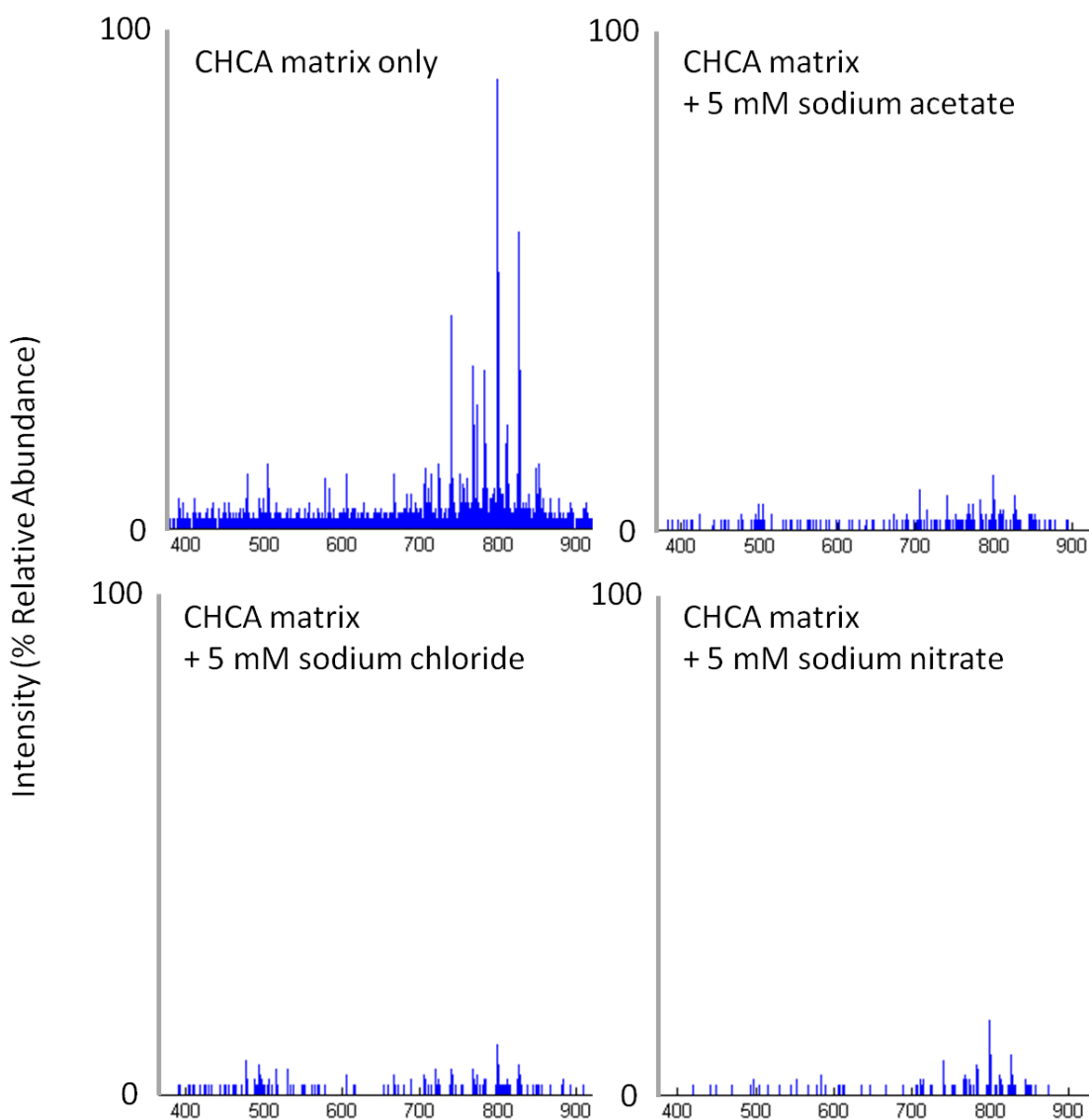
Figure 28 MALDI-MS single pixel spectra from imaging data sets acquired at a raster speed of 1 mm s^{-1} and 100 μm x 100 μm pixel resolution. Tissue sections sprayed with (clockwise from top left) CHCA matrix only, CHCA matrix containing 5 mM sodium acetate, CHCA matrix containing 5 mM sodium nitrate and CHCA matrix containing 5 mM sodium chloride are shown. Abundant lipid ions are shown in the region *m/z* 700-900 in the matrix only (control) sample. No, or very low abundances of lipid ions were detected in samples sprayed with matrix solutions containing a sodium salt.

Observation of the matrix crystals after image acquisition revealed that the crystals formed on the MALDI target plate and tissue sections were fully ablated when the tissue was sprayed with a solution of CHCA matrix. However when an additive salt was included the crystals were not fully ablated by the Nd:YVO$_4$ laser employed in this study. This laser delivers a relatively low energy per pulse at a higher repetition rate compared to traditional N$_2$ lasers [71, 75]. It seems likely that the crystals formed when an additive is included in the matrix are different; although the crystalls looked the same on the MALDI target plate, it is possible that the inclusion of a salt leads to the formation of more dense or structurally different crystals. It is conceivable that these crystals could not be fully ablated owing to reasons such as those described for THAP and DHB matrices, discussed in Chapter 3.3.1.

Previous MALDI-MS imaging studies considering the inclusion of salt additives to matrix solutions have not reported problematic acquisition at low salt concentration. Imaging data from tissue homogenates and thin tissue sections when 10 or 20 mM sodium or potassium acetate is included in the matrix solution have been described by Yuki and Mitsutoshi [184]. However a very different matrix deposition protocol, depositing only 200 µl of the matrix-salt solution in a single coating was used in the study. It is therefore unlikely that the crystals formed on tissue sections in our study (prepared by depositing 5 ml matrix solution in multiple coatings allowing drying time between applications) are comparable to those formed on tissue sections by the protocol used in the described investigation. Additionally, a Nd:YAG laser was used in Yuki and

Mitsutoshis investigation operated at a lower repetition rate than the Nd:YVO$_4$ laser used in this study.

A number of other studies have examined the use of acetate salts as cationising agents in tissue imaging studies of lipid species [135, 183]. These studies do not comment upon any problems encountered with matrix ablation, however these studies were each conducted with instrumentation fitted with either a N$_2$ or an Nd:YAG laser, both of which operate at higher laser powers in comparison to the Nd:YVO$_4$ laser used in the present study. This difference could account for the problems encountered with matrix ablation. However, the formation of compact structures when lithium citrate is included in CHCA matrix solutions and deposited onto a tissue surface has been described [145], requiring higher laser fluences to detect lipid ions in imaging experiments in comparison to control samples. Clearly additive selection, including counteranion choice, is important in MALDI-MS imaging experiments and can have a dramatic effect on the detection of lipid species.

Slowing the raster speed (which increases the laser dwell time per pixel location) showed that lipid ions were detected in tissue sections sprayed with salt-doped matrix solutions only when the slowest available raster speed was used (0.2 mm s^{-1}). Further data were therefore acquired at this raster speed. Acquiring data from a single sagittal section of mouse brain at a raster speed of 1 mm s^{-1} can be achieved in 25 minutes. Changing the raster speed to 0.2 mm s^{-1} increases the image acquistion time to 1 hour 30

minutes. This significantly reduces the potential for high-throughput analysis which is a potential disadvantage of this additive incorporation strategy.

Inclusion of 5 mM sodium acetate led to significantly lower ion counts of detected species compared to the control experiment as demonstrated in Figure 29. Moreover spectral quality was poorer; few lipid species were detected above the accepted signal to noise ratio threshold (3:1). Inclusion of TFA in the MALDI matrix solution did not improve spectral quality. Compared to lipid extract analysis this resullt is very different. Inclusion of 5 mM sodium acetate in the matrix for extract analysis reduced spectral complexity owing to decreased ion counts of other adducts, however this was not true of tissue imaging analysis. It is likely that the inclusion of TFA in matrix solutions affects the analysis of samples very differently when prepared by airspray deposition rather than dried droplet. Increasing the sodium acetate additive concentration to 20 mM did not significantly change the spectral quality. This is perhaps unsurprising; addition of increased concentrations of an acetate salt to the MALDI matrix solution in lipid extract analysis discussed in Chapter 2.3.2.2 resulted in no lipid ion detection.

A number of different lipid species were detected in tissue sections sprayed with matrix solutions containing 5 mM sodium chloride or nitrate. Potassium adducts of abundant PC lipids 32:0, 34:1, 36:1 and 38:6 were detected at *m/z* 798, 772 and 826, respectively, as shown in Figure 29. These *m/z* values correspond with lipid species detected in the control experiment when no additive salt was included in the matrix solution.

Furthermore, single ion images displaying the spatial distribution of PC 32:0, 34:1 and 36:1, illustrated in Figure 30, demonstrate that data acquired from samples sprayed with or without the inclusion of an additive salt show correlating distributions. PC 32:0 is detected preferentailly in the grey matter, PC 36:1 in the white matter and PC 34:1 is reasonably homogeneously distributed.

Clearly, these sodium salts are more useful additives in comparison to sodium acetate as they do not limit the detection of lipid ions in MALDI-MS imaging experiments. Sodium adducts of these lipids were also detected at m/z 756, 782 and 810. These lipid species were detected in the control experiment too, however the percentage relative abundances of sodium adducts detected for a single lipid species were lower than those of the potassium adducts. The relative abundance of sodium-lipid adducts was increased by addition of either of these sodium salts and were greater when sodium nitrate was included in the matrix. Here we show that both sodium chloride- and nitrate-doped matrix samples can be used to analyse tissue in imaging studies.
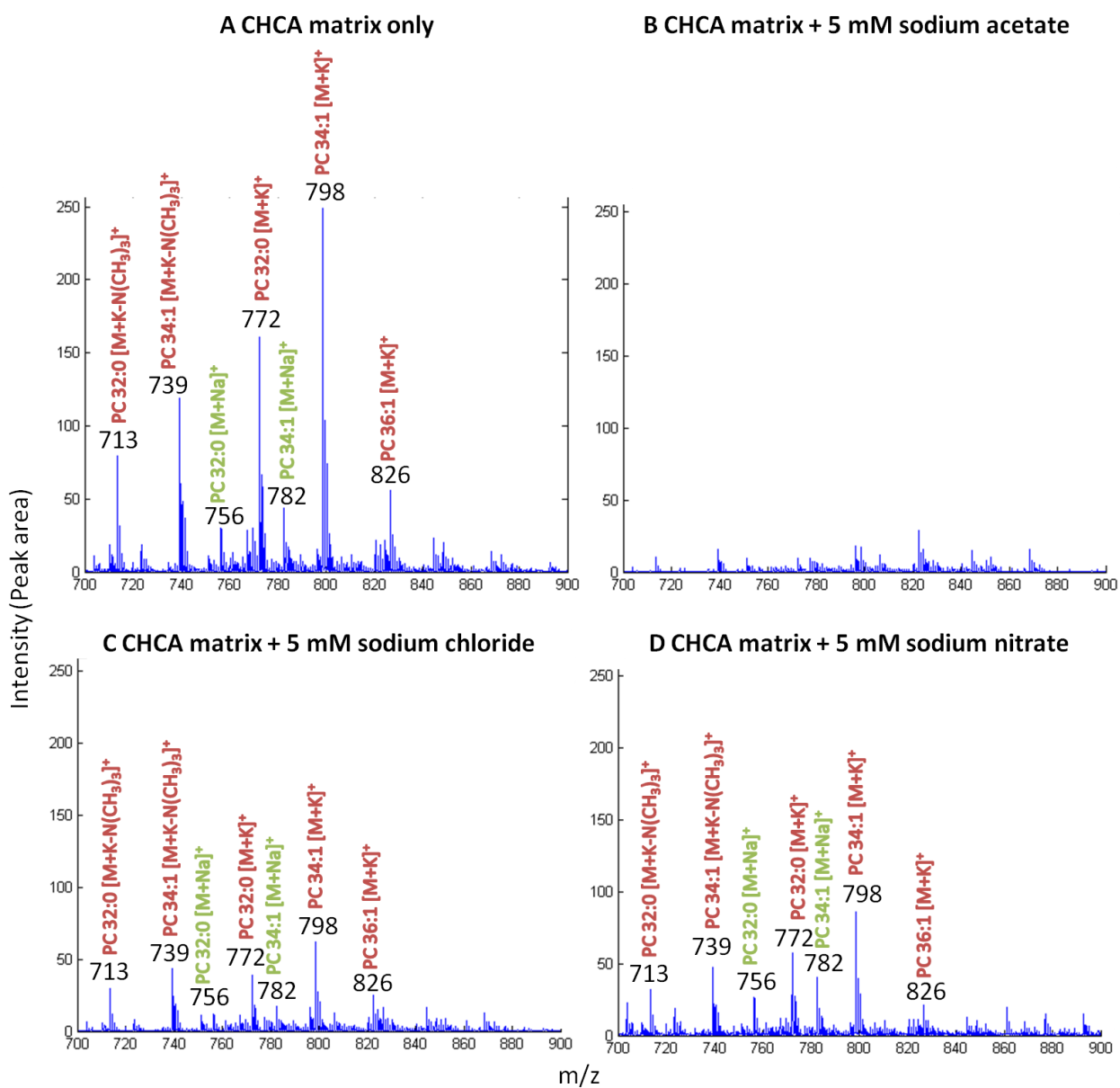
Figure 29 MALDI-MS mean spectra on tissue from imaging data sets acquired at a raster speed of 0.2 mm s^{-1} and 100 μm x 100 μm resolution. Tissue sections sprayed with A) CHCA matrix only, B) CHCA matrix containing 5 mM sodium acetate, C) CHCA matrix containing 5 mM sodium chloride and D) CHCA matrix containing 5 mM sodium nitrate are shown. Lipid ions detected in the region *m/z* 700-900 are highlighted.
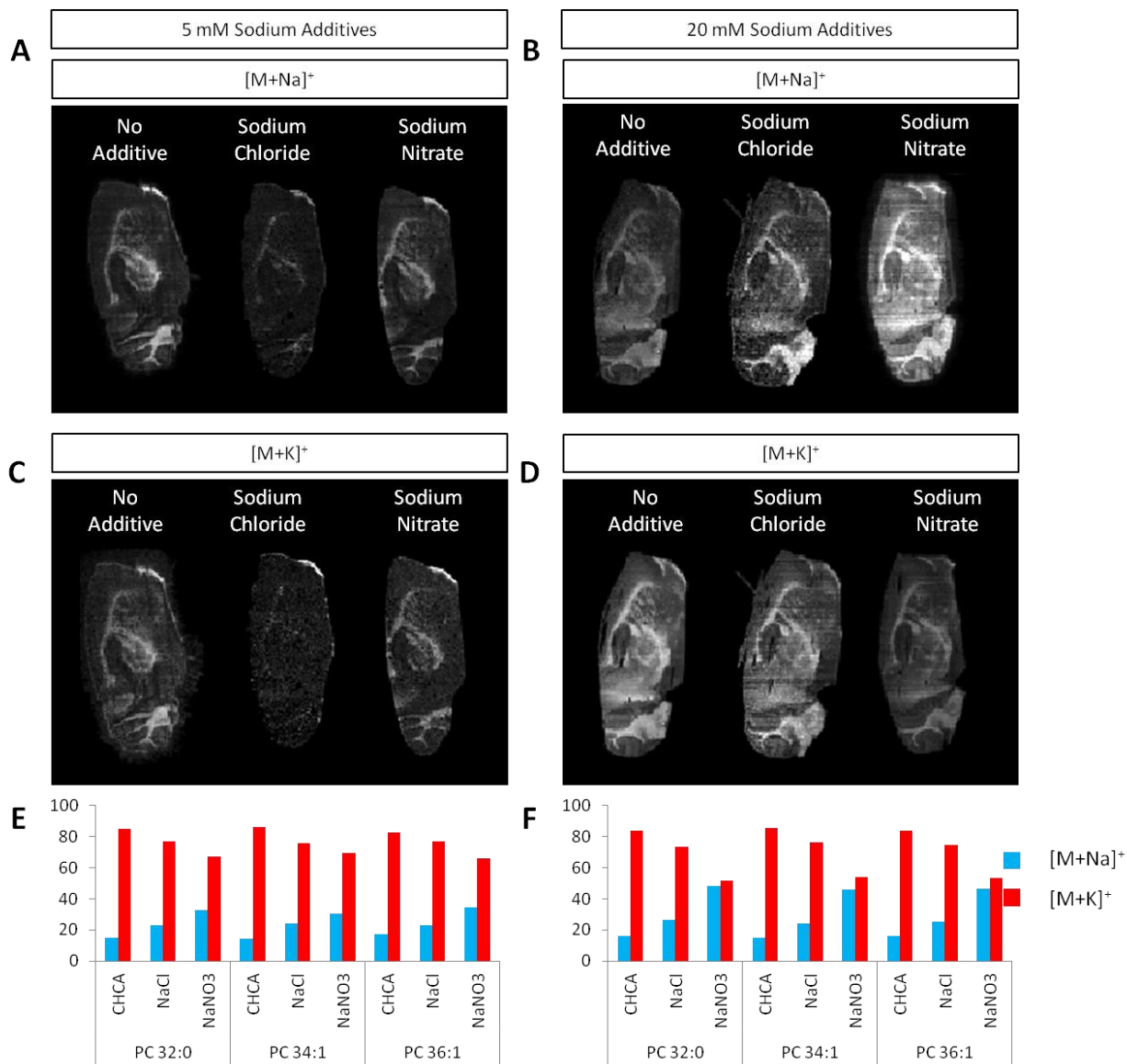
Figure 30 MALDI-MS single ion images (normalised to the total ion current (TIC)) of A) [M+Na]+ adducts and B) [M+K]+ adducts of PC 36:1 detected in mouse brain (100 µm x 100 µm pixel resolution). Images show samples sprayed with CHCA matrix including 0 or 5 mM sodium additive (left column), or CHCA matrix including 0 or 20 mM sodium additive (right column). Areas of zero counts are black and areas of maximum intensity are shown in white. The relative percentage of sodium and potassium adducts detected for three different lipid species PC lipids 32:0, 34:1 and 36:1 are shown in the bar charts E) with the inclusion of 5 mM sodium additives and F) 20 mM sodium additives.

Increasing the sodium additive concentration to 20 mM further increased the relative abundance of sodium adducts when either salt was included in the matrix solution. Nevertheless, the relative abundance of sodium adducts was more greatly increased when sodium nitrate was included in the matrix solution as shown in Figure 30 and Figure 31. Spectral quality decreased with increasing sodium chloride concentration whereas no significant change in spectral quality was observed with increasing sodium nitrate concentration. This indicates that the inclusion of sodium nitrate is more beneficial across a concentration range. Here it is shown that the nitrate counteranion yields superior results in comparison to the chloride, extending trends reported for lipid extract analysis in Chapter 2 to imaging analysis.

Increasing the additive concentration to 40 mM led to clogging of the sprayer nozzle which made the practicality of spraying additive-doped matrix solutions very difficult, hence data were not acquired at higher salt additive concentrations. Here it is reported for the first time that the inclusion of sodium nitrate can significantly increase the relative abundance of the respective cationic adduct in MALDI-MS imaging tissue studies and might therefore be more useful as a cationising agent compared to the previously reported acetate salt. The relative utility of sodium acetate, chloride and nitrate salts with respect to increasing ion counts of a lipid adduct appears to agree with our previously described lipid extract data described in Chapter 2 [235].
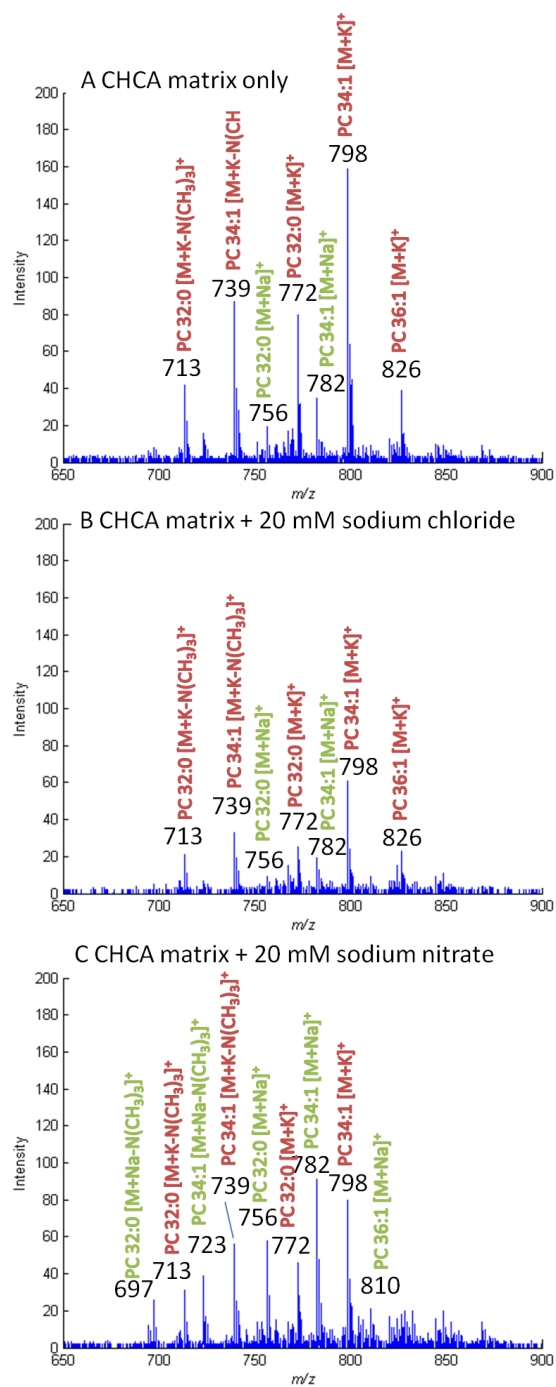
Figure 31 MALDI-MS mean spectra on tissue from imaging data sets acquired at a raster speed of 0.2 mm s-1 and 100 μm x 100 μm resolution. Tissue sections sprayed with CHCA matrix only (top), CHCA matrix containing 20 mM sodium chloride (middle) and CHCA matrix containing 20 mM sodium nitrate (bottom) are shown. Lipid ions detected in the region *m/z* 700-900 are highlighted.

The relative abundance of potassium adducts (which are naturally highly abundant in fresh tissue samples) remains high when sodium salts are incorporated, indicating that influencing adduct formation via salt addition in thin tissue sections is more challenging in comparison to lipid extract analysis. At the same additive concentrations investigated here, sodium-lipid adducts were the most abundant in lipid extract samples (except 20 mM sodium acetate). For further discussion refer to Chapter 2.However extract samples prepared by dried-droplet deposition cannot be directly compared with thin tissue sections prepared by airspray deposition.

Previous imaging studies of lipids have considered the inclusion of sodium and potassium acetate salts in matrix solutions [184]. The inclusion of potassium acetate in matrix solutions reportedly leads to increased sensitivity of the detection of polar lipids such as PC species and lower sensitivity for non-polar lipids in homogenates. It is not explicitly commented whether sodium acetate gave similar results. Our study does not show promising results when sodium acetate is included in the matrix solution. Furthermore, inclusion of any of these additive salts did not change the types of lipids (polar or non-polar) detected in murine brain. Differences in results could be accounted for by the fact that different samples (tissue homogenates) and sample preparations were considered in each investigation.

3.3.3 Incorporation of Lithium Additives via Inclusion in MALDI matrix solutions for Airspray Deposition

3.3.3.1 Airspray

Airspray deposition of matrix solutions containing 20 mM lithium chloride or nitrate led to clogging of the sprayer nozzle due to crystallisation of the salt and/or CHCA matrix at the sprayer nozzle tip. This significantly impeded the success of the deposition technique. Similar issues had been described in a previous study which examined the incorporation of lithium salts into CHCA matrix solutions, even though solutions were deposited via a heated nozzle[145]. Difficulties with additive concentration optimisation were also described by Cerruti *et al*. They described the formation of elongated clusters and compact crystal structures when some lithium salts were included in matrix solutions. These are undesirable as they can cause analyte delocalisation or require higher laser fluences for ablation.

Tissue sections sprayed with matrix solutions containing lithium salts did not lead to the detection of lithium-lipid adducts and spectra were similar to those detected when no salt additive was included in the matrix as illustrated in Figure 32.High abundances of potassium adducts of PC 32:0, 34:1 and 36:1 were detected at *m/z* 772, 798 and 826, respectively. Lower abundances of sodium adducts of these lipids were also detected at *m/z* 756, 782 and 810, as is expected in freshly frozen tissue. Lithium-lipid adducts were not detected in these samples. Clearly this route to lithium ion incorporation was

unsuccessful. Which is perhaps surprising as the abundances of sodium-lipid adducts were increased in similar preparations. However doping of MALDI matrix solutions with lithium chloride did not prove as successful in lipid extract analysis in comparison to similar preparations with a range of sodium salts.

Successful incorporation of lithium onto tissue samples via a similar strategy has been described previously and was achieved by including one of a variety of lithium salts in the matrix solution [145]. It is therefore unexpected that our lithium ion incorporation strategy proved ineffective. However, an automated deposition apparatus, with which a number of parameters such as spray heating temperature and spraying flow rate could be controlled, was used in the described study. These parameters were optimised separately for each solution deposited and could explain why it was not possible to obtain similar results using a manual deposition technique. Also, faster flow rates and a higher spray heating temperature were used for CHCA matrix including lithium chloride in comparison to CHCA matrix with no salt additive. Clearly different salt additive approaches need to be considered in order to incorporate lithium ions into tissue samples.
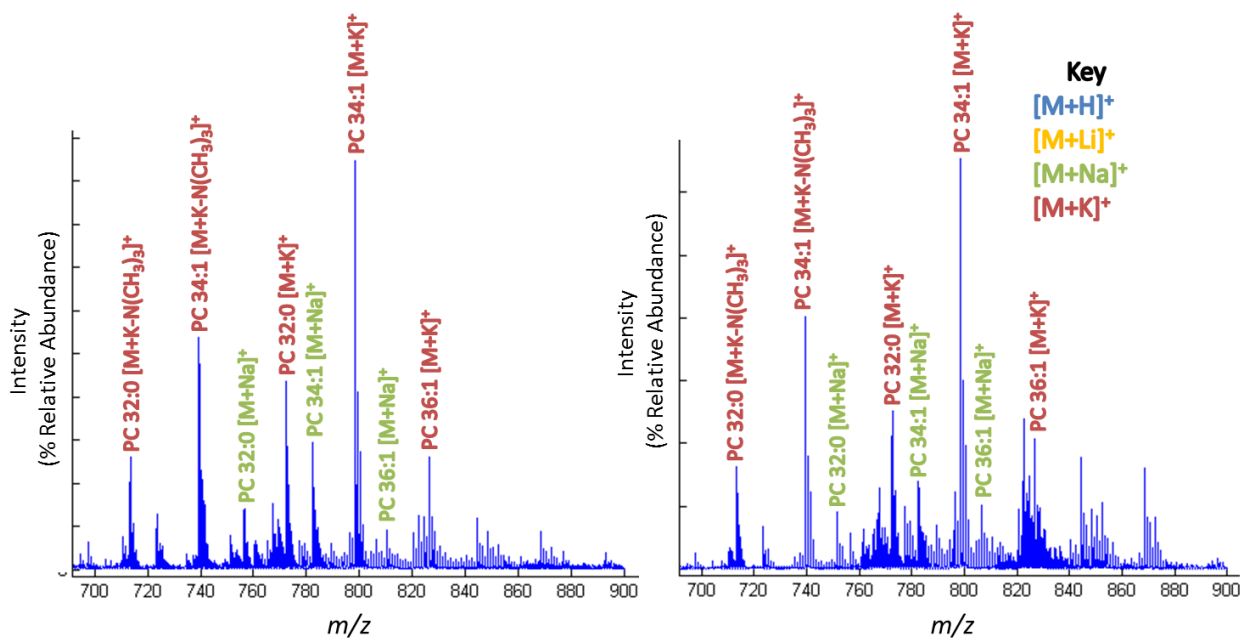
Figure 32 Mean spectrum on tissue showing phospholipid region *m/z* 700-900 showing lipid adducts ([M+H]+, [M+Li]+, [M+Na]+, [M+K]+) detected in sagittal tissue sections of mouse brain sprayed with (left) CHCA matrix (no additive) or (right) CHCA with 20 mM lithium chloride.

3.3.3.2 Dry-coating

As the main problem with lithium salt deposition appeared to be crystallisation of the salt-doped matrix solution leading to nozzle blockage of the sprayer, next the use of a solvent-free deposition technique which would eliminate the need to spray a solution was considered. In this approach, lithium salts were ground together with the CHCA matrix powder in a pestle and mortar before depositing onto the tissue via an analytical sieve. The preparation of samples for deposition by this method was relatively straightforward and less practice was required in order to deposit a homogeneous layer onto the tissue by this preparation method in comparison to airspray. Dry-coating is a solvent-free deposition method and therefore analyte delocalisation was not found to be a problem as with the airspray deposition method. This sample preparation method has previously been described as simple and used to reduce problems with delocalisation of analytes [62].

Inclusion of lithium chloride in CHCA matrix for dry-coating preparations proved troublesome. Grinding the matrix and lithium salt together led to the formation of agglomerates, probably owing to the hygroscopic nature of lithium chloride. This clumpy sample was unsuitable for this deposition technique as it could not be deposited through a 200 μm mesh sieve. A suitable sample was formed when lithium nitrate (which is less hygroscopic) was ground with CHCA matrix. Deposition of this powdered sample did not differ significantly to the salt-free sample. The employment of

this solvent-free method also eliminated the above described problems with laser ablation of the matrix-salt sample. As the powder sample adheres to the tissue surface, crystal formation is very different to that formed by airspray deposition. For this reason, data could be acquired at the optimal raster speed for 100 μm resolution images, hence the high-throughput capabilities of analysis using the Nd:YVO$_4$ laser remain upon salt inclusion by this sample preparation strategy.

This deposition method resulted in the detection of high abundances of protonated lipid adducts alongside lithium and other cationic adducts leading to very complex spectra. Very high abundances of protonated adducts at *m/z* 734, 760 and 788 (PC 32:0, 34:1 and 36:1, respectively) as well as potassium and sodium cationic adducts (*m/z* 772, 798 and 826, [M+K]$^+$ and *m/z* 756, 782 and 810, [M+Na]$^+$ of PC 32:0, 34:1 and 36:1) were evident in the control experiment as well as in experiments which included lithium nitrate, as shown in Figure 33. Relatively high abundances of protonated alongside cationic lipid adducts have been reported previously using solvent-free methods [70].

This additive incorporation strategy successfully led to the detection of lithium adducts of these lipids at *m/z* 740, 766 and 794. The detection of lithium-lipid adducts of pure fatty acid samples preloaded in Bacti plates has been reported by a similar preparation [226]. However the relative complexity of the mass spectra acquired from the tissue samples described herein was greatly increased by this deposition technique. This is in part owing to the fact that lithium-lipid adducts are detected in a similar *m/z* window to

protonated, sodium and potassium adducts, further compounding the problem of overlapping *m/z* values of different adducts of different lipids. Although solvent-free methods have proven useful for analytes which predominantly form protonated adducts [242], lipid analysis was further complicated.
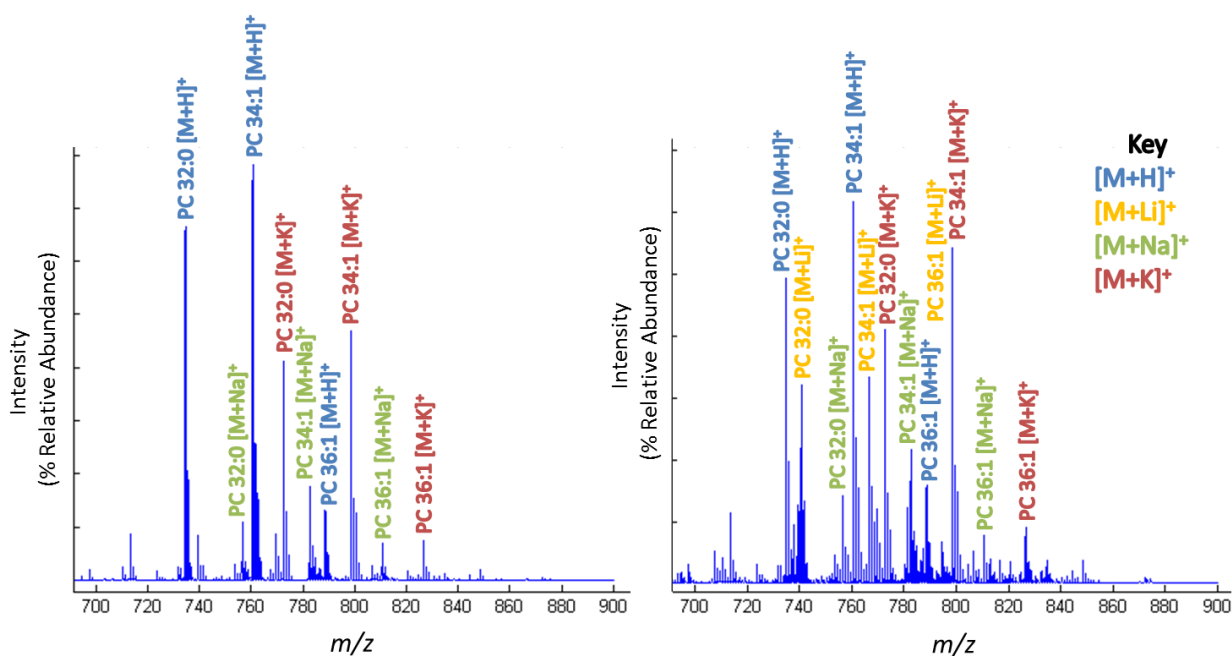
Figure 33 Mean spectrum on tissue showing phospholipid region *m/z* 700-900 showing lipid adducts ([M+H]+, [M+Li]+, [M+Na]+, [M+K]+) detected in sagittal tissue sections of mouse brain dry-coated with (left) CHCA matrix (no additive) or (right) CHCA with 5 mM lithium nitrate.

3.4 Conclusions

The inclusion of a nitrate rather than a chloride or acetate salt led to a greater change in the relative abundance of the respective (sodium) cationic lipid adducts detected, which is in agreement with the results of lipid extract studies. However it is clear from these investigations that increasing sensitivity and decreasing spectral complexity by salt addition in MALDI-MS imaging experiments is not as straightforward when compared to affecting the same pathways in lipid extract studies.

The number of experimental parameters affected by the inclusion of salts in matrix solutions is significantly increased when performing imaging experiments. Firstly, the airspray sample preparation (compared to dried droplet) is more greatly affected by salt addition as inclusion of salts in matrix solutions appears to lead to nozzle blockage with increasing salt additive concentration. The ability to acquire high-throughput data is significantly reduced, most likely owing to differences in crystal formation. Furthermore, both spectral quality and overall sensitivity is decreased when an additive salt is included in the matrix solution for airspray deposition. Finally, decreased spectral complexity or increased sensitivity of a certain adduct was not achieved (as in lipid extract experiments) by salt addition in MALDI-MS imaging experiments.

Consideration of a solvent-free matrix deposition technique as an additive incorporation strategy suffered fewer practical problems; difficulties experienced with sample deposition and laser ablation were not encountered when tissue samples were dry-

coated with an additive-doped matrix sample. However, increased spectral complexity arising from the detection of protonated alongside a variety of cationic lipid adducts leads to decreased sensitivity and introduces increased problems with overlapping *m/z* values of different adducts of different lipids. Clearly there is a need to pursue alternative cation introduction strategies for lipid imaging experiments. Further work will consider alternative routes to additive incorporation.

Analysis of fixed tissue samples by MALDI-MS imaging has shown that high abundances of sodium lipid adducts are detected in these samples [241], owing to the use of sodium salts to buffer fixative solutions. It is hypothesised that this could be a promising route to ion incorporation and will consider whether substitution of these buffering salts with lithium salts is a suitable lithium ion introduction strategy in Chapter 4.

4. Formal Lithium Fixation as a Route to Lithium Ion Incorporation into tissue for improved *in situ* analysis of phospholipids by MALDI

4.1 Introduction

Fixation of tissue samples is important to prevent proteolytic degradation[243], stabilise fine structure and obstruct bacterial growth. Formaldehyde is a non-coagulant fixative which fixes tissue via the formation of cross-linking methylene bridges between neutral amino or similar groups in proteins [244, 245]. The chemical process of formaldehyde fixation is slow and complete fixation is limited by the rate of chemical reaction and so tissue must be immersed long enough for cross-linking to occur [246, 247]. Formaldehyde is generally used as a 4% solution in water, known commercially as *formalin*.

Formalin is widely reported to be compatible with histological staining and is extensively used. With a view to tissue storage formalin is often used as an isotonic solution such as formal saline i.e.sodium chloride in formalin. The isotonic nature of such formal solutions (containing formaldehyde as a chemical tissue fixative) limits diffusion of tissue components. Formal saline is acidic. For this reason, some laboratories prefer to use sodium phosphate salts to neutrally buffer the solution. Both preparations involve sodium salts to maintain physiological conditions [248].

A number of other salts have been included in formalin (formal solutions) with a view to improving tissue studies by analytical techniques such as microscopy. Mercuric chloride has been included in formalin combined with acetic acid to enhance nuclear detail in light microscopy. Alternatives based on zinc have also proven successful for improved tissue contrast for light microscopy [249], increasing staining density of cell nuclei [250].

Contrast of tissue or cell features can be amplified for electron microscopy by staining with heavy metals which efficiently scatter electrons [251, 252]. Suitable stains should preferentially bind a particular structural constituent or species [252]. Heavy metals such as osmium [253, 254], lead [255] and uranium [256] have all been included in fixation and staining preparations for electron microscopy. Many are described in targeted approaches for a specific analyte; osmium tetroxide stains for unsaturated lipids [257], ruthenium for polymers [258], lead hydroxide for RNA containing cell components [259] and barium hydroxide for the golgi regions of hepatic cells [259]. Formal solutions can also be used as primary fixatives prior to other treatment to improve a particular analysis [260]. Clearly careful consideration of the analyte of interest is important when choosing a staining or fixation method and it is not unusual to use numerous fixation techniques for multiple analysis of a single tissue sample [247].

Mass spectrometry imaging offers analysts the opportunity to simultaneously acquire information regarding both composition and spatial distribution of analytes. Osmium

tetroxide (OsO_4) staining for targeted analysis of lipids by time-of-flight secondary ion mass spectrometry (TOF-SIMS) has been reported previously [261], hence it is possible to direct mass spectrometry analysis using stains and fixatives. Formaldehyde does not act as a fixative for lipids and is therefore a suitable medium to consider for their analysis [262, 263]. MALDI-MS imaging of tissue fixed in formal saline or phosphate buffered formalin have been shown to lead to the detection of high abundances of sodium adducts of lipids [241, 264]. Lipids form multiple adducts in tissue and dissociation studies of different adducts have shown that greater product ion information is obtained when lithium-lipid adducts are dissociated [19, 22, 143, 145, 150, 230, 235, 265, 266]. Furthermore, the *sn*-1 and *sn*-2 side-chains can be assigned; loss of the *sn*-1 fatty acid side-chain will be detected with greater abundance [223, 230]. This becomes particularly important when identifying potential disease biomarkers in complex tissue samples by mass spectrometry [163, 177, 179, 267, 268].

Lithium salts are not naturally abundant in tissue and so the task of lithium ion introduction arises. Conventional approaches to lithium incorporation into tissue, by mixing salts with the matrix compounds prior to matrix deposition, were discussed in chapter 3 of this thesis. Owing to the failure of these approaches to incorporate high abundances of lithium lipid adducts, without compromising the sensitivity of the experiment through detection of multiple lipid adduct types, the need to pursue alternative ion incorporation strategies was highlighted.

In this Chapter, fixation in a formal lithium solution is presented as a tissue treatment in a targeted approach for the improved analysis of lipid species by MALDI-MS and imaging. The formation of lithium-lipid adducts *in situ* by this route allows the analyst to acquire compositional information that can also be mapped in ion images, showing the spatial distribution of particular lipid species within the tissue, as well as enhancing their identification by CID. Using this sample preparation technique MS/MS images of lipids in which structurally characteristic product ions of a particular lipid can be mapped were also acquired, showing the spatial location of a single identifiable analyte. The compatibility of formal lithium fixation with a number of common histological staining techniques was established using sections of human liver from normal and diseased specimens, thus highlighting the potential of this approach for biomarker identification.

4.2 Experimental

4.2.1 Materials

All salts (NaCl, LiCl and LiNO$_3$), α-cyano-4-hydroxycinnamic acid matrix (CHCA) and formic acid (FA) were purchased from Sigma Aldrich (Gillingham, UK). Formaldehyde was purchased from Adams Healthcare (Swindon, UK). Methanol (HPLC grade) was purchased from Fisher Scientific (Leicestershire, UK). Water was purified by an ELGA Option 3 system (Marlow, UK). Haematoxylin and eosin (H&E), van Gieson, Oil Red O and Celestine Blue stains, Scott's tap water substitute, acid alcohol and alcohol were purchased from Leica Biosystems (UK). DPX mountant (a mix of distyrene, plasticiser, and xylene), acetone, and Immu-Mount were all purchased from Thermo Scientific (Shandon, UK). Stainless steel MALDI target plates were purchased from AB Sciex (Framingham, USA), conductive ITO-coated glass slides from Bruker Daltonik (Bremen, Germany) and plain glass and poly-lysine-coated glass slides from Leica (UK).

4.2.2 Human Tissue Samples

Explanted liver tissue from patients being transplanted for chronic end-stage liver disease (Non-alcoholic steatohepatitis, NASH) was obtained from the Queen Elizabeth Hospital, Birmingham, UK. Fresh tissue was cut into approximately 1cm^3 pieces and immediately frozen by immersion in liquid nitrogen. Samples were then stored at -80 ˚C until cryosectioning was performed. All tissue was collected with informed written consent under local ethics committee approval.

4.2.3 Fixative Solutions

Formal saline was prepared according to standard protocols, 0.154 M NaCl in formalin, where formalin is a solution of 10% formaldehyde solution (40% in methanol) in water resulting in a solution which contains 4% formaldehyde. Formal lithium solutions were prepared similarly: 0.154 M LiCl or $LiNO_3$ salt in formalin.

4.2.4 Tissue Block Fixation

A snap-frozen whole rat brain was sectioned into four. Each sector was treated differently. The first remained frozen and was stored at -80°C, the rest were immersion-fixed in either formal saline or formal lithium (LiCl or $LiNO_3$) at room temperature. Immersion fixation of tissue blocks was achieved by immersing tissue blocks in formal saline or formal lithium (LiCl or $LiNO_3$ salt) in a volume 20x their mass for 48 hours. Once fixed, tissue blocks were stored at -80 °C until sectioning at -18 °C (Leica CM 1850 Cryostat (Milton Keynes, UK)) at 12 µm before thaw-mounting onto a stainless steel MALDI imaging target or plain glass slides for LESA-ESI-MS or at 6 µm before thaw-mounted onto poly-lysine-coated glass slides for staining. Freezing of fixed tissue facilitates the preparation of tissue blocks for sectioning.

4.2.5 Single Section Fixation

Snap-frozen mouse brain tissue was sectioned differently for mass spectrometry (12 µm) and staining (6 µm) (Leica CM 1850 Cryostat (Milton Keynes, UK)). Human liver tissue blocks were sectioned 6 µm thick (Bright OTF (Cambridgeshire, UK)). Tissue sections

were thaw-mounted onto ITO coated glass slides for MALDI analysis on an ultrafleXtreme instrument, plain glass slides for LESA-ESI analysis or poly-lysine-coated glass for staining. Slides were then submerged in a fixative solution for 30 minutes. Control (fresh) sections were not treated with a fixative.

4.2.6 Staining

Serial tissue sections to those used for mass spectrometry were treated by fixation in a formal solution or not fixed (control fresh tissue) and stained. Groups of serially treated tissue sections were stained with H&E, van Gieson or Oil Red O according to standard protocols. A Ziess Axioskop 40 microscope, 10 x objectives, was used to obtain microscopic images using Ziess AxioVision software.

4.2.7 Matrix Application

Matrix solutions of CHCA (20 mg/mL, 80 % CH_3OH) were deposited using an artist's airbrush purchased from Draper (Hampshire, UK) propelled by dry N_2. Two consecutive spray passes were followed by ten seconds drying time, until 10 mL was deposited, from a distance of 20 cm from the plate.

4.2.8 Mass Spectrometry

MALDI-MSI, MS/MS and MS/MS imaging studies of murine samples were carried out on a QSTAR XL Q-TOF mass spectrometer (AB Sciex). An Elforlight (Daventry, UK) Nd:YVO$_4$ DPSS laser (355 nm) was triggered by a Thurlby Thandar Instruments

(Huntingdon, Cambridgeshire) TGP110 10 MHz pulse generator, coupled to the MALDI source via a 100 µm core diameter fiber optic patch cord (Edmund Optics, NA=0.22) and operated at 5 kHz and approximately 8 µJ. Analysis was performed in positive ion mode with a pixel size of 100 by 100 µm, *m/z* range 400-900, focusing potential (FP) of 85 and declustering potential (DP2) of 35. For MS/MS imaging, CID was performed with N_2 gas at collision energy of 40 eV. All images were collected in raster mode at a speed of 1 mm s^{-1} and acquired in ≈ 25 minutes.

MALDI-MSI of human liver tissue was acquired on an ultrafleXtreme TOF/TOF mass spectrometer (Bruker Daltonics) with a smartbeam-II Nd:YAG (355 nm) laser operated at 1 kHz and laser energy was optimised between 35%-55% of the available power. Analysis was performed in reflectron TOF and positive ion mode with a pixel size 100 by 100 µm, *m/z* region 60-1000. Images were acquired in spot-imaging mode summing 500 laser shots per pixel. Each full tissue section image was acquired in ≈ 5 hours.

4.2.9 Data Conversion and Analysis

MALDI data acquired using the QSTAR XL was analysed using Analyst QS 1.1 and MATLAB. The data were converted from the AB Sciex .wiff proprietary file format to mzML using AB MS Data Converter (AB Sciex version 1.3) and then converted to imzML using imzMLConverter [236] and processed in MATLAB (version 7.8.0 (2009a), Math Works Inc., USA). For all images displayed, peak information is the summed ion intensity from within a 0.1 Dalton window centred on the peak of interest. MALDI data acquired using the ultrafleXtreme was analysed using MATLAB. Data were converted from the Bruker proprietary format to mzML using a custom MATLAB script and then converted to imzML using imzMLConverter.

4.3 Results and Discussion

4.3.1 MALDI-MS Imaging analysis of Formal Fixed Tissues

Preparation of formal saline according to the standard protocol (0.154 M in formalin) substituting sodium chloride with a lithium salt did not alter the final pH of the solution. Furthermore, no lipids were detected by MALDI-MS analysis of the fixative solutions *post* fixation of tissue, indicating that there was no lipid migration into the supernatant solution. In addition, formal lithium fixation led to similar indicative discolouration of the tissue as that using formal saline. Sectioning of tissue fixed in formal lithium did not appear to differ to the standard formal saline preparation and thaw-mounting of the tissue sections onto either stainless steel MALDI target plates, plain or coated glass slides was unaffected by treatment in this fixative.

Preparing formal lithium fixed tissue samples for imaging analysis by the widely employed deposition method of airspray, with CHCA matrix solutions, led to similar matrix crystal homogeneity as when spraying freshly frozen and formal saline-fixed tissue sections. Introducing lithium during tissue fixation removes the need for salt inclusion in MALDI matrix solutions during the matrix deposition procedure; the crystal homogeneity is unchanged by formal preparations hence many of the problems described in Chapter 3 of this thesis in previous studies [145] are removed by immersion fixation. Furthermore, these images were acquired at a raster speed of 1 mm s^{-1}, enabling

relatively high-speed imaging of lithium adducts, and hence this methodology lends itself to high-throughput analysis.

Lipid species detected in formal saline-fixed tissue were similar to those detected in freshly frozen tissue. Predominantly sodium-lipid adducts were detected when analysing fixed tissue prepared with a sodium salt, agreeing with previous literature [241]. The three most abundant lipid peaks in the *m/z* region 700-900 in freshly frozen-tissue analysis are *m/z* 772, 798 and 826, corresponding to $[M+K]^+$ of PC 32:0, 34:1 and 36:1, respectively. The most abundant peaks in the lipid region shift to *m/z* 756, 782 and 810 in formal saline fixed tissue, indicating a change in predominant adduct formation to $[M+Na]^+$ lipid adducts, as shown in Figure 34.

The lipid species detected in formal lithium-fixed tissue were also comparable to those detected in freshly frozen and formal saline samples, with a mass shift of Δ-32 compared to freshly frozen ($[M+K]^+$ to $[M+Li]^+$). When analysing formal lithium-fixed tissue samples the most abundant peaks detected in the region *m/z* 700-900 were 740, 766 and 794, $[M+Li]^+$ of PC 32:0, 34:1 and 36:1 respectively as illustrated in Figure 34. Similar species were reported in tissue studies which describe lithium ion introduction via inclusion in matrix solutions [145]. It would appear that fixing tissue in an isotonic lithium salt fixative solution leads to a shift in predominant adduct formation similar to that previously reported in isotonic or buffered sodium salt fixative solutions.
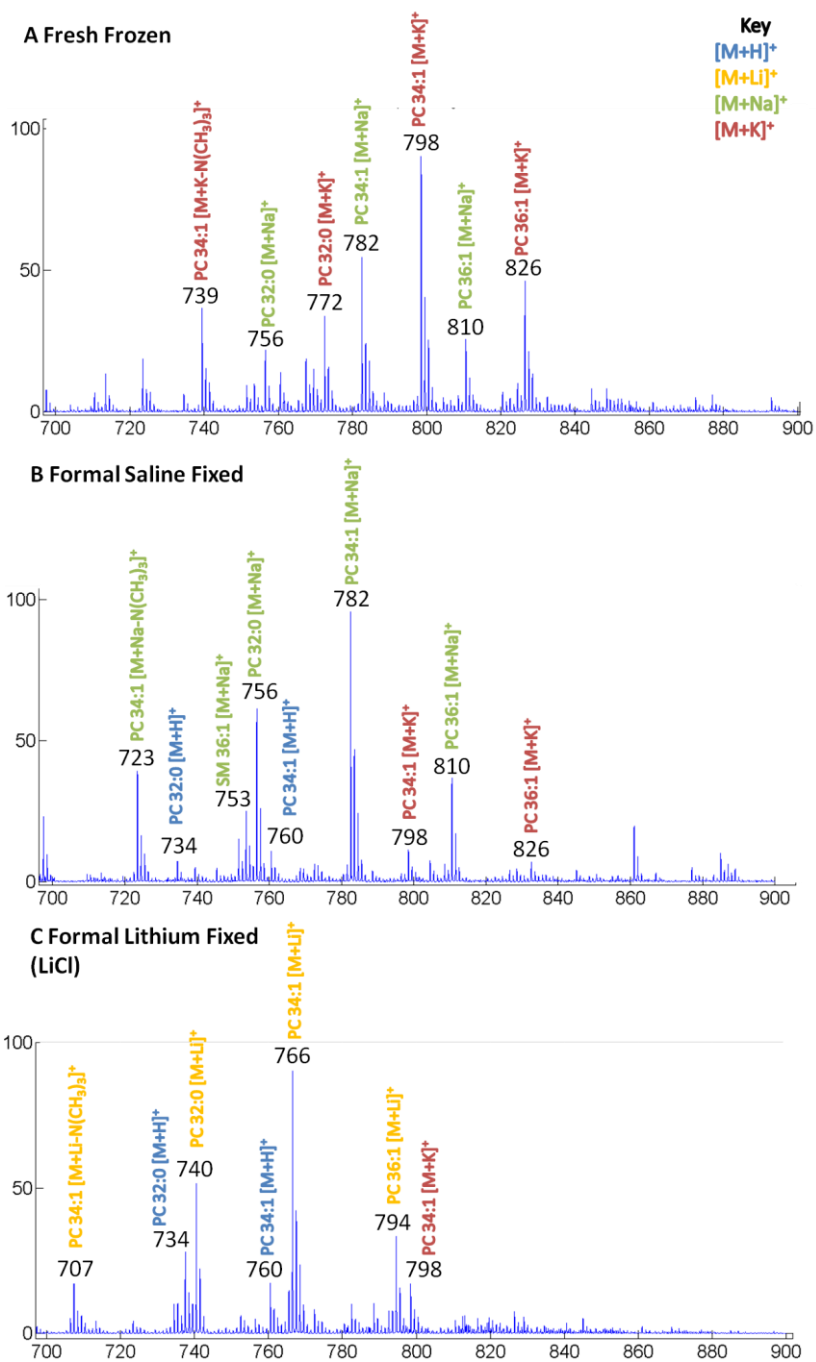
Figure 34 Mean spectra of species detected between *m/z* 700-900 on tissue during acquisition of MALDI-MS images. A) Freshly frozen tissue B) Formal saline fixed (NaCl) C) Formal lithium fixed (LiCl). Adducts of lipid species are highlighted in the spectra: potassium adducts are red, sodium adducts are green, protonated adducts are in blue and lithium adducts are yellow. The spectral quality and species detected by each sample preparation do not change, only the dominant lipid adduct.

Mean spectra of species detected in tissue during imaging analysis are shown in Figure 34. It is clear from this figure just how successful this preparation method is for forming the predominant lipid adducts detected. Further adduct confirmation can be achieved via MS/MS analysis as the head-group product ion changes corresponding to the lipid adduct dissociated [150]. The spectral quality of formal lithium-fixed samples is similar to that of freshly frozen and formal saline-fixed tissue. There did not appear to be a significant change in the signal to noise ratio by preparing the tissue using this method and the ion counts of detected lipid species were of a similar order of magnitude. In short, introducing lithium by formal lithium fixation does not appear to compromise spectral quality in any way.

However, Figure 35 showing the relative abundances of detected lipid adducts demonstrates that although lithium-lipid adducts are detected in high relative abundance in formal lithium-fixed tissue samples, they are not the only adducts detected. Potassium, sodium and protonated lipid adducts are detected in lower abundances. As the relative abundances of lithium adducts of each lipid were much higher than all other adducts, spectral complexity was not significantly increased, certainly not to the same extent as additive incorporation via tissue dry-coating (discussed in Chapter 3.3.3.2). Furthermore, immersion fixation of single sections of freshly frozen tissue sections 12-6 μm thick were thaw mounted on to MALDI target plates in a formal lithium solution for 20 minutes gave similar results (data not shown),

showing the versatility of this methodology for targeted lipid analysis of either whole

organs or single sections.
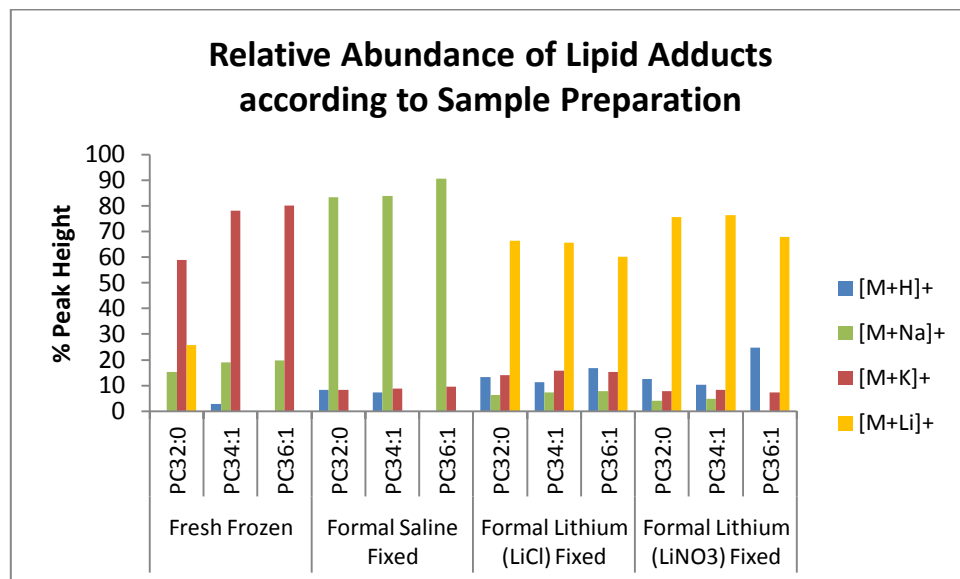
Figure 35 Graph showing the percentage relative abundance of PC 32:0, 34:1 and 36:1 detected during imaging experiments of thin tissue sections in freshly frozen tissue and tissue fixed in either a formal saline solution containing sodium chloride or a formal lithium solution containing either lithium chloride or lithium nitrate. Anomalous results for [M+Li]$^+$ of PC 32:0 in freshly frozen tissue and [M+H]$^+$ of PC 36:1 in formal lithium fixed tissue can be explained thus; [M+Li]$^+$ of PC 32:0 is expected at *m/z* 740, the high abundance of this detected in freshly frozen tissue is an isotope peak of *m/z* 739 which is a fragment ion of *m/z* 798 (PC 34:1 [M+K-N(CH$_3$)$_3$]$^+$). The [M+H]$^+$ of PC 36:1 is detected at *m/z* 788, the [M+Li]$^+$ of PC 36:4 is also detected at the same *m/z* and therefore it is likely that both contribute.

Protonated adducts are not detected in significant abundance in fresh tissue, however they are detected in both formal saline- and formal lithium-fixed tissues. It is therefore most likely that it is the formal solution and not the use of a lithium salt in such preparations that is the main contributing factor to the introduction of protonated lipid adducts. These formal solutions, although isotonic, are all acidic, which would account for the detection of protonated lipid adducts in the MALDI-MS experiment. Previous reports of the analysis of formalin-fixed tissue samples have not commented upon the relative abundances of other adducts.

Nitrate salts have recently been reported to increase ion counts of a desired lipid adduct in MALDI-MS [235] but had limited use as a matrix additive in imaging experiments described in chapter 3 of this thesis. Substitution of lithium chloride for lithium nitrate did not lead to a significant increase in ion counts of detected species. Results indicate that this method is tolerant of different salt types and differences in anatomical localisation of specific lipid species can be identified equally well with both fixatives, as demonstrated in Figure 36. The use of different counteranions of a salt has been described for a number of other formal preparations; for example with formal zinc solutions prepared with zinc salicylate [249] or both acetate and chloride salts [250]. Substitution of the lithium chloride or nitrate salt with alternative lithium salts could therefore prove advantageous. Sodium phosphate salts are routinely employed in formal solutions in order to maintain neutral pH. This could be advantageous in

MALDI-MS and imaging experiments as it may reduce the relative abundance of protonated adducts detected.
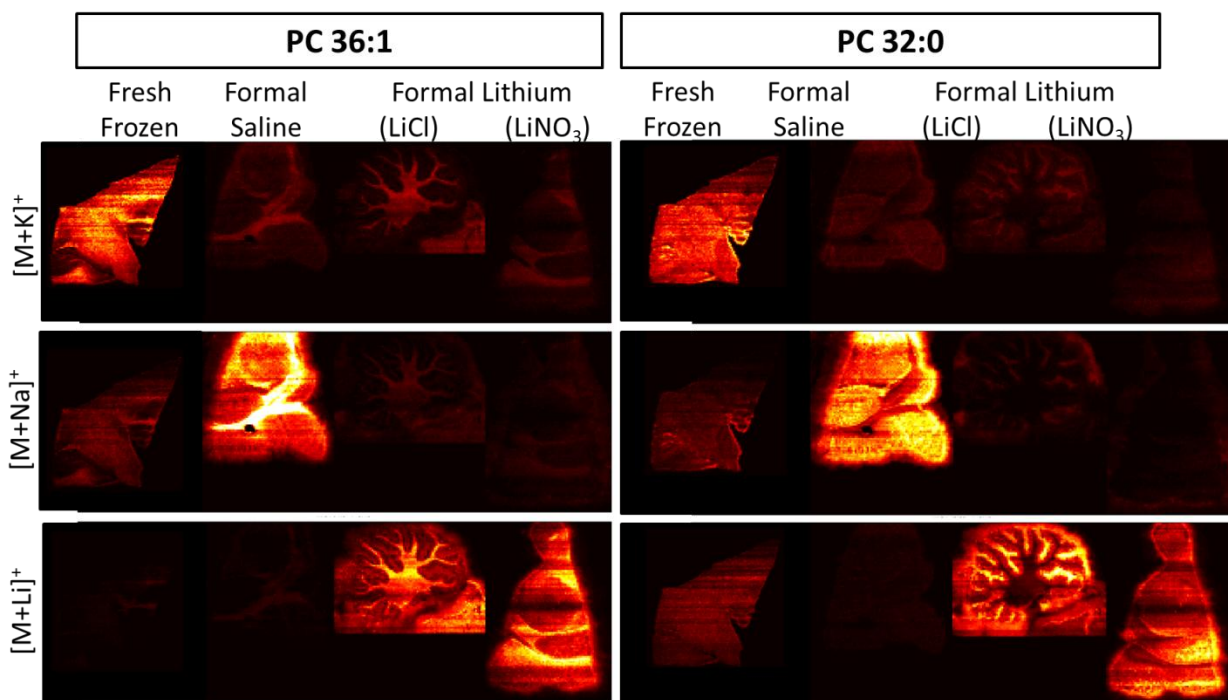
Figure 36 MALDI-MS imaging of rat brain quarters on a Q-TOF instrument. Freshly frozen (control) and formal fixative treated samples; formal saline (NaCl) or formal lithium (LiCl or LiNO₃). Single ion images of [M+K]⁺, [M+Na]⁺ and [M+Li]⁺ adducts of PC 36:1 (*m/z* 826, 810, 794 respectively) are shown on the left-hand side and the same adducts of PC 32:0 (*m/z* 772, 756, 740) are shown on the right-hand side. The intensity scale shows the peak area of all adducts for a particular lipid. Areas of zero counts are black and areas of maximum intensity are shown in white. The maximum intensity is 2000 ion counts for PC 36:1 on the left and 2500 for PC32:0 on the right. The change in the predominant lipid adduct detected as dictated by tissue treatment is shown.

There was one stark difference between spectra acquired from formal lithium- or sodium-fixed tissue and freshly frozen tissue samples. The numbers of ions detected in the region *m/z* 400-650 in data acquired from fresh tissue sections were lower in comparison to fixed tissue sections. Higher abundances of species detected in this region were evident in formal saline-fixed tissue samples in comparison to fresh tissue, as illustrated in Figure 37; however these were higher still when formal lithium tissue was analysed. Generally the peaks detected in this mass region can be accounted for by laser-induced fragmentation; peaks detected at *m/z* 451 and 478, for example, were also detected upon CID of a lipid standard of a PC 34:1 species described in chapter 2 o this thesis. This was the most abundant lipid detected in fresh tissue samples. The detection of fragment peaks is not uncommon in samples analysed with a 'hot' matrix such as CHCA[19]. This is discussed in greater detail in Chapter 2.3.1.

However, as all of these samples were analysed with the same CHCA matrix solution, it is probable that the sample preparation is responsible for these observed differences. In formal lithium-fixed tissue samples there are two distinct regions of fragment ions; between 550-650 and 400-550 u. The peaks detected in these two regions correspond to the expected *m/z* of neutral losses from the phosphocholine species detected in the region *m/z* 700-900. Neutral losses in the region *m/z* 550-650 can be attributed to neutral loss of the PC head-group and those detected in the lower region of *m/z* 400-550 can be attributed to neutral loss of fatty acid side-chains. Although MALDI-MS imaging data of lithium-lipid adducts has been described previously, data was only acquired between

m/z 700-900 [145]. Many groups acquire data in small mass windows in order to improve sensitivity in tissue studies. This unfortunately means it is not possible to comment as to whether similar observations have been made by other groups in tissue imaging studies of lithium lipid adducts.
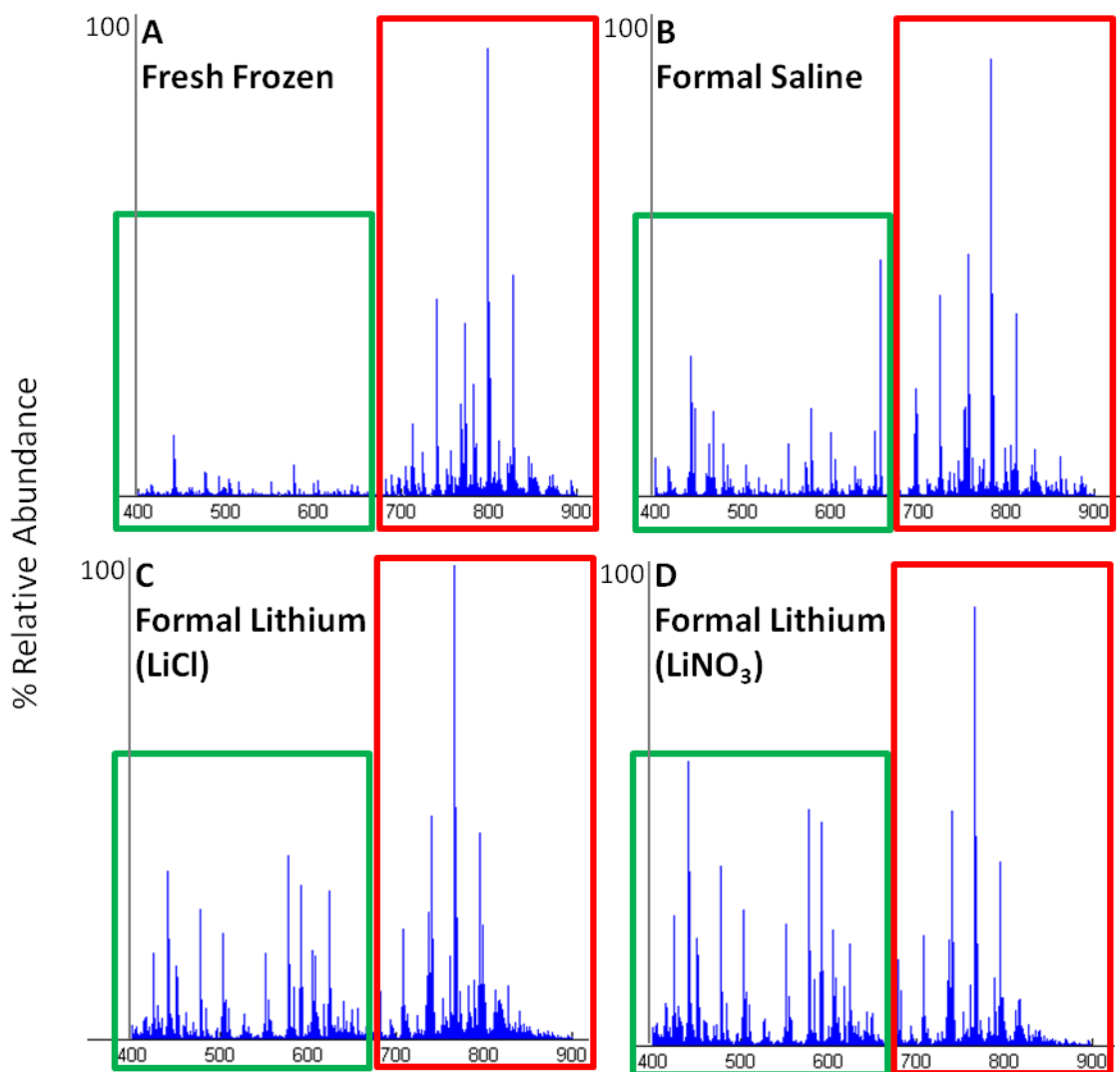
Figure 37 Mean spectra of ions detected on tissue in MALDI-MS imaging of rat brain tissue. Panels show A) Freshly frozen (control) and formal fixative treated samples; B) formal saline (NaCl) or C) and D) formal lithium (LiCl or LiNO₃). The change in the relative percentage abundance of ions detected in the region *m/z* 400-600 with varying tissue treatment is shown.

4.3.2 *In situ* **structural Characterisation of Lipids**

A particular advantage of driving ionisation towards lithium adduct formation is the improved structural characterisation afforded by CID of these adducts when compared to sodium- and potassium-lipid adducts, as discussed in Chapter 2.3.4. Lipid profiling of different lipid adducts *in situ* shows that dissociation of either the potassium-, sodium- or lithium-lipid adduct allows head-group assignment via neutral loss of 59 u (choline) and of 183 u (PC head-group) and the detection of the sodiated phosphate head-group at *m/z* 147. As described in CID of lipid standard analysis in chapter 2 of this thesis, greater structural information is expected from CID of sodium-lipid adducts as would be detected in high abundance in formal saline fixed tissue samples in comparison to potassium which are detected in high abundance in freshly frozen tissue.

Dissociation of sodium-lipid adducts enabled identification of fatty acid side-chains via the detection of product ions relating to the neutral loss of a fatty acid or a fatty acid alongside loss of the choline moiety of the PC head-group (59 u). For example, product ions detected at *m/z* 500 and 441 upon CID of the sodium ([M+Na]$^+$) adduct of PC 32:0 can be attributed to the neutral loss of 256 u and the neutral loss of 256+59 u indicating the presence of a 16:0 fatty acid. The product ion detected at *m/z* 239 supports this assignment as it can be attributed to the acyl ion (RCO$^+$) of 16:0. Previous *in situ* studies of CID analysis of sodium adducts of lipids in formal-fixed tissue samples have shown similar product ions for PC lipid species [264, 269]. However, in the presented study

similar analysis of PC 34:1 and 36:1 did not lead to the detection of all of these product ions by *in situ* profiling, as illustrated in Figure 38.

More product ions were detected in high relative abundance which inform the fatty acid side-chain identities when lithium-lipid adducts were dissociated in formal lithium fixed tissue compared to potassium adducts detected in freshly frozen tissue or sodium adducts in formal saline-fixed tissue. This is demonstrated for a number of lipid species in Figure 38 and is in agreement with previous lipid studies that lithium adducts provide greater structural information in *in situ* studies [19, 34, 143, 270].

The ability to dissociate highly abundant lithium-lipid ions *in situ* enables structural assignment via detection of the following types of product ions; neutral loss of the fatty acid, neutral loss of the fatty acid lithium salt and neutral loss of the fatty acid alongside the neutral loss of choline. The detection of three product ions in the region *m/z* 340-540 indicates that the two fatty acid side-chains are the same. Dissociation of the lithium adduct ([M+Li]$^+$) of PC 32:0 at *m/z* 740 results in three highly abundant product ions; *m/z* 484 (neutral loss of 256 u, 16:0 fatty acid), *m/z* 478 (neutral loss of 262 u, lithium salt of 16:0 fatty acid), and *m/z* 425 (neutral loss of 315 u, 16:0 fatty acid (256) and choline (59)). PC 32:0 can therefore be assigned as PC 16:0/16:0 from CID of the [M+Li]$^+$ adduct in formal lithium-fixed tissue as illustrated in Figure 39 a. This assignment is in agreement with previous reports of *in situ* lipid profiling of murine brain [130, 133] and is further supported by the detection of the acyl ion (RCO$^+$) of 16:0 fatty acid at *m/z* 239.
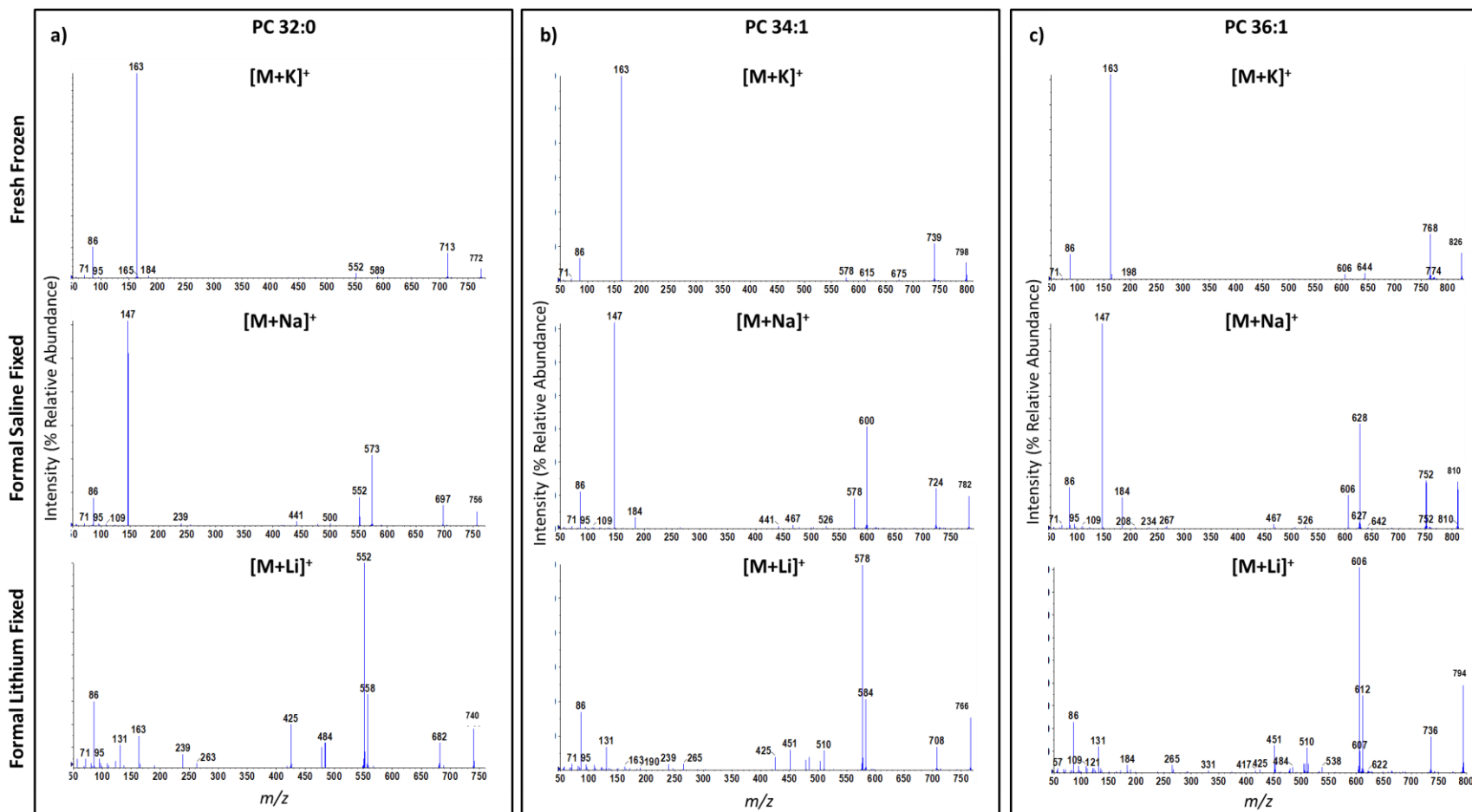
Figure 38 Representative MALDI-MS/MS spectra showing product ions detected by CID of (top) [M+K]⁺ adducts in fresh tissue , (middle) [M+Na]⁺ adducts in formal saline fixed tissue, and (bottom) [M+Li]⁺ adducts in formal lithium fixed tissue of a) PC 32:0, b) PC 34:1 and c) PC 36:1. Direct tissue profiling of formal lithium fixed tissue leads to the detection of a greater number of fatty acid side-chain informative product ions in the region *m/z* 350-540, aiding structural elucidation.
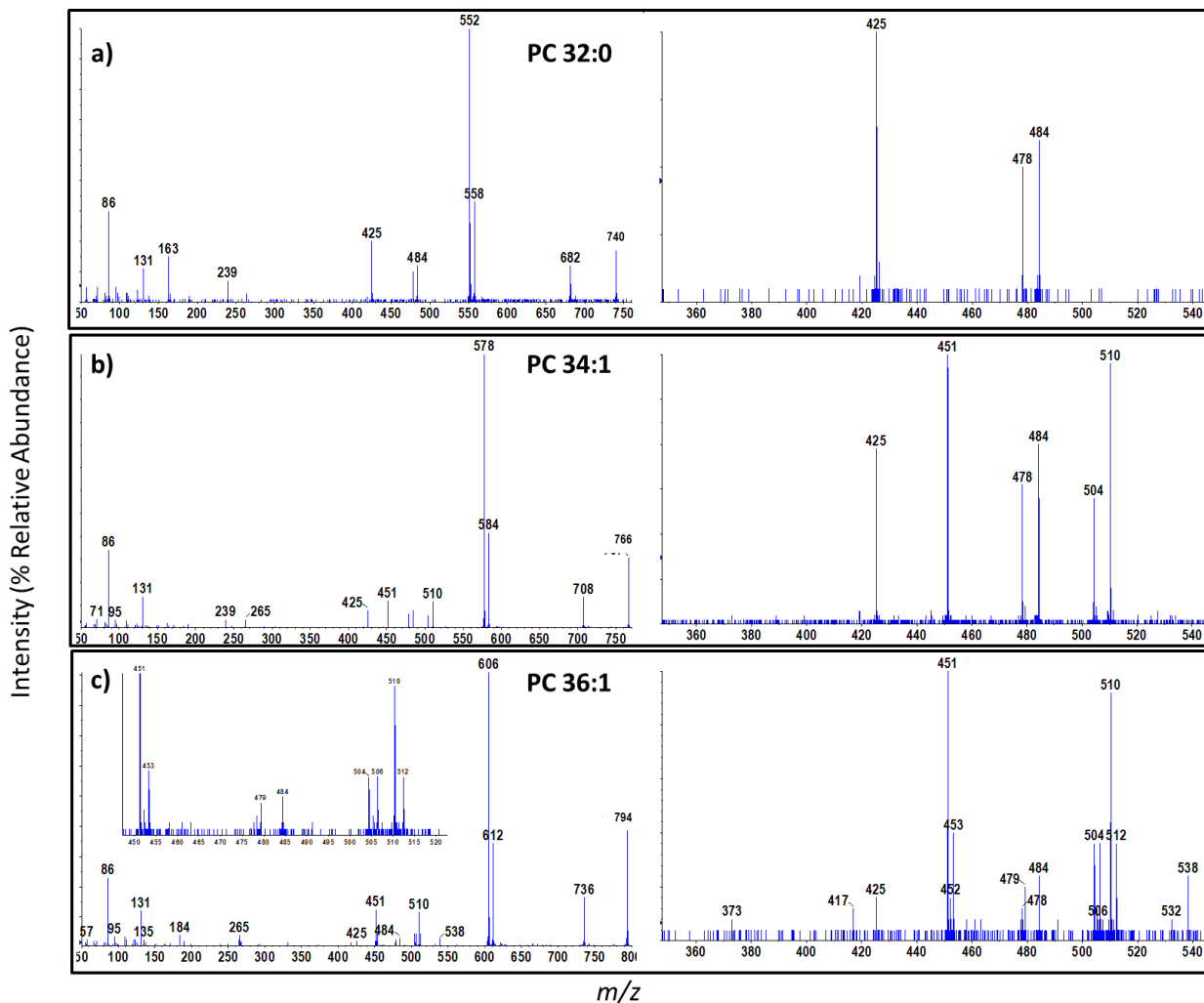
Figure 39 Representative MALDI-MS/MS spectra showing the structurally informative product ions detected by collision-induced dissociation of [M+Li]+ adducts of lipids from direct tissue profiling of formal lithium fixed tissue. [M+Li]+ adducts of a) PC 32:0 (parent ion *m/z* 740), b) PC 34:1 (parent ion *m/z* 766) and c) PC 36:1 (parent ion *m/z* 794). The full product ion mass spectrum (*m/z* 50-750, 770 or 800 respectively) is shown on the left and a magnification of the *m/z* region 350-540 showing side-chain characteristic product ions.

Dissociation of [M+Li]$^+$ of PC 34:1 at *m/z* 766 results in six product ions in the region *m/z* 340-540, as shown in Figure 39 b, indicating that the two fatty acid side-chains are different. Product ions detected at *m/z* 510 (neutral loss of 256 u), *m/z* 504 (neutral loss of 262 u), and *m/z* 451 (neutral loss of 315 u) indicate the presence of a 16:0 fatty acid in this species also. In this example, the acyl ion of this fatty acid is also detected at *m/z* 239. Further product ions at *m/z* 484 (neutral loss of 282 u), *m/z* 478 (neutral loss of 288 u, (282+6)) and *m/z* 425 (neutral loss of 341 u (282 + 59)) all indicate that the other side-chain is an 18:1 fatty acid. Again, the acyl ion is also detected at *m/z* 265 supporting this assignment. As the ions corresponding to loss of the *sn*-1 fatty acid are detected in greater abundance than those of the *sn*-2 loss [19, 271], complete structural assignment is possible. Product ions indicating loss of a 16:0 fatty acid are detected in greater abundance than those indicating an 18:1 fatty acid, signifying that the 16:0 fatty acid resides in the *sn*-1 position , therefore this lipid can be confirmed as PC 18:1/16:0 (*sn*-3 *sn*-2/*sn*-1). This data is in agreement with previous *in situ* studies of murine brain of lithium-lipid adducts where lithium was introduced to the tissue via pipetting[143].

Dissociation of [M+Li]$^+$ of PC 36:1 at *m/z* 794.6 presented in Figure 39 c results in twelve product ions indicating the presence of two isobaric lipids with two sets of different fatty acid side-chains. Product ions detected at *m/z* 538 (neutral loss of 256), *m/z* 532 (neutral loss of 262) and *m/z* 479 (neutral loss of 315) all indicate the presence of a 16:0 fatty acid. An 18:1 fatty acid side-chain is also indicated by similar product ions at *m/z* 512 (neutral loss of 282), *m/z* 506 (neutral loss of 288) and *m/z* 453 (neutral loss of 341).

Product ions detected at *m/z* 510 (neutral loss of 284), *m/z* 504 (neutral loss of 300) and *m/z* 451 (neutral loss of 343) indicate the presence of an 18:0 fatty acid. Finally, a 20:1 chain is indicated by similar characteristic ions detected at *m/z* 484 (neutral loss of 310), *m/z* 478 (neutral loss of 316) and *m/z* 425 (neutral loss of 369). In this example, acyl ions of each fatty acid were not detected; hence it was concluded that these are less reliable for assignment in comparison to the above described neutral loss product ions. The product ion at *m/z* 479 was detected in greater abundance than that at *m/z* 369 and the product ion at *m/z* 451 was detected in greater abundance than that at *m/z* 453, thus the lipid composition can be assigned as a mixture of PC 20:1/16:0 and PC 18:1/18:0.

Overall, the improved structural information obtained from CID analysis of lithium-lipid adducts detected in high abundance in formal lithium-fixed tissue in comparison to similar analysis of sodium adducts detected in formal saline-fixed tissue or potassium adducts in freshly frozen tissue is demonstrated. Furthermore, it is shown that dissociation of lithium adducts more reliably provides structural information which enables elucidation of each substituent, indicating not only the lipid head-group and both fatty acid side-chains but also informing the relative positions of each along the glycerol backbone.

Lithium-lipid adducts have been analysed *in situ* previously via depositing a small volume of a matrix solution containing lithium salt [77, 143]. This type of preparation leads to delocalisation of lipid species in the sampled region, forming a spot 800-1500 μm in size [143], and does not enable separate analysis of small tissue features. The presented methodology does not suffer from lipid delocalisation, therefore analysis of specific anatomical features is only limited by the laser beam profile incident on the tissue.

In situ analysis of lithium-lipid adducts from tissue prepared by spraying a matrix solution containing a lithium salt, has also been reported by Cerruti *et al*.[145]. This approach also maintains spatial information however the formation of compact crystals and problems encountered with deposition of these matrix-salt solutions reduces the universality of their approach[145]. Here a method which enables rapid data acquisition using standard sample preparation protocols using lithium salts which did not prove useful in Cerruti's study is described. Furthermore, as the presented methodology incorporates lithium ions independently of MALDI sample preparation it should lend itself as a suitable lithium ion introduction technique for tissue analysis by other surface-sampling techniques such as LESA (discussed in detail in Chapter 5) or SIMS, which commonly operates using ion sources with beam profiles on the nanometre scale [272]. The potential benefits of combining MS/MS analysis with spatial information are demonstrated herein by performing MS/MS imaging studies.

4.3.3 MALDI-MS/MS Imaging

MS/MS imaging of lithium-fixed tissue sections enables generation of ion images showing the spatial distribution of structurally characteristic product ions. The mean spectrum acquired from tissue regions during MS/MS imaging of PC 34:1 [M+Li]$^+$ (m/z 766.6) is shown in Figure 40 a. Mapping the spatial distribution of the most abundant product ions that were characteristic of the fatty acid side-chain identities, at m/z 425 (neutral loss of 18:1 fatty acid side-chain alongside choline) and m/z 451 (neutral loss of 16:0 fatty acid and choline), clearly shows that this lipid is detected homogeneously in the cerebellum. MS/MS imaging of PC 32:0 [M+Li]$^+$ (m/z 740.6) is shown in Figure 40 b. This time there is only one fatty acid side-chain. Mapping the spatial distribution with the most abundant fatty acid side-chain indicative peak at m/z 425 (neutral loss of 16:0 fatty acid and choline) and m/z 551 (neutral loss of the lithium adduct of the PC head-group) clearly shows that this lipid is detected only in the grey matter in the cerebellum.

These spatial distributions directly correlate and concur with the distributions in the original MS imaging data set. Therefore it is possible to map ion images of structurally characteristic product ions by preparing tissue in a formal lithium fixative. Moreover, these data were acquired by the same rapid acquisition parameters described for MALDI-MS imaging. This capability is particularly important if two different lipid species are present at the exact same m/z. For example, it should be possible to

separately show the spatial distributions of PC (18:1/18:0) and PC (20:1/16:0) by MS/MS imaging of a lithium-fixed sample.
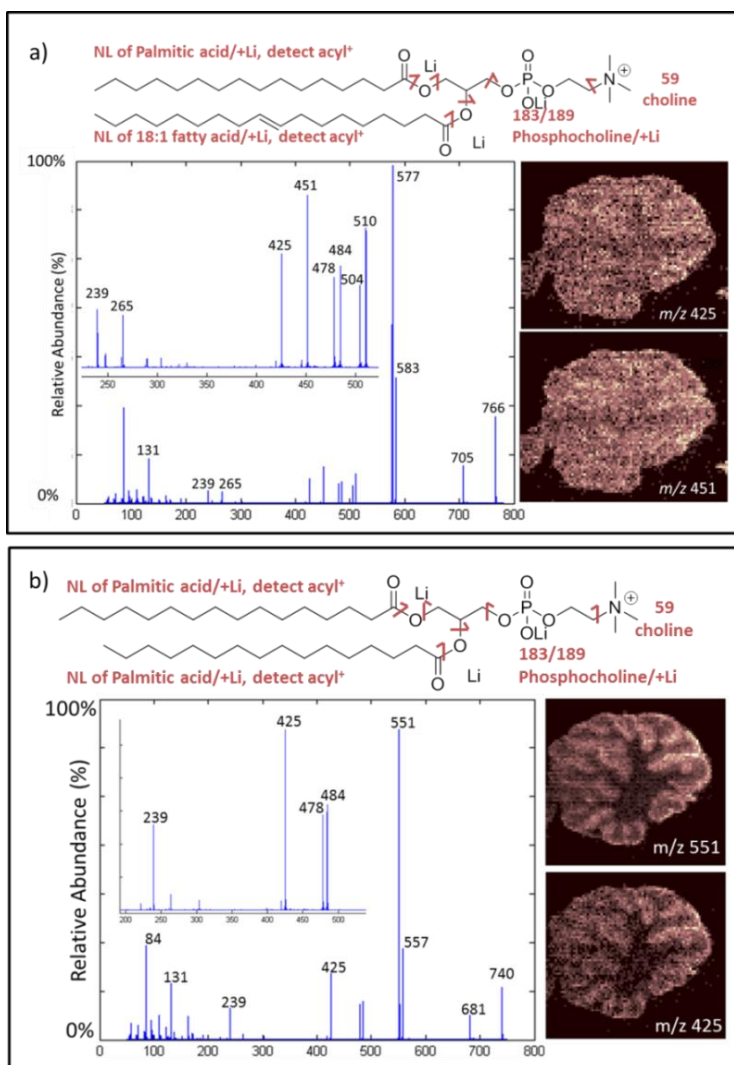
Figure 40 Panel a: MALDI-MS/MS of PC 34:1 [M+Li]+ Single ion images of *m/z* 451 (neutral loss of palmitic acid) and 425 (neutral loss of 18:1 fatty acid) and the mean spectrum of ions detected on tissue are shown. Panel b: MALDI-MS/MS of PC 32:0 [M+Li]+ Single ion images of *m/z* 551 (neutral loss of 189) and 425 (neutral loss of palmitic acid and choline) and the mean spectrum of ions detected on tissue by are shown. A schematic illustrating dissociation sites is shown above each spectrum (annotation of NL is neutral loss). Ion image areas of high signal intensity are shown in pink. The potential to spatially map distributions of a single lipid using MS/MS imaging with greater confidence than may be possible with MS imaging is shown.

MS/MS imaging is widely documented for other analytes[273-276] and recent studies have considered sodium adducts of fatty acids and triacylglycerols in fingerprints[277] and sodium adducts of phosphocholine lipids in formal saline or phosphate buffered formalin-fixed tissue samples [269, 278]. Previous reports of MS/MS imaging of sodium-lipid adducts in formal saline and phosphate-buffered formalin-fixed tissue samples have shown that fatty acid side-chain informative product ions can be spatially mapped; Steven *et al.* showed that acyl ions are detected when a number of sodium adducts of PC lipid species are analysed by MS/MS imaging of formal saline-fixed samples [278].

The detection of further product ions that are characteristic of the fatty acid side-chain identities were not commented upon and spectra are not provided, hence it is not possible to comment upon the relative abundance of these ions. However, although MS/MS imaging studies of sodium-lipid adducts detected in phosphate-buffered formalin-fixed tissue samples describe product ions relating to the neutral loss of the fatty acid side-chain upon CID [269], only head-group indicative product ion images are presented. Here it is shown that MS/MS imaging of lithium lipid ions in formal lithium fixed tissue samples leads to the detection of relatively high abundances of a range of peaks indicative of the fatty acid side-chain identities, the distributions of which can be used to show the spatial distribution of a single, identified, lipid. In this way the ability to perform MS/MS imaging from lithium lipid adducts shows real opportunity for *in situ* tissue analysis of a range of lipid species.

4.3.4 Human Liver Case Study - Compatibility of Formal Metal Fixatives with Common Staining Methods

In order to assess the compatibility of our fixing strategy with standard histological staining techniques, a study using human tissue was performed. Specimens from patients with non-alcoholic steatohepatitis (NASH) were analysed by MALDI-MS imaging. Serial sections were stained using traditional chromogenic stains to evaluate any effect of tissue fixation on histological information.

MALDI-MS images of PC 34:1 show lipid distributions that correlate well with the morphology of the tissue section. This lipid is localised within the hepatocyte nodules in the NASH specimen; intensity varies between individual features and there is a tendency for increased signal closest to the fibrotic areas. Mapping of the $[M+K]^+$ adduct in freshly frozen tissue and the $[M+Li]^+$ adduct in formal lithium-fixed tissue shows similar distributions in fresh and fixed tissue samples as illustrated in Figure 41.

Due to the heterogeneous nature and complex composition of biological samples it is extremely important to identify the composition and morphology of different tissue types. Currently diagnosis depends on the routine fixation of tissue with (pH neutral) phosphate-buffered formalin and subsequent histopathological analysis using light microscopy. However with the additional molecular information available from techniques such as MALDI-MSI, the integration of MS techniques is desirable, and

standard protocols suitable for use with histopathology and MS imaging could be

beneficial for histology-driven studies [279-282].
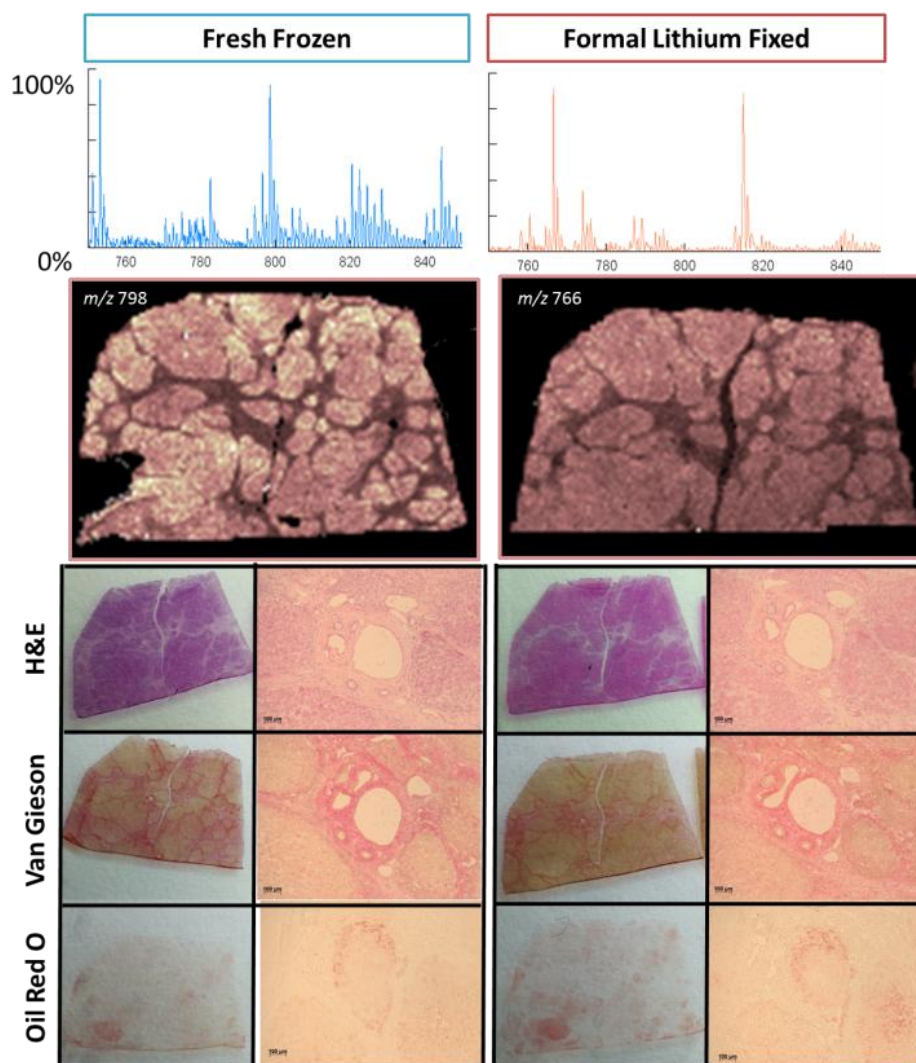
Figure 41 MALDI-MS images of lipid PC 34:1 detected in NASH liver sections. A summed spectrum of peaks detected in the region *m/z* 750-850 is presented in the top panel and ion images are shown below. There is a clear change in the predominant adduct detected in freshly frozen ([M+K]+) and formal lithium (LiCl) ([M+Li]+) fixed tissue samples. Gross and microscopic images of serial sections of tissue stained with H&E, van Gieson and Oil Red O are shown below each tissue image. Scale bars show 100 µm, larger pictures can be viewed in Figures 34 and 35. The opportunity to correlate MS images with histological staining techniques from formal lithium fixed samples, similar to fresh tissue samples, is shown.

The effect of formal metal fixation on common staining techniques (H&E, van Gieson and Oil Red O) was considered. Fresh tissue, formal saline and formal lithium prepared with either lithium chloride or nitrate were assessed. NASH liver tissue is characterised by chronic inflammation steatosis and extensive fibrosis, which causes major disruptions to the architecture of the tissue. Staining of thin tissue sections of the NASH specimen confirmed inflammation contains major fibrotic septa (stained pink in the van Giesen stain) and abundant steatosis (highlighted by red neutral lipid accumulations in the Oil Red O samples). Microscopic observation confirmed that both micro-vesicular and macro-vesicular steatosis was evident and distribution was not uniform with some regenerative nodules being more intensely steatotic than others. Visualisation of this architecture was possible irrespective of tissue treatment and all features were identifiable in all samples, as demonstrated in Figure 42 and Figure 43.

Importantly, this examination of the histological sections appears to show that all formal preparations facilitated the uptake of each dye and maintained the microarchitecture of the tissue samples. All tissue features remain evident and distinguishable when tissue sections are treated with a formal fixative and subsequently stained with common histological reagents. Formal lithium-fixed tissue sections appeared to closely resemble those from freshly frozen samples (Figure 41, 42 and 43). Therefore it would seem that treating the sample with formal lithium does not limit histology and would be suitable for histology-driven lipid imaging studies owing to the improved characterisation afforded by lithium adducts.
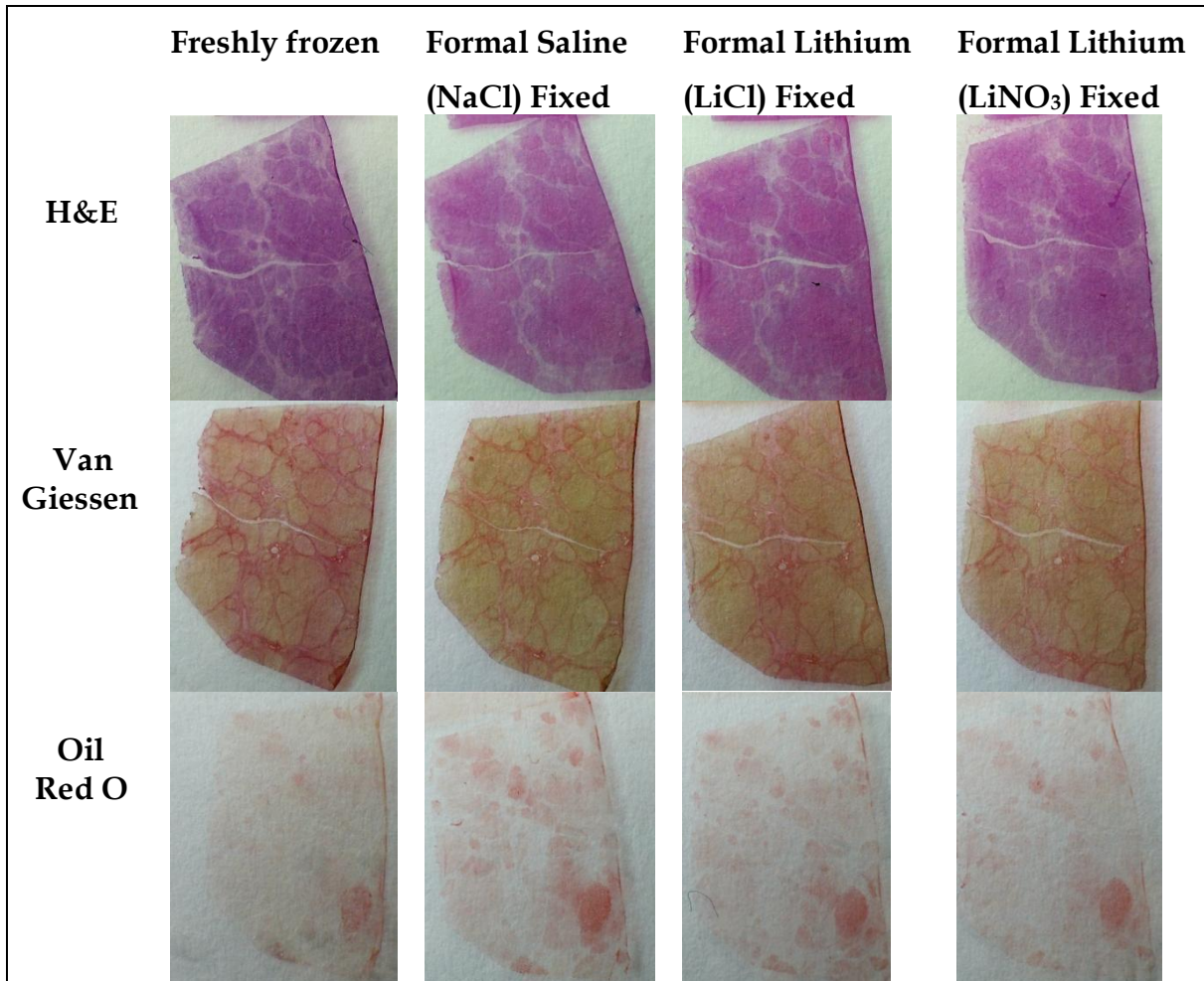
Figure 42 Representative gross images showing staining of sections from blocks of NASH tissue treated with either no fixative (freshly frozen) or formal saline (NaCl) or a formal lithium fixative solution prepared with either LiCl or $LiNO_3$ stained with either H&E, Van Giessen or Oil Red O stains. Similar results from each staining technique are observed irrespective of tissue treatment.
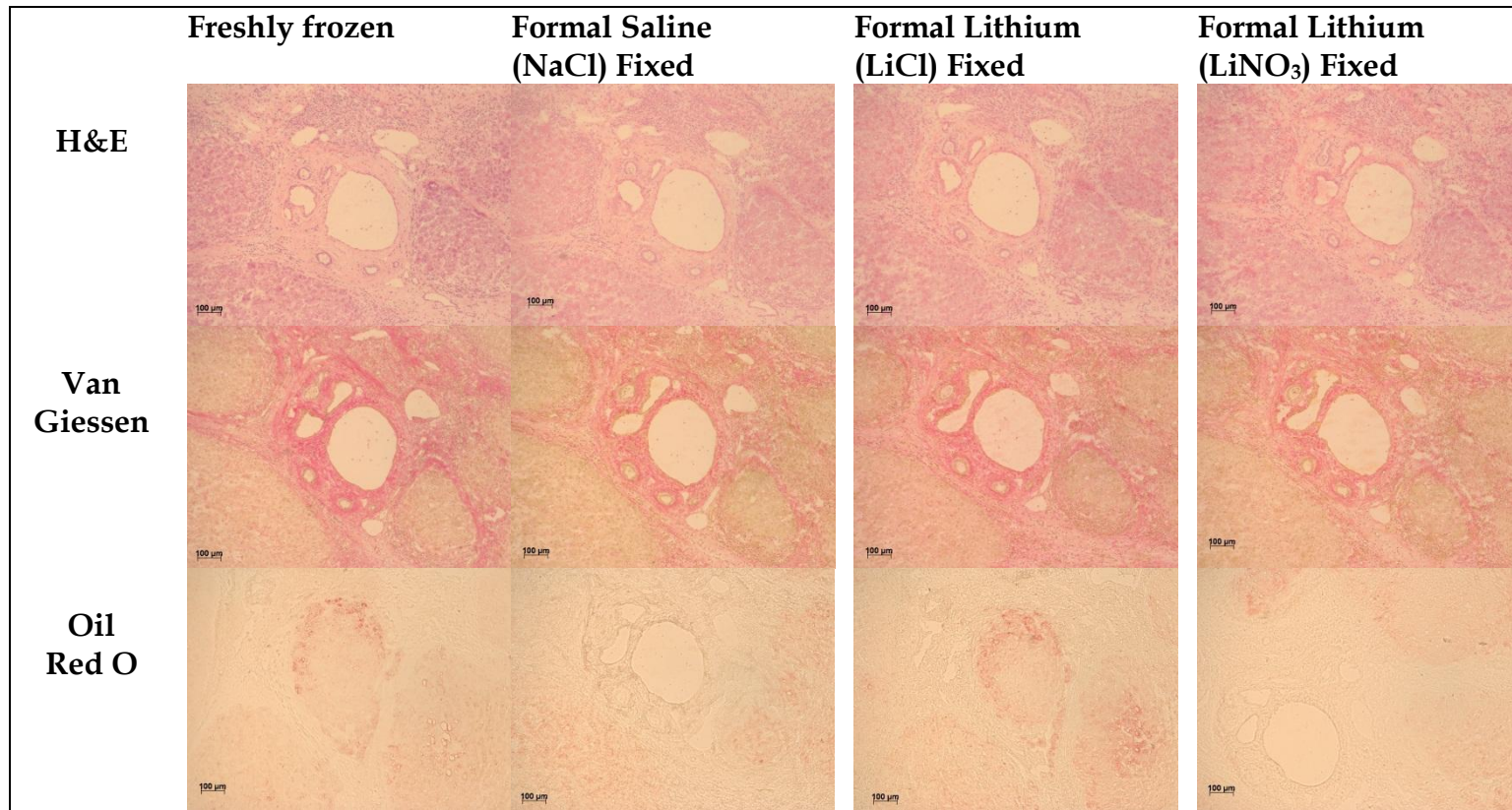
Figure 43 Representative microscopic images centred on portal areas within NASH tissue sections (matched to those in images Figure 34) treated with either no fixative (freshly frozen), formal Saline (NaCl) or a formal lithium fixative solution prepared with either LiCl or LiNO₃ stained with either H&E, Van Giessen or Oil Red O stains. Similar results from each staining technique are observed irrespective of tissue treatment.

MALDI imaging studies are typically conducted alongside standard histological evaluations of tissue sections. This is becoming increasingly important in clinical studies in which spectra and single ion images can be spatially correlated to different tissue regions in stained sections providing unrivalled insight into the molecular composition and cellular organisation of samples. Correlation of imaging data with histological information (staining) usually involves analysis of a first section by MALDI and a serial section for staining. Less commonly, the same tissue section may be surveyed by both approaches. Tissue staining has been performed both pre- and *post* MALDI imaging. Although common dyes such as haematoxylin and eosin have not lent themselves to this strategy, other routinely used dyes such as cresyl violet and methylene blue have proven more compatible [282, 283]. None the less, it is widely accepted that structural stains such as haematoxylin and eosin provide the most useful detail of cellular structure and tissue architecture which is required for histopathological surveys and grading of clinical samples.

4.4 Conclusions

Treatment of tissues by formal-lithium fixation is a simple and reproducible method for incorporating lithium salts into tissue. High abundances of lithium lipid ions are detected without compromising sensitivity or increasing spectral complexity. Importantly, the distributions of selected lipids were not found to differ between fresh and fixed tissues proving this is a viable sample preparation strategy for tissue imaging by MALDI and other mass spectrometry techniques. Moreover, CID studies show that *in situ* structural characterisation of lipids is significantly enhanced by the opportunity to dissociate lithium lipid adducts in MALDI experiments when compared to other adducts detected in freshly frozen or formal saline-fixed tissues.

The compatibility of formal lithium fixation with three common stains has also been confirmed by examination of liver tissue. Hence it is shown that formal lithium fixation not only enhances the *in situ* information that can be obtained in MALDI-MS and MS/MS imaging studies, but also that the uptake and usefulness of haematoxylin and eosin, as well as van Gieson and Oil Red O stains are not compromised. With increasing pressure to identify potential biomarkers in clinical investigations we hope that this methodology will provide lipid analysts with a single, histology-compatible protocol for multi-modal analysis of tissue sections: Formal lithium is a useful tissue preservative, offers an effective route to introducing lithium for CID in MALDI studies and is compatible with common histological stains.

5. Liquid-Extraction Surface-Analysis (LESA) –Electrospray (ESI) Mass Spectrometry of Fixed Tissue Samples

5.1 Introduction

Liquid-extraction surface-analysis (LESA) enables surfaces to be probed with a solvent by maintaining a liquid micro-junction on the sample surface prior to electrospray ionisation (ESI). As the mechanisms of ionisation of MALDI and ESI differ greatly (refer to chapter 1.x.x), analysing samples by each technique can provide supporting and complimentary data. The corroboration of results between MALDI and LESA techniques from direct surface analysis strengthens results [120]. Although LESA cannot provide spatial resolution comparable to MALDI [120], it has been shown that analysis of MALDI spot samples by LESA-ESI, *post* MALDI analysis, can support the information obtained by MALDI, ionising species which are not detected in the first analysis [119]. Furthermore, DESI imaging has been used in support of MALDI imaging to separately analyse different analytes of interest, such as both lipids and proteins [130].

A range of neutral and polar lipids have been analysed previously by ESI [106-110] [106, 107, 111-113]. However to date very few LESA experiments have considered surface sampling analysis of lipid analytes. Stegemann *et al*. considered LESA for the analysis of human atherosclerotic plaques, showing the application of direct surface-sampling and ESI of lipids [121]. Furthermore, they were able to perform MS/MS studies of analytes

extracted directly from the tissue surface. In addition, Brown *et al*. showed the applicability of LESA for the separate analysis of each side of contact lenses in order to gain an understanding of the lipid deposits on each side [126].

Furthermore, lithium adducts of a wide variety of lipid species have been shown to provide superior structural information in CID experiments performed after ionisation by electrospray, analogous to that described in MALDI. Therefore the formation of abundant lithium-lipid adducts in ESI experiments would be advantageous. In this chapter the compatibility of LESA to sample tissue surfaces of formalin fixed samples for electrospray ionisation is considered. The LESA-ESI sampling-ionisation set-up will be coupled to an orbitrap mass analyser.

5.2 Experimental

5.2.1 Materials

All salts (NaCl, LiCl and LiNO$_3$) and formic acid (FA) were purchased from Sigma Aldrich (Gillingham, UK). Formaldehyde was purchased from Adams Healthcare (Swindon, UK). Methanol (HPLC grade) was purchased from Fisher Scientific (Leicestershire, UK). Water was purified by an ELGA Option 3 system (Marlow, UK). Plain glass slides were purchased from Leica (UK).

5.2.2 Fixative Solutions

Formal Lithium was prepared according to standard protocols (0.154 M LiCl in formalin) where formalin is a solution of 10% (by volume) formaldehyde solution (40% in methanol) in water (90% volume) resulting in a solution which contains 4% formaldehyde. Formal calcium solutions were prepared similarly (0.077 M CaCl$_2$ salt in formalin).

5.2.3 Tissue Block Fixation

The cerebellum tissue from a snap-frozen mouse brain was sectioned into two. Each was treated differently; one remained frozen and was stored at -80 ˚C, the other was immersion-fixed in formal lithium (LiCl) at room temperature. Immersion fixation of tissue blocks was achieved by immersing tissue blocks in formal lithium (LiCl) in a volume 20x its mass for 48 hours. Once fixed, tissue blocks were stored at -80˚C until

sectioning at -18 ˚C (Leica CM 1850 Cryostat (Milton Keynes, UK)) at 10 μm before thaw-mounting onto plain glass slides for LESA-ESI-MS.

5.2.4 Single Tissue Section Fixation

Snap-frozen mouse brain tissue was sectioned at 10 μm (Leica CM 1850 Cryostat (Milton Keynes, UK)) and then thaw-mounted onto plain glass slides. The slides were then submerged in a formal calcium fixative solution for 30 minutes. Control (fresh) sections were not treated with a fixative.

5.2.5 LESA Sampling

Automated sample analysis was performed using the LESA Points software (Advion Ithaca, NY) which controls the TriVersa Nanomate. This platform was used to select the location or locations on the tissue surface (x and y co-ordinates) and the z position, relative to the plate height, for sampling routines using the Nanomate probe. The LESA sampling routine involved the collection of a conductive tip from the Advion tip rack before moving to a solvent well containing the electrospray solvent solution. The Nanomate probe aspirated 2.5 μL into the conductive tip and then the probe was relocated to the predetermined location on the surface and then descended to 0.4 mm above the surface. The tip dispensed a proportion of the volume of the solution (1.5 μL) for single position sampling onto the sample forming a liquid micro-junction (LMJ) between the tip and the surface. The LMJ was maintained to allow sufficient time for

analytes to dissolve (10 s). The solvent was then re-aspirated into the tip. Finally the tip was rotated and engaged with the back of the ESI chip, and nanospray ionisation was initiated. The Triversa Nanomate was coupled with a Thermo Fisher Scientific Orbitrap Velos mass spectrometer. MS data were collected for 3 minutes per extraction.

5.2.6 Mass Spectrometry

Electrospray analysis was performed on an LTQ Orbitrap Velos from Thermo Fisher Scientific (Leicestershire UK). Tissue sections were surface sampled by LESA (Advian Ithaca, NY) with solvents comprised of 70:30:0.1 $CH_3OH:H_2O:FA$. Samples were introduced at a flow rate of ~80 nL/min with a gas pressure of 0.3 psi, a tip voltage of 1.75 kV and a capillary temperature of 250 °C. MS data were collected in full scan mode (*m/z* 500-1500) with a resolution of 100 000 at *m/z* 400. Each scan comprised 20 co-added microscans. The Automatic Gain Control (AGC) was used to accumulate sufficient ions for analysis. The AGC target was $1x10^6$ with a maximum fill time of 2 s in full scan mode.

5.2.7 Data Conversion

LESA data were converted to mzML using msconvert as part of ProteoWizard [284]. Spectra acquired from a single injection were summed using a custom MATLAB script and output to mzML. The summed spectra were then converted to imzML using imzMLConverter [236] and processed in MATLAB.

5.3 Results and Discussion

5.3.1 LESA-ESI analysis of Freshly Frozen Tissue Sections

LESA coupled to electrospray ionisation (ESI) [125] and a high-resolution mass spectrometer allowed further identification of lipids in freshly frozen and formal-fixed specimens when compared to MALDI analysis on a Q-TOF instrument. The orbitrap instrumentation has high mass-resolving power and high mass-accuracy capabilities. Data acquired on a Q-TOF mass spectrometer is capable of reporting data in the region *m/z* 700-900 within 0.1 *m/z* whereas data acquired on an orbitrap mass spectrometer is reported to within 5 ppm (parts per million). Therefore, different adducts of different lipid species can be better separated on an orbitrap mass spectrometer.

The superiority in mass-resolving capabilities of the orbitrap mass analyser is demonstrated in Figure 44 over MALDI data acquired on a Q-TOF mass spectrometer. The ion detected at *m/z* 798 is shown in example spectra of data acquired on each instrument; data acquired on the orbitrap mass analyser is clearly much better resolved. The mass resolving power (R) can be determined by the following equation;

$$R = m/\Delta m \text{ at FWHM}$$

Where *m* is the mass of the ion and Δm at FWHM is the change in mass at Full Width Half Maximum of the peak. The mass-resolving power of the orbitrap mass is calculated

as 93 000 and that of the Q-TOF mass analyser is 7 000 (to the nearest thousand) for *m/z*

798.5 shown in Figure 44.
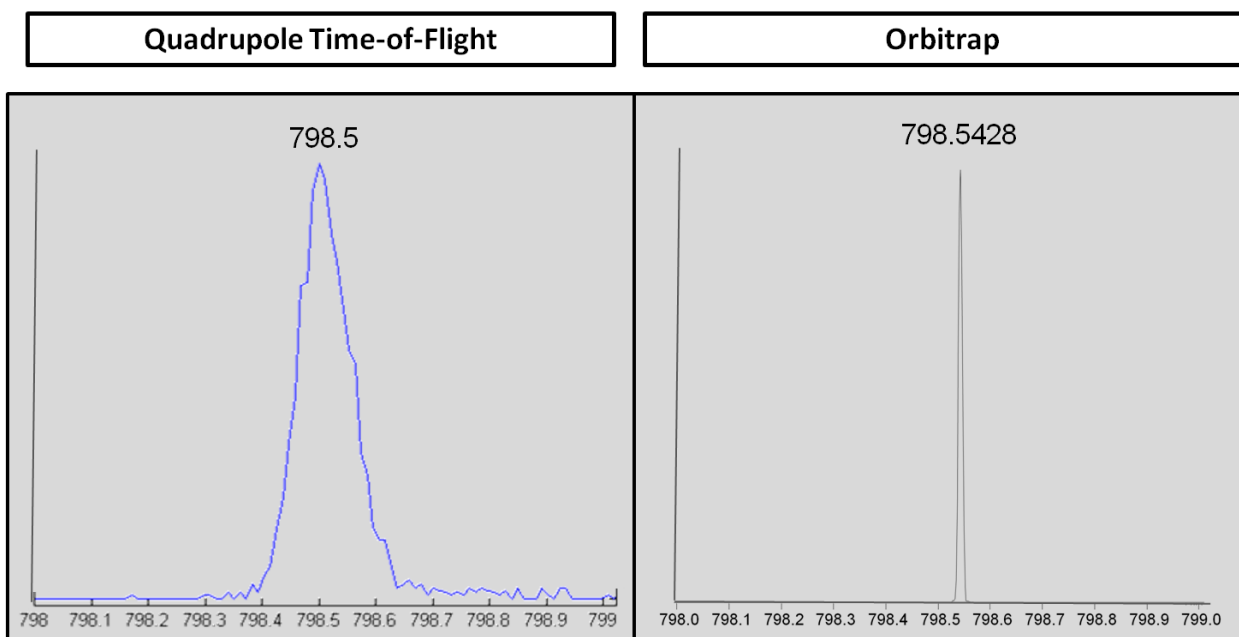
Figure 44 Example mass spectra of peak detected at *m/z* 798 in mouse brain analysis by (left) MALDI on a Q-TOF mass spectrometer and (right) by LESA-ESI on an orbitrap mass spectrometer.

Lipid species detected from surface-sampling fresh tissue sections were preferentially detected as potassium adducts. The mass spectrum displayed in Figure 45 shows phospholipid adducts assigned by accurate mass (within 5 ppm). Lower abundances of sodium and protonated adducts were also detected. A range of different phospholipid species were identified by their accurate mass in the LESA-ESI experiment. In the phospholipid region between m/z 700-900 the most abundant species detected were phosphocholine lipids. These lipids were also detected in greatest abundance in MALDI-MSI analysis of thin tissue sections of mouse brain. This is perhaps unsurprising as these are inherently charged (zwitter ionic).

It should be noted that despite the vastly improved peak resolution and mass accuracy afforded by this instrumentation, a number of different lipid species remain detected within 5 ppm of one another. Although peak assignment is enhanced in this analysis, overlapping theoretical m/z values of different adducts of different lipids remains problematic in terms of assignment by accurate mass. Hence tandem mass spectrometry experiments remain an important method of identification of lipids and routes to the formation of a single adduct type remain desirable in LESA-ESI analysis on accurate mass instrumentation.
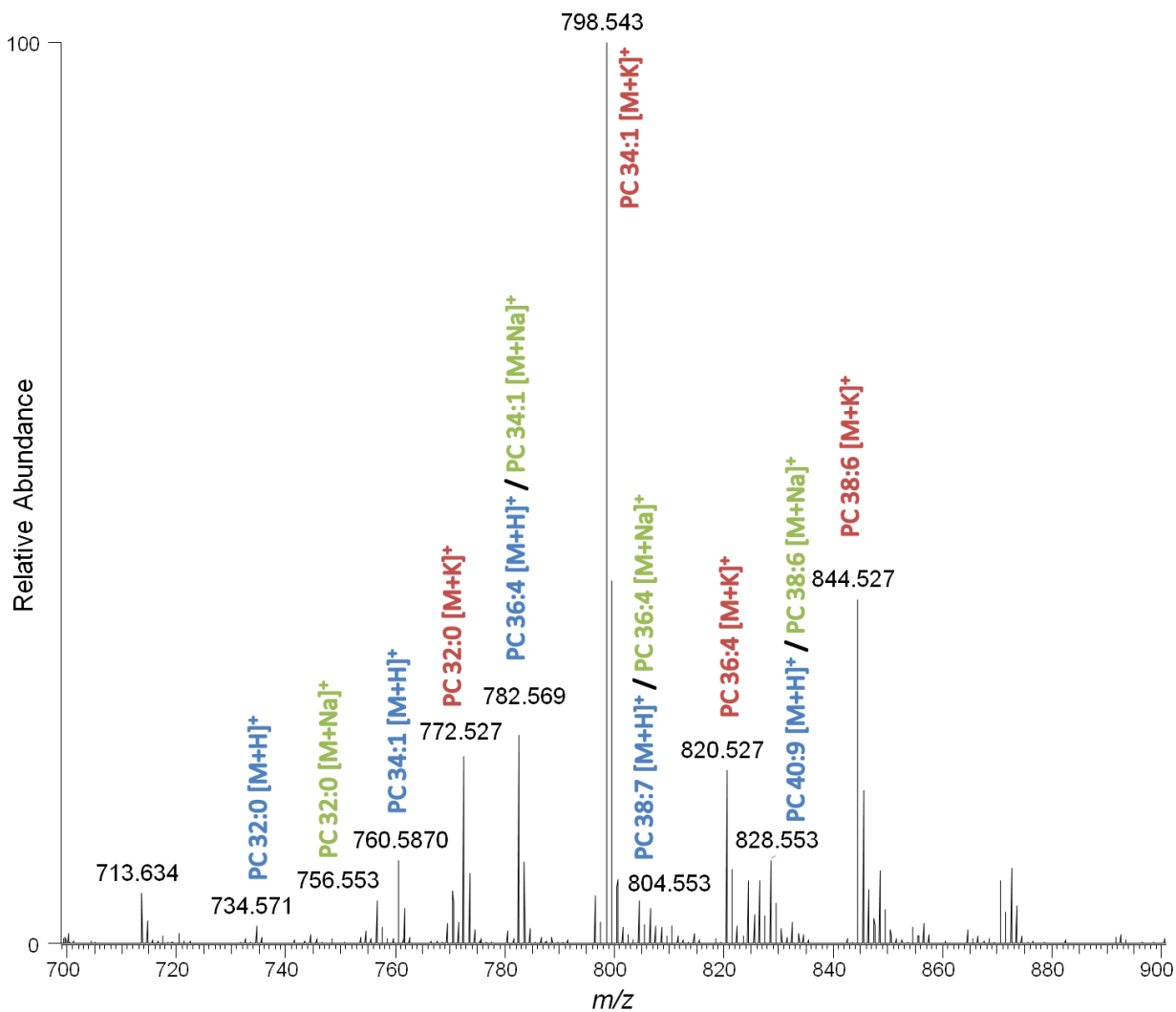
Figure 45 Typical LESA-ESI mass spectrum acquired from surface-sampling freshly frozen tissue in the *m/z* region 700-900.

Predominantly PC species, were detected in the MALDI experiment, however more species were identified by accurate mass in this analysis. Preferential detection of PC and SM species could be owing to the zwitterionic moiety facilitating ionisation and protonation/cationisation. It is possible that the increased detection of PC species and other phospholipid species, displayed in Figure 46, is owing to the improved sensitivity afforded by the orbitrap mass analyser. However, the sampling technique could also contribute to an improvement in sensitivity of the analysis.
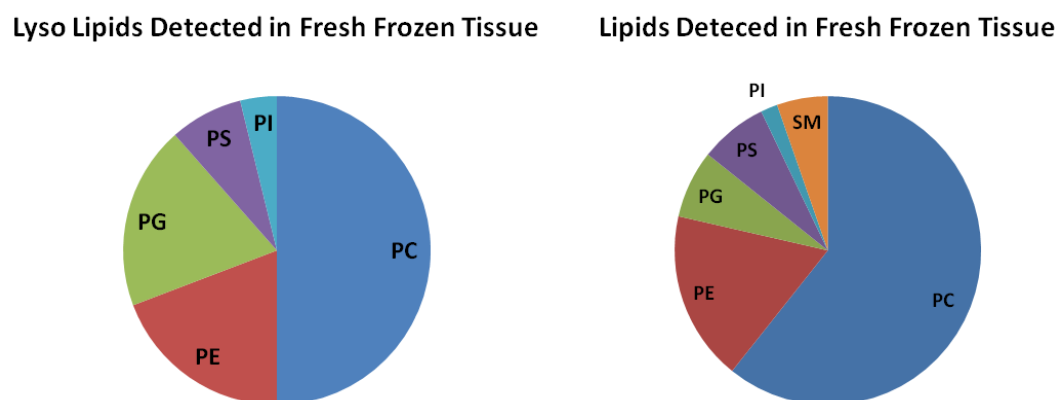
Figure 46 Pie charts showing the relative numbers of lyso-phospholipid and phospholipid species detected in LESA-ESI analysis of freshly frozen mouse tissue, assigned by accurate mass.

The formation of a liquid micro-junction on the tissue surface with 1.5 µl solvent leads to a sampling area approximately 3 mm², which is much larger than that considered in MALDI-MSI analysis presented in Chapters 2 and 3 of this thesis which is approximately 0.05 mm². This impacts on MSI data acquisition by LESA sampling; currently the highest possible spatial resolution reported in the literature is 1 mm [285], which does not enable differentiation of histological features in many tissue types. This maximum resolution is also inferior to the best achieved in MALDI-MSI; typically tissue imaging is conducted at a spatial resolution of 100 µm, however high resolution data of 10 µm has been reported recently [128]. A number of groups have reported studies considering solvent-based methods (such as LESA or DESI) and MALDI-MSI analysis to obtain improved compositional and spatial information from tissue samples [120, 130].

A number of different lyso-phospholipid species were also identified in the LESA experiment, as shown in Figure 46. Comparison of mean spectra between m/z 500-900 shown in Figure 47 reveals lyso-phospholipids were detected in high relative abundances in LESA-ESI analysis in the region m/z 500-700. However these species were not detected in MALDI experiments. Although the orbitrap mass analyser offers improved sensitivity over the Q-TOF set up, this cannot account for the poor detection of lyso-phospholipid species in MALDI experiments, which were shown to be present in higher abundance than phospholipid species in the LESA-ESI study. This is most likely due to the ionisation technique; clearly the experimental conditions of the MALDI study did not lead to efficient extraction and/or ionisation of lyso-phospholipid species. Poor

detection of lyso-phospholipid species in the MALDI study could be due to a range of different experimental factors, such as solvent or matrix selection and in source dissociation.
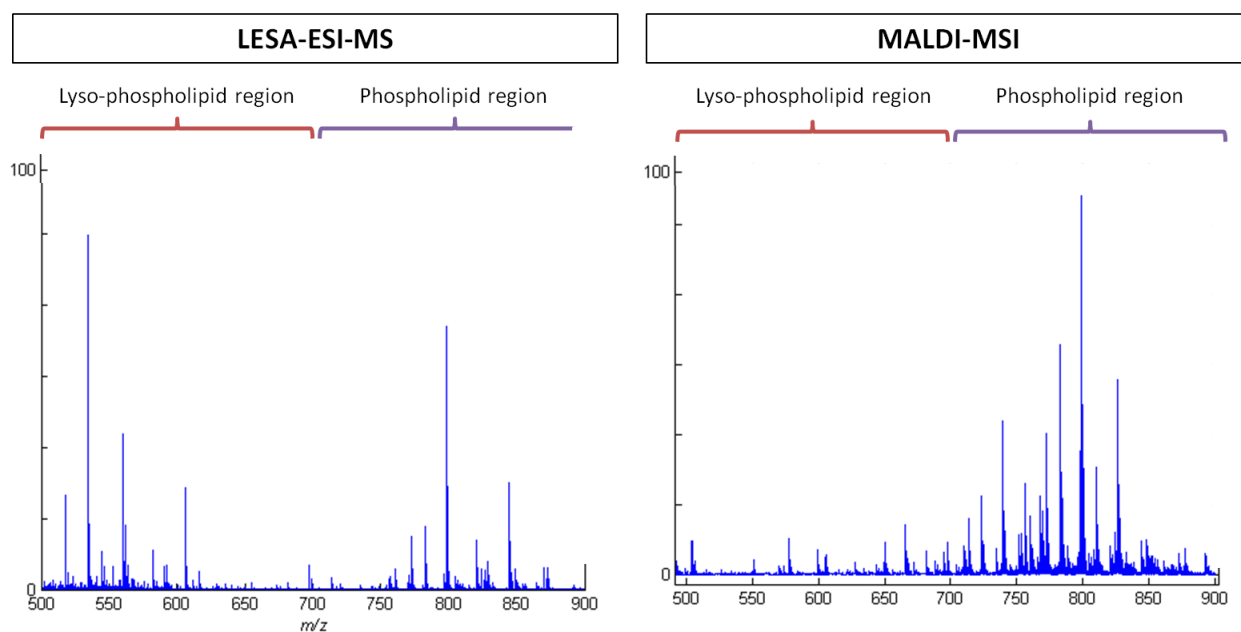
Figure 47 Mean mass spectra showing lipids detected in the region *m/z* 500-900 from (left) surface-sampling of freshly frozen tissue sections via LESA prior to ESI and (right) MALDI mass spectrometry imaging analysis. Lyso-phospholipids are detected in the region *m/z* 500-700 and phospholipids in the region *m/z* 700-900.

LESA-ESI is a relatively new surface-sampling technique. Many groups have explored the use of LESA for the analysis of drugs and/or drug metabolites [122-124, 286, 287] and protein or peptide species [125]; however only a few groups have considered its use for the analysis of lipid analytes. Brown *et al.* used LESA for the detection of both polar and non-polar lipid species, such as phosphatidylcholines and wax esters, directly from contact lens material [126]. The ability to ionise both polar and non-polar analytes under the same conditions is a particular advantage of ESI in comparison to MALDI; matrix compound selection must be carefully optimised for each analyte in MALDI, few matrix compounds lead to the simultaneous detection of both polar and non-polar species. Optimisation of these experimental parameters is a large area of research in the field of MALDI-MS and MSI. Brown's study also demonstrates the compatibility of LESA with concave surfaces; laser ablation is not so tolerant of samples with such varying heights incident to the laser beam.

A further advantage of LESA over traditional ESI analysis of lipids is the ability to extract analytes directly from the sample surface, removing the need for time-consuming extraction procedures methods such as Folch [204]. Stegemann *et al.* showed that direct extraction of lipid species from human atherosclerotic plaques provides similar results to bulk lipid extraction. Furthermore, the particular advantage of LESA to sample a single surface was exploited by Brown's analysis of both sides of contact lenses (eye side and air side). It would be difficult to ensure lipid extraction from a single side

of the lens by manual techniques and the efficiency of the process would be limited as the sample could not be homogenised.

A number of groups that have performed LESA-ESI analysis of lipids directly from tissue surfaces have also considered MS/MS profiling of detected lipid analytes in clinical samples [121, 126]. Dissociation of lithium adducts of a number of different lipid classes have been reported to provide similar improvements in structural characterisation studies when ions are formed by electrospray to those shown in Chapters 1 and 3 of this thesis by MALDI [230, 288]. Furthermore, assignment of the fatty acid residues of triacylglycerol lipids is reportedly enriched by lithium adduction [113] and double-bond assignment of unsaturated fatty acids has been enhanced by dissociation of lithium-lipid adducts [227]. Here we explore the analysis of formal lithium-fixed tissue samples by LESA-ESI; the formation of lithium adducts of a variety of lipid species is desirable for structural studies.

5.3.2 LESA-ESI analysis of Formal Lithium Fixed Tissue Sections

Lithium-lipid adducts were detected in high abundance in formal lithium-fixed tissue as shown in Figure 48. Peaks relating to protonated, sodium or potassium adducts were found to be significantly less abundant in comparison to fresh tissue sections. Protonated lipid adducts were detected in higher abundance in freshly frozen samples when sampled by LESA when compared with MALDI-MSI data. The increased relative abundances of protonated adducts detected in the LESA study could be owing to the nature of the ionisation process and/or the solvent system used to sample the tissue surface and form the spray in the experiment. A solvent system comprising 70% methanol with the addition of 0.1% formic acid was used in this analysis. As methanol and water are both protic solvents and formic acid is also a proton donor it is perhaps unsurprising that protonated adducts form in relatively high abundance. It follows that higher relative abundances of protonated adducts were also detected in LESA-ESI sampling of formal-lithium fixed tissue.
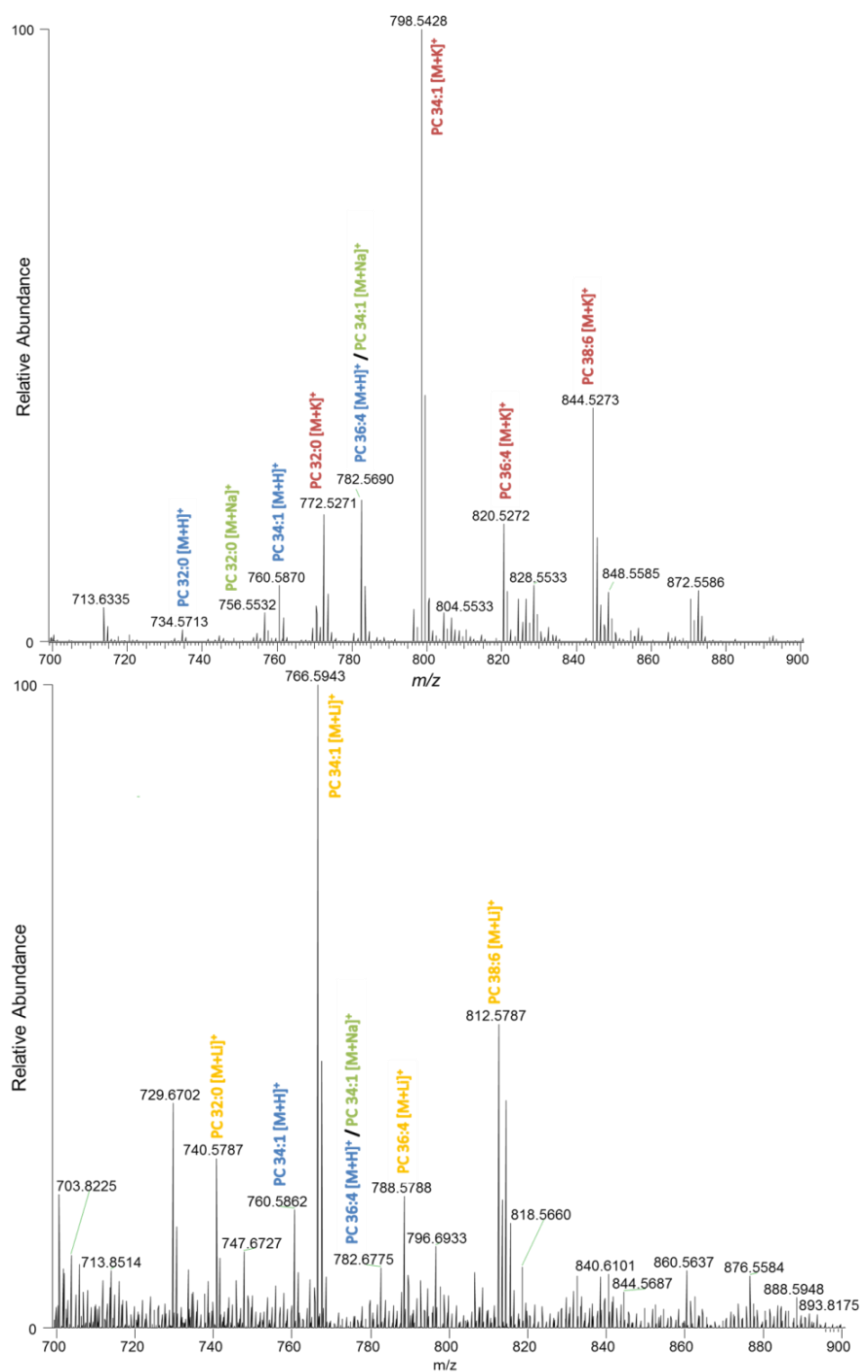
Figure 48 Mean spectra showing phospholipids species detected in the region *m/z* 700-900. Lipid adducts of three PC lipid species (PC 32:0, 34:1 and 36:4) detected in freshly frozen tissue (above) and formal lithium fixed tissue (below) are highlighted. Highly abundant lithium lipid adducts were detected in the formal lithium preparation.

Again, a range of phospholipid and lyso-phospholipid species such as phosphocholine (PC), lyso- phosphocholine (LPC), phosphethanolamine (PE) lyso-phosphethanolamine (LPE), phosposerine (PS), lyso-phosposerine (LPS), phosphoglycerol (PG) and a number of phophnositol (PI) and sphingomyelin (SM) species were detected. A number of neutral lipids such as diacylglycerol and triacylglycerol lipid species were also identified by their accurate mass. The pie charts in Figure 49 describe the range of lyso-, phospholipid and other lipid species detected in formal lithium-fixed tissue samples. Although a number of neutral lipids can be assigned by accurate mass, many of these were not lithium-lipid adducts. As tissue fixation removes protein analytes which have a high number of charged sites from the extracted sample, it is possible that a higher number of neutral lipid analytes can successfully compete for protons or cations. Furthermore, increased acidity of the fixed sample in comparison to fresh samples could explain increased detection of protonated adducts of neutral and other lipids.

Collision-induced dissociation of selected peaks in Chapter 4 of this thesis showed that lithium adducts provide structurally informative product ions relating to both the lipid head-group and fatty acid side-chain identities whereas other lipid adducts do not. It follows that analysis of formal-lithium tissue samples by imaging techniques such as desorption electrospray ionisation (DESI) should enable the acquisition of similar data to that presented herein by MALDI and LESA.

Lyso Lipids Detected in Formal Lithium Fixed Tissue   **Lipids Detected in Formal Lithium Fixed Tissue**
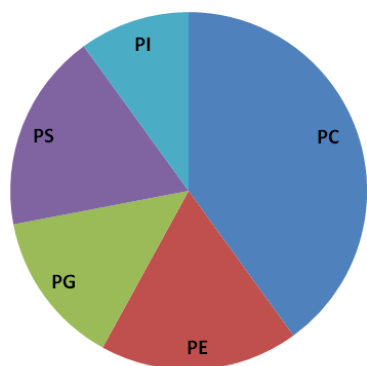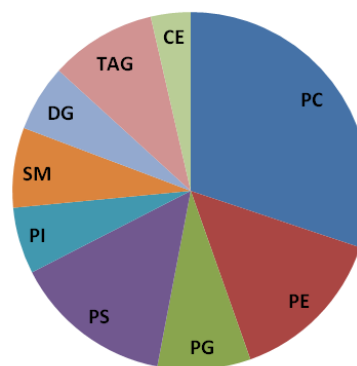
Figure 49 Pie charts showing the relative numbers of lyso-phospholipid and phospholipid species detected in LESA-ESI analysis of formal lithium-fixed tissue, assigned by accurate mass.

5.3.3 LESA-ESI analysis of Formal Calcium-Fixed Tissue Sections

Fixation of tissues in a formal calcium solution has been shown to aid lipid retention [289]. This could be beneficial in the preservation of lipid species in archived tissue samples. In order to evaluate whether this type of sample preparation is compatible with mass spectrometry analysis of lipid analytes, tissue was fixed in a solution of calcium chloride in formalin (formal calcium). LESA-ESI sampling of the tissue surface led to the detection of a number of lipid species. As shown in Figure 50, highly abundant protonated adducts of lipid analytes were detected in formal calcium-fixed tissue. The detected species in the phospholipid region *m/z* 700-900 were comparable to those detected in freshly frozen tissue described in the previous section of this chapter. The agreement in detected lipid species between freshly frozen and formal calcium-fixed tissue samples is particularly important as it shows that mass spectrometry analysis of formal-fixed samples is tolerant of a variety of salts.
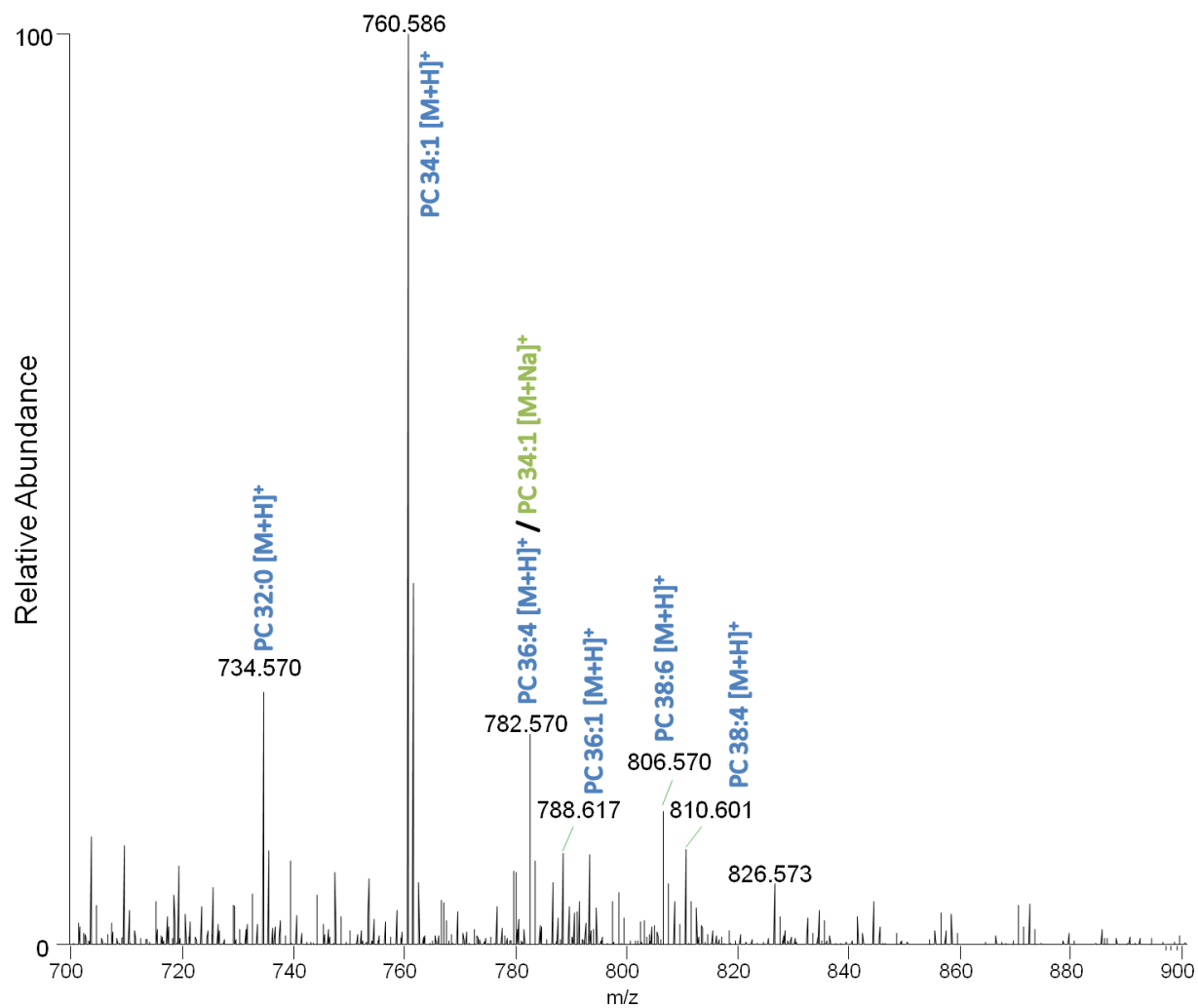
Figure 50 Mass spectrum acquired from surface sampling formal calcium-fixed murine brain by LESA in the *m/z* region 700-900.

Predominantly singly charged protonated adducts of lipid species were detected, alongside lower abundances of sodium and potassium adducts. Adducts of the most abundant phosphocholine lipid detected, PC 34:1, in both freshly frozen tissue and the formal calcium-fixed sample are shown in Figure 45 and Figure 50 respectively. There is a very clear difference in the dominant adduct formation. Potassium adducts were most abundant in freshly frozen tissue whereas protonated lipid adducts were most abundant in the formal calcium-fixed sample.

Doubly charged species were also detected in low relative abundance in the formal calcium-fixed specimen. These are most obvious above m/z 1000. A number of doubly charged species were detected in the region m/z 1140-1190 as shown in Figure 51. These doubly charged species cannot be attributed to protein species because the process of chemical fixation cross-links proteins, hence they are not detected in fixed tissue samples. Therefore these species are most likely attributed to multiply charged lipid adducts formed with the doubly charged calcium cation. For example, the doubly charged peaks centred on m/z 1159.85 could be attributed to a lipid metal complex of Ca^{2+} and three PC 34:1 lipid molecules $[Ca+(PC\ 34:1)_3]^{2+}$ and those centred on m/z 1146.84 could be attributed to a lipid metal complex of Ca^{2+}, two PC 34:1 and one PC 32:0 lipid molecules $[Ca+(PC\ 34:1)_2(PC\ 32:0)]^{2+}$.
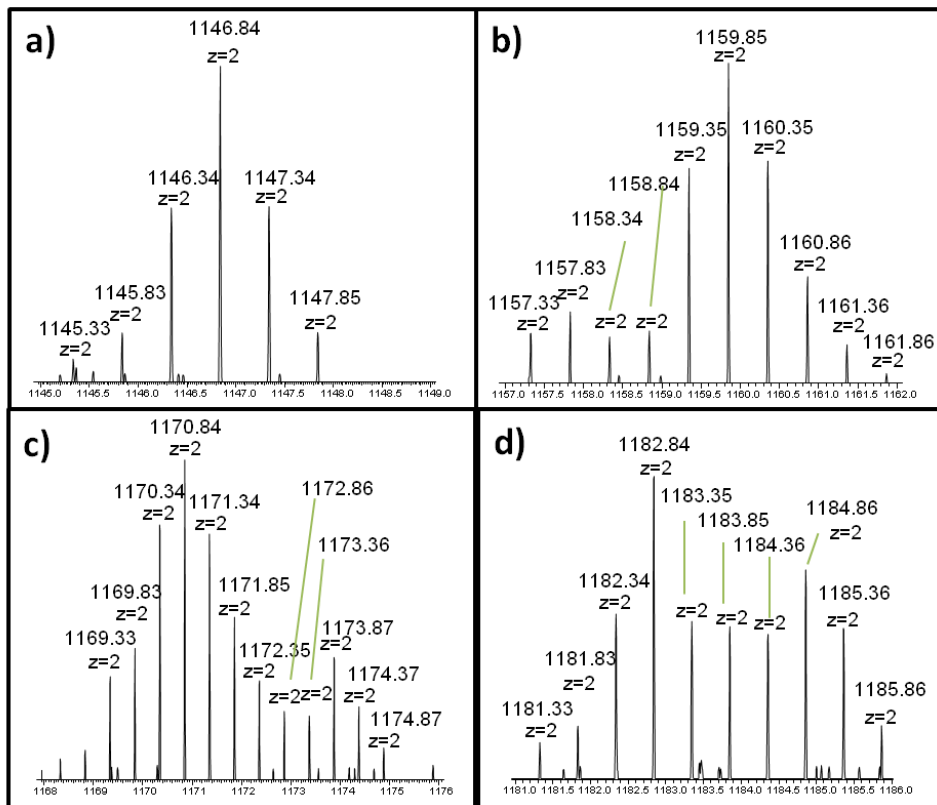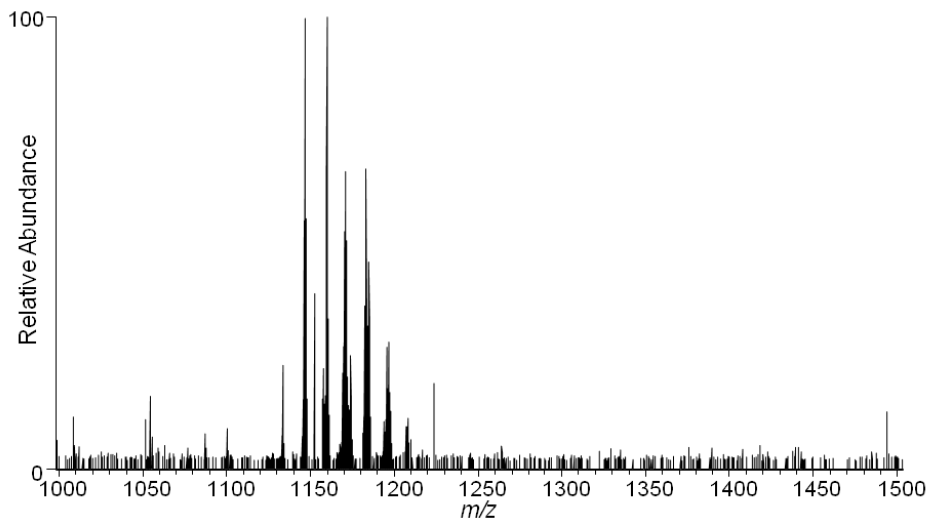
Figure 51 Mass spectrum showing species detected in the region *m/z* 1000-1500 from LESA-ESI analysis of formal calcium-fixed tissue. Insets a) to d) show magnifications of regions showing doubly charged species.

Closer inspection of the detected species in the region *m/z* 700-900, displayed in Figure 52, reveals that a number of doubly charged species were detected in low abundance. Peaks at *m/z* 779.56 can be attributed to the presence of the calcium adduct of PC 34:1 with two lipid species associated around the metal centre [Ca+(PC 34:1)$_2$]$^{2+}$ which has been detected in previous electrospray studies considering the analysis of PC lipids in the presence of calcium ions [146].

The detection of multiply charged lipid species alongside protonated adducts in complex biological samples such as tissue leads to decreased sensitivity and increased spectral complexity. However, the fact that multiply charged lipid species can be formed by the inclusion of a divalent cation enables the opportunity to explore dissociation techniques that require a multiply charged species, such as electron capture or electron transfer dissociation, which cannot usually be considered in MALDI.
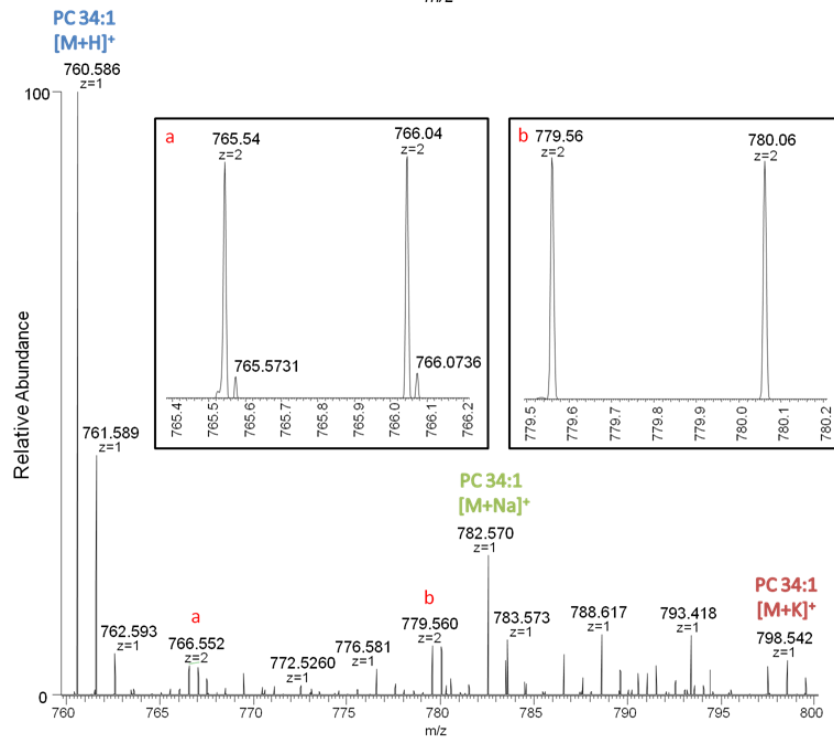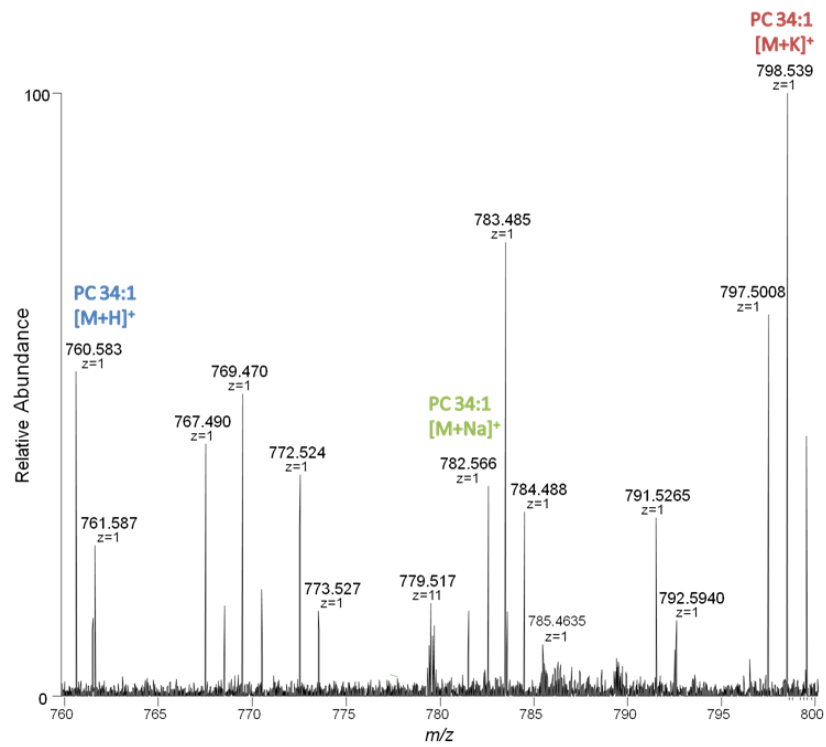
Figure 52 Mass spectra showing adducts of PC 34:1 detected in freshly frozen tissue (top) and formal calcium-fixed tissue (bottom) analysed by LESA-ESI. Insets a and b show doubly charged peaks at *m/z* 765.54 and 766.05 and 779.56 and 780.06 respectively, characterised by a separation of 0.5 u.

5.4 Conclusions

Surface sampling of thin tissue sections by LESA-ESI is shown to be compatible with both freshly frozen and formal-fixed tissue samples. Coupling sample ionisation to a high resolution mass analyser (orbitrap) enables the assignment of species with greater confidence. Furthermore, the improved sensitivity of this technique, compared to MALDI-MS on a Q-TOF mass analyser, is displayed in the number of different phospholipid species determined in this analysis. In addition, improved sensitivity for lyso phospholipid species is shown.

LESA of formal lithium-fixed tissue samples leads to the detection of abundant lithium-lipid adducts. Although lipids can be readily assigned, owing to the ability to acquire high mass accurate data, a range of different lipid adducts were still detected. Lithium ion introduction via tissue fixation in a formal fixative solution did not lead to as great an extent of control of adduct formation when compared to the MALDI-MSI data presented in Chapter 3 of this thesis; the relative abundances of, for example, protonated adducts remains high. An alternative approach to lithium ion introduction, such as in the sampling solvent system, may be more beneficial for this technique. Collision-induced dissociation of lithium adducts leads to the detection of more product ions that provide greater structural information than other lipid adducts. Hence lipid profiling of clinical samples could potentially be enhanced by the analysis of these types of samples.

Analysis of formal-fixed samples prepared with a doubly charged calcium cation is also shown to be compatible with LESA-ESI. Different lipid adducts are predominant in different samples; potassium adducts are most abundant in fresh tissue whereas protonated adducts are most abundant in formal calcium-fixed tissue sections. However, the detection of a number of doubly charged lipid species in the formal calcium sample indicates that data interpretation of these formal-fixed samples may not be as straightforward as those prepared with a singly charged metal cation, such as lithium.

Although the detection of doubly charged lipid species directly from complex biological samples may not be advantageous, the fact that these can be formed enables the opportunity to consider electron-mediated dissociation techniques for structural studies. Further work will consider the addition of doubly charged metal cations to solutions of lipid standards in dissociation studies, including electron-transfer dissociation.

6. Fragmentation chemistry of $[M^{II}+L_n]^{2+}$ complexes of phosphocholines

6.1 Introduction

The use of additive salts in collision-induced dissociation (CID) studies of lipid analytes (L) has thus far predominantly considered the inclusion of Group 1 metal salts (M), forming singly charged $[L+M]^+$ adducts in electrospray ionisation (ESI) [228, 290]. Investigations into the dissociation of singly charged lipid species by Hsu *et al.* have shown that lipid adducts of the smallest Group 1 metal (lithium) provide the most useful dissociation product ions with respect to structural information of lipid analytes [113, 228-230, 290]. Multiply charged species as well singly charged ions can be formed by ESI and the formation of such species enables the opportunity to consider electron-mediated dissociation techniques such as electron-transfer dissociation (ETD) and electron-capture dissociation (ECD).

Ho *et al.* have reported a comprehensive evaluation of CID of lipid adducts formed with monovalent, divalent and trivalent cations [265]. Salts of lithium, sodium, potassium, strontium, barium and the whole of the first transition metal series were considered for CID of a range of phospholipid standards (PE, PG and PC). CID of divalent metal-lipid adducts of the form $[L-H+M^{II}]^+$ were shown to provide product ions indicative of the identities of the head-group designated in the *sn*-3 position and the fatty acid side-chains residing in the *sn*-1 and *sn*-2 positions. Multiply charged lipid species can be readily formed by electrospray ionisation and investigations into

the dissociation of doubly charged metal-lipid samples have been recently reported in the literature [146, 291].

James *et al.* have shown that lipid-metal complexes of the form $[L_n+M^{II}]^{2+}$ up to n=8 can be detected by ESI analysis of a PC lipid in the presence of copper (II). Their study of the CID fragmentation pathways of the different lipid-metal clusters detected, showed that when n > 4 the dominant product ions indicated the neutral loss of one or more lipid molecules [291]. More informative product ions were detected by dissociation of smaller complexes.

The formation of divalent metal-lipid complexes offers the opportunity to consider ECD or ETD for which multiply charged ions are required. James *et al.* later reported ECD of PC lipid standards formed by the incorporation of 4 mM metal salt ($CaCl_2$, $MgCl_2$, $CoCl_2$ or $CuCl_2$). A number of factors were considered in the ECD analysis of divalent metal-lipid complexes; the size of the lipid ligand, the number of ligands and also the effect of changing M^{2+}. It was shown that to obtain product ions which are indicative of fatty acyl chains, calcium and magnesium divalent cations in the smallest complex form ($[L_2+M^{II}]^{2+}$) were most informative [146]. These divalent metals have not been considered previously in CID or ETD analysis of phospholipids by ESI.

ETD and CID of phospholipids were compared by Liang *et al.*; they generated multiply charged species from doubly sodiated-lipid species [148]. Electron transfer dissociation of a doubly sodiated PC lipid was shown to provide structurally informative product ions enabling assignment of *sn*-1, *sn*-2 and *sn*-3 side-chains. Although this dissociation technique has proven useful for structural analysis of lipids, to date, ETD of doubly charged lipid complexes formed with doubly charged metal cations has not been considered.

High-energy collision-induced dissociation (HE-CID) of lipid species has also been shown to be beneficial in the structural analysis of PC lipid species. Shimma *et al.* showed that the double-bond location can be determined by HE-CID analysis of singly charged Group 1 cationic metal-lipid adducts [154]. The dissociation of doubly charged lipid species by HE-CID however has not been reported.

The aim of this investigation was therefore to determine whether other divalent cations could provide useful dissociation data. The opportunity to perform electron transfer dissociation enables comparisons with the types of product ions detected with collision-induced dissociation and high energy-CID to be made. Inclusion of a Group 2 metal cation in PC lipid solutions led to the detection of a range of lipid-metal complexes of varying size (increasing number of lipid species associated with the metal centre). For simplicity, only the dissociation of the smallest lipid-metal complexes $[L_2+M]^{2+}$ formed with Group 2 metals cations will be considered (as these were shown to yield the most useful dissociation data by James *et al.*) [291]. The three smallest Group 2 metals (Be^{2+}, Mg^{2+} or Ca^{2+}) will be evaluated in order to determine

whether similar trends with respect to cation size to those reported for CID of singly charged Group 1 metal-lipid adducts are apparent. Collision-induced dissociation will be first considered and then compared to high energy-collision-induced dissociation (HE-CID) and electron-transfer dissociation (ETD).

6.2 Experimental

6.2.1 Materials

Lipid standards 1-palmitoyl-2-oleyl-*sn*-glycero-3-phosphocholine PC (18:1/16:0) and 1-palmitoyl-2-steroyl-*sn*-glycero-3-phosphocholine PC (18:0/16:0) were purchased from Avanti Polar Lipids Inc. (Delfzyl, The Netherlands). All salts ($BaSO_4$, $MgCl_2$ and $CaCl_2$) and formic acid (FA) were purchased from Sigma Aldrich (Gillingham, UK). Methanol (HPLC grade) was purchased from Fisher Scientific (Leicestershire, UK). Water was purified by an ELGA Option 3 system (Marlow, UK). Plain glass slides were purchased from Leica (UK).

6.2.2 Sample Solutions

Solutions of final concentration 5 µg ml^{-1} lipid with the inclusion of 0.5 mM salt in 70% MeOH/0.1% FA were used for direct infusion experiments.

6.2.3 Direct Infusion

Automated sample analysis was performed using the LESA Points software (Advion Ithaca, NY) which controls the TriVersa Nanomate. This platform was used to select the locations of the sample wells for sampling routines using the Nanomate probe. The LESA sampling routine involved the collection of a conductive tip from the Advion tip rack before moving to the sample well. The Nanomate probe aspirated 5 µL into the conductive tip and then the tip was rotated and engaged with the back of the ESI chip, and nanospray ionisation was initiated. The Triversa Nanomate was coupled with a Thermo Fisher Scientific Orbitrap Velos mass spectrometer.

6.2.4 Mass Spectrometry

Electrospray analysis was performed on an LTQ Orbitrap Velos from Thermo Fisher Scientific (Leicestershire UK). Samples were introduced by direct infusion (Advion Ithaca, NY) with solvents comprising 70:30:0.1 $CH_3OH:H_2O:FA$. Samples were introduced at a flow rate of ~80 nL/min with a gas pressure of 0.3 psi, a tip voltage of 1.75 kV and a capillary temperature of 250 °C. MS data were collected in full scan mode (*m/z* 500-1500) with a resolution of 100 000 at *m/z* 400. The Automatic Gain Control (AGC) was used to accumulate sufficient ions for analysis. The AGC target was $1x10^6$ with a maximum fill time of 2 s in full scan mode. For CID and HE-CID MS/MS experiments collision energy was optimised between 0-50. Nitrogen was used as a collision gas. For ETD MS/MS experiments activation time was optimised between 0-500 ms. All data were acquired for 3 minutes.

6.2.5 Data Conversion

LESA data were converted to mzML using msconvert as part of ProteoWizard [284]. Spectra acquired from a single injection were summed using a custom MATLAB script and output to mzML. The summed spectra were then converted to imzML using imzMLConverter [236] and processed in MATLAB.

6.3 Results and Discussion

6.3.1 Mass Spectrometry analysis of PC lipids in the presence of Group 2 metals

Direct infusion ESI-MS analysis of phosphocholine lipid standards PC 18:1/16:0 and PC 18:0/16:0 in the presence of 0.5 mM magnesium (Mg^{2+}) or calcium (Ca^{2+}) ions led to the detection of a number of lipid-metal adducts. Doubly charged lipid-metal complexes of the type $[L_2+M^{II}]^{2+}$ for M = Mg at m/z 774.59 and $[L_3+M]^{2+}$ m/z at 1155.39 (where M designates the divalent metal cation and L denotes the lipid species) were detected in the mass range 700-2000 alongside singly charged species of the form $[L+H]^+$ at m/z 762.60 (protonated lipid species) and $[L-H+M]^+$ at m/z 784.59 (loss of a hydrogen and association of the doubly charged metal cation). These lipid-metal adducts are shown in Figure 53.

Larger lipid-metal complexes of the form $[L_4+M]^{2+}$ and $[L_5+M]^{2+}$ were detected in some experiments, however the relative intensity of these was low. Analysis of these PC lipid standards in the presence of beryllium (Be^{2+}) ions led to variable results. The above described metal-lipid complexes were detected in some experiments however this proved irreproducible. As beryllium-lipid complexes could not be reliably formed, the dissociation of these adducts was not considered.

The detection of multiple complexes of varied size led to a complex spectrum of a single lipid species when compared to experiments where only a singly charged metal is present. James and coworkers described similar doubly charged lipid-metal complexes in their CID study of PC species upon the inclusion of copper (II) metal cations in lipid solutions [291]. This study helps explain the complicated spectra shown in Figure 51 in Chapter 4 of this thesis and could be a potential disadvantage to analysis of lipids with doubly charged cations as increasing spectral complexity is undesirable. Nevertheless if these adducts provide greater structural information than singly charged lithium-lipid adducts in dissociation experiments, their formation would be beneficial.
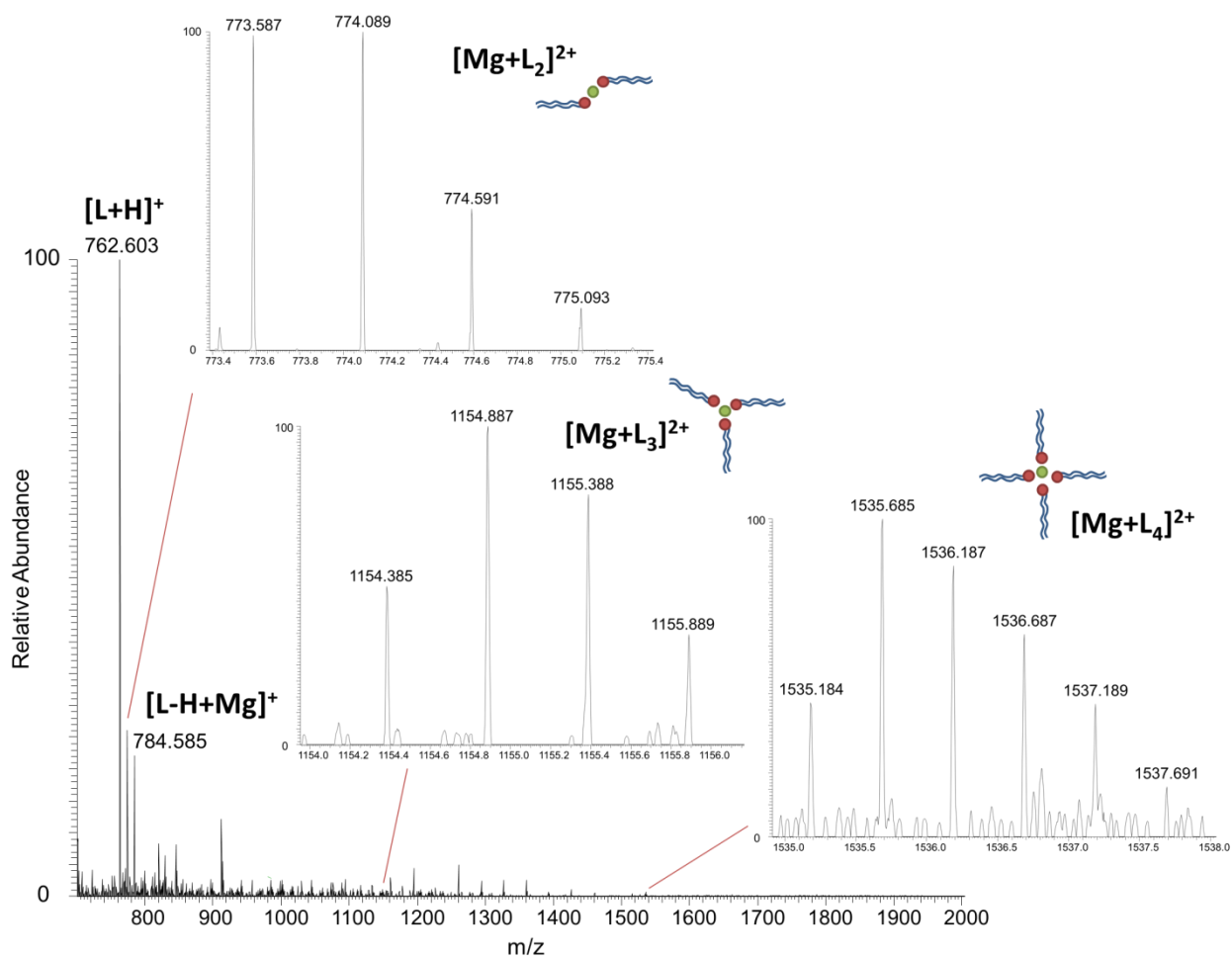
Figure 53 ESI mass spectrum showing lipid adducts and complexes detected when PC 34:0 (18:0/16:0) was analysed in the presence of magnesium ions. The full mass spectrum (*m/z* 700-2000) acquired by direct infusion ESI is presented with insets showing lipid-metal complexes of the form $[Mg+L_2]^{2+}$, $[Mg+L_3]^{2+}$ and $[Mg+L_4]^{2+}$.

When the PC lipid containing only saturated fatty acid side-chains was analysed (PC 18:0/16:0) in the presence of magnesium or calcium ions, the most abundant lipid adduct detected was the protonated lipid $[L+H]^+$ followed by the $[M^{II}+L_2]^{2+}$ complex. The opposite was true when the lipid species containing an unsaturated fatty acid side-chain was analysed (PC 18:1/16:0), which could indicate that the doubly charged metal cation associates with the electron rich double bond in the unsaturated fatty acid side-chain, hence the increased relative abundance of the doubly charged lipid-metal complex.

The singly charged $[M^{II}+L-H]^+$ adduct was also detected in each experiment, however the relative abundance of this species depended on the metal cation and lipid. Similar abundances of the $[Mg+L_2]^{2+}$ complex and $[Mg+L-H]^+$ adduct were detected when PC 18:0/16:0 was analysed. However the $[Mg+L-H]^+$ adduct was detected lower in abundance than the $[L+H]^+$ adduct and $[Mg+L_2]^{2+}$ complex when PC 18:1/16:0 was analysed. The $[Ca+L-H]^+$ adduct was detected in lowest abundance when PC 18:0/16:0 was analysed and yet this was detected in similar abundance to the $[L+H]^+$ adduct when PC 18:1/16:0 was analysed, as shown in Figure 54. It is not clear why this might be the case. As the $[M^{II}+L-H]^+$ adduct was not the most abundant in most experiments, dissociation of these singly charged species was not considered in the presented study.
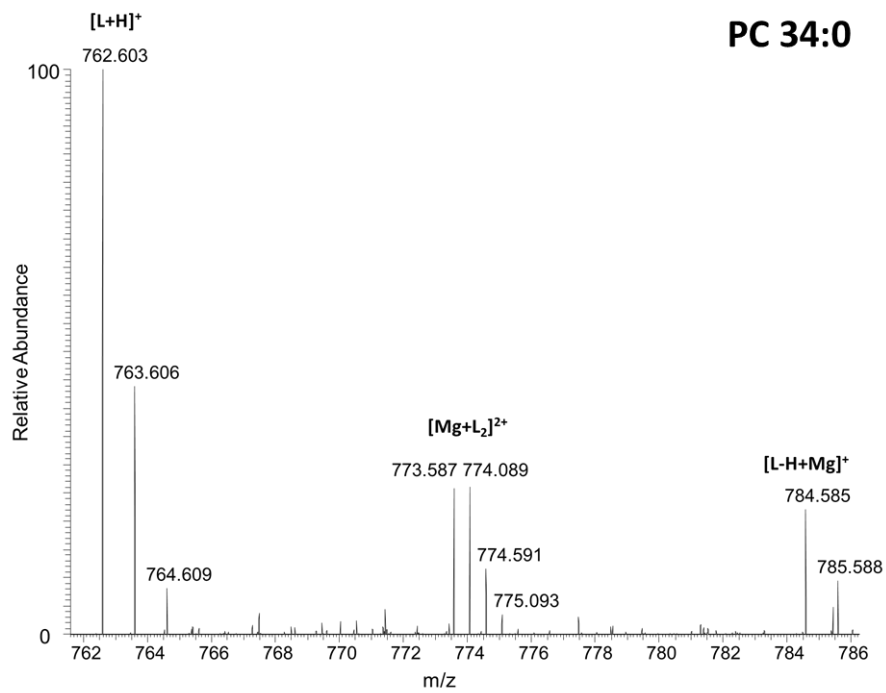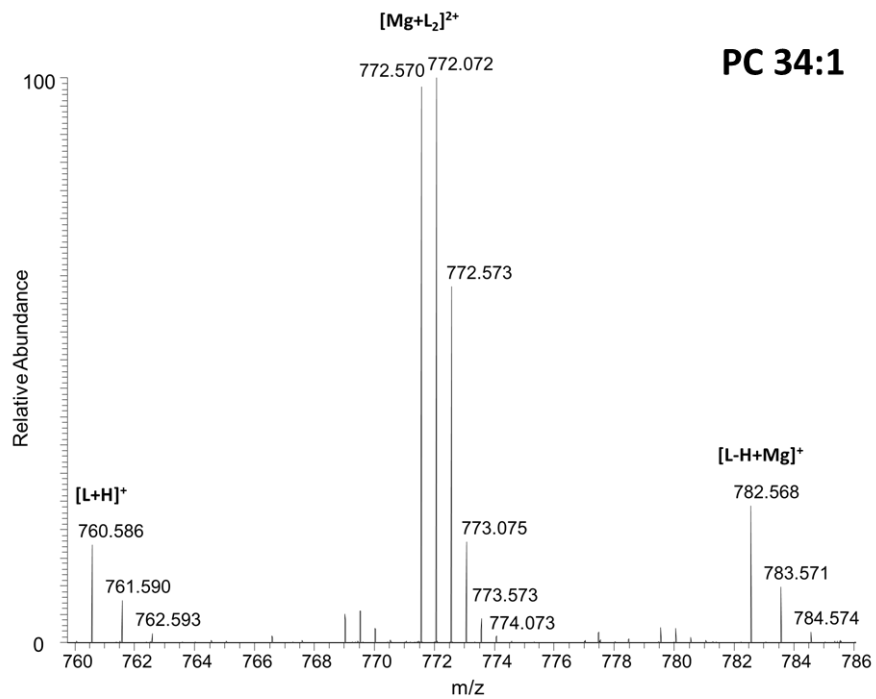
Figure 54 Mass spectra showing the relative abundance of [L+H]+, [Mg+L₂]²⁺ and [L-H+Mg]+ when PC 34:0 (18:0/16:0) and PC 34:1 (18:1/16:0) were analysed by direct infusion ESI.

Ho *et al.* investigated CID of a range of lipid-metal adducts, reporting that the inclusion of a divalent metal in lipid standard solutions leads to the formation of adducts of the form $[M^{II}+L-H]^+$ for PE and PG lipid species [265]. However, their study did not consider PC lipid species or any of the divalent cations reported in this investigation. All first row transition metals were considered alongside strontium and barium. Doubly charged lipid-metal complexes similar to those described herein were not considered in their study, only $[M^{II}+L-H]^+$ adducts are described. It is therefore possible that different lipid adducts are preferentially formed by electrospray analysis with changing Group 2 metal cation, with larger cations such as strontium and barium forming $[M^{II}+L-H]^+$ adducts preferentially to $[M^{II}+L_n]^{2+}$ lipid-metal complexes. Further studies considering a wider range of Group 2 metal cations in a single experiment could therefore be beneficial.

The relative complexity of the spectra suggests that the use of divalent cations in complex lipid samples could be limited. Mass spectrometry analysis of doubly charged lipid-metal complexes could potentially be improved by utilising an ion mobility cell which separates ions by mobility in a carrier gas as ion mobility differs for ions with the same *m/z* value. Despite these possible complexities, these doubly charged ions may still be helpful in the analysis of a single lipid species after lipid separation. The main aim of this investigation was to determine whether the use of divalent cations could provide useful dissociation data, allowing the opportunity for ETD. For simplicity, only dissociation of the $[M^{II}+L_2]^{2+}$ lipid complex formed with

Mg^{2+} or Ca^{2+} cations will be considered. CID will be first considered and then compared to ETD.

6.3.2 Collision-Induced Dissociation (CID) of [M^{II}+L$_2$]$^{2+}$ lipid-metal complexes

CID of the [Mg+L$_2$]$^{2+}$ complex of PC 18:1/16:0 (*m/z* 772.07) led to the detection of a variety of product ions, most of which were singly charged. The most abundant product ion displayed in Figure 55A was indicative of one of the fatty acid side-chain identities, detected at *m/z* 504.344. This product ion is indicative of the neutral loss of the magnesium adduct less hydrogen of the *sn*-1 16:0 fatty acid [Mg+L$_2$-H–R$_1$COOMg-H]$^+$ from the [Mg+L–H]$^+$ species detected at *m/z* 782.55. The next most abundant product ion was detected at *m/z* 478.328 and is indicative of a similar loss of the 18:1 *sn*-2 fatty acid [Mg+L$_2$-H–R$_2$COOMg-H]$^+$. Comparable product ions were detected upon CID of the [Ca+L$_2$]$^{2+}$ complex of PC 18:1/16:0 (*m/z* 780.06), and when a saturated lipid PC 18:0/16:0 was dissociated in the form [Mg+L$_2$]$^{2+}$ (*m/z* 774.08) or [Ca+L$_2$]$^{2+}$ (*m/z* 784.59), as shown in Figure 55.
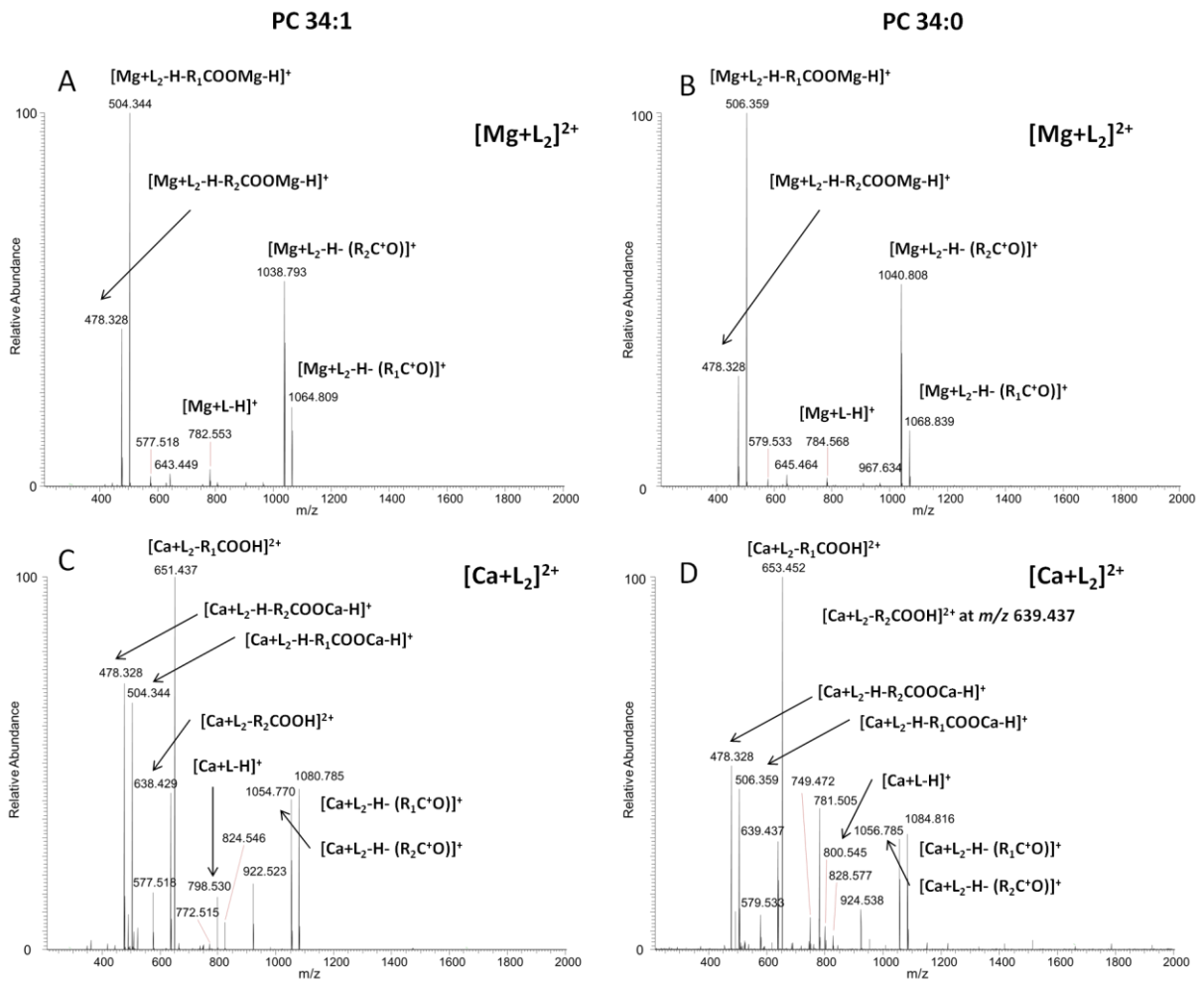
Figure 55 Representative ESI-MS/MS spectra showing product ions detected following collision-induced dissociation of (A) *m/z* 772.07 [Mg+L$_2$]$^{2+}$ lipid-metal complex of PC 34:1 (18:1/16:0), (B) *m/z* 774.08 [Mg+L$_2$]$^{2+}$ lipid-metal complex of PC 34:0 (18:0/16:0), (C) *m/z* 782.58 [Ca+L$_2$]$^{2+}$ lipid-metal complex of PC 34:1 (18:1/16:0) and (D) *m/z* 784.59 [Ca+L$_2$]$^{2+}$ lipid-metal complex of PC 34:0 (18:0/16:0).

The detection of product ions at *m/z* 504.344 and 478.328 are commonly reported in CID studies of lithium adducts $[L+Li]^+$ of PC 18:1/16:0 and are indicative of the neutral loss of the lithium salt of each respective fatty acid side-chain from the $[L+Li]^+$ parent [143, 235]. This study suggests that similar product ions are formed by CID of doubly charged Group 2 lipid-metal complexes when compared to those formed by CID of singly charged Group 1 cationic lipid adducts. However, whilst these fatty acid side-chain indicative product ions are detected in relatively low abundance in CID studies of singly charged Group 1 cationic lipid adducts, in comparison to other detected product ions, they were the most abundant product ions detected upon CID of these $[M^{II}+L_2]^{2+}$ lipid metal complexes.

Collision-induced dissociation studies conducted by Ho *et al..* of singly charged adducts of the form $[M^{II}\text{-}H+L]^+$ (where M^{II} = Sr or Ba) also led to the detection of product ions which were indicative of the neutral loss of each fatty acid along the glycerol backbone for a range of phospholipids [265]. Neutral losses of the *sn*-1 fatty acid side-chain were detected in greater abundance and enabled determination of the relative positions of each fatty acid. One stark difference between the product ion spectra described by Ho *et al.* and those presented herein is the relative abundances of product ions indicative of the head-group and fatty acid side-chain identities; neutral losses, characteristic of fatty acid losses, were detected in highest abundance in our study but were detected in lower abundance than head-group-specific product ions in Ho's study.

The next most abundant product ions detected were also indicative of the fatty acid side-chain identities. Peaks detected at m/z 1038.79 and 1064.81 upon CID of the $[Mg+L_2]^{2+}$ complex of PC 18:1/16:0 suggest the loss of 504 u and 478 u from the singly charged lipid-metal complex $[Mg+L_2]^+$. These masses correspond to the singly charged product ions detected at m/z 504 and 478 indicating the loss of each fatty acid side chain, or the detection of $[Mg(L)+C_{16}H_{31}O_2]^+$ and $[Mg(L)+C_{18}H_{33}O_2]^+$. Similar peaks detected at m/z 1040.81 and 1068.84 upon CID of the $[Mg+L_2]^{2+}$ complex of PC 18:0/16:0, suggest the loss of 506 u and 478 u from the singly charged lipid-metal complex $[Mg+L_2]^+$. Similar product ions were detected upon CID of calcium-lipid complexes of both PC species. Analogous product ions were reported by James *et al.* in their investigation of CID pathways of PC lipid-copper complexes and can be described as a carboxylate abstraction [291]. A phosphate abstraction pathway leading to the detection of $[Cu(L)+PC]^+$ was also described in the dissociation of $[Cu+L_2]^{2+}$, however comparable product ions were not detected in this study when either magnesium or calcium lipid-metal complexes were dissociated by CID.

Here it is shown that very high relative abundances of product ions informative of the fatty acid side-identities are detected upon collision-induced dissociation of $[M^{II}+L_2]^{2+}$ complexes of PC lipid species formed with either magnesium or calcium metal ions. Relatively high abundances of product ions informative of the *sn*-1 and *sn*-2 fatty acid side-chain identities were also reported by Ho *et al.* upon CID of singly charged divalent metal lipid adducts of the form $[L-H+M^{II}]^+$ [265]. Although the relative abundances of fatty acid-indicative product ions varied with changing M^{2+}

cation in Ho *et al.*'s study, generally they were detected in much greater abundance than dissociation of cationic lipid adducts of PE, PG and PS species formed with monovalent Group 1 cations. Similar benefits from CID of doubly charged complexes of the type $[M^{II}+L_2]^{2+}$ are demonstrated herein.

Additional product ions characteristic of the fatty acid side-chain identities, shown in Figure 56, were detected when the calcium $[Ca+L_2]^{2+}$ lipid-metal complexes of PC 18:1/16:0 (*m/z* 780.06) and PC 18:0/16:0 (*m/z* 782.07) were dissociated. Doubly charged peaks at *m/z* 651.94 and 638.93, detected following CID of $[Ca+L_2]^{2+}$ when L=PC 18:1/16:0 and *m/z* 653.95 and 639.94 when L=PC 18:0/16:0, correspond to neutral loss of the *sn*-1 and *sn*-2 fatty acid side-chains, respectively, from the $[Ca+L_2]^{2+}$ complex. These correspond to the neutral loss of the *sn*-1 fatty acid and the *sn*-2 fatty acid side-chain respectively from the doubly charged complex. Therefore, although the MS/MS mass spectra of calcium-lipid species contain a greater number of peaks, these are usefully informative product ions.

The relative abundance of product ions indicative of the identity of each fatty acid side-chain has been shown to be informative of the relative positions of the fatty acid side-chains along the glycerol backbone in previous ESI studies of lithium-lipid adducts[266]. In the present study (dissociation of $[M+L_2]^{2+}$ where L= either PC(18:0/16:0) or PC (18:1/16:0)), the relative abundance of the peak indicative of the loss of the metal salt of the *sn*-1 fatty acid was greater than the corresponding *sn*-2 fatty acid loss when the magnesium lipid complex was dissociated.
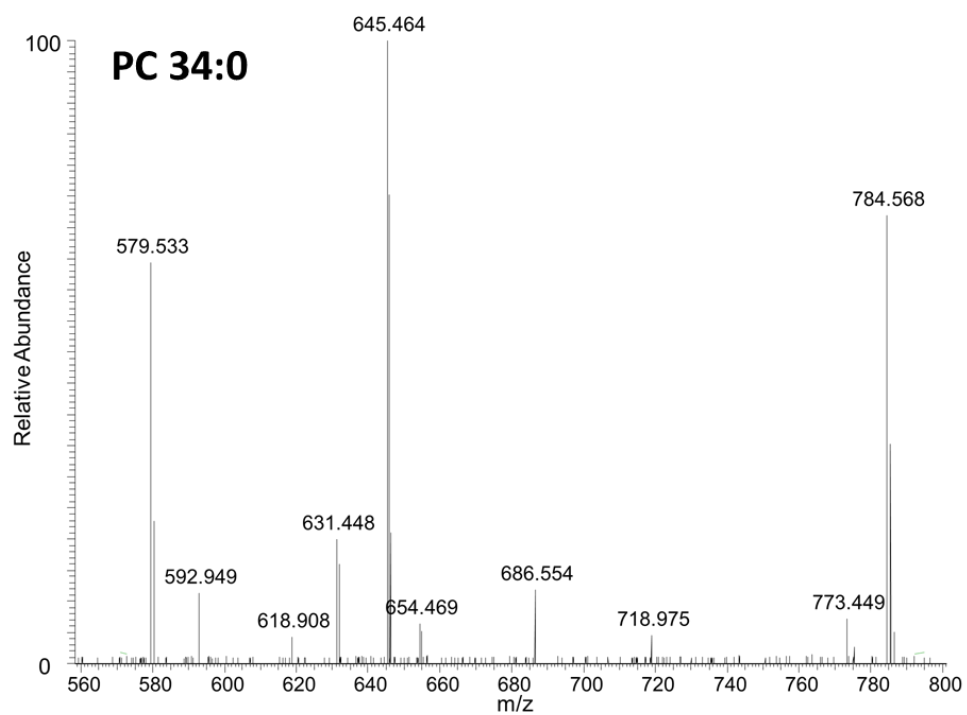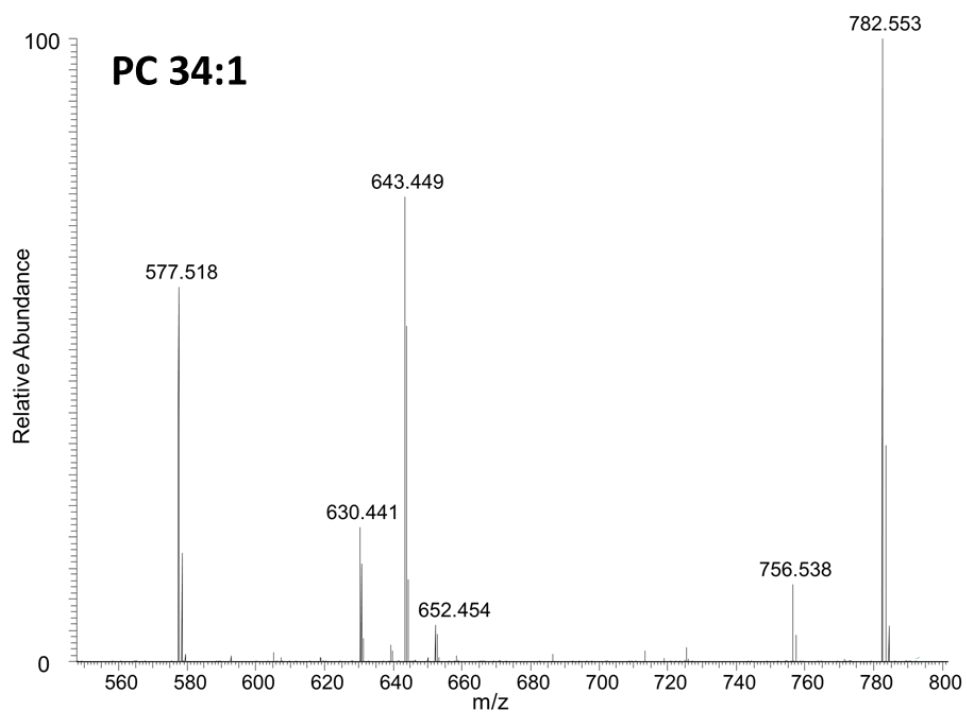
Figure 56 Representative ESI-MS/MS spectra showing product ions detected between *m/z* 560 and 800 following collision-induced dissociation of (top) [Ca+L$_2$]$^{2+}$ of PC 18:1/16:0 and (bottom) [Ca+L$_2$]$^{2+}$ of PC 18:0/16:0.

However, the opposite was true when the calcium-lipid complexes were subjected to CID. In these examples the loss of the *sn*-2 calcium lipid salt was detected in greater abundance than that of the *sn*-1 fatty acid. Moreover, further doubly charged product ions indicative of the neutral loss of each fatty acid side-chain from the calcium lipid complex were detected in the opposite relative abundance to the, similar, singly charged product ions; peaks indicative of the neutral loss of the *sn*-1 fatty acid were detected in greater relative abundance than the corresponding product ions indicative of the *sn*-2 fatty acid.

The identity of each of the *sn*-1 and *sn*-2 fatty acid side-chains is inferred by CID of these lipid-metal complexes irrespective of the metal. This result is in contrast to CID studies of monovalent cationic lipid adducts in which only dissociation of the lithium-lipid adduct has been shown to lead reliably to the detection of informative product ions in high relative abundance. CID studies of lithium-lipid adducts of a variety of different lipid species have shown that neutral loss of the *sn*-1 fatty acid (or the metal salt of such) is detected in greater relative abundance than corresponding *sn*-2 fatty acid losses. It would seem that the trends differ depending on the divalent metal cation in the presented study; however a much more detailed study considering a wider range of lipids with different fatty acid side-chains is needed to enable a more confident determination of these trends.

A further product ion was detected at *m/z* 577.518 upon CID of each lipid-metal complex ($[Mg+L_2]^{2+}$ or $[Ca+L_2]^{2+}$) when L = PC 18:1/16:0 and at *m/z* 579.533 upon CID of each lipid-metal complex ($[Mg+L_2]^{2+}$ or $[Ca+L_2]^{2+}$) when L = PC 18:0/16:0.

This product ion corresponds to the neutral loss of 205.04 from the [Mg+L-H]$^+$ adduct and is indicative of the loss of the magnesium adduct of the PC head-group minus hydrogen. This is a very important neutral loss as this indicates the head-group identity. Similar product ions have been reported upon CID of singly charged cationic lipid adducts, however these were the most abundant product ions detected when cationic lipid adducts of the type [M+L]$^+$ are dissociated but were not found to be highly abundant product ions in these investigations of divalent cationic lipid adducts.

No other product ions were detected which assist in the identification of the head-group moiety, which is in part owing to the reduced m/z window in which the data was acquired (m/z 210-2000). These settings are a function of the orbitrap instrumentation and cannot be changed in CID experiments as it is dictated by the parent ion mass selected. The magnesium or calcium adduct of the PC head-group would be expected at a lower m/z than 210. In order to determine whether these types of product ions can be detected by dissociation of these divalent metal-lipid complexes a lower m/z region can be considered by performing high-energy CID (HE-CID). This will discussed next.

6.3.3 High Energy-CID (HE-CID) of $[M^{II}+L_2]^{2+}$ lipid-metal complexes

High-energy collision-induced dissociation (HE-CID) of the magnesium $[Mg+L_2]^{2+}$ complex where L is PC 18:1/16:0 (*m/z* 772.07) led to the detection of highly abundant product ions at *m/z* 504.35 and 478.33, which are indicative of the two fatty acid side-chain identities. Similar product ions were detected in CID experiments and these product ions are discussed in greater detail above. In addition, detection of a product ion at *m/z* 577.52 when L = PC 18:1/16:0 was indicative of the loss of the PC head-group. In this way, the identity of each substituent along the glycerol backbone could be determined by this dissociation technique, see Figure 57. Corresponding product ions were detected upon HE-CID of the $[Mg+L_2]^{2+}$ complex of PC 18:0/16:0.

HE-CID of calcium $[Ca+L_2]^{2+}$ complexes of these two lipid standards led to the detection of similar product ions indicative of the fatty acid side-chain identities as well as the PC head-group. However further doubly charged product ions were detected at *m/z* 651.94 and 638.93 upon HE-CID of PC 18:1/16:0. These product ions correspond to neutral loss of the 16:0 *sn*-1 fatty acid and loss of the 18:1 *sn*-2 fatty acid side-chain, respectively, from the doubly charged complex. Similar product ions were also detected when PC 18:0/16:0 was analysed in the presence of calcium ions. These additional product ions were also detected when the calcium-lipid complexes were dissociated by CID. Again, it is unclear as to why these additional doubly charged product ions would be detected only when calcium lipid complexes were dissociated and not following dissociation of magnesium complexes.

The relative abundances of peaks that are indicative of the fatty acid side-chain identities displayed similar trends upon high-energy dissociation of either metal adduct with either lipid; the detection of the peak indicating loss of the *sn*-1 fatty acid metal salt was detected in greater abundance than that of the *sn*-2 fatty acid metal salt. The difference in relative abundances of these product ions was much larger when magnesium metal complexes were dissociated. Additional doubly charged product ions, indicative of the neutral loss of each fatty acid from the complex, were detected when calcium-lipid complexes were dissociated, showing the same preferential loss of the *sn*-1 fatty acid. The difference in relative abundances of these product ions was far greater than the singly charged product ions indicative of the loss of the lipid-metal salt. Therefore monitoring of this loss further aids assignment upon HE-CID of lipid metal adducts formed with calcium.

Head-group product ions indicative of the metal cation associated with the phosphate moiety of the head-group have been reported in CID of Group 1 cationic lipid adducts. These characteristic product ions are detected at *m/z*'s lower than those considered in CID analysis but can be monitored in HE-CID experiments. A singly charged product ion, indicative of the magnesium phosphate moiety, would be expected at *m/z* 146.97 and 162.95 for the magnesium and calcium adduct, respectively. These were not detected in HE-CID experiments which suggests that the dissociation pathways of at least the head-group differs when dissociating $[M^{II}+L_2]^{2+}$ complexes of Group 2 metals rather than $[M+L]^+$ adducts of Group 1 metals.
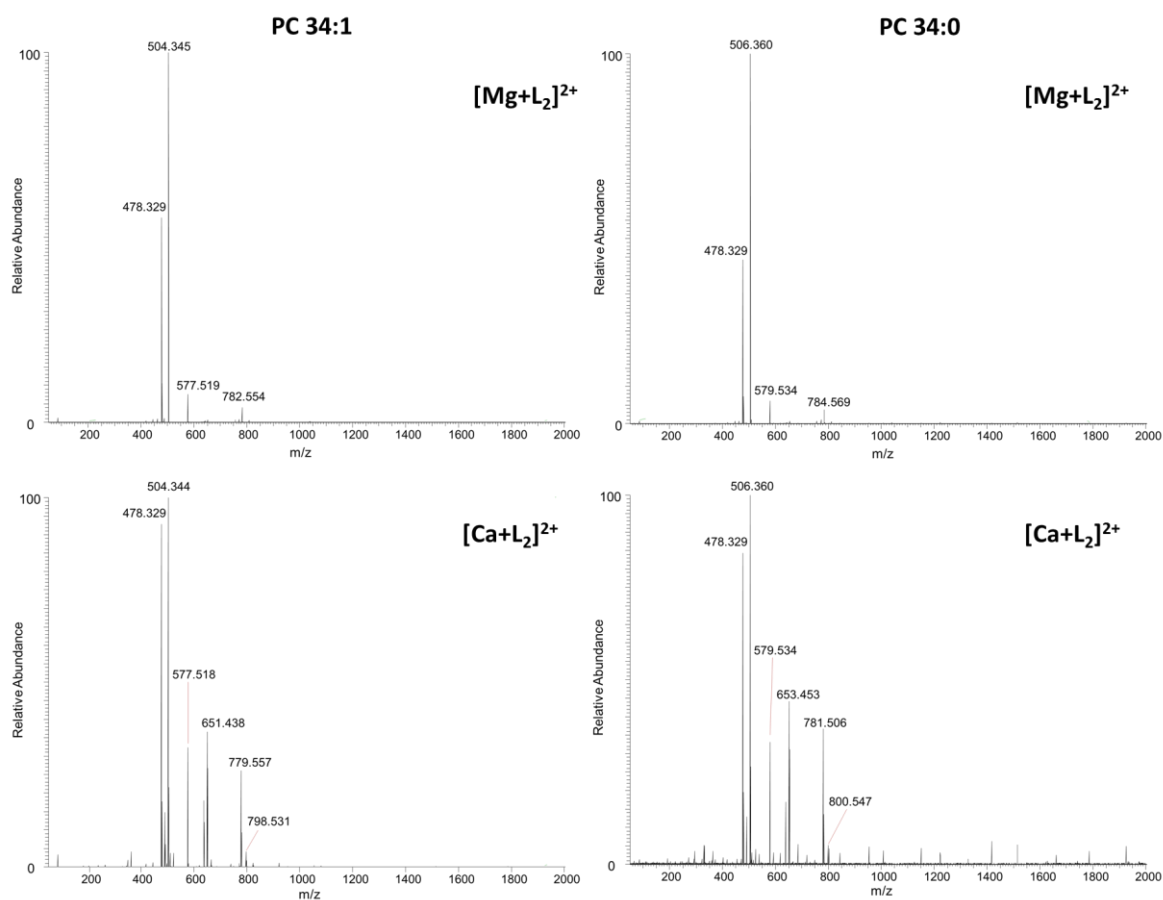
Figure 57 Representative ESI-MS/MS spectra showing product ions detected following high-energy collision-induced dissociation of (top) [Mg+L$_2$]$^{2+}$ lipid-metal complexes of PC 34:1 (18:1/16:0) and PC 34:0 (18:0/16:0) and (bottom) [Ca+L$_2$]$^{2+}$ lipid-metal complexes of PC 34:1 (18:1/16:0) and PC 34:0 (18:0/16:0).

6.3.4 Electron-Transfer Dissociation (ETD) of $[M^{II}+L_2]^{2+}$ lipid-metal complexes

Electron-transfer dissociation of the magnesium $[Mg+L_2]^{2+}$ complex led to the detection of a number of different product ions indicative of the fatty acid side-chain identities. The most abundant product ions were indicative of the loss of the acyl chain of the *sn*-1 fatty acid and *sn*-2 fatty acid side-chains, respectively. Product ions were detected at *m/z* 1303.91 and *m/z* 1307.91 upon ETD of $[Mg+L_2]^{2+}$ complexes where L = PC 18:1/16:0 and PC 18:0/16:0, respectively. The same trend was true when calcium complexes of PC 18:1/16:0 and PC 18:0/16:0 were dissociated by ETD. Therefore, as highlighted in Figure 58, it is possible that the relative positions of the *sn*-1 and *sn*-2 fatty acid side-chains can be determined by ETD of lipid-metal complexes of the type $[M^{II}+L_2]^{2+}$.

This loss of a radical RC=O has been reported previously by Liang *et al.* upon ETD of doubly sodiated $[M+2Na]^{2+}$ PC lipid adducts [148]. Doubly charged, doubly sodiated lipid adducts are not widely reported in the literature. Singly charged singly sodiated lipid adducts are more commonly reported in high abundance in lipid studies by ESI. However, Liang's study demonstrates that doubly charged lipid species can be formed with monovalent cations via doping with a salt, thus highlighting the potential benefit of future studies considering Group 1 metals in electron-mediated dissociation techniques. Loss of the acyl chain radical of PC lipid species has also been reported by James *et al.* in electron-capture dissociation (ECD) studies of calcium and magnesium lipid-metal complexes [146]. Clearly, similar product ions,

indicative of the fatty acid side-chain identities, are formed by both electron-mediated dissociation techniques.

Other abundant product ions detected in each experiment corresponded to the expected m/zs of the doubly charged parent ions $[M^{II}+L_2]^{2+}$ and singly charged complex $[M^{II}-H+L_2]^+$. Electron transfer leading to the loss of a methyl radical was detected in the present study in relatively low abundance. This type of product ion was also described by Liang $et\ al.$ in their ETD experiments of doubly sodiated PC species. Loss of the choline moiety of the head-group was also described in their study. Similar product ions were detected in this study in low abundance. It is possible that this head-group-characteristic product ion is enough to determine that a phosphocholine species has been dissociated, even though loss of the whole PC species is not indicated. James $et\ al.$ reported similar findings in their ECD study of PC lipid species: loss of the choline moiety of the PC head-group was detected, however loss of the intact PC head-group was not [146].

Overall, electron-transfer dissociation of these doubly charged Group 2 metal-lipid complexes provides highly abundant product ions that are characteristic of the two fatty acid side-chain identities. These product ions combined with the loss of 59.07 u, which is indicative of the choline $(N(CH_3)_3)$ moiety of the head-group, enables complete structural assignment of the PC lipid species. Electron transfer dissociation of lipid complexes formed with divalent metal cations has not previously been reported. Here it is shown that highly abundant structurally informative products ions are detected.
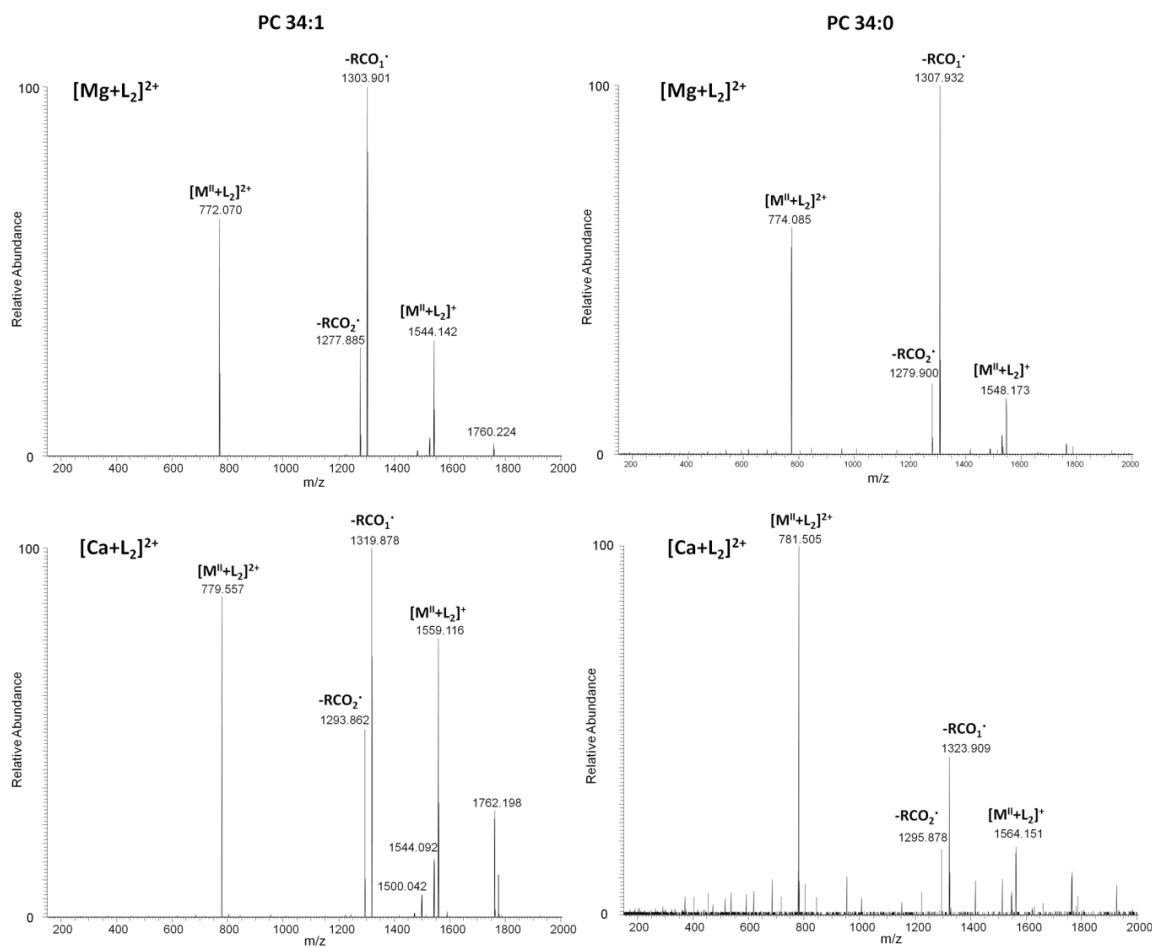
Figure 58 Representative ESI-MS/MS spectra showing product ions detected following electron- transfer dissociation of (A) $[Mg+L_2]^{2+}$ lipid-metal complexes of PC 34:1 (18:1/16:0) and PC 34:0 (18:0/16:0) and (bottom) $[Ca+L_2]^{2+}$ lipid-metal complexes of PC 34:1 (18:1/16:0) and PC 34:0 (18:0/16:0).

6.4 Conclusions

Dissociation of lipid-metal complexes of the form $[M^{II}+L_2]^{2+}$ led to the detection of highly abundant product ions indicating the fatty acid side-chain identities by collision-induced dissociation, high-energy- collision-induced dissociation and electron-transfer dissociation techniques. Therefore dissociation of these types of lipid adducts could be useful in structural characterisation studies of lipid analytes. Furthermore, there is strong indication that the relative abundances of product ions indicative of the fatty acid side-chains are informative of their relative *sn*-1 and *sn*-2 positions along the glycerol backbone.

It appears from this study that the size of the Group 2 metal cation in the lipid-metal complex does not affect dissociation to the same extent as in CID analysis of lipid adducts formed with singly charged Group 1 metal cations. Structurally informative product ions, indicating the identity of the two fatty acid side-chains, were detected irrespective of the Group 2 metal cation added.

Nonetheless, there is stark contrast between the dissociation spectra of these doubly charged metal-lipid complexes and singly charged Group 1 metal-lipid adducts in terms of the head-group ions detected. Although neutral losses characteristic of the PC head-group were detected upon CID or HE-CID dissociation of these lipid-metal complexes, no such product ions were detected when they were dissociated by ETD. Moreover, the head-group-informative peaks were detected in much lower abundance than product ions informative of the fatty acid side-chain identities. The opposite is true when Group 1 metal-lipid adducts are dissociated by CID.

Overall, dissociation of $[M^{II}+L_2]^{2+}$ lipid-metal adducts could provide more sensitive, fatty acid-informative dissociation data. Although head-group-indicative peaks were only detected by CID or HE-CID, it would be possible to perform two experiments in succession to obtain fatty acid side-chain information from ETD and then head-group information from CID or HE-CID. As even low sample concentrations can lead to long analysis times in electrospray ionisation, this should be possible even for minor components of a complex sample. This type of analysis would probably be best used *post* chromatographic separation.

Analysis of PC lipid species with a doubly charged Group 2 metal led to the formation of a wide range of different lipid-metal complexes leading to a complicated mass spectrum. Therefore the employment of these metal cations in dissociation studies of biological samples would be complicated; however they could still be incredibly useful for structural characterisation of lipids after chromatographic separation.

7. Conclusions and Further work

This study has shown that MALDI-MS and MSI techniques are practical tools for the analysis of lipids in complex lipid extracts and for direct surface analysis of tissue samples. Optimisation of sample preparation procedures for lipid analytes further improves analysis and this thesis offers sample preparation strategies for the improved analysis of lipids in complex samples by MALDI-MS and MSI.

A comprehensive survey of the inclusion of a range of salt additives in MALDI matrix solutions for the MALDI-MS analysis of a complex biological extract in Chapter 2 of this thesis revealed the significance of both cation and counteranion selection. The inclusion of a singly charged cation with a high molecular mass (such as caesium) led to the formation of cationic lipid adducts in a different *m/z* window to that of naturally abundant adducts. This significantly improves the confidence with which detected species can be assigned in MS experiments.

Acetate salts were shown to lead generally to decreased spectral complexity and nitrate salts to improved sensitivity for the respective cationic lipid adduct. Furthermore, acetate salts exhibited concentration-dependent results, whereas nitrate salts increased sensitivity across a concentration range. It is unclear why nitrate salts lead to significantly improved sensitivity and do not exhibit concentration-dependent results within the studied range. Although nitrate salts have a lower lattice enthalpy than the respective chloride or acetate salt, it cannot be assumed that the same trend is true after crystallisation with matrix molecules.

In order to improve understanding as to why certain counteranions appear to be more useful it may be beneficial to probe the crystal structure when additive salts are incorporated into matrices. Solid-state UV-vis experiments would allow determination of whether the nitrate anion associates with the matrix molecule, and changes the absorptive properties. X-ray diffraction (XRD) analysis could also offer insight as to the nature of the crystal structure, and how this changes upon inclusion of the additive salt. In addition, scanning electron microscopy (SEM) would enable analysis of the surface topography, allowing comparison of crystal structure of matrix/salt mixtures upon deposition on to the MALDI target plate with changing additive salt.

Repeating the above described study in negative ionisation mode could also prove beneficial. A number of phospholipids have been shown to ionise preferentially in negative ionisation mode [13, 22] and useful dissociation data from negative ions of a range of lipids has also been described [34]. Consideration of a range of different negative ions and counter cations in lipid MS and MS/MS experiments could therefore be of potential benefit.

As commercially available MALDI matrices often contain low abundances of metal ions such as sodium and potassium, ion removal strategies such as crown ether addition [292, 293] have also been considered as a strategy for simplifying mass spectra. This is an interesting alternative approach to the salt-doping strategy described herein. Crown ethers have a circular cavity which can hold a cation via electrostatic (dipole-dipole) interactions. The size of the crown ether can be varied

and therefore different crown ethers are selective for different cations, according to size.

Evason *et al.* included 18-crown-6 in 5-chloro-mercaptobenzothiazole (CMBT) for the analysis of bacteria [292]. A combination of formic acid for promoting protonation of analytes alongside crown ether addition for ion suppression gave favourable results in terms of spectral complexity. They comment that suppression of certain ions is achieved by chelation of the crown ether with sodium and potassium metal ions. Krader *et al.* also successfully utilised similar matrix additive systems for the analysis of archea bacteria [293]. Furthermore, Harris *et al.* successfully employed 18-crown-6 to reduce or remove cationic matrix adducts detected in the analysis of trypsin and hemoglobin protein analytes [294]. This approach aimed at mass spectra simplification is certainly an idea worth exploring in MALDI-MS analysis of lipid samples.

For structural characterisation of lipid analytes by CID MS/MS, it is also shown in Chapter 2 that adduct ion selection of parent ions is particularly important. Lithium lipid adducts provide abundant product ions indicative of the fatty acid side-chain identities, alongside head-group-indicative peaks, more reliably than any naturally abundant lipid adducts. Hence the use of additive salts in sample preparations can be a useful tool for forming abundant metal-lipid adducts which provide structurally informative information. These were considered in further detail in MALDI imaging.

Analysis of thin tissue sections by MALDI-MS imaging in Chapter 3 was shown to be a useful route to combining compositional with spatial information. A high

repetition-rate SSDP laser with high-throughput capabilities enabled the acquisition of high quality imaging data. Rapid data acquisition in this way has potential benefits in clinical applications. The inclusion of sodium salt additives in MALDI matrix solutions for airspray deposition onto thin tissue sections proved successful for MALDI imaging analysis. However, lithium salts were not successfully introduced by this strategy.

Consideration of dry-coating preparations proved problematic, leading to the detection of highly abundant protonated lipid adducts and greater spectral complexity. This observation is in agreement with previous reports and has reignited debate as to the nature of the ionisation mechanisms in MALDI. From these preparations it is clear that co-crystallisation of matrix molecules with analyte species is not imperative to the ionisation process, as previously thought. As stark differences are observed in the abundant lipid adducts detected, it seems likely that solvated deposition methods aid extraction of the endogenous salts in the tissue leading to predominant potassium adduct formation. Conversely, solvent-free methods of matrix application do not appear to aid extraction of endogenous salts. Protonated adducts are detected in high abundance by dry-coating with an acidic matrix compound. Therefore it is likely that proton transfer from matrix molecules to analyte molecules occurs.

Consideration of tissue fixation as a targeted ion introduction strategy, described in Chapter 4 , appears to be the most effective approach to introducing lithium ions into tissue samples and is a promising route to detecting lithium-lipid adducts *in situ*

without compromising spatial information. The ability to form highly abundant metal-lipid adducts in tissue, from which informative CID spectra can be obtained, is particularly important for lipid biomarker discovery studies.

Nevertheless, low abundances of other lipid adducts were also detected when formal tissues were analysed by MALDI. The presence of protonated lipid adducts could be caused by the fact that an acidic fixative solution was used. The detection of protonated-lipid adducts could be reduced by using lithium phosphate salts to prepare the formal lithium solution which would form a neutral pH solution. However, overcoming spectral complexity is less straightforward when sampling formal lithium-fixed tissue by LESA; the solvents used in lipid analysis (70% methanol with 0.1% formic acid) are an inherent source of protons. The detection of low abundances of sodium- and potassium-lipid adducts in formal lithium-fixed tissue samples could potentially be reduced by washing the tissue with a solvent to remove endogenous salts prior to fixation. Careful consideration of the solvent system would be required in order to ensure lipid analytes are not removed during cation removal, as described by Wang *et al.* and Steven *et al.* [180, 278].

Recently Steven *et al.* showed that *para*-nitroaniline is a suitable matrix compound for the analysis of lipid species in MALDI-MS imaging experiments with an Nd:YVO$_4$ laser [39]. Comparison of this matrix to CHCA for tissue imaging of thin tissue sections has revealed that image quality can be improved and suggests that *para*-nitroaniline is a cooler matrix for lipid analytes. This result is significant as it is possible that the prominent number of ions detected as a result of laser-induced

fragmentation described in the analysis of formal lithium-fixed tissue samples might be reduced if the same investigation was conducted with a cooler matrix compound.

Steven *et al.* have also described re-analysis of a single thin tissue section [278]. The methodology described gives rise to a number of exciting opportunities: firstly, the opportunity for optimal protein and lipid analysis using different matrix compounds for each analyte. As shown n this thesis, it is possible to fix a single tissue section after thaw mounting onto a MALDI or LESA target, it might be possible to acquire protein data before fixing the same tissue section in a formal lithium solution for optimised lipid data acquisition from the same tissue section.

The potential to acquire MALDI-MS data and then subsequently MS/MS imaging data of sodium adducts of lipid species from a single tissue section was also shown as a possibility by repeat analysis [278]. However detection of product ions characteristic of the fatty acid side-chain identities are not described by CID of sodium adducts. It is therefore plausible that similar data could be acquired from formal lithium-fixed tissue sections which would provide greater structural information. It would be beneficial for future biomarker discovery investigations, to know whether the sensitivity is sufficient to perform MS/MS imaging analysis on multiple analytes (*m/z* values) from a single tissue section.

A number of reports of lipid studies using the $Nd:YVO_4$ laser have reported CHCA, and not DHB matrix (which is commonly reported with nitrogen lasers) [43, 71, 77, 278]. However few groups are currently using this laser and to date the relative utility of other lasers has not been examined in detail. Clearly there is scope for an

investigation as to which MALDI matrices are useful for analysis of lipids with this particular laser as the usual matrix compounds are not exhibiting the same trends in terms of their use with lipid analytes. This is a large field of research and is generally achieved by trial and error studies using established matrix compounds and novel alternatives. This type of investigation was not within the scope of the work.

It is also shown in Chapters 5 and 6 of this thesis that the inclusion of a divalent metal cation in sample preparations leads to the formation of lipid-metal complexes of the form $[M^{II} + L_n]^{2+}$ ranging in size from n=2 to n=4. These metal additives may not therefore be useful for direct analysis of complex biological samples. However, consideration of CID, HE-CID and ETD of doubly charged metal-lipid complexes of the form $[M^{II} + L_2]^{2+}$ reveals that highly abundant structurally informative product ions are detected upon dissociation of these species. Although product ions indicative of both head-group- and fatty acid side-chain identities were not detected in very high abundance by a single dissociation technique, a combination of HE-CID and ETD provides highly abundant head-group- and side-chain-indicative product ions, respectively. It is possible that utilising both of these dissociation techniques could be a suitable method for the analysis of a complex lipid sample post chromatographic separation.

In the scope of this thesis CID, HE-CID and ETD techniques have been evaluated for structural characterisation of lipid species. However, elucidation of the double bond position of unsaturated lipids has not been achieved using the described methods. A relatively new dissociation technique, ozone-induced dissociation, has been shown to

be particularly useful for assigning double positioning of unsaturated lipids [152]. This dissociation technique provides superior information with regards to double-bond positioning in a wide range of lipid species; however this is performed in conjunction with CID, or a similar technique, as a method of obtaining additional information.

Although double bond positioning was not determined in dissociation studies presented in this thesis, preliminary ETD studies indicate that lipids containing saturated and unsaturated fatty acid side-chains preferentially form different lipid-metal adducts upon inclusion of a Group 2 metal. This is a promising result and further studies, considering a number of lipid standards with varying degrees of unsaturation, could be beneficial to determine whether the relative abundance of different lipid-metal adducts can infer the degree of unsaturation (or that a lipid is completely saturated) in a fatty acid side-chain.

However detailed mechanistic studies, considering a wide range of lipids with both saturated and unsaturated fatty acid side-chains, would be required in order to determine whether this is the case.

References

1. Fenn, J., et al., *Electrospray ionization for mass spectrometry of large biomolecules.* Science, 1989. **246**(4926): p. 64-71.

2. Tanaka, k., et al., *Protein and polymer analyses up to m/z 100 000 by laser ionisation time-of-flight mass spectrometry.* Rapid Communications in Mass Spectrometry, 1988. **2** p. 151-153, .

3. Xu, J., et al., *ToF-SIMS imaging with cluster ion beams.* Applied Surface Science, 2004. **231**: p. 159-163.

4. Takáts, Z., et al., *Mass Spectrometry Sampling Under Ambient Conditions with Desorption Electrospray Ionization.* Science, 2004. **306**(5695): p. 471-473.

5. Caprioli, R.M., T.B. Farmer, and J. Gile, *Molecular Imaging of Biological Samples: Localization of Peptides and Proteins Using MALDI-TOF-MS.* Analytical Chemistry, 1997. **69**(23): p. 4751-4760, .

6. Beckey, H.D. and H.R. Schulten, *Field Desorption Mass Spectrometry.* Angewandte Chemie International Edition in English, 1975. **14**(6): p. 403-415.

7. Schulten, H.R. and H.M. Schiebel, *Principle and technique of field-desorption mass spectrometry.* Naturwissenschaften, 1978. **65**(5): p. 223-230.

8. Posthumus, M.A., et al., *Laser desorption-mass spectrometry of polar nonvolatile bio-organic molecules.* Analytical chemistry, 1978. **50**(7): p. 985-991.

9. Opsal, R.B. and J.P. Reilly, *Ultraviolet laser induced ionization of molecules near surfaces.* Chemical Physics Letters, 1983. **99**(5–6): p. 461-464.

10. Karas, M. and F. Hillenkamp, *Laser desorption ionization of proteins with molecular masses exceeding 10,000 daltons.* Analytical chemistry, 1988. **60**(20): p. 2299-2301.

11. Duncan, M.W., G. Matanovid, and A. Cerpa-PoUak, *Quantitative Analysis of Low Molecular Weight Compounds of Biological Interest by Matrix-assisted Laser Desorption Ionization.* Rapid Communications in Mass Spectrometry, 1993. **7**: p. 1090-1094.

12. Goheen, S.C., et al., *Mass spectrometry of low molecular mass solids by matrix-assisted laser desorption/ionization.* Journal of Mass Spectrometry, 1997. **32**(8): p. 820-828.

13. Fuchs, B., R. Süß, and J. Schiller, *An update of MALDI-TOF mass spectrometry in lipid research.* Progress in Lipid Research, 2010. **49**(4): p. 450-475.

14. Kussmann, M., et al., *Matrix-assisted Laser Desorption/Ionization Mass Spectrometry Sample Preparation Techniques Designed for Various Peptide and Protein Analytes.* Journal of Mass Spectrometry, 1997. **32**(6): p. 593-601.

15. Nielen, M.W., *MALDI time-of-flight mass spectrometry of synthetic polymers.* Mass spectrometry reviews, 1999. **18**(5): p. 309-344.

16. Le, C.H., J. Han, and C.H. Borchers, *Dithranol as a MALDI Matrix for Tissue Imaging of Lipids by Fourier Transform Ion Cyclotron Resonance Mass Spectrometry.* Analytical chemistry, 2012.

17. Sauer, S., *The essence of DNA sample preparation for MALDI mass spectrometry.* Journal of Biochemical and Biophysical Methods, 2007. **70**(2): p. 311-318.

18. Harvey, D.J., *Matrix-assisted laser desorption/ionization mass spectrometry of carbohydrates.* Mass Spectrometry Reviews, 1999. **18**(6): p. 349-450.

19. Stübiger, G. and O. Belgacem, *Analysis of lipids using 2, 4, 6-trihydroxyacetophenone as a matrix for MALDI mass spectrometry.* Analytical chemistry, 2007. **79**(8): p. 3206-3213.

20. Hidaka, H., et al., *Analysis of human serum lipoprotein lipid composition using MALDI-TOF mass spectrometry.* Annals of Clinical & Laboratory Science, 2007. **37**(3): p. 213.

21. Landgraf, R.R., et al., *Considerations for quantification of lipids in nerve tissue using matrix-assisted laser desorption/ionization mass spectrometric imaging.* Rapid Communications in Mass Spectrometry, 2011. **25**(20): p. 3178-3184.

22. Jackson, S.N., H.-Y.J. Wang, and A.S. Woods, *Direct Profiling of Lipid Distribution in Brain Tissue Using MALDI-TOFMS.* Analytical Chemistry, 2005. **77**(14): p. 4523-4527.

23. Chen, Y., et al., *Imaging MALDI Mass Spectrometry Using an Oscillating Capillary Nebulizer Matrix Coating System and Its Application to Analysis of Lipids in Brain from a Mouse Model of Tayâˆ’Sachs/Sandhoff Disease.* Analytical Chemistry, 2008. **80**(8): p. 2780-2788.

24. McAvey, K., et al., *Laser-Induced Oxidation of Cholesterol Observed During MALDI-TOF Mass Spectrometry.* Journal of the American Society for Mass Spectrometry, 2011. **22**(4): p. 659-669.

25. Garrett, T., et al., *Lipid analysis of flat-mounted eye tissue by imaging mass spectrometry with identification of contaminants in preservation.* Analytical and Bioanalytical Chemistry, 2011. **401**(1): p. 103-113.

26. Hankin, J.A., et al., *MALDI Mass Spectrometric Imaging of Lipids in Rat Brain Injury Models.* Journal of the American Society for Mass Spectrometry, 2011: p. 1-8.

27. Suarez, E., et al., *Matrix-assisted laser desorption/ionization-mass spectrometry of cuticular lipid profiles can differentiate sex, age, and mating status of Anopheles gambiae mosquitoes.* Analytica Chimica Acta, 2011. **706**(1): p. 157-163.

28. Jackson, S.N., et al., *MALDI-ion mobility-TOFMS imaging of lipids in rat brain tissue.* Journal of Mass Spectrometry, 2007. **42**(8): p. 1093-1098.

29. Grove, K.J., S.L. Frappier, and R.M. Caprioli, *Matrix Pre-Coated MALDI MS Targets for Small Molecule Imaging in Tissues.* Journal of the American Society for Mass Spectrometry, 2011: p. 1-4.

30. Bresler, K., et al., *Parameters affecting the accuracy of the MALDI-TOF MS determination of the phosphatidylcholine/lysophosphatidylcholine (PC/LPC) ratio as potential marker of spermatozoa quality.* Chemistry and Physics of Lipids, 2011. **164**(7): p. 696-702.

31. Johanson, R.A., et al., *Phosphatidylcholine removal from brain lipid extracts expands lipid detection and enhances phosphoinositide quantification by matrix-assisted laser desorption/ionization time-of-flight (MALDI-TOF) mass spectrometry.* Analytical Biochemistry, 2007. **362**(2): p. 155-167.

32. Lay, J.O., et al., *Rapid characterization of lipids by MALDI MS. Part 1: Bacterial taxonomy and analysis of food oils.* Lipid Technology, 2012. **24**(1): p. 11-14.

33.   Woods, A.S., et al., *Gangliosides and Ceramides Change in a Mouse Model of Blast Induced Traumatic Brain Injury.* ACS Chemical Neuroscience, 2013.

34.   Jackson, S.N., H.-Y.J. Wang, and A.S. Woods, *In Situ Structural Characterization of Glycerophospholipids and Sulfatides in Brain Tissue Using MALDI-MS/MS.* Journal of the American Society for Mass Spectrometry, 2007. **18**(1): p. 17-26.

35.   Krist, S., et al., *Analysis of volatile compounds and triglycerides of seed oils extracted from different poppy varieties (Papaver somniferum L.).* Journal of agricultural and food chemistry, 2005. **53**(21): p. 8310-8316.

36.   Benabdellah, F., et al., *In situ primary metabolites localization on a rat brain section by chemical mass spectrometry imaging.* Analytical chemistry, 2009. **81**(13): p. 5557-5560.

37.   Stübiger, G., et al., *Influence of HSA and IgG on LDL oxidation studied by size-exclusion chromatography and phospholipid profiling using MALDI tandem-mass spectrometry.* Chemistry and Physics of Lipids, 2011. **164**(6): p. 563-572.

38.   Belgacem, O., et al., *Isolation of esterified fatty acids bound to serum albumin purified from human plasma and characterised by MALDI mass spectrometry.* Biologicals, 2007. **35**(1): p. 43-49.

39.   Steven, R., A. Race, and J. Bunch, *para-Nitroaniline is a Promising Matrix for MALDI-MS Imaging on Intermediate Pressure MS Systems.* Journal of the American Society for Mass Spectrometry, 2013: p. 1-4.

40.   Dannenberger, D., et al., *The intact muscle lipid composition of bulls: an investigation by MALDI-TOF MS and 31P NMR.* Chemistry and Physics of Lipids, 2010. **163**(2): p. 157-164.

41.   Murphy, R.C., et al., *MALDI imaging of lipids after matrix sublimation/deposition.* Biochimica et Biophysica Acta (BBA) - Molecular and Cell Biology of Lipids, 2011. **1811**(11): p. 970-975.

42.   Trim, P.J., et al., *Matrix-assisted laser desorption/ionisation mass spectrometry imaging of lipids in rat brain tissue with integrated unsupervised and supervised multivariant statistical analysis.* Rapid Communications in Mass Spectrometry, 2008. **22**(10): p. 1503-1509.

43.   Ferguson, L., et al., *Two-Step Matrix Application for the Enhancement and Imaging of Latent Fingermarks.* Analytical chemistry, 2011. **83**(14): p. 5585-5591.

44.   Vidová, V., et al., *Visualizing spatial lipid distribution in porcine lens by MALDI imaging high-resolution mass spectrometry.* Journal of lipid research, 2010. **51**(8): p. 2295-2302.

45.   Cerruti, C.D., et al., *MALDI imaging and structural analysis of rat brain lipid negative ions with 9-aminoacridine matrix.* Analytical chemistry, 2012.

46.   Astigarraga, E., et al., *Profiling and Imaging of Lipids on Brain and Liver Tissue by Matrix-Assisted Laser Desorption/Ionization Mass Spectrometry Using 2-Mercaptobenzothiazole as a Matrix.* Analytical Chemistry, 2008. **80**(23): p. 9105-9114.

47.   Yang, H.-J., et al., *Analysis of cancer cell lipids using matrix-assisted laser desorption/ionization 15-T Fourier transform ion cyclotron resonance mass spectrometry.* Rapid Communications in Mass Spectrometry, 2012. **26**(6): p. 621-630.

48.   Shanta, S.R., et al., *Binary Matrix for MALDI Imaging Mass Spectrometry of Phospholipids in Both Ion Modes.* Analytical chemistry, 2011. **83**(4): p. 1252-1259.

49.   Park, Y.S., et al., *Lipid profiles for intrahepatic cholangiocarcinoma identified using matrix-assisted laser desorption/ionization mass spectrometry.* Clinica Chimica Acta, 2011. **412**(21-22): p. 1978-1982.

50.   Kang, H., et al., *Protein and lipid MALDI profiles classify breast cancers according to the intrinsic subtype.* BMC Cancer, 2011. **11**(1): p. 465.

51.   Guo, Z. and L. He, *A binary matrix for background suppression in MALDI-MS of small molecules.* Analytical and Bioanalytical Chemistry, 2007. **387**(5): p. 1939-1944.

52.   Teuber, K., et al., *Significant sensitivity improvements by matrix optimization: a MALDI-TOF mass spectrometric study of lipids from hen egg yolk.* Chemistry and Physics of Lipids, 2010. **163**(6): p. 552-560.

53.   Thomas, A., et al., *Histology-Driven Data Mining of Lipid Signatures from Multiple Imaging Mass Spectrometry Analyses: Application to Human Colorectal Cancer Liver Metastasis Biopsies.* Analytical chemistry, 2013. **85**(5): p. 2860-2866.

54.   Park, K. and H. Kim, *Analysis of fatty acids by graphite plate laser desorption/ionization time of flight mass spectrometry.* Rapid Communications in Mass Spectrometry, 2001. **15**(16): p. 1494-1499.

55.   Liu, Y., et al., *Graphene and graphene oxide: two ideal choices for the enrichment and ionization of long-chain fatty acids free from matrix-assisted laser desorption/ionization matrix interference.* Rapid Communications in Mass Spectrometry, 2011. **25**(21): p. 3223-3234.

56.   Zhang, H., S. Cha, and E.S. Yeung, *Colloidal Graphite-Assisted Laser Desorption/Ionization MS and MSn of Small Molecules. 2. Direct Profiling and MS Imaging of Small Metabolites from Fruits.* Analytical chemistry, 2007. **79**(17): p. 6575-6584.

57.   Shrivas, K., et al., *Ionic Matrix for Enhanced MALDI Imaging Mass Spectrometry for Identification of Phospholipids in Mouse Liver and Cerebellum Tissue Sections.* Analytical chemistry, 2010.

58.   Li, Y., M. Gross, and F. Hsu, *Ionic-liquid matrices for improved analysis of phospholipids by MALDI-TOF mass spectrometry.* Journal of the American Society for Mass Spectrometry, 2005. **16**(5): p. 679-682.

59.   Karas, M., Hillenkamp, F., *Laser Desorption Ionization of Proteins with Molecular Masses Exceeding 10 000 Daltons.* Journal of Analytical Chemistry, 1988(60): p. 2299-2301.

60.   Önnerfjord, P., et al., *Homogeneous sample preparation for automated high throughput analysis with matrix-assisted laser desorption/ionisation time-of-flight mass spectrometry.* Rapid Communications in Mass Spectrometry, 1999. **13**(5): p. 315-322.

61.   Horneffer, V., et al., *Is the incorporation of analytes into matrix crystals a prerequisite for matrix-assisted laser desorption/ionization mass spectrometry? A study of five positional isomers of dihydroxybenzoic acid.* International Journal of Mass Spectrometry, 1999. **185–187**(0): p. 859-870.

62. Puolitaival, S.M., et al., *Solvent-Free Matrix Dry-Coating for MALDI Imaging of Phospholipids.* Journal of the American Society for Mass Spectrometry, 2008. **19**(6): p. 882-886.

63. Schiller, J., et al., *Lipid Analysis by Matrix-Assisted Laser Desorption and Ionization Mass Spectrometry: A Methodological Approach.* Analytical Biochemistry, 1999. **267**(1): p. 46-56.

64. Goto-Inoue, N., et al., *Imaging mass spectrometry for lipidomics.* Biochimica et Biophysica Acta (BBA) - Molecular and Cell Biology of Lipids, 2011. **1811**(11): p. 961-969.

65. Chen, Y., et al., *Imaging MALDI Mass Spectrometry Using an Oscillating Capillary Nebulizer Matrix Coating System and Its Application to Analysis of Lipids in Brain from a Mouse Model of Tay Sachs/Sandhoff Disease.* Analytical Chemistry, 2008. **80**(8): p. 2780-2788.

66. Aerni, H.-R., D.S. Cornett, and R.M. Caprioli, *Automated Acoustic Matrix Deposition for MALDI Sample Preparation.* Analytical Chemistry, 2006. **78**(3): p. 827-834.

67. Baluya, D.L., T.J. Garrett, and R.A. Yost, *Automated MALDI Matrix Deposition Method with Inkjet Printing for Imaging Mass Spectrometry.* Analytical Chemistry, 2007. **79**(17): p. 6862-6867.

68. SunChrom. *http://sepassociates.com/sunchrom-suncollect-maldi-spotter.html*.

69. Technologies, L. *http://www.leaptec.com/products/proteomics-products/tissue-maldi-platform/tm-sprayer-for-matrix-tissue-maldi-366.php*.

70. Hankin, J.A., R.M. Barkley, and R.C. Murphy, *Sublimation as a Method of Matrix Application for Mass Spectrometric Imaging.* Journal of the American Society for Mass Spectrometry, 2007. **18**(9): p. 1646-1652.

71. Trim, P.J., et al., *Introduction of a 20 kHz Nd: YVO4 laser into a hybrid quadrupole time-of-flight mass spectrometer for MALDI-MS imaging.* Analytical and Bioanalytical Chemistry, 2010: p. 1-11.

72. Sugiura, Y. and M. Setou, *Selective imaging of positively charged polar and nonpolar lipids by optimizing matrix solution composition.* Rapid Communications in Mass Spectrometry, 2009. **23**(20): p. 3269-3278.

73. Spraggins, J.M. and R.M. Caprioli, *High-Speed MALDI-TOF Imaging Mass Spectrometry: Rapid Ion Image Acquisition and Considerations for Next Generation Instrumentation.* Journal of the American Society for Mass Spectrometry: p. 1-10.

74. McLean, J.A., W.K. Russell, and D.H. Russell, *A High Repetition Rate (1 kHz) Microcrystal Laser for High Throughput Atmospheric Pressure MALDI-Quadrupole-Time-of-Flight Mass Spectrometry.* Analytical chemistry, 2002. **75**(3): p. 648-654.

75. Spraggins, J. and R. Caprioli, *High-Speed MALDI-TOF Imaging Mass Spectrometry: Rapid Ion Image Acquisition and Considerations for Next Generation Instrumentation.* Journal of the American Society for Mass Spectrometry, 2011. **22**(6): p. 1022-1031.

76. Vertes, A., et al., *Laser pulse length dependence of internal energy transfer in UV-MALDI-MS.* Applied Physics A: Materials Science & Processing, 2004. **79**(4): p. 823-825.

77. Hart, P., et al., *MALDI-MS imaging of lipids in ex vivo human skin.* Analytical and Bioanalytical Chemistry, 2011. **401**(1): p. 115-125.

78. Holle, A., et al., *Optimizing UV laser focus profiles for improved MALDI performance.* Journal of Mass Spectrometry, 2006. **41**(6): p. 705-716.

79. Qiao, H., V. Spicer, and W. Ens, *The effect of laser profile, fluence, and spot size on sensitivity in orthogonal injection matrix assisted laser desorption/ionization time of flight mass spectrometry.* Rapid Communications in Mass Spectrometry, 2008. **22**(18): p. 2779-2790.

80. Knochenmuss, R., *A quantitative model of ultraviolet matrix-assisted laser desorption/ionization including analyte ion generation.* Anal. Chem, 2003. **75**(10): p. 2199-2207.

81. Knochenmuss, R., *A quantitative model of ultraviolet matrix-assisted laser desorption/ionization.* Journal of Mass Spectrometry, 2002. **37**(8): p. 867-877.

82. Krüger, R. and M. Karas, *Formation and fate of ion pairs during MALDI analysis: anion adduct generation as an indicative tool to determine ionization processes.* Journal of the American Society for Mass Spectrometry, 2002. **13**(10): p. 1218-1226.

83. Knochenmuss, R., *Photoionization pathways and free electrons in UV-MALDI.* Anal. Chem, 2004. **76**(11): p. 3179-3184.

84. Hillenkamp, F., et al., *Positive and negative analyte ion yield in matrix-assisted laser desorption/ionization revisited.* International Journal of Mass Spectrometry, 2009. **285**(3): p. 114-119.

85. Dreisewerd, K., *The Desorption Process in MALDI.* Chemical Reviews, 2003. **103**(2): p. 395-426.

86. Jaskolla, T. and M. Karas, *Compelling Evidence for Lucky Survivor and Gas Phase Protonation: The Unified MALDI Analyte Protonation Mechanism.* Journal of the American Society for Mass Spectrometry, 2011. **22**(6): p. 976-988.

87. Loboda, A.V. and I.V. Chernushevich, *Investigation of the mechanism of matrix adduct formation in MALDI at elevated pressure.* International Journal of Mass Spectrometry, 2005. **240**(2): p. 101-105.

88. Knochenmuss, R. and R. Zenobi, *MALDI ionization: the role of in-plume processes.* Chem. Rev, 2003. **103**(2): p. 441-452.

89. Zhang, J. and R. Zenobi, *Matrix-dependent cationization in MALDI mass spectrometry.* Journal of Mass Spectrometry, 2004. **39**(7): p. 808-816.

90. Zenobi, R. and R. Knochenmuss, *Ion formation in MALDI mass spectrometry.* Mass spectrometry reviews, 1998. **17**(5): p. 337-366.

91. Moon, J., et al., *Ion Yields for Some Salts in MALDI: Mechanism for the Gas-Phase Ion Formation from Preformed Ions.* Journal of the American Society for Mass Spectrometry, 2012. **23**(1): p. 162-170.

92. Karas, M. and R. Krueger, *Ion formation in MALDI: the cluster ionization mechanism.* Chem. Rev, 2003. **103**(2): p. 427-440.

93. Luo, G., I. Marginean, and A. Vertes, *Internal Energy of Ions Generated by Matrix-Assisted Laser Desorption/Ionization.* Analytical Chemistry, 2002. **74**(24): p. 6185-6190.

94.   Jorgensen, T.J.D., G. Bojesen, and H. Rahbek-Nielsen, *The proton affinities of seven matrix-assisted laser desorption/ionization matrices correlated with the formation of multiply charged ions.* European Mass Spectrometry, 1998. **4**(1): p. 39-46.

95.   Ohanessian, G., *Interaction of MALDI matrix molecules with Na+ in the gas phase.* International Journal of Mass Spectrometry, 2002. **219**(3): p. 577-592.

96.   Zhang, J., et al., *Theoretical Calculation of Gas-Phase Sodium Binding Energies of Common MALDI Matrices.* The Journal of Physical Chemistry A, 2002. **106**(28): p. 6610-6617.

97.   Wong, C.K.L. and T.-W.D. Chan, *Cationization Processes in Matrix-assisted Laser Desorption/Ionization Mass Spectrometry: Attachment of Divalent and Trivalent Metal Ions.* Rapid Communications in Mass Spectrometry, 1997. **11**(5): p. 513-519.

98.   Karas, M., M. Glückmann, and J. Schäfer, *Ionization in matrix assisted laser desorption/ionization: singly charged molecular ions are the lucky survivors.* Journal of Mass Spectrometry, 2000. **35**(1): p. 1-12.

99.   Knochenmuss, R., *Ion formation mechanisms in UV-MALDI.* The Analyst, 2006. **131**(9): p. 966-986.

100.   Guenther, S., et al., *Laser spot size and laser power dependence of ion formation in high resolution MALDI imaging.* International Journal of Mass Spectrometry, 2010. **294**(1): p. 7-15.

101.   Dreisewerd, K., et al., *Influence of the laser intensity and spot size on the desorption of molecules and ions in matrix-assisted laser desorption/ionization with a uniform beam profile.* International Journal of Mass Spectrometry and Ion Processes, 1995. **141**(2): p. 127-148.

102.   Allwood, D., et al., *Optical absorption of matrix compounds for laser-induced desorption and ionization (MALDI).* Applied Surface Science, 1997. **109**: p. 154-157.

103.   Chen, X., J. Carroll, and R. Beavis, *Near-ultraviolet-induced matrix-assisted laser desorption/ionization as a function of wavelength.* Journal of the American Society for Mass Spectrometry, 1998. **9**(9): p. 885-891.

104.   Edmond de Hoffmann, V.S., *Mass Spectrometry Principles and Applications*, in *Mass Spectrometry Principles and Applications*, L. John Wiley & Sons, Editor. 2009, John Wiley & Sons, Ltd: Chichester. p. 43-55.

105.   Wilm, M. and M. Mann, *Analytical Properties of the Nanoelectrospray Ion Source.* Analytical chemistry, 1996. **68**(1): p. 1-8.

106.   Cutler, R.G., et al., *Involvement of oxidative stress-induced abnormalities in ceramide and cholesterol metabolism in brain aging and Alzheimer's disease.* Proceedings of the National Academy of Sciences of the United States of America, 2004. **101**(7): p. 2070-2075.

107.   Colsch, B., et al., *Characterization of the ceramide moieties of sphingoglycolipids from mouse brain by ESI-MS/MS.* Journal of lipid research, 2004. **45**(2): p. 281-286.

108.   Brügger, B., et al., *Quantitative analysis of biological membrane lipids at the low picomole level by nano-electrospray ionization tandem mass spectrometry.*

Proceedings of the National Academy of Sciences of the United States of America, 1997. **94**(6): p. 2339-2344.

109. Hsu, F.-F. and J. Turk, *Electrospray ionization with low-energy collisionally activated dissociation tandem mass spectrometry of glycerophospholipids: Mechanisms of fragmentation and structural characterization.* Journal of Chromatography B, 2009. **877**(26): p. 2673-2695.

110. Pulfer, M. and R.C. Murphy, *Electrospray mass spectrometry of phospholipids.* Mass spectrometry reviews, 2003. **22**(5): p. 332-364.

111. Sandhoff, R., et al., *Determination of cholesterol at the low picomole level by nano-electrospray ionization tandem mass spectrometry.* Journal of lipid research, 1999. **40**(1): p. 126-132.

112. Hutchins, P.M., E.E. Moore, and R.C. Murphy, *Electrospray MS/MS reveals extensive and nonspecific oxidation of cholesterol esters in human peripheral vascular lesions.* Journal of lipid research, 2011. **52**(11): p. 2070-2083.

113. Hsu, F.-F. and J. Turk, *Structural characterization of triacylglycerols as lithiated adducts by electrospray ionization mass spectrometry using low-energy collisionally activated dissociation on a triple stage quadrupole instrument.* Journal of the American Society for Mass Spectrometry, 1999. **10**(7): p. 587-599.

114. Iribarne, J.V. and B.A. Thomson, *On the evaporation of small ions from charged droplets.* The Journal of Chemical Physics, 1976. **64**(6): p. 2287-2294.

115. Nguyen, S. and J.B. Fenn, *Gas-phase ions of solute species from charged droplets of solutions.* Proceedings of the National Academy of Sciences, 2007. **104**(4): p. 1111-1117.

116. Dole, M., et al., *Molecular Beams of Macroions.* The Journal of Chemical Physics, 1968. **49**(5): p. 2240-2249.

117. Wachs, T. and J. Henion, *Electrospray Device for Coupling Microscale Separations and Other Miniaturized Devices with Electrospray Mass Spectrometry.* Analytical chemistry, 2001. **73**(3): p. 632-638.

118. Kertesz, V., M.J. Ford, and G.J. Van Berkel, *Automation of a Surface Sampling Probe/Electrospray Mass Spectrometry System.* Analytical chemistry, 2005. **77**(22): p. 7183-7189.

119. Kertesz, V. and G.J. Van Berkel, *Fully automated liquid extraction-based surface sampling and ionization using a chip-based robotic nanoelectrospray platform.* Journal of Mass Spectrometry, 2010. **45**(3): p. 252-260.

120. Marshall, P., et al., *Correlation of Skin Blanching and Percutaneous Absorption for Glucocorticoid Receptor Agonists by Matrix-Assisted Laser Desorption Ionization Mass Spectrometry Imaging and Liquid Extraction Surface Analysis with Nanoelectrospray Ionization Mass Spectrometry.* Analytical chemistry, 2010. **82**(18): p. 7787-7794.

121. Stegemann, C., et al., *Comparative Lipidomics Profiling of Human Atherosclerotic PlaquesClinical Perspective.* Circulation: Cardiovascular Genetics, 2011. **4**(3): p. 232-242.

122. Kertesz, V. and G.J. Van Berkel, *Liquid Microjunction Surface Sampling Coupled with High-Pressure Liquid Chromatography–Electrospray Ionization-Mass*

Spectrometry for Analysis of Drugs and Metabolites in Whole-Body Thin Tissue Sections. Analytical chemistry, 2010. **82**(14): p. 5917-5921.

123. Van Berkel, G.J., et al., *Liquid microjunction surface sampling probe electrospray mass spectrometry for detection of drugs and metabolites in thin tissue sections.* Journal of Mass Spectrometry, 2008. **43**(4): p. 500-508.

124. Van Berkel, G.J. and V. Kertesz, *Application of a Liquid Extraction Based Sealing Surface Sampling Probe for Mass Spectrometric Analysis of Dried Blood Spots and Mouse Whole-Body Thin Tissue Sections.* Analytical chemistry, 2009. **81**(21): p. 9146-9152.

125. Edwards, R.L., et al., *Hemoglobin Variant Analysis via Direct Surface Sampling of Dried Blood Spots Coupled with High-Resolution Mass Spectrometry.* Analytical chemistry, 2011. **83**(6): p. 2265-2270.

126. Brown, S.H.J., et al., *Automated surface sampling of lipids from worn contact lenses coupled with tandem mass spectrometry.* Analyst, 2013.

127. Girod, M., et al., *Desorption Electrospray Ionization Imaging Mass Spectrometry of Lipids in Rat Spinal Cord.* Journal of the American Society for Mass Spectrometry, 2010. **21**(7): p. 1177-1189.

128. Anderson, D.M., et al., *High-resolution matrix-assisted laser desorption ionization–imaging mass spectrometry of lipids in rodent optic nerve tissue.* Molecular vision, 2013. **19**: p. 581.

129. Touboul, D., et al., *Improvement of biological time-of-flight-secondary ion mass spectrometry imaging with a bismuth cluster ion source.* Journal of the American Society for Mass Spectrometry, 2005. **16**(10): p. 1608-1618.

130. Eberlin, L.S., et al., *Desorption Electrospray Ionization then MALDI Mass Spectrometry Imaging of Lipid and Protein Distributions in Single Tissue Sections.* Analytical chemistry, 2011. **83**(22): p. 8366-8371.

131. Estrada, R. and M.C. Yappert, *Alternative approaches for the detection of various phospholipid classes by matrix assisted laser desorption/ionization time of flight mass spectrometry.* Journal of Mass Spectrometry, 2004. **39**(4): p. 412-422.

132. Schiller, J., et al., *CsCl as an auxiliary reagent for the analysis of phosphatidylcholine mixtures by matrix-assisted laser desorption and ionization time-of-flight mass spectrometry (MALDI-TOF MS).* Chemistry and Physics of Lipids, 2001. **113**(1-2): p. 123-131.

133. Wang, H.Y.J., et al., *Direct profiling of phospholipids and lysophospholipids in rat brain sections after ischemic stroke.* Rapid Communications in Mass Spectrometry, 2010. **24**(14): p. 2057-2064.

134. Morris, H.R., et al., *High Sensitivity Collisionally-activated Decomposition Tandem Mass Spectrometry on a Novel Quadrupole/Orthogonal-acceleration Time-of-flight Mass Spectrometer.* Rapid Communications in Mass Spectrometry, 1996. **10**(8): p. 889-896.

135. Yang, H.-J., et al., *Imaging of lipids in cultured mammalian neurons by matrix assisted laser/desorption ionization and secondary ion mass spectrometry.* Surface and Interface Analysis, 2010. **42**(10-11): p. 1606-1611.

136. Chernushevich, I.V., A.V. Lododa, and B.A. Thomson, *An Introduction to quadrupole-time-of-flight mass spectrometry.* Journal of Mass Spectrometry, 2001. **36**: p. 849-865.

137. Comisarow, M.B. and A.G. Marshall, *Fourier transform ion cyclotron resonance spectroscopy.* Chemical Physics Letters, 1974. **25**(2): p. 282-283.

138. Kingdon, K.H., *A Method for the Neutralization of Electron Space Charge by Positive Ionization at Very Low Gas Pressures.* Physical Review, 1923. **21**(4): p. 408-418.

139. March, R.E., *An Introduction to Quadrupole Ion Trap Mass Spectrometry.* Journal of Mass Spectrometry, 1997. **32**(351): p. 369.

140. Makarov, A., *Electrostatic Axially Harmonic Orbital Trapping: A High-Performance Technique of Mass Analysis.* Analytical chemistry, 2000. **72**(6): p. 1156-1162.

141. Hardman, M. and A.A. Makarov, *Interfacing the Orbitrap Mass Analyzer to an Electrospray Ion Source.* Analytical chemistry, 2003. **75**(7): p. 1699-1705.

142. Hu, Q., et al., *The Orbitrap: a new mass spectrometer.* Journal of Mass Spectrometry, 2005. **40**(4): p. 430-443.

143. Jackson, S.N., H.-Y.J. Wang, and A.S. Woods, *In Situ Structural Characterization of Phosphatidylcholines in Brain Tissue Using MALDI-MS/MS.* Journal of the American Society for Mass Spectrometry, 2005. **16**(12): p. 2052-2056.

144. Castro-Perez, J., et al., *Localization of Fatty Acyl and Double Bond Positions in Phosphatidylcholines Using a Dual Stage CID Fragmentation Coupled with Ion Mobility Mass Spectrometry.* Journal of the American Society for Mass Spectrometry: p. 1-16.

145. Cerruti, C.D., et al., *MALDI imaging mass spectrometry of lipids by adding lithium salts to the matrix solution.* Analytical and Bioanalytical Chemistry, 2011: p. 1-13.

146. James, P.F., M.A. Perugini, and R.A.J. O'Hair, *Electron Capture Dissociation of Complexes of Diacylglycerophosphocholine and Divalent Metal Ions: Competition Between Charge Reduction and Radical Induced Phospholipid Fragmentation.* Journal of the American Society for Mass Spectrometry, 2008. **19**(7): p. 978-986.

147. McFarland, M.A., et al., *Structural Characterization of the GM1 Ganglioside by Infrared Multiphoton Dissociation, Electron Capture Dissociation, and Electron Detachment Dissociation Electrospray Ionization FT-ICR MS/MS.* Journal of the American Society for Mass Spectrometry, 2005. **16**(5): p. 752-762.

148. Liang, X., et al., *Electron Transfer Dissociation of Doubly Sodiated Glycerophosphocholine Lipids.* Journal of the American Society for Mass Spectrometry, 2007. **18**(10): p. 1783-1788.

149. Brown, S.H.J., T.W. Mitchell, and S.J. Blanksby, *Analysis of unsaturated lipids by ozone-induced dissociation.* Biochimica et Biophysica Acta (BBA) - Molecular and Cell Biology of Lipids, 2011. **1811**(11): p. 807-817.

150. Stubiger, G., E. Pittenauer, and G. Allmaier, *MALDI seamless postsource decay fragment ion analysis of sodiated and lithiated phospholipids.* Anal. Chem, 2008. **80**(5): p. 1664-1678.

151. Stübiger, G. and O. Belgacem, *Analysis of lipids using 2, 4, 6-trihydroxyacetophenone as a matrix for MALDI mass spectrometry.* Anal. Chem, 2007. **79**(8): p. 3206-3213.

152. Thomas, M.C., et al., *Ozone-induced dissociation: Elucidation of double bond position within mass-selected lipid ions.* Analytical chemistry, 2008. **80**(1): p. 303-311.

153. Harvey, D.J., *A new charge-associated mechanism to account for the production of fragment ions in the high-energy CID spectra of fatty acids.* Journal of the American Society for Mass Spectrometry, 2005. **16**(2): p. 280-290.

154. Shimma, S., et al., *Detailed Structural Analysis of Lipids Directly on Tissue Specimens Using a MALDI-SpiralTOF-Reflectron TOF Mass Spectrometer.* PLoS ONE, 2012. **7**(5): p. e37107.

155. Zubarev, R.A., N.L. Kelleher, and F.W. McLafferty, *Electron Capture Dissociation of Multiply Charged Protein Cations. A Nonergodic Process.* Journal of the American Chemical Society, 1998. **120**(13): p. 3265-3266.

156. Zubarev, R.A., *Electron-capture dissociation tandem mass spectrometry.* Current Opinion in Biotechnology, 2004. **15**(1): p. 12-16.

157. Syka, J.E.P., et al., *Peptide and protein sequence analysis by electron transfer dissociation mass spectrometry.* Proceedings of the National Academy of Sciences of the United States of America, 2004. **101**(26): p. 9528-9533.

158. McAlister, G.C., et al., *Implementation of Electron-Transfer Dissociation on a Hybrid Linear Ion Trap−Orbitrap Mass Spectrometer.* Analytical chemistry, 2007. **79**(10): p. 3525-3534.

159. Cunnane, S.C., et al., *Fish, docosahexaenoic acid and Alzheimer's disease.* Progress in Lipid Research, 2009. **48**(5): p. 239-256.

160. Florent-Béchard, S., et al., *The essential role of lipids in Alzheimer's disease.* Biochimie, 2009. **91**(6): p. 804-809.

161. van Echten-Deckert, G. and J. Walter, *Sphingolipids: Critical players in Alzheimer's disease.* Progress in Lipid Research, 2012. **51**(4): p. 378-393.

162. Arendt, B.S.a.B., *Comprehensive Lipid Profiling of Human Liver Tissue Extracts of Non-Alcoholic Fatty Liver Disease.* Biomarkers and Omics AB Sciex, 2010: p. 1-6.

163. Feldstein, A.E., et al., *Mass spectrometric profiling of oxidized lipid products in human nonalcoholic fatty liver disease and nonalcoholic steatohepatitis.* Journal of lipid research, 2010. **51**(10): p. 3046-3054.

164. Shimma, S., et al., *MALDI-based imaging mass spectrometry revealed abnormal distribution of phospholipids in colon cancer liver metastasis.* Journal of Chromatography B, 2007. **855**(1): p. 98-103.

165. Uchiyama, Y., et al., *Imaging mass spectrometry distinguished the cancer and stromal regions of oral squamous cell carcinoma by visualizing phosphatidylcholine (16:0/16:1) and phosphatidylcholine (18:1/20:4).* Analytical and Bioanalytical Chemistry, 2013: p. 1-10.

166. Pirman, D.A., et al., *Changes in Cancer Cell Metabolism Revealed by Direct Sample Analysis with MALDI Mass Spectrometry.* PLoS ONE, 2013. **8**(4): p. e61379.

167. Wenk, M.R., *The emerging field of lipidomics.* Nature Reviews Drug Discovery, 2005. **4**(7): p. 594-610.

168. Fahy, E., et al., *A comprehensive classification system for lipids.* J. Lipid Res., 2005. **46**(5): p. 839-862.

169. Fahy, E., et al., *Update of the LIPID MAPS comprehensive classification system for lipids.* J. Lipid Res., 2009. **50**(Supplement): p. S9-14.

170. Oster, T. and T. Pillot, *Docosahexaenoic acid and synaptic protection in Alzheimer's disease mice.* Biochimica et Biophysica Acta (BBA) - Molecular and Cell Biology of Lipids, 2010. **1801**(8): p. 791-798.

171. Quintana, F.J., et al., *Lipids and lipid-reactive antibodies as biomarkers for multiple sclerosis.* Journal of Neuroimmunology, 2012. **248**(1–2): p. 53-57.

172. Martinelli, N., et al., *FADS genotypes and desaturase activity estimated by the ratio of arachidonic acid to linoleic acid are associated with inflammation and coronary artery disease.* American Journal of Clinical Nutrition, 2008. **88**(4): p. 941.

173. Budhu, A., et al., *Integrated Metabolite and Gene Expression Profiles Identify Lipid Biomarkers Associated With Progression of Hepatocellular Carcinoma and Patient Outcomes.* Gastroenterology, 2013. **144**(5): p. 1066-1075.e1.

174. Ide, Y., et al., *Human Breast Cancer Tissues Contain Abundant Phosphatidylcholine (36∶1) with High Stearoyl-CoA Desaturase-1 Expression.* PLoS ONE, 2013. **8**(4).

175. Singhal, R., et al., *MALDI Profiles of Proteins and Lipids for the Rapid Characterisation of Upper GI-Tract Cancers.* Journal of Proteomics, (0).

176. Singhal, R., et al., *MALDI profiles of proteins and lipids for the rapid characterisation of upper GI-tract cancers.* Journal of Proteomics, 2013. **80**(0): p. 207-215.

177. De Oliveira, L., et al., *Lipid fingerprinting in women with early-onset preeclampsia: A first look.* Clinical Biochemistry, 2012. **45**(10–11): p. 852-855.

178. Eberlin, L.S., et al., *Discrimination of Human Astrocytoma Subtypes by Lipid Analysis Using Desorption Electrospray Ionization Imaging Mass Spectrometry.* Angewandte Chemie International Edition, 2010. **49**(34): p. 5953-5956.

179. Touboul, D., et al., *MALDI-TOF and cluster-TOF-SIMS imaging of Fabry disease biomarkers.* International Journal of Mass Spectrometry, 2007. **260**(2-3): p. 158-165.

180. Wang, H.-Y.J., C.B. Liu, and H.-W. Wu, *A simple desalting method for direct MALDI mass spectrometry profiling of tissue lipids.* Journal of lipid research, 2011. **52**(4): p. 840-849.

181. Stübiger, G., et al., *Analysis of Oxidized Phospholipids by MALDI Mass Spectrometry Using 6-Aza-2-thiothymine Together with Matrix Additives and Disposable Target Surfaces.* Analytical chemistry, 2010. **82**(13): p. 5502-5510.

182. Stübiger, G., et al., *Analysis of human plasma lipids and soybean lecithin by means of high performance thin layer chromatography and matrix assisted laser desorption/ionization mass spectrometry.* Rapid Communications in Mass Spectrometry, 2009. **23**(17): p. 2711-2723.

183. Garrett, T.J., et al., *Imaging of small molecules in tissue sections with a new intermediate-pressure MALDI linear ion trap mass spectrometer.* International Journal of Mass Spectrometry, 2007. **260**(2-3): p. 166-176.

184. Yuki, S. and S. Mitsutoshi, *Selective imaging of positively charged polar and nonpolar lipids by optimizing matrix solution composition.* Rapid Communications in Mass Spectrometry, 2009. **23**(20): p. 3269-3278.

185. Jackson, S.N., et al., *A Study of Phospholipids by Ion Mobility TOFMS.* Journal of the American Society for Mass Spectrometry, 2008. **19**(11): p. 1655-1662.

186. Jackson, S.N., et al., *Gangliosides' analysis by MALDI-ion mobility MS.* Analyst, 2011. **136**(3): p. 463-466.

187. Fuchs, B., et al., *Oxygen and cytokine-dependent changes in choline phospholipid saturation in hematopoietic progenitor cells detected by MALDI-TOF mass spectrometry.* Chemistry and Physics of Lipids, 2011. **164**(7): p. 636-642.

188. Müller, M., et al., *Limits for the detection of (poly-) phosphoinositides by matrix-assisted laser desorption and ionization time-of-flight mass spectrometry (MALDI-TOF MS).* Chemistry and Physics of Lipids, 2001. **110**(2): p. 151-164.

189. Zhou, P., et al., *Study on matrix additives for sensitive analysis of lipid A using MALDI mass spectrometry.* Appl. Environ. Microbiol., 2010: p. AEM.03082-09.

190. Asara, J.M. and J. Allison, *Enhanced detection of phosphopeptides in matrix-assisted laser desorption/ionization mass spectrometry using ammonium salts.* Journal of the American Society for Mass Spectrometry, 1999. **10**(1): p. 35-44.

191. Zhu, X. and I. Papayannopoulos, *Improvement in the detection of low concentration protein digests on a MALDI TOF/TOF workstation by reducing -cyano-4-hydroxycinnamic acid adduct ions.* Journal of Biomolecular Techniques: JBT, 2003. **14**(4): p. 298.

192. Zhang, Y., H.-J. Lu, and P.-Y. Yang, *Enhanced Ionization of Phosphopeptide Using Ammonium Phosphate as Matrix Additive by MALDI-MS.* Chinese Journal of Chemistry, 2008. **26**(10): p. 1863-1869.

193. Kjellström, S. and O.N. Jensen, *Phosphoric Acid as a Matrix Additive for MALDI MS Analysis of Phosphopeptides and Phosphoproteins.* Analytical chemistry, 2004. **76**(17): p. 5109-5117.

194. Wang, Y., H. Rashidzadeh, and B. Guo, *Structural effects on polyether cationization by alkali metal ions in matrix-assisted laser desorption/ionization.* Journal of the American Society for Mass Spectrometry, 2000. **11**(7): p. 639-643.

195. Pastor, S.J. and C.L. Wilkins, *Analysis of hydrocarbon polymers by matrix-assisted laser desorption/ionization-fourier transform mass spectrometry.* Journal of the American Society for Mass Spectrometry, 1997. **8**(3): p. 225-233.

196. Asara, J.M. and J. Allison, *Enhanced Detection of Oligonucleotides in UV MALDI MS Using the Tetraamine Spermine as a Matrix Additive.* Analytical chemistry, 1999. **71**(14): p. 2866-2870.

197. Vandell, V. and P. Limbach, *Polyamine co-matrices for matrix-assisted laser desorption/ionization mass spectrometry of oligonucleotides.* Rapid Communications in Mass Spectrometry, 1999. **13**(20): p. 2014-2021.

198. Howard, K.L. and G.L. Boyer, *Adduct simplification in the analysis of cyanobacterial toxins by matrix-assisted laser desorption/ionization mass spectrometry.* Rapid Communications in Mass Spectrometry, 2007. **21**(5): p. 699-706.

199.	Lacey, D., et al., *Aspirin revealed: A cationization strategy for detecting acetylsalicylic acid by MALDI mass spectrometry.* International Journal of Mass Spectrometry, 2007. **261**(2-3): p. 192-198.

200.	Choi, S.-S., et al., *Comparison of ionization behaviors of ring and linear carbohydrates in MALDI-TOFMS.* International Journal of Mass Spectrometry, 2009. **279**(1): p. 53-58.

201.	Choi, S.-S. and S.-H. Ha, *Influence of sample preparation method and silver salt types on MALDI-TOFMS analysis of polybutadiene.* Macromolecular Research, 2008. **16**(2): p. 108-112.

202.	Guan, B. and R.B. Cole, *MALDI Linear-Field Reflectron TOF Post-Source Decay Analysis of Underivatized Oligosaccharides: Determination of Glycosidic Linkages and Anomeric Configurations Using Anion Attachment.* Journal of the American Society for Mass Spectrometry, 2008. **19**(8): p. 1119-1131.

203.	Calvano, C. and C. Zambonin, *MALDI-Q-TOF-MS Ionization and Fragmentation of Phospholipids and Neutral Lipids of Dairy Interest Using Variable Doping Salts.* Adv Dairy Res, 2013. **1**(101): p. 2.

204.	Folch, J., M. Lees, and G. Sloane-Stanley, *A simple method for the isolation and purification of total lipids from animal tissues.* J. biol. Chem, 1957. **226**(1): p. 497-509.

205.	Vorm, O. and M. Mann, *Improved mass accuracy in matrix-assisted laser desorption/ionization time-of-flight mass spectrometry of peptides.* Journal of the American Society for Mass Spectrometry, 1994. **5**(11): p. 955-958.

206.	Vorm, O., P. Roepstorff, and M. Mann, *Improved resolution and very high sensitivity in MALDI TOF of matrix surfaces made by fast evaporation.* Analytical chemistry, 1994. **66**(19): p. 3281-3287.

207.	Benard, S., et al., *Experiments towards quantification of saturated and polyunsaturated diacylglycerols by matrix-assisted laser desorption and ionization time-of-flight mass spectrometry.* Chemistry and Physics of Lipids, 1999. **100**(1-2): p. 115-125.

208.	Williams, T.L., et al., *Experimental factors affecting the quality and reproducibility of MALDI TOF mass spectra obtained from whole bacteria cells.* Journal of the American Society for Mass Spectrometry, 2003. **14**(4): p. 342-351.

209.	Soltwisch, J., et al., *Ion Yields in UV-MALDI Mass Spectrometry As a Function of Excitation Laser Wavelength and Optical and Physico-Chemical Properties of Classical and Halogen-Substituted MALDI Matrixes.* Analytical chemistry, 2012. **84**(15): p. 6567-6576.

210.	Jaskolla, T., et al., *The New Matrix 4-Chloro-[alpha]-Cyanocinnamic Acid Allows the Detection of Phosphatidylethanolamine Chloramines by MALDI-TOF Mass Spectrometry.* Journal of the American Society for Mass Spectrometry, 2009. **20**(5): p. 867-874.

211.	Mirza, S.P., N.P. Raju, and M. Vairamani, *Estimation of the proton affinity values of fifteen matrix-assisted laser desorption/ionization matrices under electrospray ionization conditions using the kinetic method.* Journal of the American Society for Mass Spectrometry, 2004. **15**(3): p. 431-435.

212. Barylyuk, K., et al., *Gas-phase basicity of several common MALDI matrices measured by a simple experimental approach.* RSC Advances, 2012.

213. Garden, R. and J. Sweedler, *Heterogeneity within MALDI samples as revealed by mass spectrometric imaging.* Anal. Chem, 2000. **72**(1): p. 30-36.

214. Bouschen, W. and B. Spengler, *Artifacts of MALDI sample preparation investigated by high-resolution scanning microprobe matrix-assisted laser desorption/ionization (SMALDI) imaging mass spectrometry.* International Journal of Mass Spectrometry, 2007. **266**(1–3): p. 129-137.

215. Angel, P.M., et al., *Enhanced Sensitivity for High Spatial Resolution Lipid Analysis by Negative Ion Mode MALDI Imaging Mass Spectrometry.* Analytical chemistry, 2012.

216. Qiao, H., et al., *Analyte distributions in MALDI samples using MALDI imaging mass spectrometry.* International Journal of Mass Spectrometry, 2009. **281**(1–2): p. 41-51.

217. Monroe, E.B., et al., *Measuring salty samples without adducts with MALDI MS.* International Journal of Mass Spectrometry, 2007. **260**(2–3): p. 237-242.

218. Colantonio, S., et al., *Quantitative Analysis of Phospholipids Using Nanostructured Laser Desorption Ionization Targets.* Lipids, 2011. **46**(5): p. 469-477.

219. Lee, G., J. Son, and S. Cha, *Selective or Class-wide Mass Fingerprinting of Phosphatidylcholines and Cerebrosides from Lipid Mixtures by MALDI Mass Spectrometry.* Bull. Korean Chem. Soc, 2013. **34**(7): p. 2143.

220. http://www.axeleratio.com/ip/solids/data/lattice_energies.htm.

221. Sun, G., et al., *Matrix-Assisted Laser Desorption/Ionization Time-of-Flight Mass Spectrometric Analysis of Cellular Glycerophospholipids Enabled by Multiplexed Solvent Dependent Analyte- Matrix Interactions.* Analytical chemistry, 2008. **80**(19): p. 7576-7585.

222. Domingues, P., et al., *Characterization of sodiated glycerol phosphatidylcholine phospholipids by mass spectrometry.* Rapid Communications in Mass Spectrometry, 2001. **15**(10): p. 799-804.

223. Hsu, F.-F.u. and J. Turk, *Electrospray ionization/tandem quadrupole mass spectrometric studies on phosphatidylcholines: the fragmentation processes.* Journal of the American Society for Mass Spectrometry, 2003. **14**(4): p. 352-363.

224. Jackson, S.N., et al., *Direct tissue analysis of phospholipids in rat brain using MALDI-TOFMS and MALDI-ion mobility-TOFMS.* Journal of the American Society for Mass Spectrometry, 2005. **16**(2): p. 133-138.

225. Wang, H.-Y.J., S.N. Jackson, and A.S. Woods, *Direct MALDI-MS Analysis of Cardiolipin from Rat Organs Sections.* Journal of the American Society for Mass Spectrometry, 2007. **18**(3): p. 567-577.

226. Trimpin, S., D.E. Clemmer, and C.N. McEwen, *Charge-Remote Fragmentation of Lithiated Fatty Acids on a TOF-TOF Instrument Using Matrix-Ionization.* Journal of the American Society for Mass Spectrometry, 2007. **18**(11): p. 1967-1972.

227. Hsu, F.-F. and J. Turk, *Distinction among isomeric unsaturated fatty acids as lithiated adducts by electrospray ionization mass spectrometry using low energy collisionally activated dissociation on a triple stage quadrupole instrument.* Journal of the American Society for Mass Spectrometry, 1999. **10**(7): p. 600-612.

228. Hsu, F.-F. and J. Turk, *Structural determination of sphingomyelin by tandem mass spectrometry with electrospray ionization.* Journal of the American Society for Mass Spectrometry, 2000. **11**(5): p. 437-449.

229. Hsu, F.-F.u., et al., *Structural studies on ceramides as lithiated adducts by low energy collisional-activated dissociation tandem mass spectrometry with electrospray ionization.* Journal of the American Society for Mass Spectrometry, 2002. **13**(6): p. 680-695.

230. Hsu, F.-F., A. Bohrer, and J. Turk, *Formation of Lithiated Adducts of Glycerophosphocholine Lipids Facilitates their Identification by Electrospray Ionization Tandem Mass Spectrometry.* Journal of the American Society for Mass Spectrometry, 1998. **9**(5): p. 516-526.

231. Deininger, S.r.-O., et al., *MALDI Imaging Combined with Hierarchical Clustering as a New Tool for the Interpretation of Complex Human Cancers.* Journal of Proteome Research, 2008. **7**(12): p. 5230-5236.

232. Cva ka, J. and A. Svatoš, *Matrix assisted laser desorption/ionization analysis of lipids and high molecular weight hydrocarbons with lithium 2, 5 dihydroxybenzoate matrix.* Rapid Communications in Mass Spectrometry, 2003. **17**(19): p. 2203-2207.

233. Trimpin, S., et al., *Fractionation and Solvent-Free MALDI-MS Analysis of Polymers Using Liquid Adsorption Chromatography at Critical Conditions in Combination with a Multisample On-Target Homogenization/Transfer Sample Preparation Method.* Analytical chemistry, 2007. **79**(19): p. 7565-7570.

234. Trimpin, S. and M.L. Deinzer, *Solvent-free MALDI-MS for the analysis of biological samples via a mini-ball mill approach.* Journal of the American Society for Mass Spectrometry, 2005. **16**(4): p. 542-547.

235. Griffiths, R.L. and J. Bunch, *A survey of useful salt additives in matrix-assisted laser desorption/ionization mass spectrometry and tandem mass spectrometry of lipids: introducing nitrates for improved analysis.* Rapid Communications in Mass Spectrometry, 2012. **26**(13): p. 1557-1566.

236. Race, A.M., I.B. Styles, and J. Bunch, *Inclusive sharing of mass spectrometry imaging data requires a converter for all.* Journal of Proteomics, 2012. **75**(16): p. 5111-5112.

237. Yoshihashi-Suzuki, S., I. Sato, and K. Awazu, *Wavelength dependence of matrix-assisted laser desorption and ionization using a tunable mid-infrared laser.* International Journal of Mass Spectrometry, 2008. **270**(3): p. 134-138.

238. Armin Holle, A.H.M.K.J.H., *Optimizing UV laser focus profiles for improved MALDI performance.* Journal of Mass Spectrometry, 2006. **41**(6): p. 705-716.

239. Wiegelmann, M., et al., *Matching the laser wavelength to the absorption properties of matrices increases the ion yield in UV-MALDI mass spectrometry.* Analytical and Bioanalytical Chemistry, 2012: p. 1-8.

240. Lemaire, R., et al., *Direct Analysis and MALDI Imaging of Formalin-Fixed, Paraffin-Embedded Tissue Sections.* Journal of Proteome Research, 2007. **6**(4): p. 1295-1305.

241. Carter, C., C. McLeod, and J. Bunch, *Imaging of Phospholipids in Formalin Fixed Rat Brain Sections by Matrix Assisted Laser Desorption/Ionization Mass*

Spectrometry. Journal of the American Society for Mass Spectrometry, 2011. **22**(11): p. 1991-1998.

242. Goodwin, R.J.A., et al., *Use of a Solvent-Free Dry Matrix Coating for Quantitative Matrix-Assisted Laser Desorption Ionization Imaging of 4-Bromophenyl-1,4-diazabicyclo(3.2.2)nonane-4-carboxylate in Rat Brain and Quantitative Analysis of the Drug from Laser Microdissected Tissue Regions.* Analytical chemistry, 2010. **82**(9): p. 3868-3873.

243. Werner, M., et al., *Effect of formalin tissue fixation and processing on immunohistochemistry.* The American journal of surgical pathology, 2000. **24**(7): p. 1016.

244. Puchtler, H. and S.N. Meloan, *On the chemistry of formaldehyde fixation and its effects on immunohistochemical reactions.* Histochemistry, 1985. **82**(3): p. 201-204.

245. Kiernan, J.A., *Formaldehyde, formalin, paraformaldehyde and glutaraldehyde: what they are and what they do.* Microscopy Today, 2000. **1**: p. 8-12.

246. Buesa, R.J., *Histology without formalin?* Annals of Diagnostic Pathology, 2008. **12**(6): p. 387-396.

247. Jamie M. Nowacek, J.A.K., *Fixation and Tissue Processing*, in *Special Stains and H&E*, J.A.K. George L. Kumar, Editor. 2010, Dako North America: California. p. 141-152.

248. Glauret, A.M., *2.2 Vehicles for Fixatives*, in *Practical Methods in Electron Microscopy: Fixation, Dehydration and Embedding of Biological Specimens*, A.M. Glauret, Editor. 1978, North-Holland Publishing Company: The Netherlands. p. 7-21.

249. Mugnaini, E. and A.L. Dahl, *Zinc-aldehyde fixation for light-microscopic immunocytochemistry of nervous tissues.* Journal of Histochemistry & Cytochemistry, 1983. **31**(12): p. 1435-8.

250. Wester, K., et al., *Zinc-based fixative improves preservation of genomic DNA and proteins in histoprocessing of human tissues.* Laboratory investigation, 2003. **83**(6): p. 889-899.

251. Watson, M.L., *Staining of Tissue Sections for Electron Microscopy with Heavy Metals.* The Journal of Biophysical and Biochemical Cytology, 1958. **4**(4): p. 475-478.

252. Hall, C., M. Jakus, and F. Schmitt, *The structure of certain muscle fibrils as revealed by the use of electron stains.* Journal of Applied Physics, 1945. **16**(8): p. 459-465.

253. Palay, S.L., et al., *Fixation of neural tissues for electron microscopy by perfusion with solutions of osmium tetroxide.* The Journal of cell biology, 1962. **12**(2): p. 385-410.

254. Wigglesworth, V.B., *The Use of Osmium in the Fixation and Staining of Tissues.* Proceedings of the Royal Society of London. Series B - Biological Sciences, 1957. **147**(927): p. 185-199.

255. Reynolds, E.S., *The use of lead citrate at high pH as an electron-opaque stain in electron microscopy.* The Journal of cell biology, 1963. **17**(1): p. 208-212.

256. Stempak, J.G. and R.T. Ward, *An improved staining method for electron microscopy.* The Journal of cell biology, 1964. **22**(3): p. 697-701.

257. Adams, C.W.M., *Osmium Tetroxide and the Marchi Method: Reactions with Polar and Non-polar Lipids, Protein and Polysaccharide.* Journal of Histochemistry & Cytochemistry, 1960. **8**(4): p. 262-267.

258. Trent, J.S., J.I. Scheinbeim, and P.R. Couchman, *Ruthenium tetraoxide staining of polymers for electron microscopy.* Macromolecules, 1983. **16**(4): p. 589-598.

259. Watson, M.L., *Staining of Tissue Sections for Electron Microscopy with Heavy Metals: II. Application of Solutions Containing Lead and Barium.* The Journal of Biophysical and Biochemical Cytology, 1958. **4**(6): p. 727-730.

260. Holt, S.J. and R.M. Hicks, *Studies on Formalin Fixation for Electron Microscopy and Cytochemical Staining Purposes.* The Journal of Biophysical and Biochemical Cytology, 1961. **11**(1): p. 31-45.

261. Belazi, D., et al., *Chemical analysis of osmium tetroxide staining in adipose tissue using imaging ToF-SIMS.* Histochemistry and Cell Biology, 2009. **132**(1): p. 105-115.

262. Deierkauf, F.A. and F.J.M. Heslinga, *The Action of Formaldehyde on Rat Brain Lipids.* Journal of Histochemistry & Cytochemistry, 1962. **10**(1): p. 79-82.

263. Boskey, A.L., M.L. Cohen, and P.G. Bullough, *Hard tissue biochemistry: A comparison of fresh-frozen and formalin-fixed tissue samples.* Calcified Tissue International, 1982. **34**(1): p. 328-331.

264. Palmer, A.D., et al., *Sucrose cryo-protection facilitates imaging of whole eye sections by MALDI mass spectrometry.* Journal of Mass Spectrometry, 2012. **47**(2): p. 237-241.

265. Ho, Y.-P., P.-C. Huang, and K.-H. Deng, *Metal ion complexes in the structural analysis of phospholipids by electrospray ionization tandem mass spectrometry.* Rapid Communications in Mass Spectrometry, 2003. **17**(2): p. 114-121.

266. Turk, F.H.a.J., *Electrospray Ionisation/Tandem Quadrupole Mass Spectrometric Studies on Phosphatidylcholines: The Fragmentation Processes.* Journal of the American Society for Mass Spectrometry, 2003. **14**: p. 352-363.

267. Ashraf, M.Z., N.S. Kar, and E.A. Podrez, *Oxidized phospholipids: Biomarker for cardiovascular diseases.* The International Journal of Biochemistry & Cell Biology, 2009. **41**(6): p. 1241-1244.

268. Stauber, J., et al., *MALDI Imaging of Formalin-Fixed Paraffin-Embedded Tissues: Application to Model Animals of Parkinson Disease for Biomarker Hunting.* Journal of Proteome Research, 2008. **7**(3): p. 969-978.

269. Carter, C.L., *The Analysis and Imaging of Lipids from Complex Samples by Matrix-Assisted Laser Desorption/Ionisation Mass Spectrometry*, in *The School of Chemistry*. 2012, University of Birmingham: EThOS. p. 241.

270. Jackson, S.N. and A.S. Woods, *Direct profiling of tissue lipids by MALDI-TOFMS.* Journal of Chromatography B, 2009. **877**(26): p. 2822-2829.

271. Al-Saad, K.A., et al., *Structural analysis of phosphatidylcholines by post-source decay matrix-assisted laser desorption/ionization time-of-flight mass spectrometry.* Journal of the American Society for Mass Spectrometry, 2003. **14**(4): p. 373-382.

272. Kollmer, F., *Cluster primary ion bombardment of organic materials.* Applied Surface Science, 2004. **231–232**(0): p. 153-158.

273. Perdian, D.C. and Y.J. Lee, *Imaging MS Methodology for More Chemical Information in Less Data Acquisition Time Utilizing a Hybrid Linear Ion Trap−Orbitrap Mass Spectrometer.* Analytical chemistry, 2010. **82**(22): p. 9393-9400.

274. Prideaux, B., et al., *High-sensitivity MALDI-MRM-MS imaging of moxifloxacin distribution in tuberculosis-infected rabbit lungs and granulomatous lesions.* Analytical chemistry, 2011. **83**(6): p. 2112-2118.

275. Khatib-Shahidi, S., et al., *Direct Molecular Analysis of Whole-Body Animal Tissue Sections by Imaging MALDI Mass Spectrometry.* Analytical Chemistry, 2006. **78**(18): p. 6448-6456.

276. Reyzer, M.L., et al., *Direct analysis of drug candidates in tissue by matrix-assisted laser desorption/ionization mass spectrometry.* Journal of Mass Spectrometry, 2003. **38**(10): p. 1081-1092.

277. Yagnik, G.B., A.R. Korte, and Y.J. Lee, *Multiplex mass spectrometry imaging for latent fingerprints.* Journal of Mass Spectrometry, 2013. **48**(1): p. 100-104.

278. Steven, R. and J. Bunch, *Repeat MALDI MS imaging of a single tissue section using multiple matrices and tissue washes.* Analytical and Bioanalytical Chemistry, 2013: p. 1-10.

279. Jeon, Y.E., et al., *Histology-directed matrix-assisted laser desorption/ionization analysis reveals tissue origin and p53 status of primary liver cancers.* Pathology International, 2011. **61**(8): p. 449-455.

280. Agar, N., et al., *Matrix solution fixation: Histology-compatible tissue preparation for MALDI mass spectrometry imaging.* Anal. Chem, 2007. **79**(19): p. 7416-7423.

281. Cornett, D.S., et al., *A Novel Histology-directed Strategy for MALDI-MS Tissue Profiling That Improves Throughput and Cellular Specificity in Human Breast Cancer.* Mol Cell Proteomics, 2006. **5**(10): p. 1975-1983.

282. Chaurand, P., et al., *Integrating Histology and Imaging Mass Spectrometry.* Analytical chemistry, 2004. **76**(4): p. 1145-1155.

283. Walch, A., et al., *MALDI imaging mass spectrometry for direct tissue analysis: a new frontier for molecular histology.* 2008, Journal of Histochem Cell Biology. p. 421-434.

284. Chambers, M.C., et al., *A cross-platform toolkit for mass spectrometry and proteomics.* Nat Biotech, 2012. **30**(10): p. 918-920.

285. Eikel, D. and J. Henion, *Liquid extraction surface analysis (LESA) of food surfaces employing chip-based nano-electrospray mass spectrometry.* Rapid Commun. Mass Spectrom., 2011. **25**(16): p. 2345-2354.

286. Van Berkel, G.J., V. Kertesz, and R.C. King, *High-Throughput Mode Liquid Microjunction Surface Sampling Probe.* Analytical chemistry, 2009. **81**(16): p. 7096-7101.

287. Walworth, M.J., et al., *Direct sampling and analysis from solid-phase extraction cards using an automated liquid extraction surface analysis nanoelectrospray mass spectrometry system.* Rapid Communications in Mass Spectrometry, 2011. **25**(17): p. 2389-2396.

288. Hsu, F.-F. and J. Turk, *Studies on Phosphatidylserine by Tandem Quadrupole and Multiple Stage Quadrupole Ion-Trap Mass Spectrometry with Electrospray*

Ionization: Structural Characterization and the Fragmentation Processes. Journal of the American Society for Mass Spectrometry, 2005. **16**(9): p. 1510-1522.

289.   Holt, S., E.E. Hobbiger, and G. Pawan, *Preservation of integrity of rat tissues for cytochemical staining purposes.* The Journal of Biophysical and Biochemical Cytology, 1960. **7**(2): p. 383-386.

290.   Hsu, F.-F. and J. Turk, *Studies on phosphatidylglycerol with triple quadrupole tandem mass spectrometry with electrospray ionization: fragmentation processes and structural characterization.* Journal of the American Society for Mass Spectrometry, 2001. **12**(9): p. 1036-1043.

291.   James, P.F., M.A. Perugini, and R.A.J. O'Hair, *Size matters! Fragmentation chemistry of [Cu(L)n]2+ complexes of diacylglycerophosphocholines as a function of coordination number (n = 2–7).* Rapid Communications in Mass Spectrometry, 2007. **21**(5): p. 757-763.

292.   Evason, D.J., M.A. Claydon, and D.B. Gordon, *Effects of ion mode and matrix additives in the identification of bacteria by intact cell mass spectrometry.* Rapid Communications in Mass Spectrometry, 2000. **14**(8): p. 669-672.

293.   Krader, P. and D. Emerson, *Identification of archaea and some extremophilic bacteria using matrix-assisted laser desorption/ionization time-of-flight (MALDI-TOF) mass spectrometry.* Extremophiles, 2004. **8**(4): p. 259-268.

294.   Harris, W.A., D.J. Janecki, and J.P. Reilly, *Use of matrix clusters and trypsin autolysis fragments as mass calibrants in matrix-assisted laser desorption/ionization time-of-flight mass spectrometry.* Rapid Communications in Mass Spectrometry, 2002. **16**(18): p. 1714-1722.